BULGARIAN CHEMICAL COMMUNICATIONS

Section

Chemistry

Study of the reactivity of the generated liver metabolites of a newly synthesized derivative of bexarotene and paracetamol

I. R. Iliev[2*], Y. K. Koleva[1], S. F. Georgieva[2]

[1]*University "Prof. Assen Zlatarov", Faculty of Natural Science, Department of Chemistry, Burgas, Bulgaria*
[2]*Medical university "Prof. Paraskev Stoyanov", Faculty of Pharmacy, Department of Pharmaceutical Chemistry, Varna, Bulgaria*

The present work is focused to predict probable hepatic metabolites (*in vivo* and *in vitro* rat) and to study their reactivity mechanism (DNA and protein binding). The parent structure of the newly synthesized compound of bexarotene and paracetamol can bind to DNA but it cannot bind to protein and experimental metabolic pathways of action were not observed for rat *in vivo* and *in vitro*. The reactivity of predicted hepatic metabolites for both conditions (*in vivo* and *in vitro* rat) have different mechanisms of action (A_N^2, non-covalent interaction, non-specific, radical mechanism, S_N^1 and S_N^2) by DNA binding. The protein reactivity of the bexarotene derivative has the following mechanisms of action (Michael addition, nucleophilic addition, Schiff base formation, S_N^2).

Keywords: bexarotene derivative, predict, metabolic activation, hepatic, QSAR Toolbox

INTRODUCTION

The search for new drugs and approaches in the treatment of oncological and infectious diseases is a leading goal in medical and pharmaceutical practice around the world.

Retinoids, a group of small lipophilic molecules, are essential for a variety of biological processes. Retinoids regulate gene transcription by binding to the nuclear receptors, the retinoic acid (RA) receptors (RARs), and the retinoid X receptors (RXRs). RARs and RXRs are ligand-activated transcription factors for the regulation of RA responsive genes. The actions of RARs and RXRs on gene transcription require a highly coordinated interaction with a large number of coactivators and corepressors [1].

Bexarotene, a third-generation retinoid, exhibits its pharmacological effects through its interaction with retinoid X receptors – RXR [1]. RXRs are located primarily in visceral organs such as the liver and kidneys. Activated RXRs form homodimers or heterodimers with RAR (retinoic acid receptors), vitamin D receptors, thyroid receptors or peroxisome proliferator activator receptors (PPAR) [1]. The ability of RXRs to form heterodimers with different nuclear receptors indicates that the biological activity of bexarotene may be much more diverse than that of compounds that activate only RARs [1].

In vitro, bexarotene inhibits the growth of tumor cell lines. *In vivo*, bexarotene causes tumor regression in some animal models and prevents tumor induction in others [1].

At the heart of the toxic effects of bexarotene is its retinoid nature. Like other members of the retinoid group, it is characterized by extreme teratogenicity. Some of the more specific side effects of bexarotene therapy include central hypothyroidism, elevated cholesterol and triglyceride levels [1].

Increases in liver function tests associated with bexarotene use have been reported. Based on data from ongoing clinical trials, elevations in liver function tests suffered back development within one month in 80% of patients after dose reduction or discontinuation of treatment. Temporary or permanent discontinuation of bexarotene should be considered if the test results reach values three times higher than the upper limit for normal values of SGOT / AST, SGPT / ALT or for bilirubin [2]. Bexarotene is also contraindicated for patients with hepatic failure [2].

Hydrazones have been demonstrated to possess, among other, antimicrobial, anticonvulsant, analgesic, antiinflammatory, antiplatelet, antitubercular and antitumoral activities [3].

Paracetamol (acetaminophen) is one of the most widely used of all drugs, with a wealth of experience clearly establishing it as the standard antipyretic and analgesic for mild to moderate pain states [4]. Systematic use of high doses of paracetamol can lead to increased liver failure and is now the leading cause of acute liver failure and is the second most common cause of liver failure requiring transplantation [5]. During the 1960s and 1970s, increasing concern was raised about the

---

* To whom all correspondence should be sent:
E-mail: *i__iliev@abv.bg*

toxicity of nonprescription analgesics, but in normal use paracetamol exhibited a consistent safety profile [4].

Hepatic metabolic stability is a key parameter in drug discovery because it can prevent a drug from attaining sufficient *in vivo* exposure, producing short half-lives, poor oral bioavailability and low plasma concentrations. It is essential to identify metabolic liabilities early in drug discovery so they can be addressed during lead optimization. Metabolic stability is typically first measured *in vitro* using liver microsomes and data from this assay are used to guide structural modifications to improve stability or select the best compounds for *in vivo* pharmacokinetic (PK) and efficacy testing. Liver microsomes are enriched with cytochrome P (CYP) 450 enzymes, localized in the endoplasmic reticulum membrane, which are responsible for the metabolism of the majority (70–80%) of clinically approved drugs [6, 7].

Hybrid molecules are new class drugs. The advantages of these molecules are better bioavailability at the target site, better effect with minimal therapeutic doses, lower toxicity and cheap preclinical evaluation. The OECD QSAR Toolbox is a software designed to support hazard assessment of chemicals, as well as to increase mechanistic and other knowledge on chemical substances in a cost-efficient way. It promotes the use of assessment methods alternative to animals and minimizes unnecessary animal testing without reducing the safety of human health and environment [8].

At a glance, computational tools reduce the use of animals in laboratory tests, reduce the cost for testing and increase the number of chemicals which are assessed for their effects upon human health and the environment. The toxicity of substances can be predicted even before they are produced, facilitating sustainable product development and green chemistry [8].

The aim of this work was to study the probable reactivity of the parent structure of the newly synthesized compound of bexarotene and paracetamol and their generated hepatic metabolites (for both conditions (rat *in vivo* and *in vitro*)) with respect to DNA and protein binding.
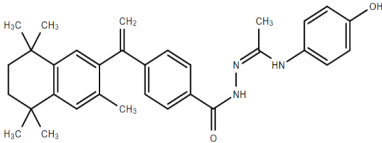
The newly synthesized hydrazone derivative was obtained according to the basic scheme of synthesis of bexarotene analogs and its structure was confirmed by its spectral data [9].

For the purpose of this study we synthesized a new hydrazone derivative of the retinoid bexarotene. The process consists of three major steps – esterification of the carboxylic group, hydrazinolysis and substitution of ketone to the newly formed hydrazone group. The result of the synthesis depends on the aldehyde or ketone used. For the purpose of this study we used paracetamol forming the new derivative of bexarotene shown in Table 1 [9]. Currently, there are no literature data of the mechanism of action of the newly synthesized derivative. The newly synthesized bexarotene derivative (N-[1-(4-hydroxyphenyl)amino ethilyden]-4-[1-(3,5,5,8,8-pentamethyl-6,7-dihydro naphtalen-2-yl)-ethenyl]phenylcarbohydrazide) is presented in Table 1 [9, 10].

Organisation for Economic Co-operation and Development (*OECD*) (*Q)SAR Toolbox (version 4.3)*. (Quantitative) structure-activity relationships [(Q)SARs] are methods for estimating properties of a chemical from its molecular structure and have the potential to provide information on the hazards of chemicals, while reducing time, monetary costs and animal testing currently needed. To facilitate practical application of (Q)SAR approaches in regulatory contexts by governments and industry and to improve their regulatory acceptance, the OECD (Q)SAR project has developed various outcomes such as the principles for the validation of (Q)SAR models, guidance documents as well as the QSAR Toolbox [11].

Observed rat in vivo metabolism. The observed (documented) metabolic pathways for 647 chemicals, extracted from the scientific literature, and associated with the *in vivo* biotransformations of xenobiotic chemicals in rodents (mostly rats) are stored in a database format that allows easy computer access to the metabolism information [11].

Table 1. Name and structural formula of the newly synthesized derivative.

Name of compound	Structural formula
N-[1-(4-hydroxyphenyl)aminoethilyden]-4-[1-(3,5,5,8,8-pentamethyl-6,7-dihydronaphtalen-2-yl)-ethenyl]phenylcarbohydrazide	

MATERIAL AND METHODS

In vivo rat metabolism simulator. The current *in vivo* rat liver metabolic simulator (transformation table) represents electronically designed set of 671 structurally generalized, hierarchically arranged abiotic and enzymatic transformation reactions, which are characteristic for the metabolism for *in vivo* experimental systems such as rodent (mostly rat). The principal applicability of this simulator is associated with the reproduction, as well as the prediction of the metabolic activation reactions and pathways of xenobiotic chemicals, which may elicit *in vivo* genotoxicity effects [11].

Observed rat liver S9 metabolism. The documented metabolic pathways for 261 chemicals observed with the use of *in vitro* experimental systems such as rodent (mostly rat) liver microsomes and S9 fraction are stored in a database format that allows easy computer access to the metabolism information [11].

Rat liver S9 metabolism simulator. The current *in vitro* rat liver metabolic simulator (transformation table) represents electronically designed set of 551 structurally generalized, hierarchically arranged biotransformation reactions, which are characteristic for the metabolism for *in vitro* experimental systems such as rodent (mostly rat) liver microsomes and S9 fraction. The principal applicability of this simulator is associated with the reproduction, as well as the prediction of the metabolic activation reactions and pathways of xenobiotic chemicals, which may elicit *in vitro* genotoxicity effects such as bacterial mutagenicity and chromosomal aberrations [11].

DNA binding by OASIS. The profiler is based on Ames mutagenicity model part of OASIS TIMES system. The profiler consists of 85 structural alerts responsible for interaction with DNA analyzed in Ames mutagenicity model. The scope of the profiler is to investigate presence of alerts within target molecules which may interact with DNA [11].

Protein binding by OASIS. The scope of the profiler is to investigate the presence of alerts within target molecules responsible for interaction with proteins. The list of 112 structural alerts has been separated into 11 mechanistic domains. Each of the mechanistic domains has been separated into more than 2 mechanistic alerts. The profiling result outcome assigns a target to the corresponding structural alert, mechanistic alerts and domain [11].

RESULTS AND DISCUSSION

QSAR Toolbox software (version 4.3) was used for predicting possible metabolites of N-[1-(4-hydroxyphenyl)aminoethilyden]-4-[1-(3,5,5,8,8-pentamethyl-6,7-dihydronaphtalen-2-yl)-ethenyl]phenylcarbohydrazide in the liver (*in vivo* and *in vitro* rat) and its DNA and protein binding. The parent structure of N-[1-(4-hydroxyphenyl)aminoethilyden]-4-[1-(3,5,5,8,8-pentamethyl-6,7-dihydronaphtalen-2-yl)-ethenyl] phenylcarbohydrazide can bind to DNA with mechanism of actions (A_N^2 (nucleophilic addition reaction with cycloisomerization (hydrazine derivatives)), non-covalent interactions (DNA intercalation (DNA intercalators with carboxamide and aminoalkylamine side chain)), radical mechanism *via* ROS formation (hydrazine derivatives) and S_N^2 (direct nucleophilic attack on diazonium cation (hydrazine derivatives))) and cannot bind to protein. Experimental metabolic pathways of activation were not observed for rat *in vivo* and *in vitro*. In the liver metabolism simulator (*in vivo* rat), twenty-four metabolites were predicted. Results of hepatic prediction (*in vivo* rat) of N-[1-(4-hydroxyphenyl)aminoethilyden]-4-[1-(3,5,5,8,8-pentamethyl-6,7-dihydronaphtalen-2-yl)-ethenyl]phenylcarbohydrazide are present in Table 2. The possible DNA binding by OASIS (mechanism of reaction) of the predicted hepatic metabolites for N-[1-(4-hydroxyphenyl)amino ethilyden]-4-[1-(3,5,5,8,8-pentamethyl-6,7-dihydronaphtalen-2-yl)-ethenyl]phenylcarbo hydrazide was estimated by QSAR Toolbox software. Results of DNA binding of the predicted hepatic metabolites for N-[1-(4-hydroxyphenyl) aminoethilyden]-4-[1-(3,5,5,8,8-pentamethyl-6,7-dihydronaphtalen-2-yl)-ethenyl]phenylcarbo hydrazide are presented in Table 3.

Twenty-four metabolites are reactive, i.e. alerts are found by DNA binding. Structural alerts (quinoneimine, thionine and phenoxazinium derivatives, hydrazine derivatives, DNA intercalators with carboxamide and aminoalkylamine side chain, specific imine and thione derivatives, epoxides and aziridines) were identified for twenty four metabolites in the mechanistic domains (radical mechanism, A_N^2, non-covalent interaction and S_N^2, S_N^1, non-specific) with mechanistic alerts (Michael-type addition, quinoid structures, nucleophilic addition reaction with cycloisomerization, DNA intercalation, incorporation into DNA/RNA, due to structural analogy with nucleoside bases, radical mechanism *via* ROS formation, ROS formation after GSH depletion, nucleophilic substitution on diazonium ion, direct nucleophilic attack on diazonium cation and alkylation, direct acting epoxides and related).

Table 2. Number and structure of the predicted hepatic metabolites (*in vivo*) of N-[1-(4-hydroxyphenyl) aminoethilyden]-4-[1-(3,5,5,8,8-pentamethyl-6,7-dihydronaphtalen-2-yl)-ethenyl]phenylcarbohydrazide by QSAR Toolbox.

1	2	3
4	5	6
7	8	9
10	11	12
13	14	15
16	17	18
19	20	21
22	23	24

Table 3. DNA binding of hepatic metabolites for N-[1-(4-hydroxyphenyl) aminoethilyden]-4-[1-(3,5,5,8,8-pentamethyl-6,7-dihydronaphtalen-2-yl)-ethenyl]phenylcarbohydrazide by QSAR Toolbox (liver *in vivo* metabolism simulator)

Number of metabolite	DNA binding by OASIS (Mechanism of reaction)		
	Structural alert	Mechanistic alert	Mechanistic domain
1-1-3,10,11 3,10,11	Quinoneimine, thionine and phenoxazinium derivatives	Michael-type addition, quinoid structures	A_N^2
1-24	Hydrazine derivatives	Nucleophilic addition reaction with cycloisomerization	A_N^2
1-24	DNA intercalators with carboxamide and aminoalkylamine side chain	DNA intercalation	Non-covalent interaction
1-3, 10,11	Quinoneimine, thionine and phenoxazinium derivatives	DNA intercalation	Non-covalent interaction
1-3, 10,11	Specific imine and thione derivatives	Incorporation into DNA/RNA, due to structural analogy with nucleoside bases	Non specific
1-24	Hydrazine derivatives	Radical mechanism via ROS formation	Radical
1-3, 10,11	Specific imine and thione derivatives	Radical mechanism via ROS formation	Radical
1-3, 10,11	Quinoneimine, thionine and phenoxazinium derivatives	ROS formation after GSH depletion	Radical
1-3, 10,11	Specific imine and thione derivatives	Nucleophilic substitution on diazonium ion	S_N^1
1-24	Hydrazine derivatives	Direct nucleophilic attack on diazonium cation	S_N^2
20-24	Epoxides and aziridines	Alkylation, direct acting epoxides and related	S_N^2

The results of protein binding of the predicted hepatic (liver *in vivo*) metabolites for N-[1-(4-hydroxyphenyl)aminoethilyden]-4-[1-(3,5,5,8,8-pentamethyl-6,7-dihydro naphtalen-2-yl)-ethenyl] phenylcarbohydrazide are presented in Table 4. Nine metabolites are not reactive and fifteen are reactive, i.e. alerts are found by protein binding. Structural alerts (quinone methide(s)/imines; quinoide oxime structure; nitroquinones, naphtaquinone(s)/imines, aldehydes, epoxides, aziridines and sulfuranes) were identified for fifteen metabolites in the mechanistic domains (Michael addition, Nucleophilic addition, Schiff base formation and S_N^2) with mechanistic alerts (Michael addition on quinoid type compounds, Addition to carbon-hetero double bond, Schiff base formation with carbonyl compounds and Ring opening S_N^2 reaction). The possible liver metabolites of N-[1-(4-hydroxyphenyl) aminoethilyden]-4-[1-(3,5,5,8,8-pentamethyl-6,7-dihydronaphtalen-2-yl)-ethenyl]phenylcarbo hydrazide that have been predicted by QSAR Toolbox (*in vitro* rat metabolism simulator) are thirteen. Results of hepatic prediction (*in vitro* rat) of N-[1-(4-hydroxyphenyl)aminoethilyden]-4-[1-

(3,5,5,8,8-pentamethyl-6,7-dihydronaphtalen-2-yl)-ethenyl] phenylcarbohydrazide are presented in Table 5. Results of DNA binding of the predicted hepatic (liver *in vitro*) metabolites for N-[1-(4-hydroxyphenyl)aminoethilyden]-4-[1-(3,5,5,8,8-pentamethyl-6,7-dihydronaphtalen-2-yl)-ethenyl] phenylcarbohydrazide are presented in Table 6.

Thirteen metabolites are reactive, i.e. alerts are found by DNA binding. Structural alerts (quinoneimine, thionine and phenoxazinium derivatives, hydrazine derivatives, DNA intercalators with carboxamide and aminoalkylamine side chain, specific imine and thione derivatives) were identified for thirteen metabolites in the mechanistic domains (radical mechanism, A_N^2, non-covalent interaction, S_N^2, nonspecific, S_N^1) with mechanistic alerts (Michael-type addition, quinoid structures, nucleophilic addition reaction with cycloisomerization, DNA intercalation, incorporation into DNA/RNA, due to structural analogy with nucleoside bases, radical mechanism via ROS formation, ROS formation after GSH depletion, nucleophilic substitution on diazonium ion and direct nucleophilic attack on diazonium cation).

Prediction results of protein binding of the predicted hepatic (liver *in vitro*) metabolites for N-[1-(4-hydroxyphenyl)aminoethilyden]-4-[1-(3,5,5,8,8-pentamethyl-6,7-dihydronaphtalen-2-yl)-ethenyl]phenylcarbohydrazide are presented in Table 7.

Seven metabolites are not reactive and six are reactive, i.e. alerts are found by protein binding. Structural alerts (quinone methide(s)/imines; quinoide oxime structure; nitroquinones,

naphtaquinone(s)/imines, ketones and aldehydes) were identified for six metabolites in the mechanistic domains (Michael addition, Schiff base formation and nucleophilic addition) with mechanistic alerts (Michael addition on quinoid type compounds, addition to carbon-hetero double bond and Schiff base formation with carbonyl compounds).

Table 4. Protein binding of hepatic metabolites for N-[1-(4-hydroxyphenyl) aminoethilyden]-4-[1-(3,5,5,8,8-pentamethyl-6,7-dihydronaphtalen-2-yl)-ethenyl] phenylcarbohydrazide by QSAR Toolbox (liver *in vivo* metabolism simulator)

Number of metabolite	Protein binding by OASIS (Mechanism of reaction)		
	Structural alert	Mechanistic alert	Mechanistic domain
5,7-9,13,14,16,17,19	No alert found	-	-
1-3,10,11	Quinone methide(s)/imines; Quinoide oxime structure; Nitroquinones, Naphtaquinone(s)/imines	Michael Addition on quinoid type compounds	Michael addition
4,6,12,15	Ketones	Addition to carbon-hetero double bond	Nucleophilic addition
18	Aldehydes	Schiff base formation with carbonyl compounds	Schiff base formation
20-24	Epoxides, Aziridines and Sulfuranes	Ring opening S_N^2 reaction	S_N^2

Table 5. Number and structure of the predicted hepatic metabolites (*in vitro*) of N-[1-(4-hydroxyphenyl)aminoethilyden]-4-[1-(3,5,5,8,8-pentamethyl-6,7-dihydronaphtalen-2-yl)-ethenyl]phenylcarbohydrazide by QSAR Toolbox.

Table 6. DNA binding of the hepatic metabolites for N-[1-(4-hydroxyphenyl) aminoethilyden]-4-[1-(3,5,5,8,8-pentamethyl-6,7-dihydronaphtalen-2-yl)-ethenyl] phenylcarbohydrazide by QSAR Toolbox (liver *in vitro* metabolism simulator)

Number of metabolite	DNA binding by OASIS (Mechanism of reaction)		
	Structural alert	Mechanistic alert	Mechanistic domain
2-4	Quinoneimine, thionine and phenoxazinium derivatives	Michael-type addition, quinoid structures	A_N2
1-13	Hydrazine derivatives	Nucleophilic addition reaction with cycloisomerization	A_N2
1-13	DNA intercalators with carboxamide and aminoalkylamine side chain	DNA intercalation	Non-covalent interaction
2-4	Quinoneimine, thionine and phenoxazinium derivatives	DNA intercalation	Non-covalent interaction
2-4		Incorporation into DNA/RNA, due to structural analogy with nucleoside bases	Non specific
2-4	Specific imine and thione derivatives	Incorporation into DNA/RNA, due to structural analogy with nucleoside bases	Non specific
1-13	Hydrazine derivatives	Radical mechanism *via* ROS formation	Radical
2-4	Specific imine and thione derivatives	Radical mechanism *via* ROS formation	Radical
2-4	Quinoneimine, thionine and phenoxazinium derivatives	ROS formation after GSH depletion	Radical
2-4	Specific imine and thione derivatives	Nucleophilic substitution on diazonium ion	S_N1
1-13	Hydrazine derivatives	Direct nucleophilic attack on diazonium cation	S_N2

Table 7. Protein binding of hepatic metabolites for N-[1-(4-hydroxyphenyl) aminoethilyden]-4-[1-(3,5,5,8,8-pentamethyl-6,7-dihydronaphtalen-2-yl)-ethenyl] phenylcarbohydrazide by QSAR Toolbox (liver *in vitro* metabolism simulator)

Number of metabolite	Protein binding by OASIS (Mechanism of reaction)		
	Structural alert	Mechanistic alert	Mechanistic domain
1,6,7,9,11-13	No alert found		
2-4	Quinone methide(s)/imines; Quinoide oxime structure; Nitroquinones, Naphtaquinone(s)/imines	Michael Addition on quinoid type compounds	Michael addition
5,8	Ketones	Addition to carbon-hetero double bond	Nucleophilic addition
10	Aldehydes	Schiff base formation with carbonyl compounds	Schiff base formation

CONCLUSIONS

The parent (basic) structure of the newly synthesized derivative of bexarotene and paracetamol after application of *in silico* methods (QSAR Toolbox software for metabolic activation in the liver of rats (*in vivo* and *in vitro*) to the OECD) was found to generate hepatic metabolites that exhibit different reactivity.

The metabolites were mainly formed through different types of mechanism – Michael type addition, nucleophilic addition, non-covalent interaction, radical mechanism and both types of nucleophilic substitution.

A total of twenty-four metabolites were predicted as positive.

The twenty-four predicted metabolites belong to diverse chemical classes, including quinoneimine, thionine, phenoxazinium derivatives, hydrazine

derivatives, DNA intercalators with carboxamide and aminoalkylamine side chain, specific imine and thione derivatives, epoxides and aziridines.

The probable active metabolites (hepatic) may be cytotoxic and enhance the potential antitumor effect of the newly synthesized compound.

It was also predicted that the parent structure of the newly synthesized derivative may be a substrate for different CYP450 enzymes.

REFERENCES

1. N. Agova, PhD thesis, 2019, https://repository.mu-varna.bg/dspviewerb/srv/viewer/eng/28f22724-afc2-4577-a401-0422e9d35477?tk=KPInJK_CRXekAQQi6dNUdwAAAABhjltI.o2fw9FwP7zMRlwvCVKve-w&dspcontext=&sequence=8&handle=nls/516

2. Targetrin - brief description of the product - https://www.ema.europa.eu/en/documents/product-information/targretin-epar-product-information_en.pdf

3. S. Rollas, Ş. Güniz Küçükgüzel, *Molecules*, **12,** 1910 (2007).

4. L. F. Prescott, *American Journal of Therapeutics*, **7(2),** 143 (2000).

5. U.B. Ghaffar, N. A. Tadvi, *J. Cont. Med. A,* **2 (3)** 12 **(**2014).

6. U. M. Zanger, M. Schwab, *Pharmacol. Ther.,* **138,** 103 (2013).

7. E. P. A. Neve, M. Ingelman-Sundberg, *Curr. Opin. Drug Discov. Devel*., **13,** 78 (2010).

8. QSAR Toolbox - https://qsartoolbox.org/about/

9. N. Agova, S. Georgieva, St. Stoeva, S. Stamova, J. Mitkov, *Bulg. Chem. Commun.*, **52 (A),** 9, (2020).

10. ChemIDplus Advanced; https://chem.nlm.nih.gov/chemidplus/.

11. The OECD QSAR Toolbox: https://www.oecd.org/chemicalsafety/risk-assessment/oecd-qsar-toolbox.htm.

Influence of skin metabolites of the newly synthesized derivative of bexarotene and paracetamol on the potential antitumor effect

I. R. Iliev[2*], Y. K. Koleva[1], S. F. Georgieva[2]

[1]*University "Prof. Assen Zlatarov", Faculty of Natural Science, Department of Chemistry, Burgas, Bulgaria*
[2]*Medical university "Prof. Paraskev Stoyanov", Faculty of Pharmacy, Department of Pharmaceutical Chemistry, Varna, Bulgaria*

The present work is structured to predict probable skin metabolites, their DNA and protein binding of the newly synthesized compound of bexarotene and paracetamol. Predicted skin metabolites of the newly synthesized derivative of bexarotene and paracetamol are three in the following mechanistic domains - A_N^2, non-covalent interaction, non-specific, radical mechanism, S_N^1 and S_N^2 by DNA binding and two reactive metabolites in the mechanistic domain (Michael addition) by protein binding. Metabolites containing structural alerts with a potential toxic effect may complement the possible antitumor effect.

Keywords: bexarotene derivative, predict, metabolic activation, skin, QSAR Toolbox

INTRODUCTION

A leading goal in medical and pharmaceutical practice around the world is the search for new drugs and approaches in the treatment of oncological and infectious diseases.

In this regard retinoic acids play an important role in cell physiology. They are essential for embryonic development, regulating organogenesis, organ homeostasis and cell growth [1]. These compounds bind to and activate one or more nuclear retinoid receptors to modulate gene expression. There are two known classes of retinoid receptors, retinoic acid receptors (RARs) and retinoid X receptors (RXRs) [2].

In keeping with their ability to induce cell growth, differentiation and apoptosis, retinoic acids have been studied and used as anti-tumor or tumor preventive agents. Several retinoid acids are currently approved by the US Food and Drug Administration (FDA) for the treatment of certain malignancies, or are in clinical trials to assess their activities in various tumors [3, 4].

Bexarotene is a third generation retinoid. It is referred to as a rexinoid as it is the first KR-selective retinoid agonist to be studied in humans. It has been approved in the USA for the treatment of cutaneous T-cell lymphoma (CTCL) in patients who are refractory to at least one prior systemic therapy. There are also some data showing the potential use of bexarotene in combination with other currently available treatment modalities for CTCL. Finally, bexarotene has been assessed for potential use in solid tumors [2].

The use of some retinoids has been associated with photosensitivity. Patients should be advised to minimize exposure to sunlight and to avoid the use of tanning beds during treatment with bexarotene, as *in vitro* data suggest that bexarotene may have a potential photosensitizing effect [5].

The most common toxicity was dose-dependent skin toxicity, with the majority being mild skin dryness. Rarely skin dryness and peeling is dose limiting at 650 mg/m²/day. Some patients report of cracking of the lips [2].

Hydrazones represent an important class of compounds for the development of new drugs. Therefore, many researchers synthesize these compounds as target structures and evaluate their biological activity. They have been demonstrated to possess, among other, antimicrobial, anticonvulsant, analgesic, antiinflammatory, antiplatelet, antitubercular and antitumoral activities, but from all significant effects the leading one is the antitumoral [6-9].

Hybrid molecules are defined as chemical entities with two or more structural domains having different biological functions and dual activity, indicating that a hybrid molecule acts as two distinct pharmacophores. Hybrid molecules can modify pharmacological effects of the parent structures. The advantages of these molecules are better bioavailability at the target site, better effect with minimal therapeutic doses, lower toxicity and cheap preclinical evaluation.

Paracetamol (acetaminophen) has become one of the most popular 'over-the-counter' non-narcotic analgesic. It is an effective mild analgesic, suitable

---

* To whom all correspondence should be sent:
E-mail: *i_iliev@abv.bg*

for treating mild to moderate pain although it does not appear to possess significant anti-inflammatory activity. Paracetamol's most troublesome side effect (methaemoglobinaemia) is due to another metabolite p-phenetidine. The mechanism of action of paracetamol is poorly defined, although it has been speculated that it may selectively inhibit prostaglandin production in the central nervous system, which would account for its analgesic/antipyretic properties. The lack of any significant influence on peripheral cyclooxygenase would explain the absence of anti-inflammatory activity [10].

There are no literature data of paracetamol being used as a topical treatment for any skin disease. There are no topical dosage forms.

The skin, like other organs in the human body, contains numerous enzymes that are capable of metabolizing endogenous substances and xenobiotics. In the past, the skin has been considered only as a physical barrier. Nowadays, it is well known that the skin also has the potential to metabolize substances with a different nature. Although the topical administration of drugs offers several advantages compared to traditional routes it is necessary to be well aware of the possibility of metabolism in the skin. The study of skin metabolism is of major importance not only in the field of transdermal drug delivery systems but also for the safe and efficient local skin treatment with topically applied substances [11].

Skin metabolism, in turn, can affect a number of processes, including skin toxicity, absorption, maintenance of homeostasis, delivery of dermal dosage forms, and efficacy. Due to the potentially wide-ranging effects that skin metabolism may affect, interest in it is increasing. This has led to the development of *in vitro* methods for predicting the potential of various substances to produce skin metabolites [11].

Recently, the possibility of the metabolism of medicinal products in the skin has been the subject of numerous studies. The barrier functions, absorption, and distribution of chemicals into and through the skin have been studied long ago. Now it is known that skin metabolism plays a key role in toxicity processes [11].

To evaluate the risk of drug use, many factors have to be considered. Of these, the absorption and permeability of the skin to different molecules, as well as the possibility of metabolic changes, are of particular importance. The risk of dermal metabolite production should be thoroughly monitored in order to assess the safety and minimize the potential for toxic reactions [11].

The Organization for Economic Co-operation and Development (OECD) (Q)SAR Application Toolbox makes it possible to predict metabolic changes and assess the risk based on the chemical structure of the compounds. In many cases, the parent chemical is not responsible for the development of an adverse reaction or toxicity. They are the result of their transformation and activation (metabolic or chemical). When a chemical changes as a result of metabolism, it may form biologically active metabolites. Experimentally identifying metabolism opportunities is difficult, expensive, and often incomplete. Therefore, the use of mathematical models to predict metabolism opportunities is increasing [12].

The present work is structured to predict probable skin metabolites, their DNA and protein binding of the newly synthesized compound of bexarotene and paracetamol.
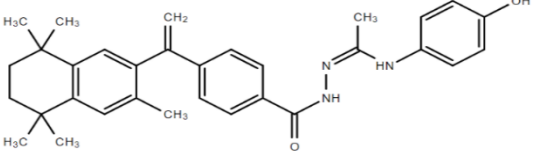
MATERIAL AND METHODS

The newly synthesized hydrazone derivative was obtained according to the basic scheme of synthesis of bexarotene analogs and its structure was confirmed by its spectral data [13,15].

For the purpose of this study we synthesized a new hydrazone derivative of the retinoid bexarotene. The process contains 3 major steps – esterification of the carboxylic group, hydrazinolysis and substitution of ketone to the newly formed hydrazone group. The result of the synthesis depends on the aldehyde or ketone used. For the purpose of this study we used paracetamol forming the new derivative of bexarotene shown in Table 1 [13].

Currently there's no literature data on the mechanism of action of the newly synthesized derivative. The compound (a newly synthesized bexarotene derivative (N-[1-(4-hydroxyphenyl) aminoethilyden]-4-[1-(3,5,5,8,8-pentamethyl-6,7-dihydronaphtalen-2-yl)-ethenyl]phenylcarbo hydrazide)) is presented in Table 1 [13, 14].

Table 1. Name and structural formula of the newly synthesized derivative.

Name of compound	Structural formula
(N-[1-(4-hydroxyphenyl) aminoethilyden]-4-[1-(3,5,5,8,8-pentamethyl-6,7-dihydronaphtalen-2-yl)- ethenyl]phenylcarbohydrazide))	

Organisation for Economic Co-operation and Development (*OECD*) (*Q)SAR Toolbox (version 4.3)*. (Quantitative) structure-activity relationships [(Q)SARs] are methods for estimating properties of a chemical from its molecular structure and have the potential to provide information on the hazards of chemicals, while reducing time, monetary costs and animal testing currently needed. To facilitate practical application of (Q)SAR approaches in regulatory contexts by governments and industry and to improve their regulatory acceptance, the OECD (Q)SAR project has developed various outcomes such as the principles for the validation of (Q)SAR models, guidance documents as well as the QSAR Toolbox [10].

Several profilers were used to predict hepatic and skin metabolic activation (observed and simulator) of the newly synthesized compound as well as DNA and protein binding:

Skin metabolism simulator. Skin metabolism simulator mimics the metabolism of chemicals in the skin compartment. Given the lack of reported skin metabolism data and the widespread hypotheses is that skin enzymes can metabolize absorbed xenobiotics *via* reactions analogous to those determined in liver, the simulator was developed as a simplified mammalian liver metabolism simulator. The skin metabolism simulator contains a list of hierarchically ordered principal transformations, which can be divided into two main types – rate-determining and non-rate-determining [10].

DNA binding by OASIS. The profiler is based on Ames Mutagenicity model part of OASIS TIMES system. The profiler consists of 85 structural alerts responsible for interaction with DNA analyzed in Ames Mutagenicity model. The scope of the profiler is to investigate presence of alerts within target molecules which may interact with DNA [10].

Protein binding by OASIS. The scope of the profiler is to investigate presence of alerts within target molecules responsible for interaction with proteins. The list of 112 structural alerts has been separated into 11 mechanistic domains. Each of the mechanistic domains has been separated into more than 2 mechanistic alerts. The profiling result outcome assigns a target to the corresponding structural alert, mechanistic alerts and domain [10].

RESULTS AND DISCUSSION

QSAR Toolbox software (version 4.3) has been used for predicting possible metabolites of (N-[1-(4-hydroxyphenyl)aminoethilyden]-4-[1-(3,5,5,8,8-pentamethyl-6,7-dihydronaphtalen-2-yl)-ethenyl] phenylcarbohydrazide)) in the skin and its DNA and protein binding. The parent structure of (N-[1-(4-hydroxyphenyl)aminoethilyden]-4-[1-(3,5,5,8,8-pentamethyl-6,7-dihydronaphtalen-2-yl)-ethenyl] phenylcarbohydrazide)) can bind to DNA with mechanism of actions (A_N^2 (Nucleophilic addition reaction with cycloisomerization (hydrazine derivatives)), Non-covalent interactions (DNA intercalation(DNA intercalators with carboxamide and aminoalkylamine side chain)), radical mechanism *via* ROS formation (hydrazine derivatives) and S_N^2(direct nucleophilic attack on diazonium cation (hydrazine derivatives))) and cannot bind to protein. After metabolic activation of the newly synthesized compound of bexarotene in the skin (skin metabolism simulator), three metabolites were predicted. Results of skin prediction of (N-[1-(4-hydroxyphenyl) amino-ethilyden]-4-[1-(3,5,5,8,8-pentamethyl-6,7-dihydro naphtalen-2-yl)-ethenyl]phenylcarbo hydrazide)) are presented in Table 2.

As shown on Table 2 the hydrazone functional group doesn't make the molecule act as a prodrug. According to the QSAR the possible metabolic pathways are oxidation of different functional groups. The possible DNA binding by OASIS (mechanism of reaction) of the skin metabolites for (N-[1-(4-hydroxyphenyl)aminoethilyden]-4-[1-(3,5,5,8,8-pentamethyl-6,7-dihydronaphtalen-2-yl)-ethenyl]phenylcarbohydrazide)) are predicted by QSAR Toolbox software. Results of DNA binding of the predicted skin metabolites for (N-[1-(4-hydroxyphenyl)aminoethilyden]-4-[1-(3,5,5,8,8-pentamethyl-6,7-dihydronaphtalen-2-yl)-ethenyl]phenylcarbohydrazide)) are presented in Table 3.

Table 2. Number and structure of the predicted skin metabolites of (N-[1-(4-hydroxy phenyl)aminoethilyden]-4-[1-(3,5,5,8,8-pentamethyl-6,7-dihydronaphtalen-2-yl)-ethenyl]phenylcarbohydrazide)) by QSAR Toolbox.
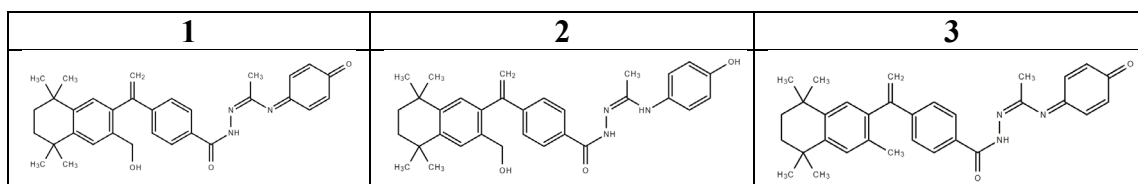
1	2	3

Table 3. DNA binding of skin metabolites for (N-[1-(4-hydroxyphenyl)aminoethilyden]-4-[1-(3,5,5,8,8-pentamethyl-6,7-dihydronaphtalen-2-yl)-ethenyl]phenylcarbo hydrazide)) by QSAR Toolbox.

Number of metabolite	DNA binding by OASIS (Mechanism of reaction)		
	Structural alert	Mechanistic alert	Mechanistic domain
1,3	Quinoneimine, Thionine and Phenoxazinium derivatives	Michael-type addition, quinoid structures	A_N^2
1-3	Hydrazine derivatives	Nucleophilic addition reaction with cycloisomerization	A_N^2
1-3	DNA intercalators with Carboxamide and Aminoalkylamine side chain	DNA intercalation	Non-covalent interaction
1,3	Quinoneimine, Thionine and Phenoxazinium derivatives	DNA intercalation	Non-covalent interaction
1,3	-	Incorporation into DNA/RNA, due to structural analogy with nucleoside bases	Non-specific
1,3	Specific imine and thione derivatives	Incorporation into DNA/RNA, due to structural analogy with nucleoside bases	Non-specific
1-3	Specific imine and thione derivatives	Nucleophilic substitution on diazonium ion	S_N^2
1-3	Hydrazine derivatives	Radical mehanism via ROS formation (indirect)	Radical
1-3	Specific imine and thione derivatives	Radical mehanism via ROS formation (indirect)	Radical

Table 4. Protein binding of skin metabolites for (N-[1-(4-hydroxyphenyl)amino ethilyden]-4-[1-(3,5,5,8,8-pentamethyl-6,7-dihydronaphtalen-2-yl)-ethenyl]phenylcarbo hydrazide)) by QSAR Toolbox (skin metabolism simulator).

Number of metabolite	Protein binding by OASIS (Mechanism of reaction)		
	Structural alert	Mechanistic alert	Mechanistic domain
2	No alert found	-	-
1,3	Quinone methide(s)/imines; Quinoide oxime structure; Nitroquinones, Naphtaquinone(s)/imines	Michael addition on quinoid type compounds	Michael addition

Three metabolites are reactive, i.e. alerts are found by DNA binding. Structural alerts (quinoneimine, thionine and phenoxazinium derivatives, hydrazine derivatives, DNA intercalators with carboxamide and aminoalkylamine side chain, specific imine and thione derivativess) were identified for three metabolites in the mechanistic domains (radical mechanism, A_N^2, non-covalent interaction and S_N^2, non-specific) with mechanistic alerts (Michael-type addition, quinoid structures, nucleophilic addition reaction with cycloisomerization, DNA intercalation, incorporation into DNA/RNA, due to structural analogy with nucleoside bases, radical mechanism *via* ROS formation).

The results of protein binding of the predicted skin metabolites for (N-[1-(4-hydroxyphenyl) aminoethilyden]-4-[1-(3,5,5,8,8-pentamethyl-6,7-dihydronaphtalen-2-yl)-ethenyl]phenylcarbo hydrazide)) are presented in Table 4.

One metabolite is not reactive and two are reactive, i.e. alerts are found by protein binding. Structural alert (Quinone methide(s)/imines; Quinoide oxime structure; Nitroquinones, Naphtaquinone(s)/imines) was identified for two metabolites in the mechanistic domains (Michael addition) with mechanistic alerts (Michael Addition on quinoid type compounds).

The QSAR method is not yet validated with other softwares or through biological testing and the generated skin metabolites for the newly synthesized derivative have not yet been synthesized.

CONCLUSIONS

The parent (basic) structure of the newly synthesized derivative of bexarotene and paracetamol after application of *in silico* methods (QSAR Toolbox software for metabolic activation in the skin to the OECD) has been found to generate skin metabolites that exhibit different reactivity.

The possible adverse effects of skin active metabolites of the bexarotene derivative are with different mechanisms of action by protein and DNA binding.

The metabolites were mainly formed through different types of mechanisms – Michael type addition, nucleophilic addition, non-covalent interaction, radical mechanism and nucleophilic substitution.

A total of three metabolites were predicted as positive.

The three predicted metabolites belong to divers chemical classes, including quinoneimine, thionine, phenoxazinium derivatives, hydrazine derivatives, DNA intercalators with carboxamide and aminoalkylamine side chain, specific imine and thione derivatives, quinone methide(s)/imines, quinoide oxime structure, nitroquinones and naphtaquinone(s)/imines.

The probable active metabolites (dermal) may be cytotoxic and to enhance the potential antitumor effect of the newly synthesized compound.

REFERENCES

1. K. Niederreither, V. Subbarayan, P Dolle, P. Chambon, *Nature Genet*., 444 (1999).
2. L. T. Farol, K. B. Hymes, *Future Drug Ltd. Exper. Rev. Anticancer Ther.*, **4(2),** 180 (2004).
3. P. Fenaux, C. Chomienne, L Degos, *Semin. Hematol.*, **38,** 13 (2001).
4. K. Mann, Sh. W. Miller, *Curr. Oncol.*, **Rep. 3,** (2001).
5. https://www.ema.europa.eu/en/documents/product-information/targretin-epar-product-information_en.pdf
6. S. Rollas, Ş. G. Küçükgüzel, *Molecules*, **12,** 1910 (2007).
7. N. Agova, I. Iliev, S. Stamova, S. Georgieva, *Management and Education*, **137** (2021).
8. G. Verma, Akranth Marella, Mohammad Shaquiquzzaman, Mymoona Akhtar, Mohammad Rahmat Ali, Mohammad Mumtaz Alam, *J. Pharm. Bioallied Sci.*, **6(2),** 69 (2014).
9. M. Asif, *International Journal of Advanced Chemistry*, **2 (2),** 85 (2014).
10. S. P. Clissold, *ADIS Drug Information Services*, Auckland, Drug **32 (Suppl. 4),** 46 (1986).
11. N. Agova, S. Georgieva, S. Stamova, Y. Koleva, *Scripta Scientifica Pharmaceutica*, *Medical University of Varna,* **7(1),** 32 (2020),
12. The OECD QSAR Toolbox: https://www.oecd.org/ chemicalsafety/risk-assessment/oecd-qsar-toolbox.htm.
13. N. Agova, S. Georgieva, St. Stoeva, S. Stamova, J. Mitkov, *Bulgarian Chemical Communications*, **52 (A), 9**, (2020).
14. ChemIDplus Advanced, https://chem.nlm.nih.gov/ chemidplus/.
15. The OECD QSAR Toolbox: https://www.oecd.org/ chemicalsafety/risk-assessment/oecd-qsar-toolbox.htm.

Hybrid supercapacitors with innovative binder - *ex-situ* structural and morphological studies

B. A. Karamanova[1*], P. S. Ublekov[2], L. S. Soserov[1], Ch. P. Novakov[2], I. V. Dimitrov[2], A. E. Stoyanova[1]

[1]*Institute of Electrochemistry and Energy Systems, Bulgarian Academy of Sciences, Acad. G. Bonchev Str, 10, 1113 Sofia, Bulgaria*
[2]*Institute of Polymers, Bulgarian Academy of Sciences, Acad. G. Bonchev Str, 103, 1113 Sofia, Bulgaria*

In this study are presented the results from *ex-situ* physicochemical analyses of electrodes with synthesized poly(vinylidene fluoride-co-hexafluoropropylene) (P(VDF-co-HFP) used as binder in the active electrode mass of hybrid supercapacitors. The cells based on biogenic activated carbon, $\alpha\beta$-Ni(OH)$_2$ composite electrode, ionic liquid (1-ethyl-3-methylimidazolium tetrafluoroborate) as electrolyte and P(VDF-co-HFP) exhibit improved capacitive characteristics. The crystal structure of the electrodes is studied using X-ray diffraction analysis. The profiles of pristine Ni(OH)$_2$ electrode before and after the electrochemical tests are similar, however, decreases in peak intensity were observed in (001) and (110) directions. In contrast, the peak intensity of (100) and (101) increased, suggesting the formation of more perfect crystals. The electrode morphology is visualized by optical microscope and AFM techniques.

Keywords: hybrid supercapacitor, polymer binder, ionic liquid, electrochemical tests, *ex-situ* study

INTRODUCTION

The supercapacitors are a relatively new generation of energy-storage devices. The function of supercapacitors (SCs) is based on the reversible adsorption of electrolyte ions into electrode materials. The interaction involving the electrode and electrolyte acts as an essential function in their overall performance. Therefore, the appropriate selection of electrode materials and electrolyte determines the SC performance.

Ionic liquids (ILs) show an enormous potential in electrochemistry due to the mobility and flexibility of ions [1]. ILs are good candidates for supercapacitors, particularly those working based on the double layer charging [2, 3]. The primary task of the electrolyte is to provide charge species at the electrode/electrolyte interface instead of diffusion of specific electroactive species. The specific energy strongly depends on the potential window, which in turn depends on the electrolyte used [4, 5]. For aqueous electrolytes-based SCs the electrochemical stability potential region is about 1.0–1.2 V, while the organic electrolytes and ionic liquids (ILs)-based SCs have the potential windows 2.7–3.0 V and 3.5–4.0 V, respectively [6-10]. Therefore, the wide stable potential window of ILs guarantees high energy densities [11, 12].

Many ILs have lower conductivity, higher viscosity and therefore a narrower operating limit at lower temperatures than aqueous and non-aqueous electrolytes. However, compared to volatile aqueous and organic electrolytes, they are much safer in SC applications, especially in the case of high current densities [13, 14]. All components of this system - electrode materials and electrolyte, as well as electrolyte additives are crucial for the development of a supercapacitor with high energy and power characteristics, as well as high Faraday efficiency [15].

In spite of the potential of ILs and the growing interest in their application in these systems, there is still only a limited number of fundamental studies (mostly theoretical) focused on the electrode / electrolyte interface of supercapacitors in IL [16-19]. It is good to keep in mind that the complexity of ILs is due to the novelty of these media compared to conventional electrolytes.

In recent years, the P(VDF-co-HFP) fluorocopolymers are attracting more attention and depending on the HFP content they can act as thermoplastics, elastomers or thermoplastic elastomers [20]. P(VDF-co-HFP) copolymers exhibit high thermostability, high hydrophobicity and enhanced mechanical properties. These copolymers have already been involved in numerous applications, and more recently for various uses in the field of energy (polymer electrolyte membranes for fuel cells, Li-ion batteries, solar cells, etc.) [21].

* To whom all correspondence should be sent:
E-mail: boriana.karamanova@iees.bas.bg

The aim of the present work is to develop a hybrid supercapacitor with improved characteristics by introducing an effective polymer binder poly(vinylidene fluoride-co-hexafluoropropylene) (P(VDF-co-HFP)) in the mass of the active electrode, to perform impact conducting electrochemical tests and *ex-situ* physicochemical analyses of the electrodes.

EXPERIMENTAL

Reagents and Materials

The reagents used in the copolymerization procedure were purchased from Sigma-Aldrich. Vinylidene fluoride (VDF, $\geq$ 99%) and hexafluoropropylene (HFP, $\geq$ 99%) were used as received. Ammonium persulfate (($NH_4)_2S_2O_8$), reagent grade, 98%) was recrystallized from distilled water prior to use. Ionic liquid (1-ethyl-3-methylimidazolium tetrafluoroborate (EMIMBF$_4$), Alfa Aesar, 98%) with acetonitrile (AN, Alfa Aesar, 99,7%) and polypropylene (PC, Alfa Aesar, 99%) additives in different concentrations was used as an electrolyte.

The active components in the electrode active mass are commercial activated carbon (YP-50F, Kurary Europe GmbH) and interstratified $\alpha\beta_{IS}$-Ni(OH)$_2$, prepared by precipitation from 0.5 M NiSO$_4$ solution with KOH at pH = 12 and temperature 70-80 °C [22].

Synthesis of poly(vinylidene fluoride-co-hexafluoropropylene) (P(VDF-co-HFP))

The copolymer synthesis was performed according to a previously described procedure [23]. Briefly, a 0.16 M aqueous solution of the radical initiator ammonium persulfate was introduced into an autoclave, degassed and purged with 2 MPa of nitrogen pressure. In the next step predetermined amounts of VDF (0.156 mol) and HFP (0.034 mol) at ratio 82/18 mol% were added and the copolymerization was carried out at 85°C for 7 h under pressure. Upon polymerization completion the autoclave was cooled down to room temperature and the emulsion was degassed in order to remove any residual unreacted VDF and/or HFP. The reaction mixture was frozen using liquid nitrogen and the copolymer was recovered through lyophilization.

Preparation of supercapacitor cells

The composite electrodes are made of activated carbon (AC) matrix with addition of $\alpha\beta_{IS}$-Ni(OH)$_2$ in content of 25%. The other electrode consists of only AC. The mass ratio between the two electrodes is 1:1, the mass loading is about 0.018 – 0.020 g. Graphite ABG 1005 EG1 (10 wt.%) and binder (10 wt. %) are added previously to the activated carbon using standardized procedure. The formed sheet electrodes are dried at 140ºC for 12 h, pressed under 20 MPa and mounted in coin-type cell with Glassmat separator.

Physicochemical and electrochemical characterization

The capacitor cells were subjected to galvanostatic charge/discharge using Arbin Instrument System BU-2000 electrochemical equipment. The test program was carried out at constant current mode at different current loads and room temperature. Some cells were subjected to continuous cycling charge/discharge at a current rate of 240 mAg^{-1} up to 5000 cycles.

The specific discharge capacitance (F g^{-1}) was calculated by the equation [24]:

$$C = (I \times \Delta t)/(m \times \Delta V) \tag{1},$$

where I, Δt, m and ΔV are discharge current, discharge time, mass of active material and voltage window, respectively. On the basis of the specific discharge capacitance, the energy density (E) can be expressed as [25]:

$$E = C \Delta V^2 /7.2 \tag{2}$$

The surface and morphology changes in the electrodes during supercapacitor testing were analyzed by means of *ex-situ* XRD and optical microscopy techniques. The crystal structure of the samples was studied using X-ray diffraction (XRD) analysis using the Bruker D8 Advance ECO diffractometer in reflection mode with Ni-filtered Cu Kα radiation over the 2θ range of 5-60°.

Size exclusion chromatography (SEC) was conducted on a combined SEC/multi-angle laser light scattering (MALLS) system consisting of Alliance e2695 HPLC separations module (Waters Corp.), 2998 PDA (Waters Corp.), DAWN Heleos II MALLS and OptilabT-rEX DRI (Wyatt Tech.) detectors. Chromatographic separation was achieved by a set of three Novema GPC columns (PSS Polymer Standards Service GmbH) with NH-functionalized acrylate copolymer network with a nominal pore size of 30, 1000 and 1000 Å. Analyses were performed in 0.2 mol formic acid aqueous solution containing 100 mmol of NaCl as eluent at 40ºC and flow rate of 1 mL.min^{-1}.

The morphology of the electrode surface was visualized with a Stemi 305 optical microscope.

The atomic-force microscopy (AFM) observations were performed on three separate areas from each sample. The measurement conditions were as follows: square zones with linear size 49.5

μm, equal to 2.459 nm^2 of surface area for each observation; resolution equal to 256 points per line for 256 lines; acquired imaging rate of 1 second per line, only the reference sample required much lower imaging rate of 10 s/per line; scanning in dynamic regime at 17 kHz of cantilever vibration at amplitude of 600 mV; images in *scan forward* mode per line, and *from down to up* for image recording. The AFM observations were conducted by AFM EasyScan 2 produced by Nanosurf (Switzerland), equipped by TAP190Al-G.

The contact angle measurements were performed on an Easy Drop DSA20E KRÜSS GmbH apparatus, Germany. Drops from the electrolyte with a volume of 6.3 μl were deposited on the electrode surface and the mean contact angle value was obtained by averaging at least 5 measurements for each sample.

RESULTS AND DISCUSSION

For the current investigations P(VDF-co-HFP) was synthesized *via* free radical emulsion copolymerization of vinylidene fluoride and hexafluoropropylene initiated by $(NH_4)_2S_2O_8$ [23] (Fig. 1). The molar content of HFP was kept around 18% in order to ensure the thermoplastic properties of the copolymer obtained. There was no need of using emulsifier in the polymerization process since the latex particles were stabilized by the ionic chain ends of the macromolecules exposed on the particles' surfaces. The molar-mass characteristics of the copolymer obtained were determined by size exclusion chromatography (SEC). The SEC-elugram reveals a monomodal molar mass distribution for the copolymer with Mn = 78 400 g/mol (Fig. 2). The copolymer dispersity (Mw/Mn) is 2.86 which is quite good result considering the polymerization technique used for P(VDF-co-HFP) preparation.

The synthesized poly(vinylidene fluoride-co-hexafluoropropylene) P(VDF-co-HFP) was used as a binder in the mass of the active electrode and was compared with traditionally used binders (polytetrafluoroethylene (PTFE) and polyvinylidene fluoride (PVDF)).

Figure 3 compares the galvanostatic charge/discharge curves of the supercapacitor cells with different binders and electrolyte additives.

The results of Figure 3 demonstrate the effect of electrolyte additives on one hand and the kind of binders in active electrode masse on the other on the supercapacitor properties. The comparison reveals that capacitance on the SC in electrolyte contains 22 wt.% AN and P(VDF-co-HFP) show higher values. The voltage profiles are typical for hybrid systems (Fig. 3b), as the calculated values for iR-drop in these SCs do not differ significantly (0.30 V for SC with P(VDF-co-HFP) and 0.46 V - for SC with PTFE).

The results obtained suggest that the binder acts differently on the macro- and micropores of the electrode materials and thus on their adsorption ability.

From Figure 3 can be noticed that AN-additive favors the SC characteristics. The reason for the observed effect may be the increase in the conductivity of the electrolyte. The next factor is the wetting of the electrode determined by the contact angle (listed in Table 1). In general, the electrolyte with additives wet the composite electrode better in comparison with electrolyte without additive. The wettability of electrode with P(VDF-co-HFP) copolymer as innovative binder is better (the contact angle decreases twice). This can be related to the improved performance of these SCs.

Although the contact angle in the electrolyte with PC addition is lower than that in the electrolyte with AN addition (Table 1), this SC shows worse performance. This result shows that the ongoing processes are complex and further electrochemical studies and *ex-situ* physicochemical analyses are needed for their more detailed interpretation.

The results demonstrate that the developed hybrid supercapacitor based on activated carbon and 25 wt.% αβ-Ni (OH)$_2$, polymer binder P(VDF-co-HFP) and 22 wt.% AN in the electrolyte (EMIMBF$_4$) shows highest capacitance and stable behavior. For 5000 charge/discharge cycles, this SC displays only 10% drop in discharge capacitance and over 97% efficiency (Fig. 4).
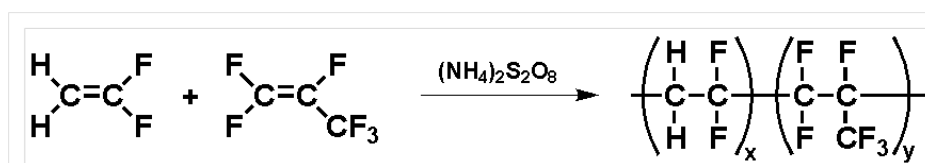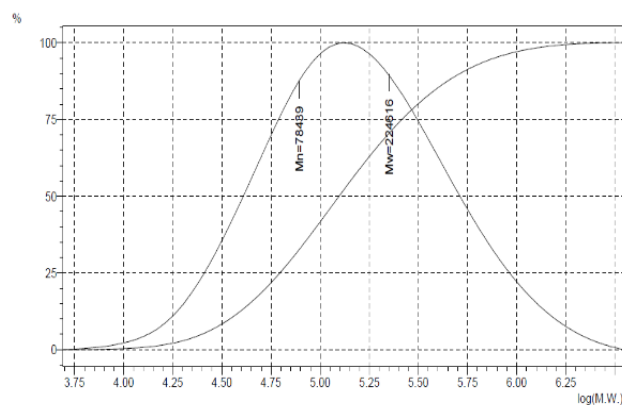

Figure 1. Synthetic route to P(VDF-co-HFP).

Figure 2. Size exclusion chromatogram (SEC) of P(VDF-co-HFP)

Table 1. Contact angles of composite electrode

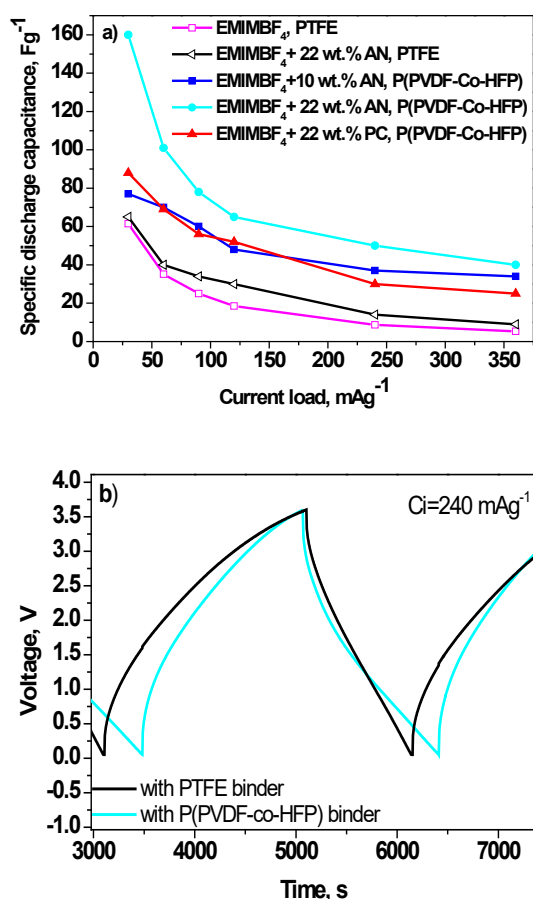| Electrolyte	Contact angle of AC/$\alpha\beta$-Ni(OH)$_2$
EMIMBF$_4$(PTFE)	98.9 ° ± 2.53 °
EMIMBF$_4$+ 22 wt.% AN (PTFE)	61.9 ° ± 4.01 °
EMIMBF$_4$+ 22 wt.% AN (PVDF-co-HFP)	32.8 ° ± 2.10 °
EMIMBF$_4$+ 22 wt.% PC (PVDF-co-HFP)	19.1 ° ± 2.30 °

Figure 3. Discharge capacitance as a function of current load for hybrid supercapacitors (a) and galvanostatic charge/discharge profiles of SCs with different binders (b) with different binders and electrolyte additives.
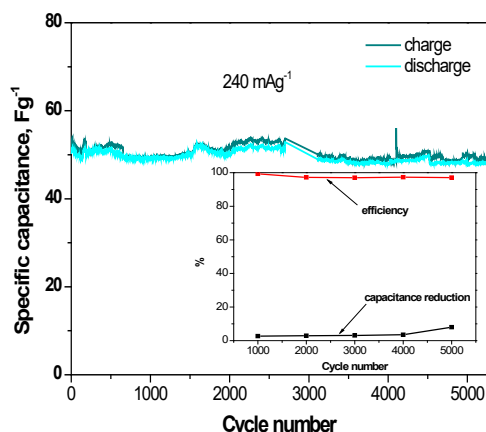
Fig. 4. Specific capacitance as a function of cycle number for SC with EMIMBF$_4$+ 22 wt.% + P(VDF-coHFP) (the inset figure shows the change in discharge capacitance and cycling efficiency during prolonged cycling)

Figure 5 compares the energy density values of supercapacitors with traditional and innovative binder. The data show a higher cell energy density with the PVDF-co-HFP binder. In interpreting the results of the electrochemical tests, it must be borne in mind that the binder has a significant effect on the pores of the activated carbon and hence on the ongoing electrochemical processes. For example, PVDF has been found to affect micro- and macropores, while PTFE predominantly attacks activated carbon macropores [26].

..
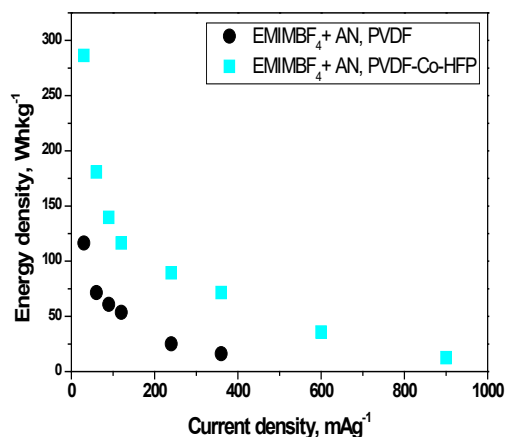
Fig. 5. Energy density as a function of current load for supercapacitors with different binders

Last but not least, the nature of the electrolyte must be taken into account. Detailed *ex-situ* physicochemical studies could serve to better clarify the positive role of the synthesized binder P(VDF-co-HFP) in the developed supercapacitor system and its further successful application in others. For this purpose, both the pristine electrodes (carbon and composite) and those after electrochemical tests were analysed.

Figure 6 compares the XRD patterns of the pristine electrodes and electrodes cycled in ionic liquid electrolyte with different binders. The XRD patterns obtained for the electrodes before and after electrochemical tests are shown in Fig. 6.
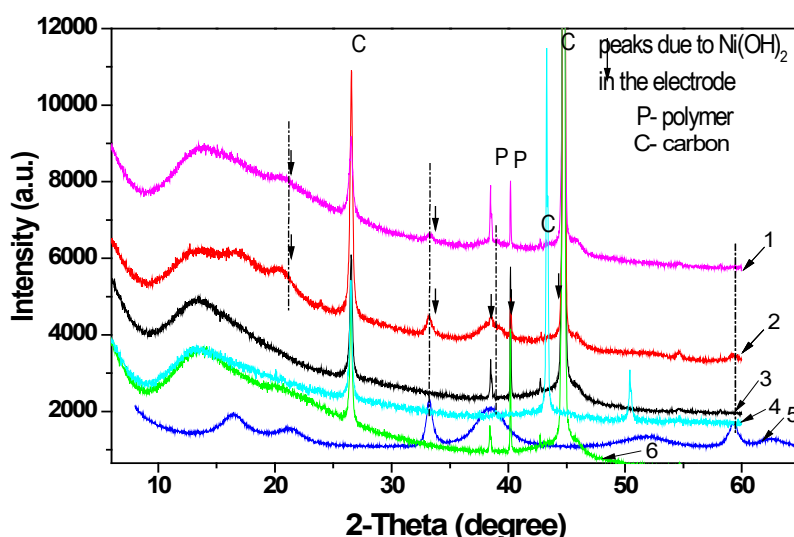
Fig. 6. XRD patterns of: 1) AC_Ni(OH)$_2$/P(VDF-co-HFP)- electrode, after electrochemical test; 2) AC_Ni(OH)$_2$/P(VDF-co-HFP) - pristine electrode; 3) AC/ P(VDF-co-HFP) - pristine electrode; 4) AC/PVDF – pristine electrode; 5) Ni(OH)$_2$; 6) AC/ P(VDF-co-HFP) - electrode, after electrochemical test

The profile of pristine Ni(OH)$_2$ exhibited 5 prominent peaks at $2\theta = 26.6°, 33.2°, 38.4°, 40.1°$ and $44.8°$, corresponding to (001), (110), (100), (101), and (004) reflections of α- and β-Ni(OH)$_2$. The diffraction pattern of Ni(OH)$_2$ after electrochemical testing is similar to that of pristine α-, β-Ni(OH)2. However, decreases in peak intensity were observed in (001) and (110) directions. In contrast, the peak intensity of (100) and (101) increased, suggesting the formation of more perfect crystals of β-Ni(OH)$_2$. The α-Ni(OH)$_2$ polymorph of nickel hydroxide consists of layers of β-Ni(OH)$_2$, oriented parallel to the crystallographic ab-plane, intercalated by water molecules. The intercalated water molecules do not occupy fixed sites, but rather they have some freedom to rotate and translate? within the ab-plane. In addition to the two fundamental phases of nickel hydroxide, there are several possible types of structural disorder, including the incorporation of foreign ions, variable hydration and crystal defects including stacking faults. The effects of the structural disorder can impart very important properties. The XRD results revealed the formation of preferentially disordered β-Ni(OH)$_2$ after electrochemical testing leading to better electrochemical activity [27].

The changes in the morphology of the electrode surface after the electrochemical examination are shown in Fig. 7 (visualized with an optical microscope).
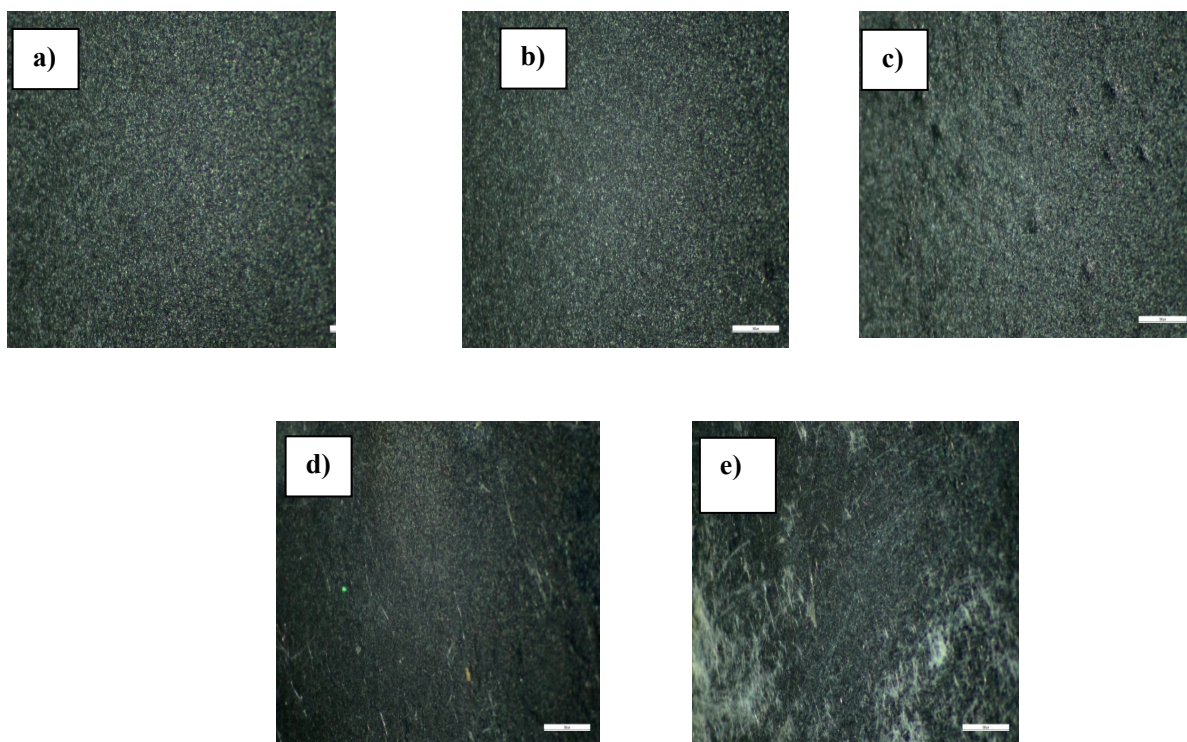

Fig. 7. Optical image of pristine and electrodes after electrochemical tests: a) C/PVDF -pristine, b) C/ P(VDF-co-HFP)- pristine, c) C_Ni(OH)$_2$/ P(VDF-co-HFP) - pristine, d) C/ P(VDF-co-HFP)- after electrochemical test, e) C_Ni(OH)$_2$/ P(VDF-co-HFP)- after electrochemical test.
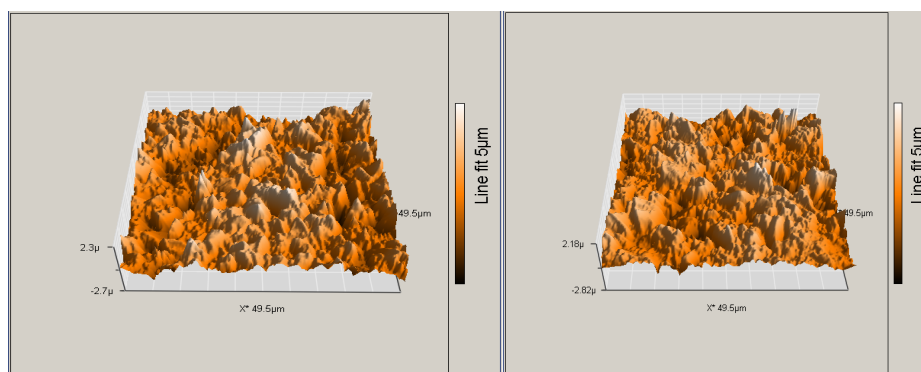

Fig. 8. 3D AFM image of the pristine electrodes: C/PVDF (left) and C/ P(VDF-co-HFP) (right)

The images show that the surface of the P(VDF-co-HFP)-modified carbon electrode is relatively smoothest, especially after electrochemical tests.

To quantify the electrode roughness AFM measurements were performed. Fig. 8 illustrates 3D AFM images of pristine carbon electrodes with classical and innovative co-polymer binders.

The results of the AFM topological observations were quantitatively evaluated. As a measure of the surface roughness are used the average value Sa, expressed by the average sum of the module of distances of all points from the measured surface, in direction, perpendicular to the conditional plane. The comparison of AFM images shows that the roughness of electrode with polymer binder is lower, Sa drops from 503.8 nm for electrode with traditional binder to 439.13 nm for the electrode with P(VDF-co-HFP). Electrode surface smoothing reactions provide more homogeneous contact with the electrolyte, resulting in higher capacitance. *Ex-situ* AFM observations of electrochemically tested carbon electrodes, as well as of composite electrodes in hybrid supercapacitor cells are forthcoming.

CONCLUSION

A new hybrid supercapacitor is demonstrated based on introduction of a synthesized specific functional co-polymer as binder in the active mass in electrode matrix. Its presence favors the wettability of the electrode while smoothing its surface thus ensuring easier penetration of IL into the pores of the carbon material. *Ex-situ* physicochemical analyzes show that the P(VDF-co-HFP) does not undergo a change during the course of electrochemical tests in contrast to the AC/Ni(OH)$_2$ – part of crystals of α-Ni(OH)$_2$ polymorph morphology transforms into disordered β-Ni(OH)$_2$ thus playing a significant role in improving the electrochemical characteristics of the studied systems.

REFERENCES

1. A. Eftekhari, Y. Liu, P. Chen, *J Power Sources,* **334,** 221 (2016).
2. R. Jamil, D. Silvester, *Curr. Opin. Electrochem.,* **35,** 101046 (2022).
3. S. Pan, M. Yao, J. Zhang, B. Li, C. Xing, X. Song, P. Su, H. Zhang, *Front. Chem.***, 8**, 261 (2020).
4. A. Eftekhar, *Energy Storage Mater.*, **9**, 47 (2017).
5. C. Zhong, Y. Deng, W. Hu, J. Qiao, L. Zhangd, J. Zhang, *Chem. Soc. Rev.*, **44**, 7484 (2015).
6. L. Siinor, C. Siimenson, K. Lust, E. Lust, *Electrochem. Commun.*, **35**, 5 (2013).
7. S. Yamazaki, T. Ito, M. Yamagata, M. Ishikawa, *Electrochim. Acta,* **86**, 294 (2012).
8. C. Siimenson, M. Lembinen, O. Oll, L. Lall, M. Tarkanovskaja, V. Ivaništšev, L. Siinor, T. Thomberg, K. Lust, E. Lust, *J. Electrochem. Soc.*, **163**, H723 (2016).
9. N. Ma, N. Phattharasupakun, J. Wutthiprom, C. Tanggarnjanavalukul, P. Wuanprakhon, P. Kidkhunthod, M. Sawangphruk, *Electrochim. Acta*, **271**, 110 (2018).
10. J. Zhao, G. Gorbatovski, O. Oll, T. Thomberg, E. Lust, *Electrochim. Acta,* **31**, 82 (2019).
11. K. Aken, M. Beidaghi, Y. Gogotsi, *Angew. Chem. Int. Ed.*, **54**, 4806 (2015).
12. M. Watanabe, M. Thomas, S. Zhang, K. Ueno, T. Yasuda, K. Dokko, *Chem. Rev.,* **117, 7190** (2017).
13. L. Wei, G. Yushin, *J. Power Sources,* **196**, 4072 (2011).
14. B. Scrosati, J. Hassoun, Y.-K. Sun, *Energy Environ. Sci.*, **4**, 3287 (2011).
15. F. Malchik, N. Shpigel, M.D. Levi, T. Mathis, A. Mor, Y. Gogotsi, D. Aurbach, *J. Mater. Chem. A.,* **7,** 19761 (2019).
16. C. Merlet, C. Péan, B. Rotenberg, P. Madden, P. Simon, M. Salanne, *J. Phys. Chem. Lett.,* **4,** 264 (2013).
17. C. Merlet, B. Rotenberg, P. Madden, P. Taberna, P. Simon, Y. Gogotsi, M. Salanne, *Nat. Mater.*, **11,** 306 (2012).
18. C. Merlet, C. Pean, B. Rotenberg, P.A. Madden, B. Daffos, P. Taberna, P. Simon, M. Salanne, *Nat. Commun.*, **4**, 2701 (2013).
19. C. Péan, C. Merlet, B. Rotenberg, P.A. Madden, P. Taberna, B. Daffos, M. Salanne, P. Simon, *ACS Nano*, **8**, 1576 (2014).
20. T. Ahmed, J. DeSimone, J. G. Roberts, *Macromolecules,* **40,** 9322 (2007).
21. B. Ameduri, *Chem. Rev.,* **109,** 6632 (2009).
22. L. Soserov, A. Stoyanova, T. Boyadzhieva, V. Koleva, M. Kalapsazova, *Electrochim. Acta*, **283,** 1063 (2018).
23. M. Apostolo, V. Arcella, G. Storti, M. Morbidelli, *Macromolecules* **32**, 989 (1999).
24. T. Wang, S. Zhang, X. Yan, M. Lyu, L. Wang, J. Bell, *ACS Appl. Mater. Interfaces,* **9,** 15510 (2017).
25. J. Huang, P. Xu, D. Cao, X. Zhou, G. Wang, *J. Power Sources*, **246**, 371 (2014).
26. L. Soserov, A. Stoyanova, R. Stoyanova, *Bulg. Chem. Commun.*, **49,** 15 (2017).
27. D. Hall, D. Lockwood, C. Bock, B. MacDougal, *Proc. R. Soc. A,* **471**, 20140792 (2015).

The probable reactivity of a petroleum component

Y. K. Koleva

Department of Chemistry, University 'Prof. Assen Zlatarov', 1 Prof. Yakimov Street, 8010 Burgas, Bulgaria;

Oil spills threaten the global and local environment in both short and long term. Therefore, the fate and environmental impact of crude oil and its petroleum products requires serious study. Most of the studies at this stage have focused on the main hydrocarbons in crude oil while a minor fraction of hydrocarbons containing heteroatoms such as nitrogen (N), sulfur (S) and oxygen (O) have been neglected. However, these heterocyclic compounds may be disproportionately important to ecosystem health, necessitating their study. Toxicological data of organosulfur compounds in oil are limited. This necessitates the use of alternative methods to assess their toxicological properties. In the present work, the probable reactivity of the parent structure (2,3-dimethyl-1-benzothiophene) and its generated hepatic metabolites (for both conditions (rat *in vivo* and *in vitro*)) with respect to DNA and protein binding were studied by the QSAR Toolbox software. The reactive hepatic metabolites in both conditions (rat *in vivo* and *in vitro*) have different mechanisms of action (radical mechanism, A_N^2 and non-covalent interaction) with respect to DNA binding and the following mechanisms of action (Michael addition and Schiff base formation) with respect to protein binding.

INTRODUCTION

An oil spill is the release of a liquid petroleum hydrocarbon into the environment, especially the marine ecosystem, due to human activity, and is a form of pollution. The term is usually given to marine oil spills, where oil is released into the ocean or coastal waters. When oil is released into the sea, not only it increases pollution, but it is also difficult to clean. In fact, most of the methods for cleaning oil spills are ineffective, and often damage the marine life and environment. So these countermeasures should be applied depending on interrelated factors like ecological protection, socioeconomic effects and health risks. Crude oil is a mixture of hydrocarbons, but each kind has a different composition of molecular compounds, for example: sulfur, nitrogen, oxygen, metals, and other elements [1].

The petroleum industry has continually been troubled with various problems related to sulfur compounds in petroleum and its products, such as product odor and storage stability, catalyst poisoning, corrosion of processing equipment, and pollution emitted during usage. Sulfur is usually the most abundant hetero element in petroleum. Most of the sulfur present in crude oils is organically bound sulfur while elemental sulfur and hydrogen sulfide usually represent a very minor portion [2]. Furthermore, noxious sulfur dioxide is produced during combustion of sulfur-containing fuels. As such they are toxic and some of them are suspected mutagens and/or carcinogens. Better knowledge of the forms in which sulfur occurs in fossil fuels might aid the development of methods for its removal [3].

The sulfur content is in the range of 0.1—3.0% in most crudes [4] but can reach 8% in the vacuum residue of heavy crudes [5]. Organic sulfur compounds in crude oils are distributed over a wide range of molecular structures: aliphatic thiols, mono- and disulfides [6], as well as alkyl phenyl disulfides [7], but a large amount occurs in aromatic structures, especially as alkylated thiophene benzologues [8]. After distillation, mercaptanes, sulfides, and thiophenes are concentrated in the gasoline-range products [9] while benzothiophenes (BTs), dibenzothiophene (DBT), and alkylated dibenzothiophenes (DBTs) are concentrated in the middle distillate fractions. They may represent up to 70% of the sulfur present in diesel fuel.

A major part of the organic sulfur present in these materials occurs as thiophenic compounds, which makes this an important class of sulfur compounds to study. In petroleums the thiophene ring is mostly present as part of ring systems (primarily benzo- and dibenzothiophenes) [10-12] but alkylated thiophenes also occur [13] and are the most abundant thiophenic compounds present in shale oils [14].

The presence of organosulfur compounds in petroleum poses important production, environmental and health problems. In 1998, the

To whom all correspondence should be sent:
E-mail: *ykoleva@btu.bg*

European Union first mandated new sulfur specifications for drastically reduced levels that started to be phased in from the year 2000 [15].

However, the knowledge about the possible toxicities caused by this type of compounds is limited, necessitating the application of alternative methods (*in silico*) for their evaluation. Some theoretical studies show that the parent compounds (the basic structure) of organosulfur compounds are not reactive, but under certain conditions (e.g. in the liver) they can generate metabolites that are reactive, i.e. can cause health problems [16, 17].

The aim of the present work is to study the probable reactivity of the parent structure (2,3-dimethyl-1-benzothiophene) and its generated hepatic metabolites (for both conditions (rat *in vivo* and *in vitro*)) with respect to DNA and protein binding, using the QSAR Toolbox software.

MATERIAL AND METHODS

Compound. Heterocyclic sulfur compounds such as alkyl benzothiophenes (2,3-dimethyl-1-benzothiophene) are major sulfur components in the hydrodesulfurized oil fractions because they are highly recalcitrant to chemical catalysts [18]. The structural formula of 2,3-dimethyl-1-benzothiophene with CAS number 4923-91-5 is presented in Figure 1 [19].
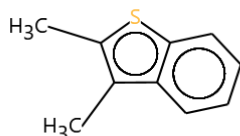

Figure 1. Structural formula of 2,3-dimethyl-1-benzothiophene

Organisation for Economic Co-operation and Development (*OECD*) (*Q*)*SAR Toolbox (version 4.3)*. (Quantitative) Structure - Activity Relationships [(Q)SARs] are methods for estimating properties of a chemical from its molecular structure and have the potential to provide information on the hazards of chemicals, while reducing time, monetary costs and animal testing currently needed [20].

METAPATH is a software platform to manage experimental data for the observed metabolism (*in vivo* and *in vitro*), providing very powerful and flexible search capabilities in identifying of metabolites, biotransformations and relative

biotransformation rates observed in specific test environments, as well as specific enzymes responsible for a given biotransformation [20]. The metabolism databases assembled in METAPATH may be used as stand-alone datasets to increase efficiency of metabolism data evaluation and assessment by searching for specific compounds and identification of metabolism commonalities and, also, differences across chemical classes, species and dose-groups. These databases can be also employed for development and improvement of existing metabolic simulators that are used to perform metabolic predictions for chemical lists of concern [20].

Observed rat in vivo metabolism. The observed (documented) metabolic pathways for 647 chemicals, extracted from the scientific literature, and associated with the *in vivo* biotransformations of xenobiotic chemicals in rodents (mostly rats) are stored in a database format that allows easy computer access to the metabolism information. This database includes structurally different chemicals of various functionalities [20].

In vivo rat metabolism simulator. The current *in vivo* rat liver metabolic simulator (transformation table) represents an electronically designed set of 671 structurally generalized, hierarchically arranged abiotic and enzymatic transformation reactions which are characteristic for the metabolism for *in vivo* experimental systems such as rodent (mostly rat). The principal applicability of this simulator is associated with the reproduction, as well as the prediction of the metabolic activation reactions and pathways of xenobiotic chemicals, which may elicit *in vivo* genotoxicity effects [20].

Observed rat liver S9 metabolism. The documented metabolic pathways for 261 chemicals observed with the use of *in vitro* experimental systems such as rodent (mostly rat) liver microsomes and S9 fraction are stored in a database format that allows easy computer access to the metabolism information. This database includes structurally different chemicals of various functionalities and fields of application [20].

Rat liver S9 metabolism simulator. The current *in vitro* rat liver metabolic simulator (transformation table) represents an electronically designed set of 551 structurally generalized, hierarchically arranged biotransformation reactions which are characteristic for the metabolism for *in vitro* experimental systems such as rodent (mostly rat) liver microsomes and S9 fraction [20].

DNA binding by OASIS. The profiler is based on Ames Mutagenicity model part of OASIS TIMES system. The profiler consists of 85 structural alerts

responsible for interaction with DNA analyzed in Ames Mutagenicity model. The scope of the profiler is to investigate the presence of alerts within target molecules which may interact with DNA [20].

Protein binding by OASIS. The scope of the profiler is to investigate the presence of alerts within target molecules responsible for interaction with proteins. The list of 112 structural alerts has been separated into 11 mechanistic domains. Each of the mechanistic domains has been separated into more than 2 mechanistic alerts. The profiling result outcome assigns a target to the corresponding structural alert, mechanistic alerts and domain [20].

RESULTS AND DISCUSSION

Toxicology is undergoing a paradigm shift, from predominantly observational science (based on animal testing), to predominantly predictive science focusing on target-specific, mechanism-based biological observations, contingent upon *in vitro* data and *in silico* predictions, often referred to as toxicology for the twenty-first century [21]. The development and application of modern tools can provide deeper insights into the molecular mechanisms underlying toxicity in a high throughput manner [22, 23]. Such developments are being driven by the need to improve the safety evaluation of chemicals in a more efficient, human-relevant context [24] to meet changing regulations and promote the use of non-animal models to predict toxicity [25].

Generally, toxicity studies require large numbers of animals, take several months to years to complete, are usually very costly, and can only test low numbers of compounds in a given time period. Current animal testing is primarily performed in rats and mice, and although these rodents exhibit many of the same responses to chemicals as humans, there are qualitative and particularly quantitative differences [26].

The software QSAR Toolbox (version 4.3) was applied to predict the possible metabolites of 2,3-dimethyl-1-benzothiophene in the liver (rat *in vivo* and *in vitro*) and their probable DNA and protein binding. The parent structure of 2,3-dimethyl-1-benzothiophene cannot bind to DNA and protein. The experimental pathways of metabolic activation were not observed in both conditions (rats *in vivo* and *in vitro*). The generated hepatic metabolites of 2,3-dimethyl-1-benzothiophene in the software QSAR Toolbox (rat *in vivo*) are presented in Table 1.

The possible DNA binding by OASIS (reaction mechanism) of the generated hepatic metabolites of 2,3-dimethyl-1-benzothiophene was predicted using the QSAR Toolbox software. The probable DNA binding of the generated hepatic metabolites of 2,3-dimethyl-1-benzothiophene is presented in Table 2.

Twenty metabolites are non-reactive and two are reactive, i.e. structural alerts are found for DNA binding. The structural alerts (quinones and trihydroxybenzenes) of the two metabolites were identified in the mechanistic domains (radical mechanism, A_N^2 and non-covalent interaction) with mechanistic alerts (radical mechanism *via* ROS formation, Michael-type addition, quinoid structures and DNA intercalation). The probable protein binding of the generated hepatic metabolites (liver *in vivo*) of 2,3-dimethyl-1-benzothiophene is presented in Table 3. Eleven metabolites are not reactive and eleven are reactive, i.e. structural alerts are found for protein binding. The structural alerts (polarised alkenes – sulfinyl, di-substituted α,β-unsaturated aldehydes and aldehydes) of the eleven metabolites were identified in the mechanistic domains (Michael addition and Schiff base formation) with mechanistic alerts (Michael addition on polarized alkenes, direct acting Schiff base formers and Schiff base formation with carbonyl compounds).

The probable hepatic metabolites of 2,3-dimethyl-1-benzothiophene that were generated using the QSAR Toolbox (*in vitro* rat metabolism simulator) are fourteen. The generated hepatic metabolites of 2,3-dimethyl-1-benzothiophene in the software QSAR Toolbox (rat *in vitro*) are presented in Table 4.

The probable DNA binding of the generated hepatic metabolites (*in vitro*) of 2,3-dimethyl-1-benzothiophene is presented in Table 5. Twelve metabolites are not reactive and two are reactive, i.e. structural alerts are found for DNA binding. The structural alerts (quinones and trihydroxybenzenes) of the two metabolites were identified in the mechanistic domains (radical mechanism, A_N^2 and non-covalent interaction) with mechanistic alerts (radical mechanism via ROS formation, Michael-type addition, quinoid structures and DNA intercalation).

The probable protein binding of the generated hepatic metabolites (*in vitro*) of 2,3-dimethyl-1-benzothiophene is presented in Table 6. Nine metabolites are not reactive and five are reactive, i.e. structural alerts are found for protein binding. The structural alerts (polarized alkenes – sulfinyl and aldehydes) of the five metabolites were identified in the mechanistic domains (Michael addition and Schiff base formation) with mechanistic alerts (Michael addition on polarized alkenes and Schiff base formation with carbonyl compounds).

29

Table 1. Number and structure of the generated hepatic metabolites (*in vivo*) of 2,3-dimethyl-1-benzothiophene
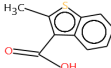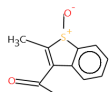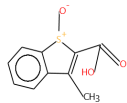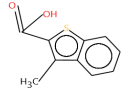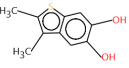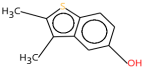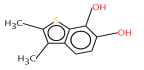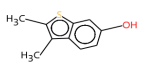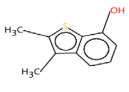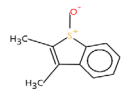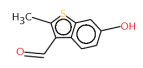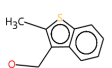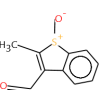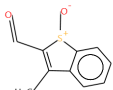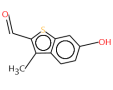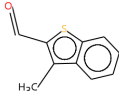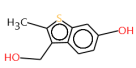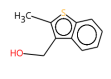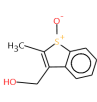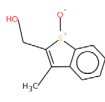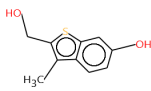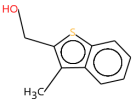

Table 2. DNA binding of hepatic metabolites of 2,3-dimethyl-1-benzothiophene by QSAR Toolbox (liver *in vivo* metabolism simulator)

Number of metabolite	DNA binding by OASIS (Mechanism of reaction)		
	Structural alert	Mechanistic alert	Mechanistic domain
1-4,6,8-22	No alert found		
5,7	Quinones and trihydroxybenzenes	Radical mechanism *via* ROS formation	Radical mechanism
5,7	Quinones and trihydroxybenzenes	Michael-type addition, quinoid structures	A_N^2
5,7	Quinones and trihydroxybenzenes	DNA intercalation	Non-covalent interaction

Table 3. Protein binding of hepatic metabolites of 2,3-dimethyl-1-benzothiophene by QSAR Toolbox (liver *in vivo* metabolism simulator)

Number of metabolite	Protein binding by OASIS (Mechanism of reaction)		
	Structural alert	Mechanistic alert	Mechanistic domain
1,4-9,17,18,21,22	No alert found		
2,3,10,13,14,19,20	Polarised alkenes - sulfinyl	Michael addition on polarized alkenes	Michael addition
14	Di-substituted α,β-unsaturated aldehydes	Direct acting Schiff base formers	Schiff base formation
11-16	Aldehydes	Schiff base formation with carbonyl compounds	Schiff base formation

Table 4. Number and structure of the predicted hepatic metabolites (*in vitro*) of 2,3-dimethyl-1-benzothiophene
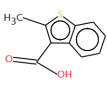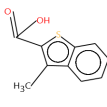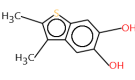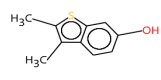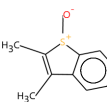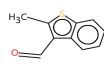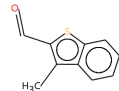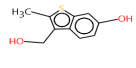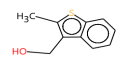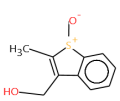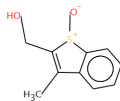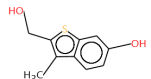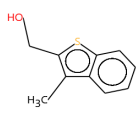
1	2	3	4	5

6	7	8	9	10

11	12	13	14	

Table 5. DNA binding of the hepatic metabolites of 2,3-dimethyl-1-benzothiophene by QSAR Toolbox (liver *in vitro* metabolism simulator)

Number of metabolite	DNA binding by OASIS (Mechanism of reaction)		
	Structural alert	Mechanistic alert	Mechanistic domain
1,2,5-14	No alert found		
3,4	Quinones and trihydroxybenzenes	Radical mechanism *via* ROS formation	Radical mechanism
3,4	Quinones and trihydroxybenzenes	Michael-type addition, quinoid structures	A_N^2
3,4	Quinones and trihydroxybenzenes	DNA intercalation	Non-covalent interaction

Table 6. Protein binding of hepatic metabolites of 2,3-dimethyl-1-benzothiophene by QSAR Toolbox (liver *in vitro* metabolism simulator)

Number of metabolite	Protein binding by OASIS (Mechanism of reaction)		
	Structural alert	Mechanistic alert	Mechanistic domain
1-5,9,10,13,14	No alert found		
6,11,12	Polarised alkenes - sulfinyl	Michael addition on polarized alkenes	Michael addition
7,8	Aldehydes	Schiff base formation with carbonyl compounds	Schiff base formation

CONCLUSIONS

The presence of sulfur organic compounds in oil can lead to various harmful effects on the environment and living organisms. There are no toxicological data of 2,3-dimethyl-1-benzothiophene, which requires the use of alternative methods (*in silico*) to study its reactivity. The probability of 2,3-dimethyl-1-benzothiophene to generate metabolites in the liver and their possible reactivity was investigated using the QSAR Toolbox software. Some of the generated hepatic metabolites of 2,3-dimethyl-1-benzothiophene are reactive to DNA and protein, i.e. have an electrophilic effect. Therefore, 2,3-dimethyl-1-benzothiophene may have toxic effects on living organisms.

REFERENCES

1. Possible environment alteration: http://www.aquaticlifelab.eu/4-10-oil-spills/.
2. A. H. Hegazi, J. T. Andersson, *Oil Spill Environmental Forensics: Fingerprinting and Source Identification*, 147 (2007).
3. J. S. Sinninghe Damste, A. C. Kock-van Dalen, J. W. de Leeuw, P. A. Schenck, *J. Chromatogr.*, **435**, 435 (1988).
4. R. D. Morrison, in: Environmental Forensics, Principles & Applications, CRC Press, Boca Raton, FL, 1999, Chap. 2, p. 51.
5. D. Severin, O. Glinzer, Characterization of heavy crude oils and petroleum residues, Technip, Paris, **19** (1984).
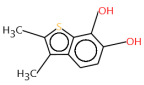6. K. J. Rygle, G. P. Feulmer, R. F. Scheideman, *J. Chromatogr. Sci.*, **22**(11), 514 (1984).
7. M. Nishioka, *Energy & Fuels*, **2**(2), 214 (1988).
8. P. J. Arpino, I. Ignatiadis, G. de Rycke, *J. Chromatogr.*, **390**(2), 329 (1987).
9. Á. Stumpf, K. Tolvaj, M. Juhász, *J. Chromatogr. A*, **819**, 67 (1998).
10. R. L. Martin, J. A. Grant, *Anal. Chem.*, **37**, 649 (1965).
11. W. B. Hughes, in: J. G. Palacas (ed.), Petroleum Geochemistry and Source Rock Potential of Carbonate Rocks (AAPG Studies in Geology, No. 18), AAPG, Tulsa, 1984, p. 181.
12. P. J. Arpino, I. Ignatiadis, G. de Rycke, *J. Chromatogr.*, **390**, 329 (1987).
13. W. L. Orr, in: O. P. Strausz and E. M. Lown (eds.), Oil Sand & Oil Shale Chemistry, Verlag Chemie, New York, 1978, p. 223.
14. W. J. Joyce, P. C. Uden, *Anal. Chem.*, **55**, 540 (1983).
15. K. Sripada, Metal ion containing liquid chromatographic stationary phases for the analysis of polycyclic aromatic sulfur heterocycles in fossil fuels, PhD Thesis, Universität Münster, 2005.
16. Y. Koleva, *Industrial Technologies*, **8 (1)**, 139 (2021).
17. Y. Koleva, Predicting hepatic transformations of the petroleum organosulfur compounds using *in silico* methods, Edition of Assen Zlatarov University, Libra Scorp Publisher, Bulgaria, 2022 (in press).
18. M. Kobayashi, T. Onaka, Y. Ishii, J. Konishi, M. Takaki, H. Okada, Y. Ohta, K. Koizumi, M. Suzuki, *FEMS Microbiology Letters*, **187**, 123 (2000).
19. ChemIDplus Advanced, https://chem.nlm.nih.Gov/chemidplus/.
20. The OECD QSAR Toolbox: https://www.oecd.org/chemicalsafety/risk-assessment/oecd-qsar-toolbox.htm.
21. T. Hartung, *Nature*, **460**, 208 (2009).
22. M. S. Attene-Ramos, R. Huang, S. Michael et al., *Environ. Health Perspect.*, **123**, 49 (2015).
23. J. Liu, K. Mansouri, R. S. Judson et al., *Chem. Res. Toxicol.*, **28**, 738 (2015).
24. R. Judson, K. Houck, M. Martin et al., *Basic Clin. Pharmacol. Toxicol.*, **115**, 69 (2014).
25. T. Ramirez, N. Bordag, W. Mellert et al., *Toxicol. Lett.*, **221**, S194 (2013).
26. H. Olson, G. Betton, D. Robinson et al., *Regul. Toxicol. Pharmacol.*, **32**, 56 (2000).

Synthesis and characterization of carbon xerogels and MnO_2 as electrode materials for energy storage systems

B. B. Mladenova*, T. E. Stankulov, B. A. Karamanova, S. K. Veleva, V. G. Ilcheva, A. E. Stoyanova

Institute of Electrochemistry and Energy Systems, Bulgarian Academy of Sciences, G. Bonchev Str. 10, Sofia, Bulgaria

The current investigation presents some results of the synthesis of carbon xerogels and MnO_2-based materials with predefined phase composition and surface for potential application as electrodes in supercapacitors. Organic xerogels were prepared by polycondensation of resorcinol and formaldehyde. Two different methods were used for heat treatment of the previously obtained solution: microwave heating and thermal treatment in vacuum. The obtained materials were subsequently carbonized and activated in order to increase their specific surface. MnO_2-based materials were synthesized by chemical reduction in aqueous solution. All synthesized samples were structurally and morphologically characterized. The results of the current analyses demonstrate differences in the phase composition and structure of the obtained materials, reflecting on their surface properties. This creates prerequisites for in-depth study of the influence of the synthesis method, which will reflect on the electrochemical characteristics of the studied and further tested supercapacitors.

Keywords: carbon xerogels, MnO_2, electrode materials, supercapacitors, physical and electrochemical study

INTRODUCTION

In recent years, the scientific interest in cheap and environmentally friendly materials and their application in energy storage systems has increased. Their characteristics strongly depend on the electrode materials used. For example, in electrochemical supercapacitors mainly used are carbon materials with specific parameters corresponding to a number of requirements, as high electrical conductivity, high surface area, controlled surface morphology, good corrosion resistance and thermal stability, good processability and low cost of production [1, 2]. A promising carbon material is the carbon xerogel, which possesses more than the mentioned parameters - very high active surface and electrical conductivity, significant micropore volume and well-defined mesoporosity, tunable according to the synthesis conditions, and a fast and simple production process. These properties make it an ideal electrode material in various electrochemical systems and in particular in supercapacitors [3, 4].

The synthesis of carbon xerogel can be performed using sol-gel technique by drying under ambient conditions, as well as by pyrolysis of organic gel obtained by polycondensation of resorcinol and formaldehyde [5, 6]. The meso / macroporosity of carbon gels can be designed by modifying the synthesis conditions, and the microporosity can be improved by subsequent carbonization and activation treatments [7, 8].

Carbonization and activation also lead to an increase in the surface area of the xerogels, as well as in their electrical conductivity which can be further increased by introducing conductive additives into its structure [9, 10].

Different working mechanisms of hybrid supercapacitors are possible due to the electrode materials used, which in this case are usually a carbon electrode and a composite carbon matrix electrode containing an electrochemically active component. In this case, nanostructured oxides and hydroxides, providing a high reaction area, and high porosity in order to achieve better contact with the electrolytes used are very suitable [11].

A very promising electrode material for supercapacitor systems is MnO_2. This material is characterized by a high specific theoretical capacity ($\sim$ 1370 Fg^{-1}), low cost and environmental friendliness [12]. The charge storage mechanism for MnO_2 is based on the surface adsorption of cations in the electrolyte. Due to its low electronic conductivity ($\sim 10^{-6}$ Scm^{-1}), and in order to achieve high theoretical specific capacity, MnO_2 has to be used in combination with other materials with high conductivity (e.g. carbon materials and metal nanostructures, carbon nanotubes, etc.) [13].

MnO_2 exists in different crystal modifications such as α-(hollandite), β-(pyrolusite), γ-(nsutite), δ-(birnessite), k-(akhtenskite), etc. and only some of them are suitable for a particular application [14-17]. For example, according to the research of Song

* To whom all correspondence should be sent:
E-mail: *borislava.mladenova@iees.bas.bg*

[14] it has been established that α-MnO_2 shows very good electrochemical properties as an electrode material in electrochemical current sources and especially in supercapacitors. Depending on the synthesis methods used, different structural modifications of MnO_2 can be obtained.

The most commonly used methods for the preparation of manganese dioxide are: microwave-assisted reflux rapid synthesis [18], hydrothermal process [19, 20], electrochemical method [21], biosynthesis [22], co-precipitation method [23, 24], sonochemical synthesis [25], etc.

The aim of the present work is to synthesize carbon xerogel and MnO_2 as electrode materials in energy storage systems, as well as to trace the effect of the synthesis conditions on the morphology and structure of the obtained carbons. Preliminary galvanostatic charge/ discharge tests in a two-electrode symmetric supercapacitor cell will be applied to evaluate the electrochemical characteristics of the electrode materials and their stability.

EXPERIMENTAL

Synthesis of materials

Carbon xerogels. Organic xerogels were synthesized by polycondensation of mixtures of resorcinol $C_6H_6O_2$ (99%, Valerus Co., Bulgaria) and formalin (37% aqueous solution, Valerus Co., Bulgaria) in deionized water, following the procedure described by Canal-Rodriguez *et al.* [26]. The pH of the solution is a very important factor controlling the porosity of the final carbon and therefore its precise control is very important [7]. In this case, the pH of the solution was adjusted with NaOH. Two different approaches were used for gelling, curing and gel preparing: microwave heating (treatment time about 25 minutes, RFCA_MW) and vacuum heat treatment (treatment time about 50 hours, RFCA_TT).

Manganese oxide was synthesized by precipitation from an aqueous solution of potassium permanganate (VII) $KMnO_4$ (Valerus Co., Bulgaria) and manganese (II) chloride $MnCl_2$ (Valerus Co., Bulgaria) [27]. A solution containing 0.05M $MnCl_2$ was added dropwise during 60 minutes under continuous stirring to a solution containing 0.05M $KMnO_4$. The so-obtained suspension was stirred for 6 h during which a precipitate was formed. The liquid was decanted for 24 h and a suspension of two distinct phases was formed consisting of a fine precipitate and a supernatant liquor. The precipitate was washed with deionized water. The formed precipitate was finally dried at 80 °C under vacuum and then the manganese oxide powder was thermally treated at 200 °C.

The obtained materials were structurally characterized by X-ray diffraction (XRD) using a Philips X-ray diffractometer PW 10301030 having θ-2θ Bragg-Brentano geometry, with Cu Kα radiation (30 kV, 20 mA) at a wavelength λ = 1.5418 Å. The porous texture of the samples was examined by low-temperature (77.4 K) nitrogen adsorption using Quantachrome Autosorb iQ Station 3 instrument. The specific surface area was evaluated by the Brunauer-Emmett-Teller (BET) method at a relative pressure p/p_o in the range of 0.10-0.30. The total pore volume was calculated according to Gurwitsch's rule at p/p_o = 0.99. The pore size distribution was estimated by using the Barrett-Joyner-Halenda method.

The thermal behavior was investigated by differential thermal analysis (DTA) and thermogravimetric (TG) technique by means of a Perkin Elmer-Diamond apparatus, in air atmosphere and corundum crucibles. Powder samples with weight of 10-12 mg were heat- treated at 20 °C/min up to 1000 °C.

The samples morphology was observed by transmission electron microscopy (TEM) on a JEOL JEM 2100, 80-200 kV (Jeol Ltd. Japan) and scanning electron microscopy (SEM) using SEM Philips 515.

The obtained carbon xerogels were analysed by galvanostatic experiments. The supercapacitor cell comprised two identical electrodes containing activated carbon (80 wt.%), graphite ABG 1005 EG-1 (10 wt.%) and polytetrafluoroethylene binder (PTFE, 10 wt.%). The electrodes were assembled in a cell using Viledon 700/18 F separator and basic electrolyte 6 M KOH. The charge-discharge cycling tests were performed using an Arbin Instrument System BT-2000. The supercapacitor cells were cycled between 0.05 and 1.2 V at a current load increasing stepwise from 30 to 1200 mAg^{-1} for 25 cycles per step. Selected cells were charged/discharged up to 5000 cycles at a current rate of 240 mAg^{-1}.

The specific discharge capacitance (F g^{-1}) was calculated by the Equation [28]:

$$C = (I \times \Delta t)/(m \times \Delta V) \qquad (1)$$

where I, Δt, m and ΔV are discharge current, discharge time, mass of active material and voltage window, respectively. On the basis of the specific discharge capacitance, the energy density (E) and power density (P) can be expressed as [12]:

$$E = C \Delta V^2 /7.2 \qquad (2)$$
$$P = E/t \qquad (3).$$

RESULTS AND DISCUSSION

Physicochemical characterization

Carbon xerogels. The thermal decomposition of the two xerogels was analyzed by DTA / TG experiments. Figure 1 compares the thermogravimetric and DTA curves for RFCA_MW and RFCA_TT. The results show that at low temperatures, up to 300-400 °C, the carbon materials stay almost unchanged with a slight mass loss of 2-5 %, due to the presence of water. This fact is supported by the small peak of DTA between 50-80 °C. It can also be seen that the complete combustion of RFCA_RW takes place between 450 and 750 °C with only negligible residue (1%). For RFCA_TT this range is narrower, in the range of 300 and 550 °C, i.e. RFCA_TT burns relatively faster than RFCA_MW. The observed difference in the thermal decomposition of carbon xerogels obtained by different methods is probably related to the difference in their structures. For RFCA_MW, it is more complex and obviously more difficult to burn.
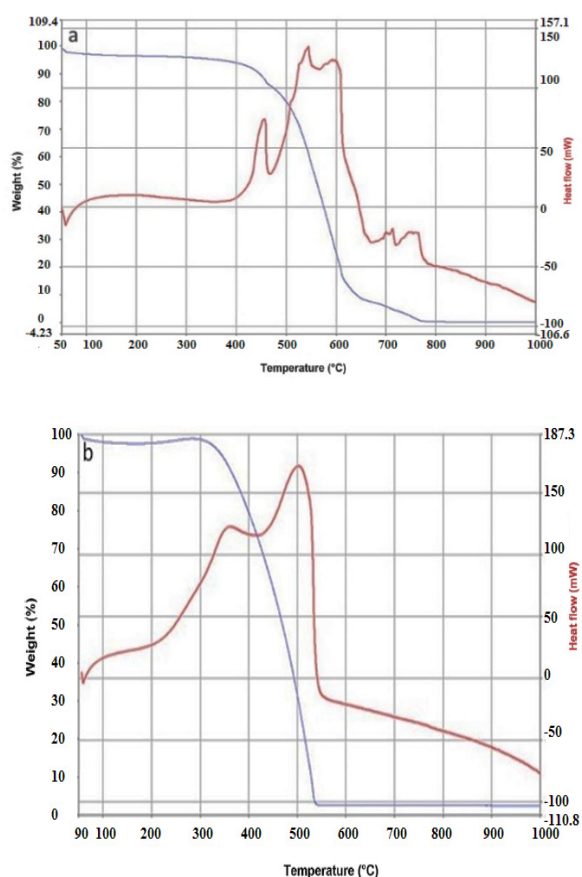
Fig. 1. Thermogravimetric and DTA curves for RFCA_MW (a) and and RFCA_TT (b)

To check the sample morphology, TEM images were taken (Fig. 2). The micrographs of both carbon xerogels show the formation of a micro layered structure with crystalline and amorphous sections. The layers are interconnected and overlap with each other.
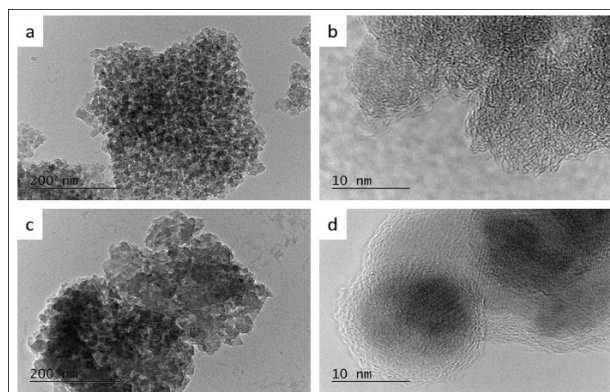
Fig. 2. TEM micrographs of carbon xerogel obtained by: microwave-induced synthesis (a, b) and vacuum heat treatment (c, d)

Figure 3 gives the pore size distribution curves for RFCA_MW and RFCA_TT together with adsorption/desorption curves. The calculated specific surface area and the total pore volume for both carbons are listed on Table 1. In general, both samples display high specific surface area, especially for RFCA_MW reaching a value higher than 660 m^2g^{-1}. The average pore diameter is very close for both RFCA_MW and RFCA_TT: 3.8 *versus* 3.7 nm (Table 1). However, the pore size distribution is different. For RFCA_TT, the distribution curve is extremely narrow with a higher peak at about 6 nm, while for RFCA_MW the distribution curve shows two peaks at 5.2 and 7.1 nm. Both isotherms are of type II and III, which is characteristic of macroporous structures [29].

Characterization of MnO₂

X-ray diffraction pattern of the synthesized MnO₂ is shown in Fig. 4. The analysis shows the presence of two broad peaks (211, 112) located at 37 ° and 66.5 °. These peaks indicate the presence of α-MnO₂ with a crystalline structure, which is confirmed by PCPDFMIN, ICDD, 2021, № 00-044-0141 database [30].
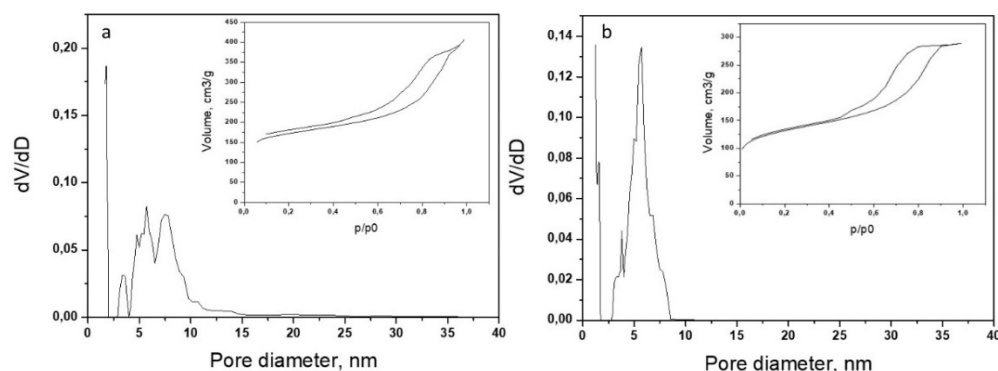
Fig. 3. Pore size distribution curves for RFCA_MW (a) and RFCA_TT (b)

Table 1. Main texture parameters of the obtained carbon xerogels: specific surface area (S_{BET}), micropore surface area (S_{micro}), external surface area (S_{ext}), total pore volume (V_t), micropore volume (V_{micro}) and average pore diameter (D_{av})

Sample	S_{BET}, $m^2 g^{-1}$	S_{micro}, $m^2 g^{-1}$	S_{ext}, $m^2 g^{-1}$	V_t, $cm^3 g^{-1}$	V_{micro} $cm^3 g^{-1}$	D_{av} nm
RFCA_MW	667	457	210	0.63	0.18	3.8
RFCA_TT	482	291	191	0.45	0.12	3.7
MnO₂	255	-	17	0.07	-	16
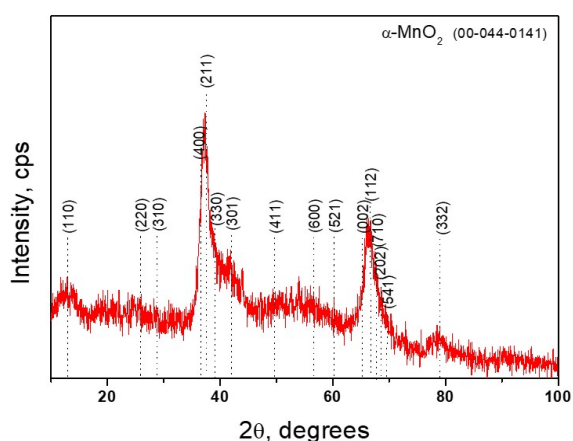
Fig. 4: X-ray powder diffraction pattern of MnO₂, compared to a database PCPDFMIN, ICDD, 2021, № 00-044-0141.

Fig. 5. Thermogravimetric and DTA curves for MnO₂.

The thermal decomposition of MnO₂ was analyzed by DTA/TG experiments, and its thermogravimetric and DTA curves are compared in Figure 5. The results show that no intensive combustion takes place in this case.

The loss of mass up to about 200 °C can be explained by the separation of water from MnO₂ nanoparticles. At higher temperatures, however, a loss of about 5% of the sample mass is observed, which indicates the presence of impurities in it. The endothermic peak, observed on the DTA curve at ~ 520 ^{0}C is, could be ascribed to α-MnO₂ – γ-MnO₂ phase transition.

The morphology of the samples was studied by SEM and TEM. Figs. 6 and 7 show the morphology of α-MnO₂ nanoparticles at different magnification. Fig. 6 shows that the prepared MnO₂ nanoparticles are homogeneous with a spherical shape and dimensions of about 50 nm. The formation of individual agglomerates with sizes over 200 nm is observed in places.

TEM images show particle aggregation, a network, which is a prerequisite for a high surface area and better electrical conductivity of the material.
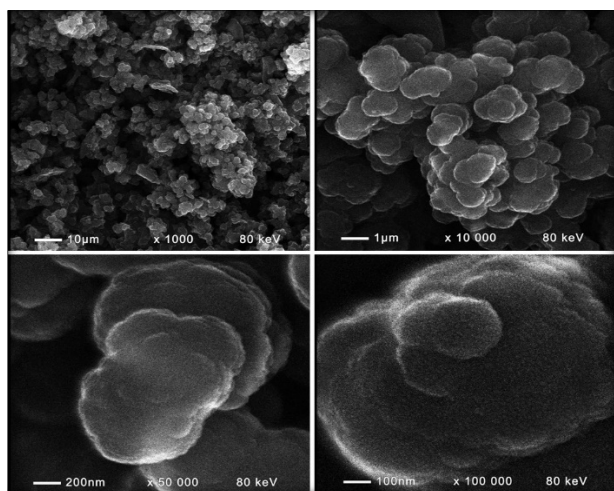
Fig. 6. SEM image for α-MnO$_2$ nanoparticles at different magnifications.
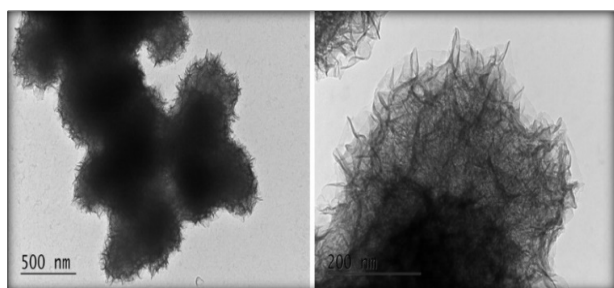
Fig. 7. TEM image for α-MnO$_2$ nanoparticles at different magnifications.

The BET analysis and main texture parameters of the obtained α-MnO$_2$ confirm this assumption. The synthesized manganese oxide shows a high specific surface area of 255 m^{2}g^{-1} (Table 1) with isotherm type III [29] and a relatively low total pore volume. There is a narrow pore size distribution mainly in the range between 3 and 5 nm, as well as presence of macropores with sizes over 50 nm (Fig. 8).

Electrochemical results

The results of the physicochemical analysis indicate that the synthesis methods used are suitable for the preparation of electrode materials applicable in energy storage systems. It was also demonstrated that the synthesis conditions affect the structural and morphological characteristics of the obtained carbon xerogels. The RFCA_MW texture parameters show a higher surface area and volume of the micropores compared to the vacuum heat treated carbon (RFCA_TT) (Table 1).
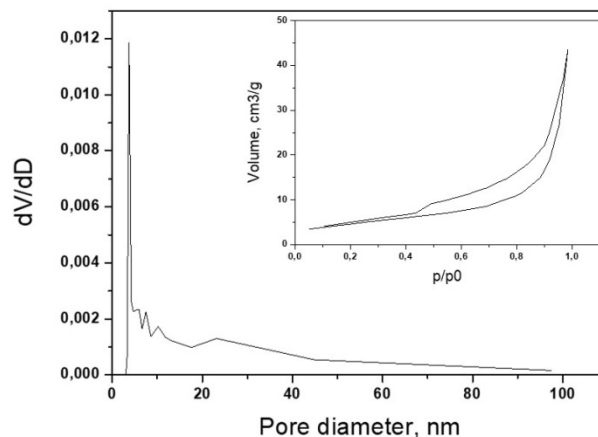
Fig. 8. Pore size distribution curves for the obtained MnO$_2$ (the inset shows the adsorption-desorption isotherms).

This result gave us reason to start electrochemical tests with carbon xerogel obtained by microwave synthesis as an electrode material in symmetrical supercapacitors. In Figure 9 its capacitive behavior as a function of current density in the current range from 60 to approximately 1200 mA g^{-1}, as well as the conducted long-term test can be seen.

The results demonstrate that the developed supercapacitor based on carbon xerogel RWCA_MW shows stable discharge capacitance of the charge-discharge process in the whole range of current loads. As one can also see, the discharge curve is clearly symmetric with its corresponding charge counterparts that exhibit a negligible voltage drop (iR-drop), indicating a rapid I-V response and an excellent electrochemical reversibility. For 5000 charge/discharge cycles, this SC displays only 5-7 % drop in discharge capacitance and over 97% efficiency (Fig. 9).
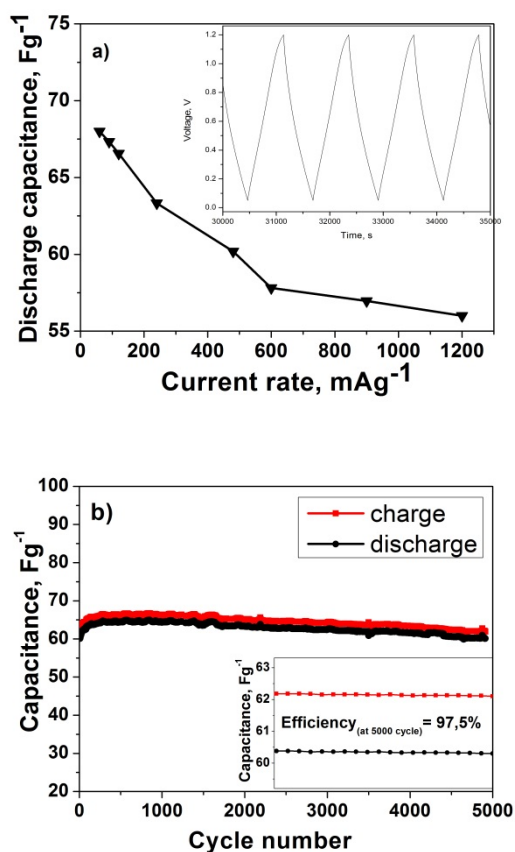
Fig. 9. Discharge capacitance as a function of current rate (a) and long-term tests at 240 mAg^{-1} (b) for symmetric supercapacitors with RWCA_MW carbon xerogel in 6 M KOH. The inset shows the galvanostatic charge-discharge curves at 240 mAg^{-1}.
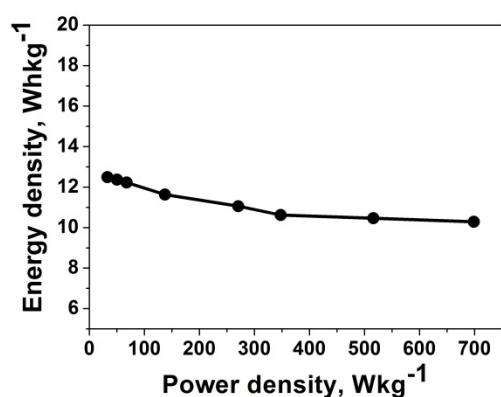
Fig. 10. Ragone plot of a symmetric supercapacitor with RWCA_MW carbon xerogel.

To evaluate the electrochemical performance of the synthesized xerogel, Figure 10 shows the Ragone plot for the assembled supercapacitor. The data indicate that the SC delivers a specific energy density of 12Wh kg^{-1} at a power density of 50 W kg^{-1}, and maintains a relatively high energy density of 10 Wh kg^{-1} even at a high power density of 700 W kg^{-1}. These values of energy density are

comparable and, in some cases, higher than those obtained for symmetric SCs in aqueous electrolyte, summarized by Zhong *et al*. [31].

CONCLUSION

Carbon xerogels and α-MnO₂ were successfully synthesized and structurally and morphologically characterized. The results of the physicochemical analysis indicate that the synthesized materials are suitable for application as electrode materials in supercapacitors. The carbon xerogels produced by microwave heating show a larger surface area and micropore volume compared to carbon materials obtained by vacuum heat treatment (RFCA_TT) and therefore this material was subjected to electrochemical test in symmetric supercapacitors.

The symmetrical supercapacitor based on RFCA_MW in 6M KOH electrolyte demonstrates a stable discharge capacitance and a high effectiveness of charge-discharge process. These results could be used as an initial research and a guide for further improvement of the carbon xerogels activation conditions in order to achieve a larger surface area and a correspondingly higher capacitance, as well as to develop a hybrid supercapacitor with the α-MnO₂ obtained.

REFERENCES

1. H. Chen, L. Hu, Y. Yan, R. Che, M. Chen, L. Wu, *Adv. Energy Mater.*, **3,** 163611 (2013).
2. G. Ramos-Fernández, M. Canal-Rodríguez, A. Arenillas, J. Menéndez, I. Rodríguez-Pastor, I. Martin-Gullon, *Carbon,* **126,** 456 (2018).
3. E. G. Calvo, E. J. Juárez-Pérez, J. A. Menéndez, A. Arenillas, *J. Colloid Interface Sci*., **357,** 541 (2011).
4. E. J. Juárez-Pérez, E. G. Calvo, A. Arenillas, J. A. Menéndez, *Carbon,* **48,** 3293 (2010).
5. M. Samanc, E. Daş, A. B. Yurtcan, *Carbon Lett.,* **31,** 1287 (2021).
6. C. Alegre, M. E. Gálvez, R. Moliner, V. Baglio, A. S. Aricò, M. J. Lázaro, *Appl. Catal.,* B, **147,** 947 (2014).
7. S. A. Al-Muhtaseb, J. A. Ritter, *Adv. Mater.,* **15,** 101 (2003)
8. N. Rey-Raap, J. A. Menendez, A. Arenillas*, Carbon,* **78,** 490 (2014).
9. M. Canal-Rodríguez, J. A. Menendez, A. Arenillas, *IntechOpen*, 69 (2017).
10. M. Canal-Rodríguez, J. A. Menendez, M. A. Montes-Moran, A. Arenillas, *J. Electroanal. Chem.,* **836,** 45 (2019).
11. A. G. Pandolfoand, A. F. Hollenkamp, *J. Power Sources*, **157,** 11 (2006).

12. J. Huang, P. Xu, D. Cao, X. Zhou, S. Yang, Y. Li, *J. Power Sources,* **246**, 371 (2014).
13. Ch. Du, N. Pan, *Nanotechnology Law & Business*, 569 (2007).
14. Zh. Song, Wei Liu, M. Zhao, Y. Zhang, G. Liu, Ch. Yu, J. Qiu, *J. Alloys Compd.*, **560**, 151 (2013).
15. M. Najafpour, S. Allakhverdiev*, Int. J. Hydrogen Energy,* **37**, 8753 (2012).
16. T. Lin T, L. Yu, M. Sun, G. Cheng, B. Lan, Z. Fu, *Chem. Eng. J.*, **286**, 114 (2016).
17. V. Štengl, D. Králová, F. Opluštil, T. Němec, *Microporous and Mesoporous Mater.*, **156**, 224 (2012).
18. X. Zhang, X. Sun, H. Zhang, D. Zhang, Y. Ma, *Electrochim. Acta,* **87**, 637 (2013).
19. M. Babu Poudel, M. Shin, H. Joo Kim, *Int. J. Hydrogen Energy*, **46**, 474 (2021).
20. X. Bai, X. Tong, Y. Gao, W. Zhu, C. Fu, J. Ma, T. Tan, C. Wang, Y. Luo, H. Sun, *Electrochim. Acta,* **281***, 525 (2018).
21. M. Mahmudi, W. Widiyastuti, P. Nurlilasari, S. Affandi, H. Setyawan, *J. Ceram. Soc. Japan,* **126**, 906 (2018).
22. S. O. Ogunyemi, F. Zhang, Y. Abdallah, M. Zhan, Y. Wang, G. Sun, W. Qiu, B. Li, Artif, *Cells Nanomed. Biotechnol.*, **47,** 2230 (2019).
23. C. Kahattha, S. Santhaveesuk, *Ferroelectrics,* **552**, 121 (2019).
24. K. A. Omar, *International Journal of Research in Engineering & Technology*, **2**, 241 (2014)
25. B. S. Raj, A. M. Asiri, A. H. Qusti, J. J. Wu, *Ultrason. Sonochem.*, **21**, 1933 (2014).
26. M. Canal-Rodríguez, L. A. Ramírez-Montoya, S. F. Villanueva, S. L. Flores-López, J. A. Menéndez, A. Arenillas, M. A. Montes-Morán, *Carbon*, **152**, 704 (2019).
27. P. Staiti, F. Lufrano, *Electrochim. Acta*, **55**, 7436 (2010).
28. T. Wang, S. Zhang, X. Yan, M. Lyu, L. Wang, J. Bell, *ACS Appl. Mater. Interfaces*, **9**, 15510 (2017).
29. K. S. W. Sing, *Pure Appl. Chem.*, **57,** 603, (1985).
30. P. Wang, Y.-J. Zhao, L.-X. Wen, J. Chen, Zh.-G. Lei, *Ind. Eng. Chem. Res.*, **53**, 20116 (2014).
31. C. Zhong, G. Deng, H. Hu, J. Qiao, L. Zhang, J. Zhang, J. *Chem. Soc. Rev.*, **44**, 7484 (2015).

Mathematical modeling, software simulation and directions of development for waste gas purification from SO_2

K. Vl. Stefanova*, N. Dr. Shukova

Institute of Chemical Engineering, Bulgarian Academy of Sciences, Acad. G. Bonchev Str. Bl.103, 1113 Sofia, Bulgaria

The environment is still awaiting the development of better technologies, apparatus and equipment to reduce gas emissions in the atmosphere, where one of the most hazardous atmospheric air pollutants is sulfur dioxide. The aim of the present work is to study and evaluate the part of the mathematical modeling and software simulations for purification of waste gases from SO_2 in the scientific literature in recent years. For this purpose, the selected articles are grouped and analyzed according to the type of their content and directions of development in order to outline the current approaches to sulfur dioxide removal. Some future development guidelines are also highlighted. The innovative approaches for SO_2 purification of the Institute of Chemical Engineering, Bulgarian Academy of Sciences, are summarized too.

INTRODUCTION

Prolonged global pollution with SO_2 is the cause of various respiratory diseases and is one of the main components of acid rain and urban smog. According to World Health Organization'2021 the average human exposure to SO_2 is 20 $\mu g\,m^{-3}$ per day or 500 $\mu g\,m^{-3}$ for 10 min [1]. Anthropogenic sources of SO_2 are fossil fuels with a substantial sulfur content and pyrometallurgical processes; another 30% of global SO_2 emissions are of natural origin in form of volcanic eruptions and sea contribution. The annual SO_2 loads from 2012 to 2015 over eastern China, Mexico and South Africa are given in [2]. Losses in Chinese agriculture and assessment of accumulated sulfur concentrations in pine needles as a criterion for SO_2 pollution were analyzed in [3] and [4], respectively.

Approaches to reduce SO_2 emissions aim at increasing the efficiency of standard or new technologies by optimizing related processes and environmental use of the raw materials, byproduct and disposal products. In many cases, determining better technology requires a detailed cost-effectiveness analysis.

Increasingly, mathematical modeling and software simulations are being used to generate an effective solution by optimizing existing technologies or predicting the success of innovations. Theoretical approaches are preferred due to low cost, fast results, reduced number of experiments and environmental safety. Some mathematical models of technological processes are so complex that only computer programs can solve them.

The aim of the present work is to study and evaluate the part of the of mathematical modeling and software simulations for SO_2 removal in terms of purification and desulfurization of waste or flue gas in the scientific literature in recent years. The scope of the study is focused on the scientific articles from the years 2020 and 2021. Demand has been extended until 2015, when some of the last limits of permissible harmful emissions into the atmosphere have been adopted. The selected articles are grouped in several sections and are analyzed according to the set criteria for content and direction of development. Some modern presentations of scientific results using software applications are also shown. The role of the Institute of Chemical Engineering, Bulgarian Academy of Sciences in the field of purification of gases from SO_2 is summarized too.

RESULTS AND DISCUSSION

Report of the available literature on the topic

The study began with a search for articles on SO_2 purification in the last 2021 and 2020, including mathematical modeling and software simulations. Most of the first significant articles are only experimental studies. Studies involving mathematical modeling and software simulations are less common, for the 200 articles reviewed, only 11. Then the keywords *modeling* and *simulation* were added to find more articles using theoretical approaches in 2020/2021 and as a result of the search 18 more articles were found. The same approach was implemented for the period down to 2014. As a result of this search, 43 more articles were collected.

---

* To whom all correspondence should be sent:
E-mail: *k.stefanova@iche.bas.bg*

Some modern trends in the presentation of scientific results for SO_2 purification are also listed.

Analyzes according to the type of content

The articles are divided into those containing experiments, mathematical modeling, software simulation and their combinations, a total of six types, see Fig. 1. Fig. 1 shows that the articles are mainly experimental studies with mathematical models of the processes. Unfortunately, theoretical approaches are rarely discussed in reviews, and are found only in Dzhonova-Atanasova *et al.* [5] and Wang *et al.* [6].
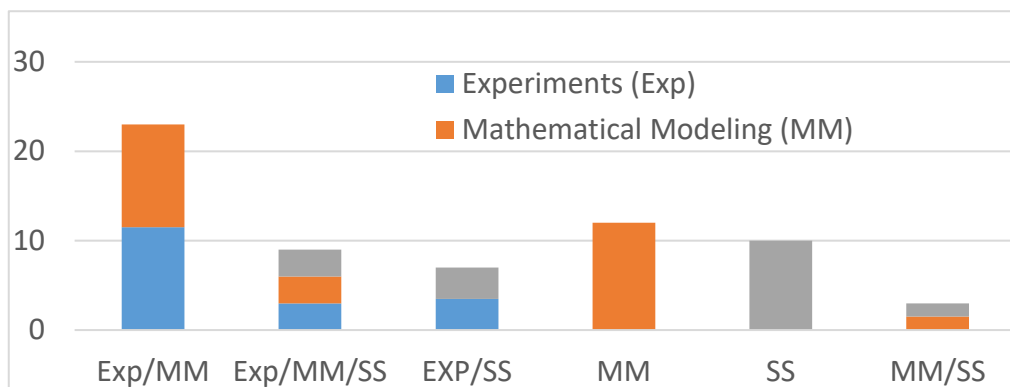
Fig. 1. All chosen articles on SO_2 purification during the years 2015 - 2021 in the study.

Scientific papers presenting only a theoretical approach to new technology, the choice of apparatus and the optimization of equipment for the purification of waste gas from SO_2 and applications of byproduct also occupy a significant part of the considered articles.

There is a tendency to derive mathematical models for each specific process, which allows accurate predicting of future innovative proposals. Valera *et al.* created a neural network to predict the efficiency of SO_2 removal in a spray tower [7]. Models obtained by Vermeulen and an improved linear driving force rate equation were studied for the adsorption of SO_2 on activated carbon particles of different sizes [8].

Mathematical modeling studies are published independently and usually much later after the experiments as the second stage of the research, for example, the proposal of Guo *et al.* for accurate modeling method to predict outlet concentration of wet flue gas desulfurization (FGD) and comprehensive cost model for real - time operational cost estimation [9]. Also in the work of Boyadjiev *et al.* a new approach of the convection-diffusion type model in column apparatuses for gas purification at a low SO_2 concentration in the thermal power plants is proposed. The convection-diffusion type of models allows to create models of average concentration and to give a quantitative description of the absorption processes [10-13]. The team of the Institute of Chemical Engineering, Bulgarian Academy of Sciences, has been working on innovative approaches for SO_2 purification since +1965, leading to many patents and utility models, some of which have been industrially applied, e.g. in the copper mining plant, Elisejna, Bulgaria [14-21]. A waste-free technology for waste gases purification from SO_2 has also been developed by means of regenerable absorbent and adsorbent [22, 23].

Wang *et al.* summarized that compared to the experimental method, the numerical simulation method is more convenient, cheaper and easier to evaluate the overall performances of the tower for SO_2 purification [24]. Abdulrasheed *et al.* clearly state that for further development and understanding of adsorption or cost optimization, computational tools are necessary such as density functional theory, grand canonical Monte Carlo and reactive force field and conductor [25].

The least represented are articles with combinations using software simulation. The reason is that software simulation studies have a rich database of independent operation and reliability of results as using literature data for verification. ASPEN Plus is used for detailed reactor simulations of CuO+CaO supported on inert SiC for coal combustion and separation of the streams of CO_2 and SO_2 and thermodynamic analysis of the process [26]. The energy-minimized structure models of boron nitride nanoflake for hazardous SO_2 capturing are created by a Gaussian program [27]. A disadvantage of the current software simulation is that it is still difficult to insert the established mathematical dependencies for the specific processes in practice, review of the CFD applications [28]. CFD simulations are used when measurements are difficult, relying mainly on generalized equations as analyzing only part of the process. An example for

41

this is the study by Tomanović *et al.* where the gas phase is modeled in Eulerian field, while the particles are tracked in Lagrangian field to predict a boiler unit efficiency [29]. The population balance model combined with CFD is used to characterize the behavior of droplets in the venture scrubber [30].

Analyzes according to the directions of development

The available technologies for SO_2 removal can be divided into two main categories: non-regenerable and regenerable processes. The predominant process for flue gas desulfurization is wet scrubbing using a lime or a limestone slurry. This process can provide 90%-99% sulfur dioxide removal using cheaper raw materials and marketable byproducts (NH_3, gypsum, H_2, N_2O, N_2). The disadvantages are the high cost of installation and large quantities of waste water. Where lower removal efficiencies can be tolerated, spray drying and dry injection processes are more economical. Some improvements with a rare commercial application are the combined removal processes of $SO_2/NO_X/CO_2/VOC$. The disadvantages of the available technologies are the regeneration of catalysts or scrubbing solutions, clogging, corrosion and the accumulation of other pollutants.

The considered articles using theoretical approaches for purification of waste gases from sulfur dioxide are presented in five directions of development (DD), see Fig. 2 and Table 1: DD_1. Innovation absorbents, adsorbents, membranes - types, effective interface surface area, characteristic, quantities; DD_2. Operating conditions - flow rate, pressure drop, inlet and outlet sulfur dioxide concentrations, pH, t, removal efficiency; DD_3. Construction - ease and time of installation, operating and maintenance labor and material, space and sparing requirements; DD_4. New *vs*. retrofit method/ technology/ constructions; DD_5. Cost material and Energy *vs*. Ecological risk. What happens with disposal and byproducts after gas purification?

The efforts of scientists are mainly focused on the use of activated carbon as a proposal for renewable engineering solutions [8, 25] and combined removal processes of $SO_2/ NO_X/ CO_2/ VOC$ [31-39]. The found studies using seawater are for hybrid technologies combined electron beam [9] and wet scrubber to control SO_2 and NOx from a diesel generator [40]. Ionic liquids are characterized by excellent chemical and thermal stability, low vapor pressure and environmental properties. The conclusions are that the costs of some kinds of ionic liquids are extremely high and are still limited [41-43]. Xin *et al*. present a membrane contactor technology as a promising alternative technology for capturing SO_2 using liquid absorbent [44]. Fig. 2 and Table 1 show that mathematical modeling and software simulation regarding operating conditions at waste gas purification from SO_2 are used more frequently. From the distribution of the selected articles by type of content and directions of development it can be seen that only mathematical modeling for innovation material is not found, Table 1.

Our study shows that it is not a small part of the scientific papers using mathematical modeling and software simulation presenting an optimization of the auxiliary equipment, cost material and energy through environmentally friendly solutions.

Future directions of development on the topic

Future development guidelines suggest to use the solar energy in the hybrid systems, as well as the sustainable green conversion of waste into valuable products in order to protect the environment. Koralegedara *et al.* have summarized applications using waste construction materials [80] as a raw material for flue gas desulfurization.
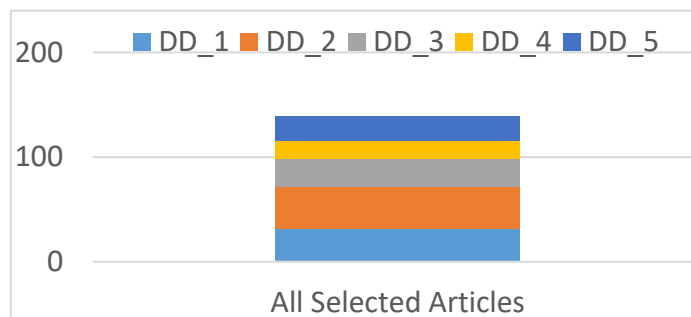
Fig. 2. All selected articles on SO_2 purification during the years 2015 - 2021 by the directions of development. DD_1 Innovation materials; DD_2 Operating conditions; DD_3 Construction adjustment; DD_4 New *vs*. retrofit; DD_5 Cost material and Energy *vs*. Ecological risk.

Table 1. All selected articles on SO_2 purification during the years 2015 - 2021 distributed by the directions of development and the content.

	DD_1	DD_2	DD_3	DD_4	DD_5
Exp/MM	8, 32, 35, 36, 42, 43, 47, 57, 58, 63, 65, 66, 80	7, 8, 31, 32, 33, 34, 35, 36 40, 43, 45, 47 53, 57, 63, 64, 65, 66	7, 8, 33, 34 35, 36, 40, 43, 45, 47, 57, 65	8, 33, 40, 43, 47, 54	8, 33, 43, 45, 47, 63
Exp/MM/SS	29, 30, 38, 51, 55, 60, 72, 73	29, 30, 38, 50, 55, 72, 73	30, 50, 73	30	29, 30, 38, 51
Exp/SS	5, 48, 49, 78	5, 39	5, 39, 56	5, 39, 56	5, 56
MM	no	9, 67, 75, 76, 77	10, 11	10, 11, 61	6, 9, 61, 74, 75, 76
SS	24, 27, 59, 70, 71	24, 46, 59, 68, 69, 70, 71	24, 26, 46, 68, 69	46, 62, 69	26, 46, 62, 69
MM/SS	37	37, 52	37	28, 52	28

(a)

(b)
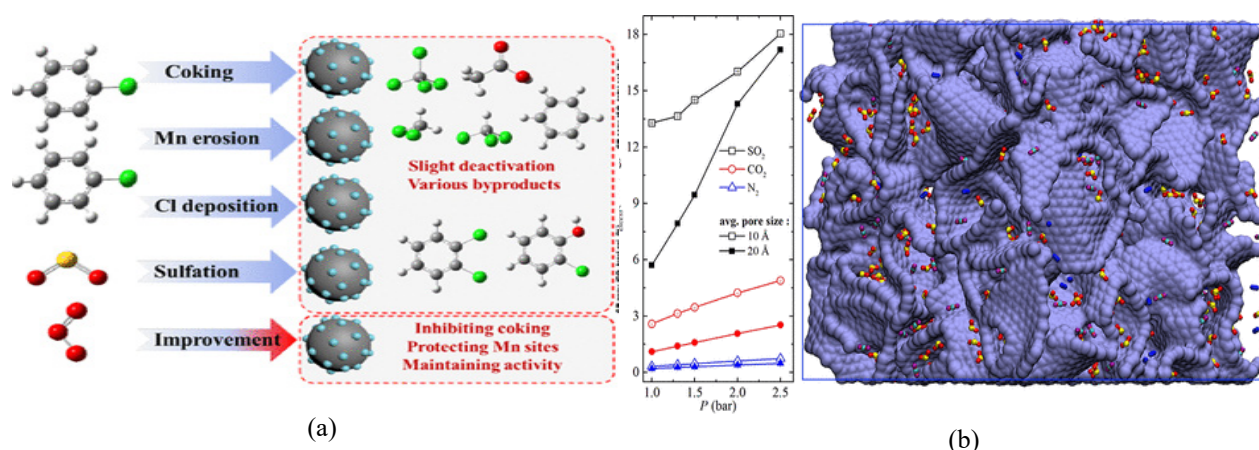
Fig. 3. Presentation of innovation materials (a) Adsorption mechanism by Grand canonical Monte Carlo simulations of a 3D graphene sponge for flue gas stream, Maurya *et al.* [70]; (b) Results and 3D graphics of chlorobenzene oxidation by oxygen and ozone over a simple Mn/Al$_2$O$_3$ catalyst, Tseng and Li [82].

Some new applications in the field are for fertilizer and soil amendment in agriculture and water treatment. The bioscrubbers are proposed as an environmentally friendly and economical alternative for flue gas purification. Advanced oxidation processes (AOPs) as with ozone, UV, hydrogen peroxide are the alternative that is looking for its place for a wider application in SO$_2$ adsorption. Our team is trying to contribute to the development of a waste gas purification process through a technology using an integrated absorption-adsorption process for waste-free decontamination of gas containing SO$_2$ [81].

Some modern trends in presentation of scientific results for SO$_2$ purification for adsorption mechanism using computational tools are shown in Fig. 3. The graphs are characterized by a good visualization of the topic of studies and the corresponding results.

CONCLUSIONS

Analysis was made of articles using mathematical modeling and software simulations as approaches to study of purification of waste gases from SO$_2$ in the scientific literature in recent years. The significance of mathematical modeling and software simulations in terms of the type of content and field of research are discussed and the results are presented graphically and tabular. It seems that among the first articles for sulfur dioxide removal there are rarely articles using mathematical modeling and software simulation, including reviews. Studies still rarely rely on mathematical modeling and software simulations, although they save time and materials for experiments. When laboratory tests cannot be performed, theoretical approaches are used for larger and more difficult objects and tasks.

Our review of modern trends in science in the field of purification of waste gases from SO_2 using mathematical modeling and software simulations provides opportunities to gather ideas and applications. The main problems about the considered multi-stage recycling system are: the need for recovery of the materials after SO_2 removal processes and the difficulty in finding practical realization of the byproducts.

REFERENCES

1. World Health Organization, WHO, Regional Office for Europe (2010).
2. Y. Zhang, C. Li, N. A. Krotkov, J. Joiner, V. Fioletov, C. McLinden, *Atmos. Meas. Tech.*, **10**(4), 1495 (2017).
3. J. Wei, X. Guo, D. Marinova, J. Fan, *J. Cleaner Prod.*, **64**, 404 (2014).
4. J. Likus-Cieślik, J. Socha, P. Gruba, M. Pietrzykowski, *Environ. Pollut.*, **258**, 113559 (2020).
5. D. B. Dzhonova-Atanasova, E. N. Razkazova-Velkova, L. A. Ljutzkanov, *Materials, methods and technologies (CD-ROM)*, **5** (2011).
6. Y. Wang, Z. Wang, Y. Liu, *Energy & Fuels* (2021).
7. V. Y. Valera, M. C. Codolo, T. D. Martins, *Chem. Eng. Res. Des.*, **170**, 1 (2021).
8. Z. Li, Y. Liu, H. Wang, C. J. Tsai, X. Yang, Y. Xing, P. A. Webley, *Chem. Eng. J.*, **353**, 858 (2018).
9. Y. Guo, Z. Xu, C. Zheng, J. Shu, H. Dong, Y. Zhang, X. Gao, *J. Air Waste Manage. Assoc.*, **69**(5), 565 (2019).
10. C. Boyadjiev, M. Doichinova, P. Popova-Krumova, B. Boyadjiev, *Recent Innovations Chem. Eng.*, **7**(1), 39 (2015).
11. C. Boyadjiev, M. Doichinova, P. Popova-Krumova, B. Boyadjiev, *Int. J. Eng. Res.*, **4**(10), 550 (2015).
12. Chr. Boyadjiev, M. Doichinova, B. Boyadjiev, P. Popova-Krumova, Modeling of Column Apparatus Processes, Springer-Verlag, Berlin Heidelberg, 2016, 313 pp.
13. Chr. Boyadjiev, M. Doichinova, B. Boyadjiev, P. Popova-Krumova, Modeling of Column Apparatus Processes (Second edition), Springer-Verlag, Berlin Heidelberg, 2018, 456 pp.
14. D. Elenkov, Chr. Bojadgiev, *IGIC – BAS*, **4**, 167 (1966).
15. D. Elenkov, H. Boyadjiev, *Comptes rendus de l' Academie bulgare des Sciences*, **18**(12), 1141 (1965).
16. D. Elenkov, Chr. Bojadgiev, *Int. Chem. Eng.*, **7**(2), 191 (1967).
17. D. Elenkov, H. Boyadjiev, I. Krastev, L. Boyadjiev, *IGIC – BAS*, **4**, 153 (1966).
18. L. V. Pantofchieva, Chr. Boyadjiev, **28** (3-4), 780 (1995).
19. Chr. Boyadjiev, *Hungarian J. of Ind. and Chem.*, **30**(2), 103 (2002).
20. Chr. Boyadjiev, B. Boyadjiev, M. Doichinova, P. Popova-Krumova, BG Patent 111168 (2012).
21. Chr. Boyadjiev, B. Boyadjiev, M. Doichinova, P. Popova-Krumova, BG Patent 111473 (2013).
22. Chr. Boyadjiev, M. Doichinova, P. Popova-Krumova, B. Boyadjiev, *Chem. Eng. & Technol.*, **37**(7), 1243 (2014).
23. Chr. Boyadjiev, M. Doichinova, P. Popova-Krumova, B. Boyadjiev, *Int. J. Eng. Res.* **4**(10), 557, 2015.
24. S. J. Wang, P. Zhu, G. Zhang, Q. Zhang, Z. Y. Wang, L. Zhao, *J. Energy Inst.,* **88**(3), 284 (2015).
25. A. A. Abdulrasheed, A. A. Jalil, S. Triwahyono, M. A. A. Zaini, Y. Gambo, M. Ibrahim, *Renewable Sustainable Energy Rev.*, **94**, 1067 (2018).
26. R. Joshi, Y. Pottimurthy, V. Shah, P. Mohapatra, S. Kumar, O. Jones, L. S. Fan, *Ind. Eng. Chem. Res.* (2021).
27. M. Mirzaei, E. Karimi, M. Yousefi, *Biointerface Res. Appl. Chem.*, **12**(1), 359 (2022)
28. H. H. Sarakikya, *Doctoral dissertation, Kenyatta University* (2020).
29. I. D. Tomanović, S. Belošević, A. Milićević, N. Đ. Crnomarković, D. R. Tucaković, *Therm. Sci.*, **21**, S759 (2017).
30. S. Zhang, W. Cui, C. Wang, T. Wu, X. Zhao, *Complexity*, (2020).
31. B. Zach, M. Šyc, K. Svoboda, M. Pohořelý, R. Šomplák, J. Brynda, M. Punčochář, *Energy & Fuels*, **35**(6), 5064 (2021).
32. T. L. Chen, Y. H. Chen, P. C. Chiang, *Chem. Eng. J.*, **393**, 124678 (2020).
33. M. A. Fakhari, A. Rahimi, M. S. Hatamipour, A. Fozooni, *Process Saf. Environ. Prot.*, **98**, 342 (2015).
34. V. Gogulancea, V. Lavric, *Plasma Chem. Plasma Process.*, **35**(1), 259 (2015).
35. I. Iliuta, F. Larachi, *Catalysts*, **9**(6), 489 (2019).
36. E. Zwolińska, V. Gogulancea, Y. Sun, V. Lavric, A. Chmielewski, *Radiat. Phys. Chem.*, **138**, 29 (2017).
37. A. Hosseinzadeh, M. Hosseinzadeh, A. Vatani, T. Mohammadi, *Chem. Eng. Process.: Process Intensif.*, **111**, 35 (2017).
38. J. L. Wolf, A. Niemi, J. Bensabat, D. Rebscher, *Int. J. Greenhouse Gas Control*, **54**, 610 (2016).
39. A. G. Chmielewski, E. Zwolińska, J. Licki, Y. Sun, Z. Zimek, S. Bułka, *Radiat. Phys. Chem.*, **144**, 1 (2018).
40. S. Darake, M. S. Hatamipour, A. Rahimi, P. Hamzeloui, *Chem. Eng. Res. Des.*, **109**, 180 (2016).
41. S. Ren, Y. Hou, K. Zhang, W. Wu, *Green Energy Environ.*, **3**(3), 179 (2018).
42. L. Jiang, K. Mei, K. Chen, R. Dao, H. Li, C. Wang, *Green Energy Environ.* (2020).
43. Y. Zhao, J. Dou, A. Wei, S. Khoshkrish, J. Yu, *J. Mol. Liq.*, 117228 (2021).
44. Q. Xin, K. An, Y. Zhang, M. Yun, S. Wang, L. Lin, Y. Zhang, *J. Membr. Sci.*, **620**, 118908, (2021).
45. Y. Liu, N. Sun, Z. Li, P. Xiao, Y. Xing, X. Yang, P. A. Webley, *Sep. Purif. Technol.*, **264**, 118308 (2021).

46. M. I. Lamas, C. G. Rodriguez, J. D. Rodriguez, J. Telmo, *Polish Maritime Research*, **42**(2), (2016).

47. J. Zhu, P. Zhao, S. Yang, L. Chen, Q. Zhang, Q. Yan, *Fuel*, **292**, 120263 (2021).

48. H. Wang, J. Q. Bai, Y. Yin, S. F. Wang, *J. Mol. Graphics and Modell.*, **96**, 107533 (2020).

49. I. Ibarra, E. Martínez-Ahumada, D. He, V. Berryman, V. Jancik, V. Martis, M. Hernandez, *Angew. Chem., Int. Edn.* (2021).

50. X. Kong, P. Xu, K. Fu, D. Gong, X. Chen, M. Qiu, Y. Fan, *Chem. Eng. Sci.*, **231**, 116327 (2021).

51. J. Lee, K. Lee, J. Kim, *ACS Appl. Mater. Interfaces*, **13**(1), 1620 (2021).

52. J. Qu, N. Qi, Z. Li, K. Zhang, P. Wang, L. Li, *Chem. Eng. Process.-Process Intensification,* 108478 (2021).

53. J. Dou, Y. Zhao, X. Duan, H. Chai, L. Li, J. Yu, *ACS omega*, **5**(30), 19194 (2020).

54. H. I. Gonul, M. Bilen, *J. Energy Resour. Technol.*, **142**(8), 082103 (2020).

55. X. Guo, L. Yin, L. Hu, J. Cao, H. Shen, J. Xu, D. Chen, *Fuel*, **280**, 118480 (2020).

56. M. A. Hanif, N. Ibrahim, A. *Environ. Sci. Pollut. Res.*, **27**(22) (2020).

57. K. H. Lejre, P. Glarborg, H. Christensen, S. Mayer, S. Kiil, *Chem. Eng. J.*, **388**, 124188 (2020).

58. K. Silas, W. W. Ab Karim Ghani, T. S. Y. Choong, U. Rashid, *Combust. Sci. Technol.*, **192**(5), 786 (2020).

59. S. Tian, C. Zhang, D. Huang, R. Wang, G. Zeng, M. Yan, W. Wang, *Chem. Eng. J.*, **389**, 123423 (2020).

60. Q. Xin, Z. Hua, Y. Fu, Y. Yang, S. Liu, H. Song, X. Gao, *Fuel*, **279**, 118420 (2020).

61. J. Kim, J. Lee, H. Cho, Y. Ahn, *J. Ind. Eng. Chem.,* **100,** 270 (2021).

62. J. Lee, H. Cho, I. Moon, I. Lubomirsky, V. Kaplan, J. Kim, Y. Ahn, *Comput. Chem. Eng.*, **146**, 107227 (2021).

63. C. K. Rojas-Mayorga, I. A. Aguayo-Villarreal, J. Moreno-Pérez, R. Muniz-Valencia, M. Á. Montes-Morán, R. Ocampo-Pérez, *J. Environ. Chem. Eng.*, **9**(1), 104810 (2021).

64. D. Jaćimovski, R. Garić-Grulović, N. Vučetić, R. Pjanović, N. Bošković-Vragolović, *Powder Technol.*, **303**, 68 (2016).

65. Y. Jia, L. Yin, Y. Xu, Y. Chen, X. Ding, *Chem. Eng. Process.: Process Intensif.*, **116**, 60 (2017).

66. H. Moshiri, H. Ale Ebrahim, B. Nasernejad, *Int. J. Coal Prep. Util.*, **36**(5), 231 (2016).

67. Z. Zhang, Y. Yan, D. A. Wood, W. Zhang, L. Li, L. Zhang, B. Van der Bruggen, *Ind. Eng. Chem. Res.*, **54**(46), 11619 (2015).

68. R. R. AL-Hussari, A. D. AL-Fatlawy, M. H. Al-Aqad, *Am. J. Chem. Eng.*, **3**(1), 19 (2015).

69. A. Arif, C. Stephen, D. Branken, R. Everson, H. Neomagus, S. Piketh, *Conference of the National Association for Clean Air (NACA 2015)*.

70. M. Maurya, J. K. Singh, *J. Phys. Chem. C*, **122**(26), 14654 (2018).

71. D. Zhang, X. Jing, D. S. Sholl, S. B. Sinnott, *J. Phys. Chem. C*, **122**(32), 18456 (2018).

72. Y. Tang, Y. Gao, D. Liu, F. Zhang, S. Qu, Z. Hao, Z. T. Liu, *RSC Adv.*, **7**(38), 23591 (2017).

73. C. Zheng, L. Xiao, R. Qu, S. Liu, Q. Xin, P. Ji, X. Gao, *Chem. Eng. J.*, **361**, 874 (2019).

74. G. Asadollahfardi, A. Khajoo'e, *Modares Civ. Eng. J.*, **16**(2), 9 (2016).

75. V. Gogulancea, I. Calinescu, V. Lavric, *Rev. Chim.*, **66**(11), 1896 (2015).

76. L. D. Pliatsuk, I. Y. Ablieieva, R. A. Vaskin, L. L. Hurets, M. Yeskendirov, *J. Eng. Sci.*, **5**(2), (2018).

77. I. I. Stefas, S. I. Manavi, F. E. Paloukis, D. N. Spartinos, *J. Chem. Technol. Biotechnol.*, **93**(9), 2681 (2018).

78. M. Qiu, X. Kong, K. Fu, S. Han, X. Gao, X. Chen, Y. Fan, *AIChE J.*, **65**(1), 409 (2019).

79. Z. Zhao, Y. Zhang, W. Gao, J. Baleta, C. Liu, W. Li. X. Gao, *Process Saf. Environ. Prot.*, **150**, 453 (2021).

80. N. H. Koralegedara, P. X. Pinto, D. D. Dionysiou, S. R. Al-Abed, *J. Environ. Manage.*, **251**, 109572 (2019).

81. Chr. Boyadjiev, B. Boyadjiev, M. Doichinova, P. Popova-Krumova, BG Patent 111398 (2014).

82. C. C. Tseng, C. J. Li, *Int. J. Heat Mass Transfer*, **116**, 329 (2018).

In vivo comparative assessment of incised wound healing in rats after application of hydrogel/organogel formulation containing St. John's wort methanol extract

S. Stefanov[1]*, S. Stoeva[2], S. Georgieva[3], M. Hristova[5], K. Nikolova[4], M. Dobreva[1],
V. Andonova[1]

[1]Medical University of Varna, Faculty of Pharmacy, Department of Pharmaceutical Technologies, 55 Marin Drinov str., Varna 9000, Bulgaria
[2]Medical University of Varna, Faculty of Pharmacy, Department of Pharmacology, Toxicology, and Pharmacotherapy, 55 Marin Drinov str., Varna 9000, Bulgaria
[3]Medical University of Varna, Faculty of Pharmacy, Department of Pharmaceutical Chemistry, 55 Marin Drinov str., Varna 9000, Bulgaria
[4]Medical University of Varna, Faculty of Pharmacy, Department of Physics and Biophysics, 55 Marin Drinov str., Varna 9000, Bulgaria
[5]Medical University of Varna, Faculty of Medicine, Department of Physiology and Pathophysiology, Training Sector of Pathophysiology, 55 Marin Drinov str., Varna 9002, Bulgaria

Over the years, St. John's wort (*Hypericum perforatum* L.) has been shown to contain important bioactive ingredients with substantial physiological and pharmacological activity. The present study aims to evaluate the healing intensity of incised wounds on rats treated with a semi-solid hydrogel/organogel (bigel) formulation containing a hyperforin-rich extract from St. John's wort. Three methods to obtain hyperforin-rich methanol extract from St. John's wort were applied and evaluated for effectiveness – percolation method, ultrasonic extraction, and Soxhlet extraction. The extracted amount of hyperforin was determined by reverse-phase HPLC analysis. The Soxhlet extraction technique was most appropriate for this study's purposes (3.552 mg/mL). Hyperforin-rich methanol extract was included in a bigel as a semi-solid formulation. The therapeutic potential of the developed formulation was evaluated for healing intensity and compared with a commercial product. Both were applied for 10 days on incised wounds (50 mm) inflicted on rats. The efficacy parameter is defined as the tensile strength applied on already healed wounds through a particular experimental setup. An *in vivo* experiment was performed with 21 male Wistar rats, divided into three groups at random. Group A was not treated with therapeutic products. Groups B and C were treated with a commercial product, and with bigel containing an extract of St. John's wort, respectively. The tensile strength registered for group B ((3.7±0.2) N) was lower than that stated for group C ((6.4±0.7) N). The obtained differences are statistically significant (p<0.05). As a result of the study accelerated and most effective wound healing was found in the experimental group treated with bigel containing St. John's wort extract rich in hyperforin.

Keywords: bigel, *Hypericum perforatum* L., hyperforin, tensile strength.

INTRODUCTION

Plants have long been used as wound healing agents, being a good source of diverse phytocomponents that, compared to synthetic molecules, are easily absorbed by humans and animals and are therefore an alternative model for drug development.

St. John's wort (SJW) has a rich historical background, one of the oldest used in traditional medicine and, therefore, the most extensively investigated medicinal herbs [1]. The medicinal properties of this species were known even back in Hippocrates' time due to its wound/burn healing and anti-inflammatory action [2]. Modern methods of qualitative and quantitative analysis prove the content of a rich palette of biologically active substances (BAS), which are used in the healing of wounds and various skin disorders, as well as in the treatment of diseases of the gastrointestinal, respiratory, and nervous systems (depression) [3].

SJW is the main source of active pharmaceutical ingredients (APIs) such as hyperforins (phloroglucinols) and hypericins (naphtho-dianthrones), and many other BAS, as a broad range of flavonoids (rutin, quercetin, miquelianin, quercitrin, amentoflavone, hyperoside). It has been found that the major BAS in SJW is hyperforin (HPF). The highest HPF concentrations were found in leaves, flowers, and fruits [4].

HPF belongs to the polycyclic polyprenylated acylphloroglucinols family and has a unique architecture. HPF is a mixture of bicyclic interconverting tautomers derived from SJW. The structure contains asymmetric vicinal quaternary centers and a densely functionalized tetracarbonyl

---

* To whom all correspondence should be sent:
E-mail: *stefan.stefanov@mu-varna.bg*

array (Fig. 1) [5]. HPF is poorly stable when exposed to light and oxygen [6]. However, it is quite stable in protic solvents such as methanol and in *in vivo* systems, as well as at low temperatures, which to some extent explains its broad therapeutic potential [7, 8]. HPF exhibits good protective and potent antioxidant and anti-inflammatory activity in topical applications.
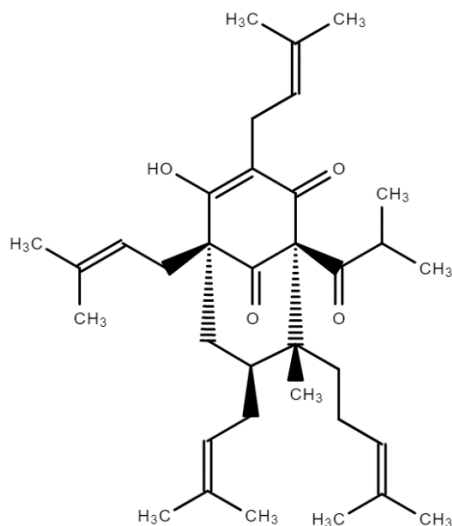
Figure 1. Chemical structure of hyperforin.

Furthermore, HPF does not induce phototoxicity. In dermal application, HPF is used for the treatment of skin diseases, such as neurodermatitis. The treatment with hyperforin-rich extract dermal products leads to improvement of the stratum corneum moisture, subjective skin parameters and reduces skin surface dryness, indicating stabilization and improvement of the barrier [9].

For effective administration of hyperforin, alone or in combination, it is indispensable that an optimal topical formulation has to be used. Furthermore, to ensure the dermal carrier's compliance, compatibility, and stability, it is desirable to consider the lipophilic characteristics of hyperforin and the necessary conditions for skin hydration [10]. In this relation, in the interest of the study, an inherently innovative hybrid dermal dosage form was chosen, optimally meeting the listed criteria.

In the family of semi-solid formulations, bigels are innovative structurally hybridized systems of two different phases – hydrogel and organogel. The symbiosis between these two types of gels allows overcoming some of the main disadvantages of the initial semi-solid systems, namely the limited ability of the hydrogel to penetrate the skin's lipophilic barriers and the low patient compliance of organogel due to its stickiness and oily residues [11]. At the same time, they expressly combine the advantages of the two precursor forms: 1) the ability to include both hydrophilic and lipophilic drug substances; 2) enrichment of hydration of stratum corneum; 3) provision of opportunities for local, transdermal, and modified drug delivery; and 4) improved patient compliance [12].

The present study evaluates the healing intensity of incised wounds on rats treated with a bigel formulation containing a hyperforin-rich extract from SJW. The article describes extracts preparation from SJW (flowers and leaves), determination of HPF, obtaining a bigel for topical application, and wound modeling and assessment.

MATERIALS AND METHODS

Materials

All materials used in the study including SJW dried flowers and leaves powdered to approx. 2 mm (Bilec Company, Bulgaria); methanol (≥99.9%, analytical grade, Fisher Chemical); hyperforin standard (≥ 85%, HPLC grade, Merck, Germany); acetonitrile (> 99.8%, HPLC grade, Fisher Chemicals UK), phosphoric acid (HPLC grade, Acros Organics Germany); double-distilled water (Gesellschaft für Labortechnik mbH, Germany), borago oil (Alteya Organics Bulgaria), poloxamer 407 (Sigma Life Science, USA), sorbitan monostearate (Span® 60, Thermo Fisher Kandel GmbH, Germany), ketamine 5% (Bremer Pharma GmbH, Germany), xylazine 2% (Alfasan Int., Netherlands), jodseptadon 10% (Chemax Pharma Ltd., Bulgaria), sodium chloride 0.9% solution (B. Braun Melsungen AG, Germany) were of pharmaceutical grade.

Methods

Preparation of the experimental extracts. Three different methods for SJW extracts preparation were used – percolation, sonication, and hot Soxhlet extraction, as all of them were performed with methanol in the absence of light.

Extract 1 **(E1)** was obtained by a percolation method in a closed vessel for 24 hours. First, 1 g of SJW was extracted at room temperature with 100 mL of MeOH. Next, the solvent was removed, and the solid residue from the extraction process was compressed to optimize yield. Finally, the liquid obtained after the compression and the solvent removed earlier were mixed and concentrated to a final volume of 50 mL.

Extract 2 **(E2)** was obtained by a sonication method. First, 1 g of dried SJW material was extracted with 100 mL of MeOH for 30 minutes at 40°C in an ultrasonic bath. Then, the reagent used was removed, and a new extraction was performed with 100 mL of MeOH for 30 min at 40°C. Finally,

the two extracts were combined and concentrated to a final volume of 50 mL.

Extract 3 **(E3)** was obtained by the Soxhlet extraction method**.** The plant material of SJW (5 g) was extracted with MeOH (500 mL) for 5 h (approximately nine cycles) in the Soxhlet apparatus [8].

After the condensation, as a general procedure, 1 mL sample of each of the extracts was taken for HPLC analysis, whereafter extracts obtained were shielded from light in dark bottles and stored in a refrigerator at -18°C until subsequent use.

HPF HPLC determination

Chromatographic conditions. The HPLC-UV analysis of HPF was performed with a Thermo Scientific UltiMate 3000 Analytical LC System, equipped with a variable wavelength vibration detector (Dionex UltiMate 3000 VWD) and a diode array detector (Dionex UltiMate 3000 DAD-3000 Diode Array Detector) (Thermo Scientific, USA). Thermo Scientific HYPERSIL GOLD AQ C$_{18}$ (150 mm × 4.6 mm, 5 µm) analytical column, protected by an HYPERSIL GOLD AQ C$_{18}$ (10 mm × 4.6 mm, 5 µm) guard-column, was used. The elution was in isocratic mode with a mobile phase consisting of 0.3 % phosphoric acid and acetonitrile (10/90, v/v). The flow rate was set at 0.8 mL/min, and the temperature of the columns and the autosampler was maintained at 25°C and 10°C, respectively. The wavelength of the UV detector was set at 273 nm, and the injection volume was 20.0 µL. Thermo Scientific™ Chromeleon™ 7.2 Chromatography Data System software™ was used for the systemic control and data analysis.

The qualitative and the quantitative determination of HPF were made according to the retention time and UV spectrum of the substance in the standard samples. In addition, quantitative analysis was performed using the method of external standardization.

Sample preparation

Standard solutions – A standard stock solution of HPF with concentration of 50.0 µg/mL was prepared in methanol. During the development of the method it was found that isocratic elution with acetonitrile and 0.3% aqueous solution of phosphoric acid is most suitable and provides sharp and symmetrical peaks of HPF. After serial dilutions working standard solutions with concentration of 50.0, 40.0, 30.0, 20.0, 10.0 and 1.0 µg/mL were obtained. They were used for calibration curve construction (x = concentration of the standard solutions [µg/mL] and y = peak area [mAU*min]) and method validation.

For method validation, the parameters proposed by the International Conference on Harmonisation (ICH) were evaluated [13].

Test solutions – samples of herbal extracts were filtered with syringe filters Minisart® NY25 (0.2 µm, d = 25.0 mm, Sartorius™, Germany). The so-obtained samples were serially diluted with methanol to obtain specimens with a final concentration of 5.0 µg/mL. After that, six aliquots of each extract were injected into the HPLC system.

Bigel preparation

The two phases (hydrophilic and lipophilic) required for the bigel composition were prepared separately. The hydrogel contains Poloxamer 407 25.0% and purified water 75.0 % (w/w). The organogel contains borago oil 85.0 % (w/w) and Span® 60 15.0 % (w/w). The weighed poloxamer 407 was dispersed in the purified water (25°C, 400 rpm). A stable hydrogel was formed. Span® 60 and E3 (1 mL) were dissolved in borago oil (60°C, 100 rpm). A bigel was obtained at hydrogel/organogel ratio of 70:30. The heated organogel was added step by step to the hydrogel under continuous stirring (500 rpm) to obtain a homogeneous mixture and cool to ambient temperature. Color, homogeneity, consistency, and phase separation of the bigel were inspected visually [14].

Experimental animals

The study was performed on 21 male Wistar rats weighing between 200 and 250g each, provided by the Medical University of Varna, Bulgaria. The animals were situated in plastic cages in a well-ventilated room at a temperature of 22 ± 1°C, relative humidity about 55%, and a 12/12 light/dark cycle was maintained. They were subjected to a standard pellet diet and water *ad libitum* throughout the experiment in the Vivarium of MU-Varna.

The experimental protocol was implemented with the approval of the Commission for Ethical Treatment of Animals at the Bulgarian Food Safety Agency (permit number: 265/02.06.2020). Furthermore, all empirical procedures were conducted according to the relevant institutional and national rules and regulations following the international guidelines (EU Directive, 2010/63/EU for animal experiments), the Basel Declaration [15], and the International Council for Laboratory Animal Science ethical guideline for researchers [16].

Wound modeling by incision

The experimental animals were anesthetized by intramuscular application of 5% ketamine (35.0 mg/kg) and 2% xylazine (5.0 mg/kg). The skin

of the dorsum (thoracolumbar region) of each rat was prepared for aseptic surgery by shaving and sterilization with povidone-iodine (10% cutaneous solution) [17]. Two paravertebral incisions, 5 cm long, located 1.5 cm from the midline on both sides of the rat, were made through the entire thickness of the skin. The wounds were closed with three interrupted surgical sutures and cleaned daily with 0.9% saline [18].

Experimental rats were randomly divided into three experimental groups with 7 animals per group. Group A was defined as a control group without treatment. Group B was defined as a reference group where rats were treated with a medicinal product – multifunctional cream, a blend of herbal extracts from *Aloe Vera*, *Prunus amygdalus*, *Vitex negundo*, and *Rubia cordifolia*. Group C was defined as an experimental group, and animals were treated with a bigel contained SJW extract. The test formulations were administered topically, once daily for a research period of ten days. The sutures were eliminated on the 9th day. On the 10th day, the wound healing strength was determined by measuring the force required to disrupt its integrity. By tensiometer was measured the tensile strength of the repaired skin after simulated surgical wounds with an experimental setup [19], which was constructed in our laboratory (Fig. 2).

Figure 2. Experimental setup for determination of the force of rupture of the wound.

Determination of the force of rupture of the wound

The tensile strength of the treated restored skin is considered a parameter for skin repairing. A force gauge Halda Haldex AB 150 Switzerland, was used to measure the rupture force of the wounds. A calibration model was created to establish the range of values measured with the force meter *(y=0.2086x, R²=0.9991)*.

Statistical analysis

All measurements during the *in vivo* experiment were made seven times. The results shown in the tables are averaged. The standard deviation is calculated. The experimental data were approximated by linear dependences, and the coefficient of determination was obtained. ANOVA: single factor analysis was performed. The rate for statistical significance is defined as the accepted significance level p <0.05.

RESULTS AND DISCUSSION

Three types of extracts were obtained by the described methods and then concentrated to a final volume of 50 mL. Their color and odor were assessed for compliance with the investigated herb. A validated HPLC method was used to quantify HPF in the extracts samples.

Results from the HPLC-UV analysis

Linearity in the range of 1.0 - 50.0 μg/mL was assessed (sixfold analysis) by the straight-line equation (*y = 0.3028x - 0.0053*) and the correlation coefficient (R² > 0.999).

The LOQ of HPF was found to be 1.0 μg/mL referring to a signal-to-noise ratio (S/N ≥ 10). In addition, the comparison of series blank and standard samples showed the ability of the system to detect the target analyte unequivocally (Fig. 3).
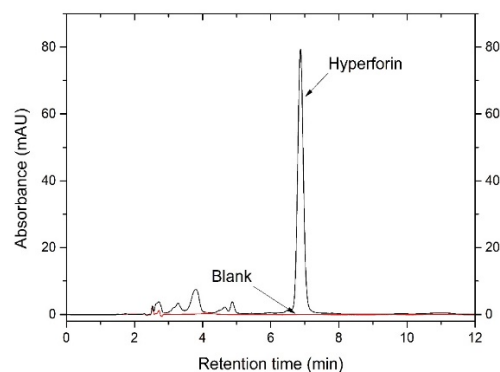
Figure 3. Comparison between a standard sample of HPF (black) and a blank sample (red).

Table 2. Quantitative analysis of HPF in samples.

№	Name of the sample	Peak area [mAU*min]	Sample concentration [µg/mL]	Concentration of plant extract [mg/mL]
1	E1	3.33	11.01	2.20
2	E2	1.93	6.38	1.28
3	**E3**	**5.37**	**17.76**	**3.55**

The developed HPLC method was used to evaluate the analytical yield of the extraction procedures.

The presented results are an argument for the choice of extract E3 obtained by the Soxhlet extraction method, as it provides the highest extraction yield of HPF (Fig. 4 and Table 2).

Bigel preparation

A stable biphasic semi-solid formulation (bigel) for topical use as a vehicle of hyperforin-rich extract of SJW was obtained. A tube inversion test confirmed the gel formation. The bigel formulation had a white color with a creamy appearance and a pleasant scent of borage oil.
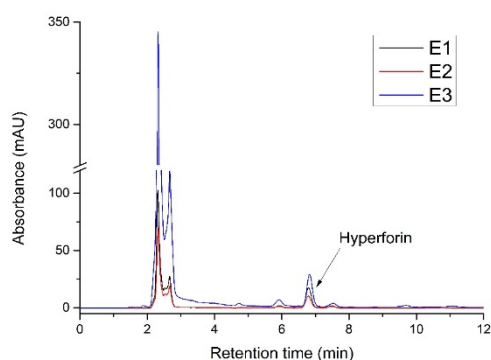
Figure 4. Overlapped chromatograms of test samples (E1 - black; E2 – red; E3 – blue).

Results from in vivo experiment

The effects of the bigel containing E3 extract of SJW were tested over 10 days in an experimental group of 7 rats. The average mass (m, g) required to tear the wounds of rats and the average values for calculated tensile forces (P, N) by groups and their standard deviations are shown in Table 3.

Table 3. Average of tensile forces by groups

Group	m, g	P, N	SD, N
A	397.55	3.95	0.20
B	382.26	3.75	0.23
C	666.67	6.41	0.70

Similar experimental results were found between control group A (without treatment) and reference group B (treatment with the commercial product). The average values of tensile forces for these groups are similar, because they lie in the same confidence interval. The experimental group C, composed of rats treated with bigel containing SJW extract, showed a significant difference and greater forces required to tear the wounds compared to the other 2 groups.

The results obtained from one-way analysis of variance (ANOVA) are presented in Tables 4, 5 and 6.

A statistical difference was found between control and experimental groups as well as between reference and experimental groups. A comparison was made between groups A and B. There is not a statistically significant difference between groups A and B ($F_{critical} > F$). The results demonstrate that the hyperforin-rich SJW extract containing bigel significantly increases the rupture resistance of the healed wound more than in the control and reference groups. These results complement the trends identified in previous studies and confirm the role of hyperforin as a potent anti-inflammatory and antioxidant agent [20, 21]. Undoubtedly, the included borage oil, which has been proven to have broad therapeutic potential, also contributes to these results [22].

Table 4. ANOVA analysis between control group A and reference group B

Source of Variation	SS	df	MS	F	P-value	F crit
Between Groups A and B	0.06	1	0.06	0.33	0.58	4.97
Within Groups A and B	1.85	10	0.19			
Total	1.91	11				

Table 5. ANOVA analysis between control group A and experimental group C

Source of Variation	SS	df	MS	F	P-value	F crit
Between Groups A and C	21.12	1	21.12	19.91	0.0012	4.96
Within Groups A and C	10.60	10	1.06			
Total	31.73	11				

Table 6. ANOVA analysis between reference group B and experimental group C

Source of Variation	SS	df	MS	F	P-value	F crit
Between Groups B and C	23.44	1	23.44	19.81	0.0012	4.96
Within Groups B and C	11.83	10	1.18			
Total	35.27	11				

CONCLUSIONS

The lack of specific wound healing products other than antibiotics, anti-inflammatory, and analgesic medicinal products used in allopathic treatment is one of the main reasons for the continued search for effective alternative resources for this purpose.

This study found accelerated and most effective wound healing in the experimental group treated with bigel containing SJW extract rich in HPF. Further studies of SJW and hyperforin, respectively, for its wound healing properties, will help determine its efficacy and range of application.

REFERENCES

1. A.L. Budantsev, V.A. Prikhodko, I.V. Varganova, S.V. Okovityi, *Pharmacy & Pharmacology*, **9**, 17 (2021).
2. A. Kotsiou, N. Seferos, M. G. Hudu. C. Tesseromatis, *J. Med. Plants Stud.,* **4**, 256 (2016).
3. I.A. Schepetkin, G. Özek, T. Özek, L.N. Kirpotina, A.I. Khlebnikov, M.T. Quinn, *Biomolecules,* **10**, 916 (2020).
4. M. Gaid, P. Haasb, T. Beuerlea, S. Schollb, L. Beerhuesa, *J. Biotechnol.*, **222**, 47 (2016).
5. X-W Yang, R. B. Grossman, G. Xu, *Chem. Rev.*, **118**, 3508 (2018).
6. J. Füller, T. Kellner, M. Gaid, L. Beerhues, C.C. Müller-Goymann, *Eur. J. Pharm. Biopharm.,* **126**, 115 (2018).
7. J-A. Richard, *Eur. J. Org. Chem.,* **2014** ,273 (2014).
8. A. Oreopoulou, E. Choulitoudi, D. Tsimogiannis, V. Oreopoulou, *Molecules*, **26**, 2920 (2021).
9. M. Gaid, E. Biedermann, J. Füller, P. Haas, S. Behrends, R. Krull, S. Scholl, U. Wittstock, C. Müller-Goymann, L. Beerhues, *Eur. J. Pharm. Biopharm.,* **126**, 10 (2018).
10. S. van Rensburg, A. Franken, J. L. Du Plessis, *Skin Res. Technol.,* **25**, 595 (2019).
11. V. Andonova, P. Peneva, G. Georgiev, V. Toncheva, E. Apostolova, Z. Peychev, S. Dimitrova, M. Katsarova, N. Petrova, M. Kassarova, *Trop. J. Pharm. Res.,* **16**, 1455 (2017).
12. A. Shakeel, F.R. Lupi, D. Gabriele, N. Baldino, B. de Cindio, *Soft Materials,* **16**, 77 (2018).
13. ICH Topic Q 2 (R1). Validation of Analytical Procedures: Text and Methodology. European Medicines Agency (1995). https://www.ema.europa.eu/en/documents/scientific-guideline/ich-q-2-r1-validation-analytical-procedures-text-methodology-step-5_en.pdf (Accessed October 26, 2021).
14. V. Andonova, P. Peneva, G. Georgiev, V. Toncheva, E. Apostolova, Z. Peychev, S. Dimitrova, M. Katsarova, N. Petrova, M. Kassarova, *Int. J. Nanomedicine,* **12**, 6221 (2017).
15. The Basel Declaration [cited 2022 Jan 28]. Available from: http://www.basel-declaration.org/basel-declaration/.
16. ICLAS Ethics and Animal Welfare Committee. ICLAS Ethical Guideline for Researchers [cited 2022 Jan 28]. Available from: http://iclas.org/committees/ethics-andanimal-welfare-committee.
17. D. Eyarefe, D. Kuforiji, T. Jarikre, B. Emikpe, *Int. J. Vet. Sci. Med*., **5**, 128 (2017).
18. I. Süntar, E. Akkol, H. Keleş, A. Oktem, K. Başer, E. Yeşilada, *J. Ethnopharmacol.,* **134**, 89 (2011).
19. A. Gomez-Beloz, J. Rucinski, M. Balick, C. Tipton, *J. Ethnopharmacol.,* **88**, 169 (2003).
20. M. Meinke, S. Schanzer, S. Haag, F. Casetti, M. Müller, U. Wölfle, A. Kleemann, J. Lademann, C. Schempp, *Eur. J. Pharm. Biopharm.,* **81**, 346 (2012).
21. U. Wölfle1, G. Seelinger, C. Schempp, *Planta Med*,. **80**, 109 (2014).
22. T.-K. Lin, L. Zhong, J. Santiago, *Int. J. Mol. Sci.,* **19**, 70 (2017).

Drinking water purification in integrated system

M. Stoev*, N. Ivanova, E. Chorbadzhiyska

*Department of Chemistry, Faculty of Mathematics and Natural Sciences, South-West University "Neofit Rilski",
Blagoevgrad, Bulgaria*

The drinking water resources of South-West Bulgaria and particularly in the region of Blagoevgrad are discussed. The main contaminants of tap water, spring water and ground water for drinking purposes are shown. Tap water is that which we get directly from the tap and it may or may not be suitable for drinking purposes. It is used for household purposes such as cleaning, cooking, gardening, laundry and more. The quality of drinking water must comply with the rules set by local municipal authorities. The national and EC requirements for the quality of drinking water are presented. The quality of drinking water is improved locally by filtration, reverse osmosis (RO) and UV disinfection. The applications of local water purification systems as a 7-stage system with RO and UV disinfection and a simple system with filtration, UV disinfection and pump are critically discussed. The 7-stage reverse osmosis system is a system that removes up to 99% of all harmful impurities from water: fluorine, pesticides, chlorine, chloramines, heavy metals, radioactive elements, microorganisms. After chemical analysis of water purification recommendations for a local improving quality of water by applications of advanced innovative water purification systems are presented.

Keywords: Drinking water, Filtration, Reverse osmosis, UV disinfection, Water purification systems

INTRODUCTION

Water is one of the most important natural resources on the Earth [1]. Although a large part of our planet (71%) is covered with water, only a small part can be used for drinking purposes (about 1%) [2]. Water consumption depends on various factors. The daily requirement of water for an adult male is 3 *l/day,* and for an adult female – 2.2 *l/day.* Water performs important functions to support the human body:

- is a vital nutrient for the life of every cell in the human body;
- regulates external body temperature through sweating and breathing;
- metabolizes and transports in the blood carbohydrates and proteins that the human body uses as food;
- physiologically removes waste from the human body through urination;
- lubricates the joints;
- forms saliva.

There are organic, inorganic and microbiological contaminants in the water.

Organic pollution is related to the pollution of water with organic matter. The latter comes from domestic, agricultural or industrial sources. The organic matter is then decomposed by microorganisms and the process is accompanied by the consumption of dissolved oxygen in the water. Toxic metals and organic pollutants have become serious environment issues because these contaminants can cause indelible damage to human health and aquatic organisms [3]. Human activities such as mining, coal burning, and manufacturing (especially battery production) contribute to the discharge of toxic metal pollutants into surrounding water bodies, and there are negative health impacts coming from intake of these pollutants even at low concentrations [4, 5]. Organic pollutants threaten human health and deteriorate water quality due to their biotoxicity and carcinogenesis [6].

Microbiological - the contamination of water with pathogenic bacteria, viruses, some fungi, parasitic worms, etc.

Inorganic pollution is associated with the entry into the water of minerals, chemicals and toxic substances. The most serious sources of inorganic pollutants are the enterprises of the metallurgical, machine-building, ore-mining and coal-mining industries; plants for the production of acids, building materials and mineral fertilizers; the timber industry and the woodworking industry; water transport and others [7].

The composition of natural waters depends on the geo - and biochemical characteristics of the region, on the natural course of physical, chemical and biological processes, as well as on human activity. The chemical composition of natural waters depends on their origin, climatic, chemical, geological and biological characteristics of the region and ongoing processes. Depending on the concentration, the chemical elements are divided into:

Main (> 1 g/l) - Na, K, Mg, Ca, Cl, S, C, O;

---

* To whom all correspondence should be sent:
E-mail: *mstoev@mail.bg*

P, Si, Sr, Mn;

Remains (< 10^{-4} g/l) - Pb, Cd, Ni, Co, Cr, etc. [8].

In recent years, due to the ever-increasing pollution of water from human activity, the need to find a way to its purification and protection is constantly growing. However, some scientists suggest that a "water crisis" is approaching. In order to slow-down and even eliminate the possibility of a water crisis, the following methods of water purification have been developed:

- Physical purification (mechanical, primary);
- Physico-chemical purification;
- Dry cleaning;
- Biological (secondary) treatment;
- Purification (tertiary);
- Decontamination;
- Sludge treatment.

The choice of treatment method depends on the nature of the contamination and the degree of harmfulness of the impurities [9].

When consuming water with indicators above the permissible limits, various pathogenic conditions are observed. With prolonged consumption of water with higher than the acceptable concentrations of arsenic, it accumulates in the thyroid gland and develops endemic goiter. Arsenic also affects the nervous, cardiovascular and respiratory systems, skin and other organs.

Chromium is a carcinogen. According to the World Health Organization Guidelines for Drinking Water Quality (2004), the permissible limit for chromium in drinking water (0.05 mg/l) is indicative only, as there is no conclusive evidence that chromium entering human organism through drinking water causes an immediate health risk [10].

In normal countries for arsenic-contaminated areas drinking water treatment plants are built for the purpose of continuous water quality monitoring and sustainable guarantee of arsenic values in the water below 10 µg/l. For example, to eliminate highly toxic concentrations of arsenic and chromium from water a three-layer filter is constructed, representing ionosorption column [11]. There are also Bulgarian funds for removal of arsenic from polluted waters [12-15].

Nitrates are a major contaminant of groundwater in Bulgaria. Excess levels of nitrates are the most common problem in terms of the physicochemical characteristics of drinking water. Excessive levels of nitrates in the water can cause the development of the disease "water-nitrate methemoglobinemia" in infants and young children. In iodine-deficient areas, it can lead to an increase in the frequency of endemic goiter in adolescents. The methods for reducing nitrates in the waters used for drinking and

household needs, known in practice, are ion exchange and reverse osmosis [10].

If the acceptable concentration of fluorides is exceeded, the disease dental fluorosis may be developed, in which fluoride accumulates in the teeth, changes their color, and damages their enamel, which makes them brittle and crumbly. Prolonged exposure to high levels of fluoride through drinking water can also lead to the development of skeletal fluorosis, which affects the entire skeletal system. Several methods are known reducing the content of fluorides in drinking water – filtration by reverse osmosis, distillation filtration, activated carbon filter for defluorination of aluminum and others.

Manganese belongs to the group of heavy metals. Studies show that consuming water with manganese exceeding the acceptable concentration of the metal leads to a decrease in children's intellectual abilities. Constant use of such water can provoke the appearance of serious diseases of the skeletal system. Manganese is an extremely toxic element that has a destructive effect on the nervous and blood systems.

Water chlorination is the most common way to disinfect drinking water, using chlorine gas or chlorine-containing compounds that react with water or salts dissolved in it, but it is also very harmful to the body. The use of chlorinated water during pregnancy can lead to birth defects in children - in particular, heart and brain defects. With prolonged consumption of chlorinated water, different types of diseases develop - cancer, endemic goiter, heart disease, anemia, hypertension and others.

Drinking water is fresh water with a high degree of purity. It must be free of heavy metals, pesticide residues, hormones, antibiotics, bacteria, viruses and other toxic impurities. The content of mineral substances should not exceed the permissible limits [16]. Chlorine compounds are used in the central water supply for disinfection of water and pipelines to destroy harmful microorganisms that cause diseases.

Bulgaria is one of the countries in the world richest in mineral waters of natural origin, with unique composition and drinking qualities. According to the National Register of the Ministry of Health (2019) 22 companies bottle natural mineral waters in Bulgaria [17].

In Bulgaria, the quality of water intended for drinking and household purposes is controlled by Ordinances 9 and 12 on the Quality of water for drinking and household purposes [18, 19]. In recent years, due to the ever-increasing water contamination from human activity, the need for its purification is constantly growing.

53

There are various methods for water purification:

- Physical purification - used for coarse substances separation;
- Physico-chemical purification - used for finely suspended particles in water;
- Chemical purification - used for pH adjustment and removal of some solutes;
- Biological purification - used for conversion of biological substances from wastewater into biomass;
- Filtration - used for removal of suspended, colloidal and dissolved contaminants;
- Disinfection - used for pathogenic bacteria removal [9].

The hardness of water is due to the calcium and magnesium ions contained in it, usually bound as carbonates. Water hardness (Table 1) is most often expressed as the equivalent of milligrams of $CaCO_3$ per liter or measured in degrees (°dH). 1°dH = 17.8 mg / l $CaCO_3$. Hardness can also be determined by what salts remain in the water after boiling. The salts determining the carbonate hardness fall to the bottom as a precipitate. For example, for calcium:

$$Ca(HCO_3)_2 \leftrightarrow CaCO_3\downarrow + H_2O + CO_2 \uparrow$$

CO_2 evaporates at boiling, and sparingly soluble $CaCO_3$ precipitates and forms white deposits on the walls of the vessel.

Table 1. Scale for assessing water hardness [24]

$Ca^{2+} + Mg^{2+}$ mg/l	°dH	Hardness
0-17	0-4	Very soft water
17-60	4-5	Soft water
60-120	9-12	Medium hardness
120-180	19-25	Moderate hardness
>180	>25	Hard water

Sixty years ago, Kobayashi [20] reported a link between water chemistry and the risk of cardiovascular disease [21]. A lot of the data show that harder water has a lower risk of disease and an association may explain why heart disease deaths are more common in the coastal areas of the United States than in the Midwest [22].

Distilled water or demineralized water is that in which the water has been subjected to a treatment which removes all its minerals and salts by reverse osmosis and distillation. This is an absolutely pure form of water, but is not usually recommended for drinking. It can cause mineral deficiency because it is devoid of any salts and most of the natural minerals in the water have been removed as a result of this process. Drinking this water can lead to rapid loss of sodium, potassium, chloride and magnesium [23].

In different regions of Bulgaria, the water has different hardness (see Fig. 1).

The purpose of this research is quality improvement of tap and spring water in Blagoevgrad region for drinking purposes through the use of local purification systems with filtration, reverse osmosis and UV disinfection. Physico-chemical characteristics of water from the water supply network, drilling and spring waters in the Blagoevgrad region were determined. A 7 - stage system with reverse osmosis and UV disinfection for tap water purification was used. Water filtration system and UV disinfection for spring water purification was used too. A cascade system for spring water purification for drinking and technical purposes was constructed and applied.

Reverse osmosis is increasingly used in drinking water supply for treatment of fresh water sources which can directly result in high-quality water. In practice reverse osmosis is never applied directly on fresh water sources, predominantly because of the occurrence of membrane fouling [25].

MATERIALS AND METHODS

Eleven different water types were analyzed (see Table 2). The tap water from Blagoevgrad was additionally purified through a 7-stage reverse osmosis system with UV disinfection (module 1). Some of the waters have been treated by a filtration and UV disinfection system (module 2). Some of the samples also passed through a cascade system (modules 1 and 2).

The groundwater from the villages of Bistritsa, Kovachevica, Blagoevgrad District was not subjected to the systems for additional purification and quality of the driver, as it has very good indicators and no improvement is necessary.

Drilling water from the village of Buchino - 6 m depth was not further purified through the system as it has a very high hardness and electrical conductivity and after additional purification the filters will have to be replaced with new ones because they will be quite dirty.

For the same reason, tap water and drilling water - 55 m depth from the village of Bozduganovo, Stara Zagora District, were not allowed through the systems.

For the bottled Pirinska mineral water "PREDELA" only analyses of the physico-chemical characteristics were made and then they were compared with those of the groundwater from the

"Predela" area. Some of the main physico-chemical characteristics according to Ordinances 9 and 12 for Water quality for drinking and household purposes of these waters were determined: physico-chemical characteristics: total hardness (°dH), Ca^{2+} (mg/l), Mg^{2+} (mg/l), pH; electrical conductivity.

The electrical conductivity was determined with a Hanna DIST 4 EC Tester conductometer with 0.01 μS / cm resolution - HI98303 calibrated with NaCl solution.

Fig. 1. Water hardness map of Bulgaria, measured in °dH [24]

Table 2. Analyzed waters and systems for improving their quality.

№	Samples	Module 1	Module 2	Module 1 and Module 2
1	Tap water located in Blagoevgrad	yes	-	-
2	Groundwater located in Park „Bachinovo", Blagoevgrad	-	yes	yes
3	Groundwater located in the village of Bistritsa, Kovachevitsa area, Blagoevgrad District	-	-	-
4	Groundwater located in the village of Belo Pole, Blagoevgrad District	-	yes	yes
5	Drilling water located in "Strumsko" Housing Estate, Blagoevgrad, drilling - 11 m	-	yes	yes
6	Drilling water located in the village of Buchino, drilling - 33 m	-	yes	yes
7	Drilling water located in the village of Buchino, drilling - 6 m	-	-	-
8	Tap water located in the village of Bozduganovo, Stara Zagora District	-	-	-
9	Drilling water located in the town of Radnevo, Stara Zagora District, drilling - 55 m.	-	-	-
10	Groundwater (Rilska water) located in the "Predela" area		yes	yes
11	Bottled Pirinska mineral water "PREDELA"	-	-	-

Fig. 2. 7 - stage reverse osmosis system with UV – disinfection (Module 1).

Fig. 3. Spring water purification system with filtration and UV – disinfection (Module 2).

The water hardness is related to the determination of the concentration of Ca^{2+} and Mg^{2+}. First, the total concentration of the two ions was determined. Mg^{2+} was then precipitated in a separate sample by raising the pH and only Ca^{2+} was titrated in this solution. The difference in the two titrations gives the amount of Mg^{2+}. The hardness of water is calculated in German degrees by the formula:

$$\frac{V_T \ N_T EM_{CaO}}{V_{pr}} \cdot 100$$

where V_T is the volume of the titrant; N_T is the normality of the titrant; EM_{CaO} - the equivalent mass of CaO; Vpr - the volume of the sample. pH was measured on a Hanna pH meter. Reverse osmosis system with UV disinfection was used (see Fig. 2). Additional information is presented in Supplementary.

This sytem was delivered to the Department of Chemistry, part of Faculty of Mathematics and Natural Sciences at the South-West University "Neofit Rilski" by "Pavirani" company. The 7-stage reverse osmosis system with UV disinfection purifies the water from all available contaminants [26].

With the three pre-filters - a 20 micrometer filter, an activated carbon filter and a 5 micrometer filter, the water is purified from sludge and chlorine and prepared for fine filtration with a reverse osmosis membrane. After passing through the membrane, the water is clean, without chemical compounds, without heavy metals and other substances. Up to this stage the so-called technical water is obtained - it has not passed through the mineralizer. It is suitable for technical purposes. In the next stage, the water passes through a filter of activated carbon from coconut shells, which aims to remove chlorine,

pesticides, and organic compounds. The mineralizer enriches the water with useful minerals such as calcium and magnesium, giving the water the qualities of slightly mineralized table water. The system also contains an ionizer, a UV sterilizer and a TDS meter [26, 27]. A spring groundwater purification system with filtration and UV disinfection, which consists of a reverse osmosis diaphragm pump, necessary to supply water to the system through a certain pressure; filter column with mechanical filter of 20 and 5 micrometers, activated carbon filter, UV lamp, TDS meter and tank for collecting purified water are presented in Fig. 3. Characteristics of the diaphragm pump for reverse osmosis and of grid tie PV generator are presented in Supplementary.

Figure 4 shows the cascade system (consisting of two modules – Module 1 and Module 2) for spring water purification, which is assembled by us. It is a combination of the two systems - a system with filtration and UV disinfection and a purification system with reverse osmosis. The electricity consumed for the pump and UV lamps is "green" from building integrated photovoltaic systems to the laboratory. Thus, such a water purification system together with the photovoltaic system can be used in regions that are isolated from the energy system.

Fig. 4. Cascade spring water purification system

RESULTS AND DISCUSSION

The results of Blagoevgrad tap water (without prior purification), water purified with a 7-stage reverse osmosis system for obtaining drinking and technical water and tap water from Bozduganovo are presented in Fig. 5. The physico-chemical indicators - total hardness (°dH), Ca^{2+} (mg/l), Mg^{2+} (mg/l), pH and the electrical conductivity are compared.

The technical water is a better solvent for detergents, better extracts coffee and tea and leaves no traces after washing glass surfaces.

From the analyses made technical water has the lowest hardness (lowest content of Ca^{2+} and Mg^{2+}) and conductivity compared to the other two waters. This result is related to the fact that the technical

water hasn´t passed through the mineralizer, but only through the three filters and the reverse osmosis membrane.

The water from the pipeline in Blagoevgrad is soft. After passing through the system, it is enriched with Ca^{2+} and Mg^{2+} and purified.

The wastewater during the treatment of water from the pipeline in Blagoevgrad has low mineralization and this allows it to be collected and fed into the cascade system for additional treatment. This saves water.
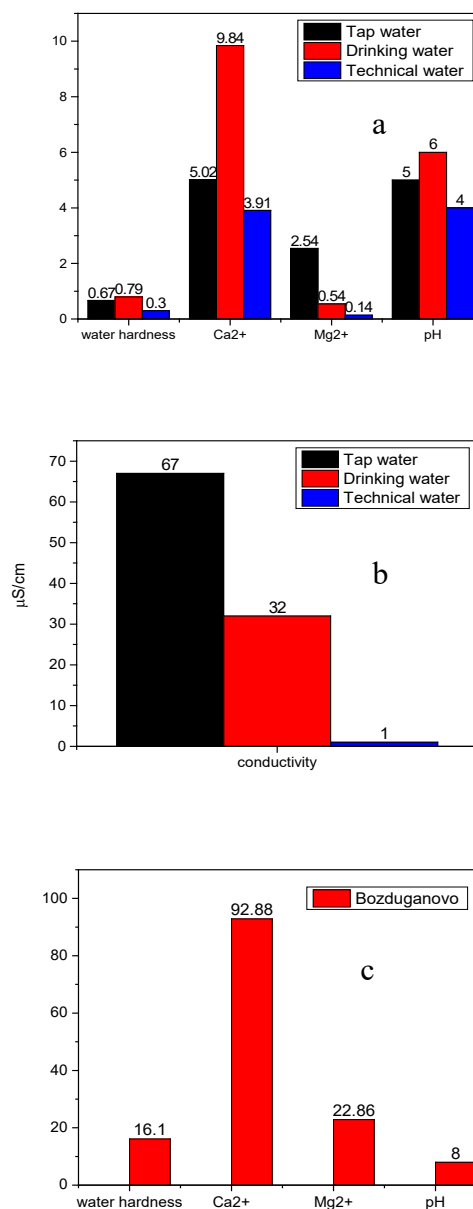

Fig. 5. Blagoevgrad tap water (without prior purification), purified with a 7-stage reverse osmosis system for obtaining drinking and technical water: a) Comparison of physico-chemical characteristics; b) Comparison of the electrical conductivity; c) Tap water from Bozduganovo – physico-chemical characteristics.

There is a significant difference in the content of Ca^{2+}, Mg^{2+}, total hardness and pH of tap water from Blagoevgrad and Bozduganovo. The high levels of these physico-chemical characteristics of the tap water in the village of Bozduganovo in comparison with those of the tap water from Blagoevgrad show that the water is much harder.

The results of the physico-chemical characteristics and the electrical conductivity research of groundwater located in the village of Bistritsa, from Park "Bachinovo" and the village of Belo Pole are presented in Figure 6. The groundwater from the village of Bistritsa has the best characteristics. It is softer compared to the water from "Bachinovo" and the village of Belo Pole due to the lower levels of Ca^{2+} and Mg^{2+}. The water from the village of Bistritsa has the lowest electrical conductivity again, which makes it best for drinking and for technical purposes in comparison with the other two water sources.
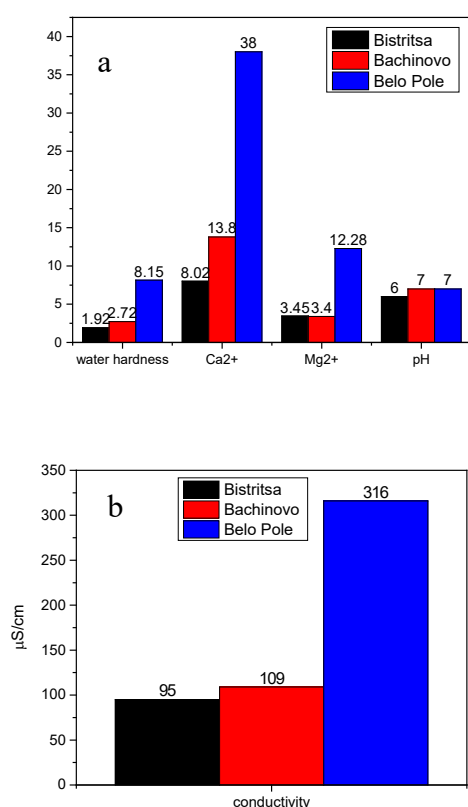
mineralization – medium-hard water. This water is suitable for drinking needs for daily consumption. Figure 7 shows the results of the physico-chemical characteristics - total hardness (°dH), Ca^{2+} (mg/l), Mg^{2+} (mg/l), pH analyses of drilling waters taken from different sources. The water from groundwater drilling in the village of Buchino - 6 m depth is the hardest one and the water taken from the groundwater drilling in the town of Radnevo (55 m depth) is the softest due to several factors. For instance: deep water is cold and the solubility of salts is lower than in other water, which is at a higher level. Water up to 6 m is more suitable for watering than for drinking purposes, as there may be various impurities due to soil fertilization. The EU is considering a ban on the use of manure, as there are no guaranteed ingredients, i.e. it may contain heavy metals, which can lead to water contamination. And to impose the use of fertilizer, which has a certain composition.

Fig. 6. Groundwater water: a) Comparison of physico-chemical characteristics; b) Comparison of the electrical conductivity.

The analyses of groundwater drilling water located in the village of Buchino - 33 m depth of the incoming water, revealed that the water has a high electrical conductivity, a higher content of magnesium than calcium ions and a high
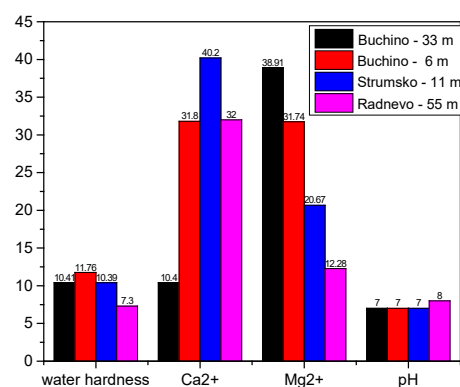
Fig. 7. Drilling groundwater - physico-chemical characteristics of a water located in the village of Buchino, "Strumsko" Housing Estate, Town of Radnevo.

The groundwater water in Predela area is softer compared to the Predel mineral water due to the higher levels of Ca^{2+} and Mg^{2+} (see Fig. 8). The electrical conductivity depends on the water mineralization; the water purity is judged by the electrical conductivity. For this purpose, there are conductometers mounted on the system.

The conductivity of different water types (tap water located in Blagoevgrad, tap water located in the village of Bozduganovo, drilling located in the village of Buchino - 33 m depth, drilling located in the village of Buchino - 6 m depth, drilling located in "Strumsko" Housing Estate - 11 m, drilling located in the town of Radnevo - 55 m depth, groundwater from "Predela" area and bottled mineral water "PREDELA") are presented in Figure 9.
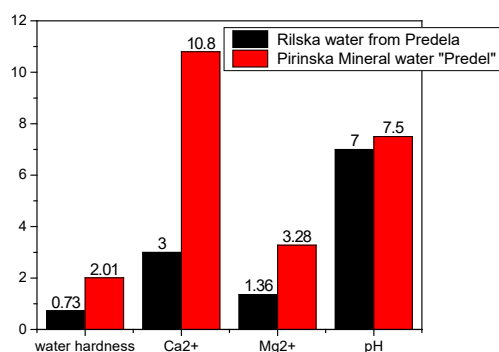
Fig. 8. Comparison of physico-chemical characteristics of groundwater.

The drilling water from the town of Radnevo (55 m depth) has the highest electrical conductivity, and the Pirin groundwater water from the "Predela" area has the lowest one.
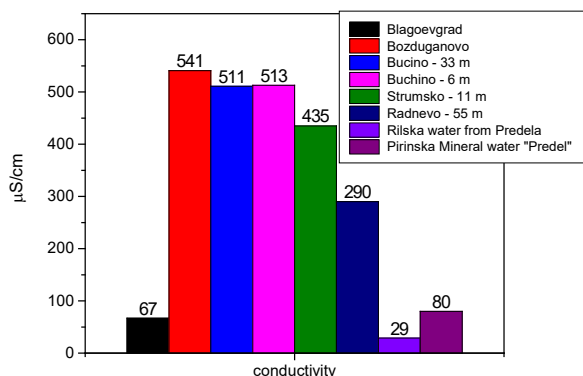
Fig. 9. Comparison of the electrical conductivity.

CONCLUSION

Local purification of tap water with a 7 - stage reverse osmosis system with UV disinfection improves its quality for drinking and technical purposes. The quality of groundwater for drinking purposes is improved by means of a local purification system with filtration and UV disinfection. By using a cascade system with a pump, powered by a photovoltaic generator in isolated areas of the energy system, local purification of groundwater for drinking purposes with initial and lower mineralization, as well as technical water is achieved. The most suitable waters for drinking purposes in Blagoevgrad Region are:

(i) Groundwater located in the villages of Bistritsa, Kovachevitsa, Blagoevgrad District;
(ii) Groundwater located in Park „Bachinovo", Blagoevgrad;

(iii) Groundwater (Rilska water) located in the "Predela" area;
(iv) Bottled Pirinska mineral water "PREDELA";
(v) Blagoevgrad tap water after local purification at home.

Suitable for drinking purposes, from drilled ground waters, after local filtration and UV disinfection are those located in the town of Radnevo (55 m depth) and in the village of Belo Pole (33 m depth).

REFERENCES

1. http://vikblg.com/.
2. Development of a Rural Water and Sanitation Safety Plan Guide - Part B, Second Revised Edition https://www.wecf.org/wp-content/uploads/2017/02/WSSP-compendium-Part-B-Bulgarian.pdf
3. J. Wanga, S. Zhanga, H. Caoa, J. Maa, L. Huanga, S. Yub, X. Maa, G. Songc, M. Qiud, X. Wanga, *Journal of Cleaner Production*, **331**, 130023 (2022).
4. X. Chen, L. Huang, J. Liu, D. Song, S. Yang, *Energy,* **239**, 121897 (2022). https://doi.org/10.1016/j.energy.2021.121897.
5. J. Wang, J. Zhang, L. Han, J. Wang, L. Zhu, H. Zeng, *Adv. Colloid Interface,* **289**, 102360 (2021). https://doi.org/10.1016/j. cis.2021.102360.
6. Y. Wu, B. Li, X. Wang, S. Yu, H. Pang, Y. Liu, X. Liu, X. Wang, *Chem. Eng. J.* **378**, 122105 (2019a). https://doi.org/10.1016/j.cej.2019.122105.
7. D. Bardukova, Pollution and water protection, University of agribusiness and rural development edition, ISSN 1314-5703.
8. T. Todorov, Forms of existence of transition metals in surface waters. Bulgarian Academy of Sciences, Institute of General and Inorganic Chemistry, 2011. http://www.igic.bas.bg/wp-content/uploads/2020/08/Abstract_BG.pdf
9. Ju. Chervenkova, Methods for water purification, University of agribusiness and rural development edition, ISSN 1314-5703.
10. http://eea.government.bg/bg/soer/2014/water/kachestvo-na-piteynite-vodi
11. V. Campos, J. I. Sayeg, P. M. Buchler, *Communications in Soil Science and Plant Analysis*. **39** (11 &12), 1670 (2008).
12. T. Budinov, N. Petrov, G. Bardarska, *Water Problems*, **35**, 39 (2005).
13. Hr. Dobrev, P. Dobrev, G. Bardarska, *Water Affairs*, **1**, 28 (1994).
14. Hr. Dobrev, G. Bardarska, *Water Case*, **1/2,** 25 (2001).
15. T. Budinova, N. Petrov, M. Razvigorova, J. Parra, P. Galiatsatou, *Ind. Eng. Chem. Res.*, **45**, 1896(2006).
16. https://bg.wikipedia.org/wiki/%D0%9F%D0%B8%D1%82%D0%B5%D0%B9%D0%BD%D0%B0_%D0%B2%D0%BE%D0%B4%D0%B0

17. V. Lyubomirova, V. Mihaylova, R. Djingova, *J. of Food Composition and Analysis,* **93,** 103595 (2020), https://doi.org/10.1016/j.jfca.2020.103595.

18. Ordinance № 9 of 16 March 2001 on the quality of water intended for drinking and household purposes.

19. Ordinance № 12 of 18.06.2002 on the quality requirements for surface waters intended for drinking and domestic water supply.

20. J. Kobayashi, *Berichte d. Ohara Instituts*, **11,** 12 (1957).

21. L. M. Klevay, G. F. Combs, Jr., Mineral elements related to cardiovascular health. Nutrients in drinking water, World Health Organization, Geneva, 2005, p. 92.

22. P. E. Enterline, A. E. Rikli, H. I. Sauer, Hyman, M. Geographic Variations in CHD risk. Pub. Health Rep. 75, 1960, p. 759.

23. S. Sengupta, Types of Water: 7 Different Types of Water And Their Purposes, https://food.ndtv.com/food-drinks/types-of-water-7-different-types-of-waters-and-their-purposes-1770281

24. http://energywater.bg/mapa-tvrdosti-vody/

25. E. R. Cornelissen, D. J. H. Harmsen, B. Blankert, L. P. Wessels, W. G. J. van der Meer, *Desalination*, **509,** 115056 (2021). https://doi.org/10.1016/j.desal.2021.115056.

26. https://pavirani.com/7_%D1%81%D1%82%D0%B5%D0%BF%D0%B5%D0%BD%D0%BD%D0%B0_%D1%81%D0%B8%D1%81%D1%82%D0%B5%D0%BC%D0%B0_%D0%B7%D0%B0_%D0%BE%D0%B1%D1%80%D0%B0%D1%82%D0%BD%D0%B0_%D0%BE%D1%81%D0%BC%D0%BE%D0%B7%D0%B0_%D1%81_tds_%D0%BC%D0%B5%D1%82%D1%8A%D1%80-1953.html

27. https://aquafilter.com/en/product/29/105/afxpomp.

DFT investigation of the radical-scavenging activity of biogenic amines

Y. Nacheva[1], A. Garkinin[2], I. Trenchev[2], Zh. Velkov[1*]

South-West University "Neofit Rilski", Blagoevgrad, Bulgaria
[2]University of Library Studies and Information Technologies (ULSIT), Sofia, Bulgaria

It is known that some biogenic amines reduce the level of active radicals in the body. On the other hand, they have a catechol fragment in their molecule. The presence of this fragment is directly related to radical scavenging activity in flavonoids and phenolic acids. To date, however, there is no comprehensive theoretical investigation of the structural causes of such activity in biogenic amines. In this study, 13 biogenic amines were investigated using the DFT/UB3LYP functional and the orbital basis 6-311++G(d,p). It was found that their radical scavenging activity is comparable and in some cases greater than that of phenolic acids. The role of the side chain and of the amino group was evaluated.

Keywords: biogenic amines; radical-scavenging activity; DFT, enthalpy changes.

INTRODUCTION

Biogenic amines (BA) are polar or low-polar nitrogen bases (Scheme 1) comprising an aliphatic chain (putrescine, cadaverine, spermine, and spermidine), a benzene (tyramine, phenylethylamine) or heterocyclic ring (histamine, pyrrolidine) [1]. According to their physiological functions and the number of amino groups [2] they can be divided into (i) monoamines – containing one amino group and acting as neuromodulators or neurotransmitters [3], their reduced level in the organisms is a cause of neurodegenerative diseases [4]; and (ii) polyamines – which own two or more amino groups and are involved in physiological processes such as cell growth and differentiation [5].

At neutral pH they form ammonium cations which stabilize the structure of chromosomes and membranes by electrostatic interactions with negative charges of nucleic acids and phospholipids [6-8]. These compounds can be toxic when present in higher concentrations [9], but on the other hand,

BAs are compounds that are crucial for maintaining cell viability, as well as the right direction of the organism's metabolic processes, such as protein synthesis, hormone synthesis and DNA replication.

A possible antioxidant role of BA has been reported in the literature. Catecholamines and their metabolites appear to play a key role in the redox balance for the formation of new synapses and the removal of old ones [10], while melatonin and its metabolites are involved in the reduction of oxidative stress [11]. Among polyamines, it has been found that spermine acts as a free radicals' scavenger in nuclei, mitochondria and brain [12-14] and as a radical-scavenger in lipoperoxidation *in vivo* [15].

The ability of phenols to react directly with radicals can be assessed by the enthalpy change of the dissociation of its readily breakable O-H bonds. Calculating the enthalpies of dissociation of the O-H bond by different mechanisms shows the most preferred among them and the proclivity of compounds to participate in reactions with active radicals – radical-scavenging activity.
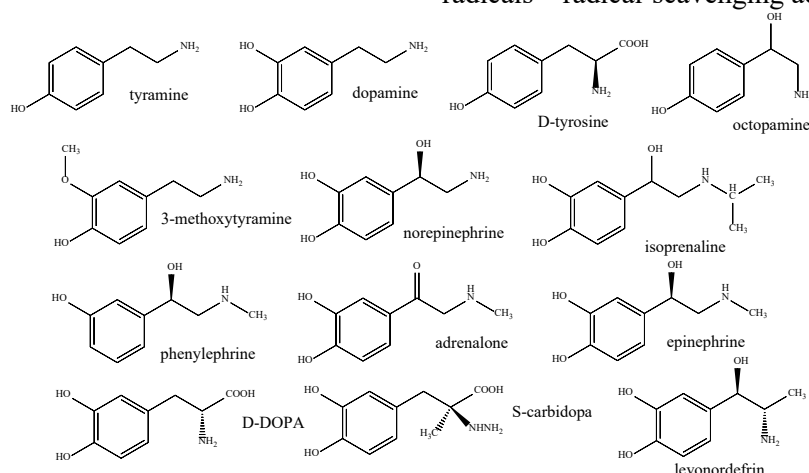
Scheme 1. Investigated BA
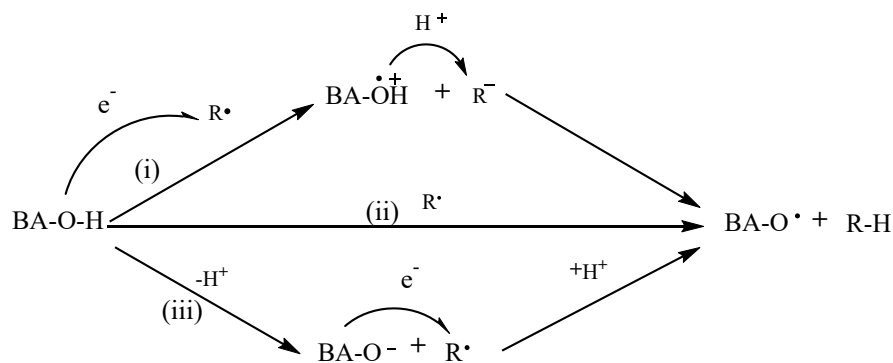
Scheme 2. Mechanisms of O-H bond dissociation

The reaction between phenolic antioxidants and active radicals can proceed following different mechanisms, but three of them are most often discussed in the literature [6–9] (Scheme 2): (i) electron transfer from the phenol to the active radical, which produces a cation-radical and the radical is converted into an anion; the electron transfer is followed by a proton transfer from the cation-radical to the anion (SET-PT); (ii) direct hydrogen atom transfer between the antioxidant and the active radical (HAT); (iii) deprotonation of the antioxidant followed by an electron transfer from the resulting anion to the active radical; the next step is the protonation of the anion produced by the active radical (SPLET).

Since the selected BAs possess phenolic hydroxyl groups, their radical scavenging potential could be evaluated by the same way as the other phenolic type radical-scavengers.

Computational details

The calculations were carried out using the density functional theory (DFT) [16], as implemented in the Gaussian09 program package [17]. The optimization of the geometry was performed with the Becke 3-parameter hybrid exchange functional combined with the Lee-Yang-Parr correlation functional (B3LYP) [18, 19] with the standard 6-311++G(d,p) basis set [20]. All possible intramolecular interactions were taken into account in the initial geometries. For all structures the harmonic vibrational frequencies were computed to confirm the true minima on the calculated potential surface.

Solvent effects on the calculated structures were investigated with the self-consistent reaction field (SCRF) method *via* the polarized continuum method (PCM) [21].

The total enthalpies of the species X are usually estimated from the equation:

$$H(X) = E_0 + ZPE + \Delta H_{trans} + \Delta H_{rot} + \Delta H_{vib} + RT, \quad (1)$$

where E_0 is the calculated total electronic energy, ZPE stands for zero-point energy, ΔH_{trans}, ΔH_{rot}, and ΔH_{vib} are the translational, rotational and vibrational contributions to the enthalpy. Finally, RT represents the pV-work term added to convert the internal energy into enthalpy. The total enthalpies were calculated at T = 298 K. The ZPE values were not scaled.

The enthalpy changes in the three possible reaction mechanisms of an O-H bond dissociation were calculated according to the scheme:

HAT
BA-O-H → BA-O· + H·   BDE = H(BA-O·)+H(H·) − H(BA-O-H)

SET-PT
BA-O-H → BA-Ȯ-H + e−   IP = H(BA-Ȯ-H)+H(e−) − H(BA-O-H)
BA-Ȯ-H → BA-O· + H+   PDE = H(BA-O·)+H(H+) − H(BA-Ȯ-H)

SPLET
BA-O-H → BA-O− + H+   PA = H(BA-O−)+H(H+) − H(BA-O-H)
BA-O− → BA-O· + e−   ETE = H(BA-O·)+H(e−) − H(BA-O−)
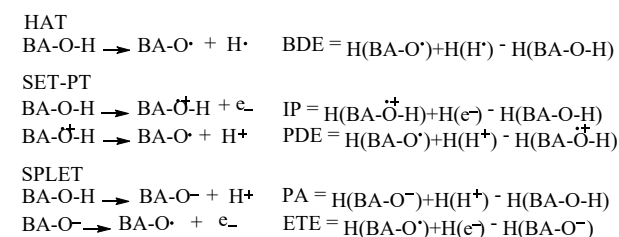
Scheme 3. Possible mechanisms of O-H bond dissociations and their corresponding enthalpy changes

The enthalpies of the hydrogen atom, proton and electron in water are taken from the literature [22], the used proton enthalpy (H_{H+}) in water is −1083.803 kJ.mol^{-1} (6.197 kJ.mol^{-1} in vacuum); the used enthalpy of an electron ($H_{e−}$) in water is −232.676 kJ.mol^{-1} (3.145 kJ.mol-1 in vacuum), the used enthalpy of a hydrogen atom ($H_{H·}$) in water is −1316.479 kJ.mol^{-1} (-1312.479 kJ.mol^{-1} in vacuum).

RESULTS AND DISCUSSION

In vacuum

BDE

According to the O-H BDE values, the hydroxyl groups of the studied BAs can be divided into three groups. In the first group are hydroxyl groups with low reactivity and BDE above 338 kJ.mol^{-1}. In the second group are hydroxyl groups with BDE from 310 to 338 kJ.mol^{-1} and in the third group are hydroxyl groups with high reactivity and BDE below 310 kJ.mol^{-1}.

Table 1. Calculated enthalpy changes in vacuum and in water (in kJ.mol^{-1})

Compound	Vacuum	Water				
	BDE	BDE	IP	PDE	PA	ETE
3-methoxytyramine	338.99	326.52	312.34	5.00	74.38	242.77
adrenalone (3)	324.48	331.39	324.85	-2.65	105.74	216.28
adrenalone (4)	321.29	330.13	324.85	-3.91	90.06	230.71
D DOPA (3)	305.23	315.88	331.20	-24.51	118.14	188.47
D DOPA (4)	303.80	312.81	331.20	-27.58	118.89	184.55
dopamine (3)	307.47	314.28	322.77	-17.68	119.92	185.00
dopamine (4)	303.64	309.94	322.77	-22.03	121.16	179.41
D-tyrosine	340.53	341.27	354.97	-22.89	141.39	190.51
epinephrine (3)	306.17	315.47	327.97	-21.69	118.42	187.68
epinephrine (4)	304.09	312.70	327.97	-24.45	118.08	185.26
isoprenaline (3)	305.97	315.36	327.52	-21.35	118.56	187.43
isoprenaline (4)	303.72	312.48	327.52	-24.22	118.34	184.78
levonordefrin (3)	303.70	313.24	325.11	-21.06	119.62	184.25
levonordefrin (4)	302.74	313.09	325.11	-21.21	115.97	187.75
norepinephrine (3)	308.82	317.22	333.55	-25.52	118.44	189.41
norepinephrine (4)	305.81	313.35	333.55	-29.39	119.58	184.4
octopamine	340.35	342.05	348.39	-15.53	138.49	194.20
phenylephrine	345.60	348.25	363.58	-24.52	136.99	201.90
S-carbidopa (3)	305.92	314.82	330.42	-24.79	118.84	186.61
S-carbidopa (4)	304.37	312.72	330.42	-26.89	118.45	184.90
tyramine	339.38	341.31	333.28	-1.16	144.86	187.08

In the first group is the hydroxyl group of phenylephrine, followed by octopamine, D-tyrosine, tyramine and 3-methoxytyramine. All these compounds own one phenolic hydroxyl group. Only in 3-methoxytyramine, there is a second substituent in the phenyl ring – a methoxy group at the 3rd position in the phenyl ring. In phenylephrine, the hydroxyl group is in the 3rd position relative to the aliphatic side chain, while in all other first-group BAs the hydroxyl group is in the 4th position.

The methoxy group in 3-methoxytyramine increases the electron density in the aromatic system, which usually reduces the O-H BDE of phenolic hydroxyl groups, but on the other hand, the hydrogen of the dissociable hydroxyl group is engaged in a hydrogen bond with the oxygen of the methoxy group, which stabilizes the compound and additional energy is needed to be detached. Ultimately, the positive mesomeric effect is in practice offset by the negative effect of the hydrogen bond on the ability of the O-H bond to dissociate to a radical and a hydrogen atom.

The compound adrenalone has two phenolic hydroxyl groups at adjacent positions in the phenyl ring (catechol structure) and occupies an intermediate place according to BDE. Their BDEs in vacuum are 321.29 and 324.48 kJ.mol^{-1}, which is

significantly less than the BDE of the first-group compounds. At the same time, this value is much higher than the BDE values for the other catechol-containing compounds. However, only adrenalone has a carbonyl group attached directly to the aromatic ring. Therefore, it is the only compound in which the π-electron system is extended to the side chain. Among the other compounds studied, there is no one in which a functional group so effectively draws electron density from the aromatic system. The expansion of the system has a favorable effect on reactivity, when anions are formed in the reaction. This is not the case when radicals are formed during the reaction. On the other hand, however, the charge transfer in the aromatic system stabilizes the input compound and increases the BDE. This is the reason BDE in adrenalone to have an intermediate value.

All other amines have a catechol ring. The presence of such a fragment in the organic compounds is sufficient for the manifestation of radical scavenging properties. The least reactive among the third group compounds is the hydroxyl group at the 3rd position in norepinephrine (308.82 kJ.mol^{-1}). The small differences in the reactivity of these compounds are due to the influence of the side

chain: the more efficiently it donates electron density to the aromatic system, the lower the BDE value is.

Seven of the compounds have O-H BDE about 308 kJ.mol^{-1} and the most reactive hydroxyl group is that at the 4th position in the phenol ring of levonordefrine (302.74 kJ.mol^{-1}). The side chain is composed of three sp3-hybrid carbon atoms and an amine group. All other compounds have a side chain of two carbon atoms and one amine group. In the structure of S-carbidopa and D-DOPA there is a carboxyl group at the end of the side chain and there is no hydroxyl group adjacent to the aromatic ring. As a result, the O-H BDE of these compounds are greater than the others.

In water

BDE

The polarizing effect of water affects the BDE of the O-H bonds in different ways. There is a significant decrease of BDE upon transition from vacuum to an aqueous medium in 3-methoxytyramine with 12.47 kJ.mol^{-1}. In all other compounds there is an increase of the BDE, which is the expected change. Typically, the decrease in BDE in any environment is due to greater radical stabilization than the input compound. However, the large decrease of O-H BDE in 3-methoxytyramine is due to a decrease in the stability of the input compound.

In an aqueous medium, the strength of the intramolecular hydrogen bond in the compound decreases. Hydrogen bonds in an aqueous medium are weaker than in a vacuum, which reduces the stability of the catecholic radicals (where the stabilization effect of the hydrogen bond is more essential) resulting in an increase of the BDEs. The water alters the BDE of these compounds by the strength of the hydrogen bonds in the compounds and in the corresponding radicals.

The increase in BDE of the hydroxyl group at the 4th position of adrenalone by about 4 kJ.mol^{-1} is due to the additional polarization of the carbonyl group and the stronger charge transfer from the aromatic ring to this group. Withdrawal of electron density from the aromatic ring always increases the BDE of the OH bonds. Despite the significant difference in the structure of this amine - the phenyl ring-conjugated carbonyl group, there is no significant difference in its properties.

The other amine that differs from the others is the phenylephrine. It has one hydroxyl group at the 3rd position relative to the side chain. Probably this is why the phenylephrine has the highest BDE in vacuum (345.60 kJ.mol^{-1}) and in water (348.25 kJ.mol^{-1}), and the highest IP (363.58 kJ.mol^{-1}).

IP

The ionization potential is a descriptor of the compounds ability to donate electrons: to be a reducing agent. However, oxy-reduction reactions take place in polar solvents and the calculation of IP in vacuum has less practical value. In fact, our calculations show that the IP values of the investigated compounds are by about 200 kJ.mol^{-1} lower in water than in vacuum.

The three compounds with the highest IP in the aqueous medium are: phenylephrine (363.58 kJ.mol^{-1}), followed by D-tyrosine (354.97 kJ.mol^{-1}) and octopamine (348.39 kJ.mol^{-1}). These are the weakest reducing agents among the studied amines.

The most reactive compound is 3-methoxytyramine (312.34 kJ.mol^{-1}), followed by dopamine (322.77 kJ.mol^{-1}), adrenalone (324.85 kJ.mol^{-1}), levonordefrine (325.11 kJ.mol^{-1}), isoprenaline (327.52 kJ.mol^{-1}) and epinephrine (327.97 kJ.mol^{-1}). The only compound with an intermediate IP is the norepinephrine (333.55 kJ.mol^{-1}). The SET-PT mechanism was found to be more probable than the HAT mechanism in aqueous media for three of them: 3-methoxytyramine, adrenalone and tyramine. For the other compounds, the opposite is true - the HAT mechanism is more probable.

PDE

Hence, the proton abstraction from the cation-radical is not the rate determining step. In this step of the SET-PT mechanism, the detachment of a proton from the cation-radical implies a significantly smaller positive (3-methoxytyramine) or negave (all other compounds) change in enthalpy.

PDE reflects the electron density distribution of the cation-radical and the uncharged radical that is obtained from it after proton detachment. PDE is a descriptor of the acidity of the cation-radical, but because this process takes place with significantly less change in enthalpy, it is much more probable.

Lowest acidity possesses the cation-radical of 3-methoxytyramine (5.00 kJ.mol^{-1}), followed by the cation-radical or tyramine (-1.16 kJ.mol^{-1}) and adrenalone (-2.65 kJ.mol^{-1}). The strongest proton acids are the cation-radicals of norepinephrine, D-DOPA and S-carbidopa (See Table 1).

With the exception of PDE of 3-methoxytyramine (4.99 kJ.mol^{-1}), all others have negative values for PDE, which indicates a spontaneous deprotonation process at room temperature.

PA

The strongest acids among the test compounds are 3-methoxytyramine (74.38 kJ.mol^{-1}) and adrenalone ((4) 90.06 kJ.mol^{-1} and (3) 105.74

kJ.mol^{-1}). They are followed by a series of compounds with intermediate acidity (between 118 and 122 kJ.mol^{-1}) and four compounds with PA above 135 kJ.mol^{-1}, all of them featuring a single O-H-phenolic group.

It can be argued on the significance of this descriptor, but we believe that the acidity of hydroxyl groups is decisive for the behavior of a phenolic radical scavenger. If the acidity of a phenol is high enough and it maintains a sufficiently high concentration of deprotonated phenolic hydroxyl groups, this will almost certainly direct the reaction to the SPLET mechanism instead the SET-PT mechanism. The oxidation of an anion in the second step is always easier than the oxidation of the compound itself.

According to this logic, the listed compounds are also candidates for interaction with radicals by the SPLET mechanism. Other compounds may also interact by this mechanism.

ETE

The anions are too unstable in a vacuum. When the molecules are immersed in water (implicitly), the anions they produce are much more stable. This is the reason for a strong decrease in PA in water and an increase in ETE to the range of 179.41 to 242 kJ.mol^{-1}.

It turns out that from the strongest acid (PA=74.38 kJ.mol^{-1}) in water (3-methoxytyramine) is the most difficult to tear off an electron (242.77 kJ.mol^{-1}). The next compound in this ranking is with 12 kJ/mol less ETE. All other compounds have an ETE below 200 kJ.mol^{-1}. Three of them have an ETE above 190 kJ.mol^{-1}, and the others, the most reactive, have an ETE below 190 kJ.mol^{-1}.

It is easiest to detach an electron from the anion which is obtained after deprotonation of the hydroxyl group at the 4th position in dopamine (179.41 kJ.mol^{-1}). And this is the strongest radical-scavenger among the studied BAs.

CONCLUSION

Thirteen BA have been investigated using the reliable DFT functional and a high theoretical level orbital basis. It has been found that their radical scavenging activity is comparable and in some cases greater than that of phenolic acids from our previous investigations. The role of the side chain amino group was evaluated. It has the strongest impact on

their reducing properties and makes the SET-PT mechanism much more likely compared to most of the phenolic acids. However, after the deprotonation of a hydroxyl group, the SPLET mechanism provides the least change in the enthalpy of electron detachment and this is the preferred mechanism for all BAs.

REFERENCES

1. M. Papageorgiou, D. Lambropoulou, C. Morrison, E. Kłodzinska, J. Namiesnik, J. Płotka-Wasylka, *Trends Anal. Chem.,* **98,** 128 (2018).
2. R. Stevanato, M. Bertelle, S. Fabris, *Pharmacology & Pharmacy,* **4,** 696 (2013).
3. S. H. Snyder, *Science,* **224,** 22 (1984).
4. S. Surendran, S. Rajasankar, *Neurol. Sci.,* **31**, 531 (2010).
5. C. Tabor, H. Tabor, *Ann. Rev. Biochem.,* **53,** 749 (1984).
6. R. Kaur-Sawhney, A. Altman, W. Galston, *Plant Physiol.,* **2**, 158 (1978).
7. R. Stevanato, A. Wisniewska, F. Momo, *Arch. Biochem. Biophys.,* **346,** 203 (1997).
8. F. Momo, S. Fabris, R. Stevanato, *Arch, Biochem. Biophys.,* **382,** 224 (2000).
9. A. Shashank, A. K. Gupta, Sh. Singh, R. Ranjan, *Curr. Nutr. Food Sci.*, **17**, 1 (2021).
10. J. Smythies, *Antioxid. Redox Signalings*, **2**, 575 (2000).
11. A. Galano, D. Xian Tan, R. J. Reiter, *J. Pineal Res.*, **51**, 1 (2011).
12. H. C. Ha, N. S. Sirisoma, P. Kuppusamy, J. L. Zweier, P. M. Woster, R. A. Casero, *Proc. Natl. Acad. Sci. U. S. A.*, **95**, 11140 (1998).
13. I. G. Sava, V. Battaglia, C. A. Rossi, M. Salvi, A. Toninello, *Free Radical Biol. Med.*, **41**, 1272 (2006).
14. N. A. Velloso Bellé, G. Dalmolin, G. Fonini, M. A. Rubin, J. B. Teixeira Rocha, *Brain Res.*, **1008**, 245 (2004).
15. S. M. Hernandez, M. S. Sanchez, M. N. Schwarcz de Tarlovsky, *Acta Trop.*, **98**, 94 (2006).
16. W. Kohn, A. D. Becke, R. G. Parr, *J. Phys. Chem.*, **100**, 12974 (1996).
17. http://gaussian.com/.
18. A. D. Becke, *Phys. Rev.* A, **38**, 3098 (1988).
19. C. Lee, W. Yang, R. G. Parr, *Phys. Rev. B,* **37**, 785 (1988).
20. R. G. Parr, *Horiz. Quant. Chem.,* **3**, 5 (1980).
21. J. B. Foresman, T. A. Keith, K. B. Wiberg, *J. Phys. Chem.,* **100**, 16098 (1996).
22. J. Rimarčík, V. Lukeš, E. Klein, M. Ilčin, *J. Mol. Struct.: THEOCHEM,* **952,** 25 (2010).

Biodegradation of polycaproamide textile materials

E. L. Pekhtasheva[1]*, E. Yu. Raykova[1], T. I. Chalykh[1], M. A. Polozhishnikova[1], M. P. Slavova[2,3]

[1]*Academic Department of Commodity Science and Commodity Examination, G. V. Plekhanov Russian Economic University, 36, Stremyannyi way, 117997 Moscow, Russia*
[2]*Institute of Electrochemistry and Energy Systems, 10, Acad. Georgi Bonchev Str. 1113, Sofia, Bulgaria*
[3]*Department Machine Elements and Chemistry, Faculty of Transport Management, Todor Kableshkov University of Transport, Sofia, 158, Geo Milev Str., Sofia, Bulgaria*

The work solves the problem of biodegradation of synthetic polymers that have exhausted the resource of their work, and the choice of microorganisms that are capable of biodegradation. As synthetic polymers, the most common ones used for the production of clothing, decorative and technical fabrics, etc., polyamides are taken. For research purposes, polycaproamide (PCA) in the form of model porous-fibrous systems of different densities was used. As objects of microbiological impact, bacterial cultures adaptive to PCA fibers (microflora of active wastewater sludge, spontaneous microflora of nylon) were used. *Bacillus subtilis k1* was identified as the most active strain of PCA biodegradable bacteria. The presumptive mechanism of degradation with ε-aminocaproic acid release is established, in which bacteria affect the weak amide bond in the macromolecular chain of polycaproamide.

Keywords: bacteria-biodegraders, ε-aminocapronic acid, polycaproamide fibers

INTRODUCTION

Currently, elimination of polymer waste is an urgent problem. Most synthetic polymers were developed in due time as analogues of the well-known natural materials, for example, glass or metals, for the purpose of their full replacement and, therefore, they have high structural strength, hardness, durability, and biological resistance. In recent years, as the service life of polymeric materials depletes, the problem of their utilization began to arise, which has become more urgent. There are various recycling programs for this purpose, but nevertheless, when polymer waste enters the natural environment, the best way out is to assimilate it to carbon dioxide and water, as it happens with natural polymers. There are different mechanisms for this process, and the most famous is biodegradation. Biostability and biodegradability are two fundamentally different properties of materials in general, and polymers in particular. As a rule, polymers are highly biostable that gives rise to the problem of protecting the environment against polymer waste. The biostability of polymers can substantially be estimated by calculation methods, for example, by the rate of aging or by extrapolating the biodegradation process. Statements that polymers do not degrade for 200 to 400 years have not yet been verified as they are industrially produced since the mid-XXth century.

Bibliographic Review

Biostability of fibrous textile materials, including polyamide materials, has been studied in many works [1-3]. It has also been established that microorganisms can use synthetic polymers as a source of energy and nutrition [4-10].

Chemical fibers, unlike natural ones, do not have their own permanent and specific microflora. Therefore, in the biodegradation of these materials, the most common types of microorganisms characterized by increased adaptability can play a major role.

The emergence and progression of biological degradation of polyamide fibers is largely due to their properties and the properties of influencing microorganisms and their species composition. Basically, the type of microorganisms that damage polyamide and other chemical fibers is determined by the conditions of their operation that form the microflora, and its adaptive capabilities.

Extraction, cultivation and use of such adaptive strains is of both scientific and practical interest. Using strains of bacteria adaptive to nylon, the waste from polyamide production, products that have become obsolete, and potentially toxic substances, can be disposed which will make it possible to obtain secondary raw materials and solve the problem of environmental protection.

---

* To whom all correspondence should be sent:
E-mail: *Pekhtasheva.EL@rea.ru*

Table 1. Indicators of physical and mechanical properties of nylon nonwoven needle-punched materials

Sample	Surface density, g/m^2	Breaking load, N		Breaking elongation, %	
		length	width	length	width
No.1	535 (0.7 tex)	1050	486	94.8	118.6
No.2	250 (0.3 tex)	347	461	70.9	117.7

The purpose of this work is to study biodegradation of synthetic polymers using an example of polyamide fibers and to identify strains of microorganisms that are capable of causing their biodegradation. To reveal the mechanism of action of microorganisms on synthetic fibers, nonwoven fibrous materials obtained from poly-ε-caproamide (PCA) were selected.

EXPERIMENTAL

The study included fibrous nonwoven materials from polycaproamide fibers obtained from the melt of secondary PCA, with linear density of 0.7 tex and 0.3 tex. The molecular weight of the polymer was 30-35 kDa. The canvas was bound mechanically by needle-punching machines. Table 1 shows the main parameters of nonwoven PCA fabrics included in the study. As objects of microbiological action on PCA materials, bacteria extracted from PCA fibers previously inoculated and damaged by microorganisms in activated sludge of wastewater, as well as damaged by spontaneous microflora formed on the fiber during its exposure in a humid chamber to a relative humidity of 100% and 30– 35 °C were used. PCA fibers served as sources of energy and nutrition for microorganisms in the metabolic process. Using the method of batch cultivation, 11 cultures were extracted from damaged polyamide fibers:

– cultures of bacteria extracted from fibers damaged by spontaneous microflora: 6a; 62a; 63a; 64a;
– cultures of bacteria extracted from PCA fibers damaged by microflora of active wastewater sludge: 5 nylon 2, 5 nylon 5, 5 nylon 6.

The degree of biological damage was assessed based on optical microscopy results by Yermilova's method [1] *via* quantifying the number of fiber damages. Fiber damage was divided into three categories: Class A – fouling by microorganisms and their metabolic products; Class B – more severe degradation: swelling, thinning, and wall damage; Class C – strong and deep damage to fibers by microorganisms: stratification and disintegration of fibers to separate conglomerates. Changes in the damage coefficient (degradation index) of the fiber in the range of 0 to 0.3 correspond to the initial changes in the fiber surface, without affecting its internal structure. If the coefficient falls within the range of 0.3 to 3.55, degradation is observed both on the surface and in the inner sections of the fibers, and at values ranged within 3.55 to 42.25 deep biological degradation of the fiber structure is observed at all its levels.

To assess the effect of bacteria on the structure and properties of materials, the samples were sterilized by UV-radiation for two hours and placed in sterile desiccators. They were inoculated with an aqueous suspension of daily pure cultures of bacteria (1.1 billion cells per 1 ml), kept in a thermostat at 35 °C to 37 °C and relative humidity of 100%.

To assess the ability of bacteria to degrade PCA fibers to ε-aminocaproic acid, a polarographic method was used. Fixed volumes of mineral media containing PCA fibers as a carbon source were sterilized. Then, they were inoculated with a daily broth culture of bacteria in a volume of 31×10^6 cells per 1 ml and incubated at 35 °C. Samples were taken every day and the content of ε-aminocaproic acid formed was determined. The content of ε-aminocaproic acid was determined on the polarograph PU-1 (Germany).

The amount of ε-aminocaproic acid formed under the action of bacteria was determined and measured in the studied media (initial and after inoculation for 10 days), as well as in the control media without bacterial inoculation. The ε-aminocaproic acid content was determined from a calibration curve. A method for determining the sorption capacity of polyamide fibers (CE), which is based on the neutralization reaction of basic or acidic groups with a 0.1N acid or alkali solution with back titration of the excess of acid or alkali was also used.

RESULTS AND DISCUSSION

Table 2 shows the research results. The most active culture turned out to be a bacterial strain under the code designation "6a" extracted from spontaneous microflora of nylon fibers. After 3 weeks of exposure, the biodegradation index (k = 0.52) verifies degradation of both the surface and the inner sections of the fiber.

Table 2. PCA-fiber damaging by bacteria *

Type of culture	Exposure time, days	Damage coefficient by classes:			Biodegradation index K, unit
		A $\overline{x}_1$	B $\overline{x}_2$	C $\overline{x}_3$	
Microflora of active sludges:	7	4.7	0	0	0.009
5 nylon 2	21	5.9	0	0	0.012
5 nylon 5	7	7.9	1.5	0	0.053
	21	24.2	5.4	0	0.183
5 nylon 6	7	15.5	1.3	0	0.064
	21	53.1	4.5	0	0.219
Spontaneous microflora of nylon:	7	22.4	2.4	0	0.105
6a	21	47.9	5.7	0	0.519
62a	7	5.3	0	0	0.011
	21	9.1	0	0	0.018
63a	7	5.4	0	0	0.011
	21	8.3	0	0	0.017
64a	7	27.9	0	0	0.056
	21	64.2	0	0	0.128
	21	73.7	0	0	0.199

*Developed by the authors

Table 3. Degree of biodegradation of nonwoven polycaproamide material fibers of different surface density by the culture of the bacterium *Bacillus subtilis k1**

Sample	Exposure time, days	Damage coefficient by classes:			Total number of damages, N, units	Biodegradation index, K, units
		A($\overline{x}_1$), unit	B($\overline{x}_2$), unit	C($\overline{x}_3$), unit		
Original	–	0	0	0	0	0
No. 1	30	34.3	10.7	1.3	46.3	0.67
No. 2	30	61.3	6.3	1.3	68.9	0.63
No. 1	90	48.6	15.3	4.2	68.1	1.5
No. 2	90	83.5	16.4	5.6	105.5	2.01
No. 1	180	76.3	19.4	7.1	102.8	2.45
No. 2	180	115.1	28.3	10.2	153.6	3.54
No. 1	270	89.4	25.7	12.4	127.5	3.98
No. 2	270	122.3	33.5	17.1	172.9	5.44
No. 1	360	110.5	39.3	15.7	165.5	5.2
No. 2	360	155.7	49.9	23.3	228.9	7.5

*Developed by the authors

The purpose of further research was to identify the bacterial strain that degrades PCA fibers, which can be used to develop an express method for assessing the bacteriological resistance of textile materials containing polycaproamide fibers. According to Bergey's Manual, the resulting strain 6a was identified as a strain of the species *Bacillus subtilis* [11].

The degree of PCA biodegradation of fibrous materials was assessed by Yermilova's method after inoculation of textile nonwoven PCA materials with the bacterial strain *Bacillus subtilis k1* [1].

Table 3 shows the results of changes in the degree of damage to polyamide nonwoven fabrics No. 1 and No. 2 under the impact of the bacterium *Bacillus subtilis k1* for 360 days. Control (initial) samples of nonwoven materials that are not damaged.

The nature and degree of bacterial degradation of polycaproamide fibrous materials was studied on nonwoven needle-punched polyamide fabrics with surface density of 535 g/m^2 and fiber fineness of

0.7 tex (No. 1), surface density of 250 g/m² and fiber fineness of 0.3 tex (No. 2) using *Bacillus subtilis k1*, the most active of bacteria-biodegraders strain.

Nonwoven fabric No. 1 had a biodegradation index of K = 067, and nonwoven fabric No. 2 had K = 0.63 30 days after inoculation with a pure culture of *Bacillus subtilis k1* that indicates damage on both the surface and in the inner sections of the fibers. At the same time, a large amount of Class A damage of the biomass fouling type was observed in nonwoven fabric No. 2. Fibers of nonwoven fabric No. 1 showed almost 2 times less fouling and, at the same time, stronger structural changes, such as damage to the fiber walls, were observed.
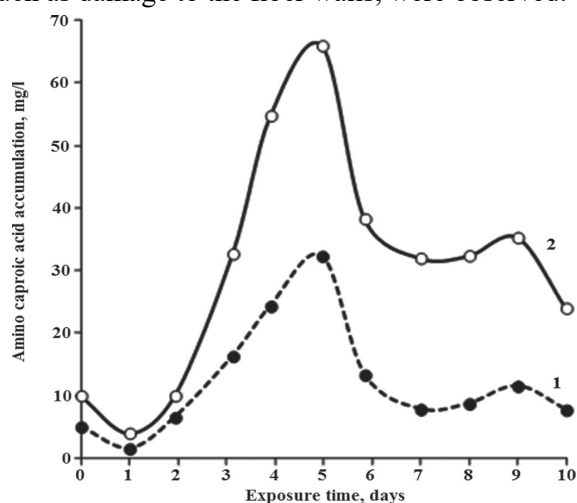

Figure 1. Change in α-amino caproic acid concentration during *Bacillus subtilis k1* development on PCA material fibers: 1 – 0.7 tex; 2 – 0.3 tex. * Developed by the authors.

After 360 days, the index of fiber biodegradation in nonwoven fabric No. 2 was 1.4 times higher than that in fibers of material No. 1, and this dependence was observed throughout the entire study. This is apparently due to the fact that, firstly, the nonwoven fabric No. 2 fiber fineness is almost 2 times less than that of the nonwoven fabric No. 1. (No. 1 – 7 tex, No. 2 – 0.3 tex), This is related to the fact that thinner fibers have a more developed porous structure and adsorb a larger number of microorganisms, and, therefore, are more intensively damaged. Secondly, the surface density of the nonwoven material No. 2 itself creates favorable conditions for the contact of fibers with microorganisms, since its total surface of interaction with microorganisms is 2 times greater.

To study the effect of microorganisms on the chemical structure of PCA fibers and elucidate the mechanism of degradation, the possibility of

accumulation of ε-aminocaproic acid by *Bacillus subtilis k1* culture was investigated. The control was a mineral medium without carbon sources inoculated with bacteria; a mineral medium with carbon sources in the form of polycaproamide nonwoven materials, but without inoculation; and a mineral medium with a carbon source in the form of ε-aminocaproic acid (10 mg/l). In a mineral medium with ε-aminocaproic acid, it was not detected after one day.

Figure 1 shows the results obtained. As follows from the data obtained, the maximum amount of ε-aminocaproic acid affected by *Bacillus subtilis k1* strain on PCA fibrous materials is released on the fifth day: 32 mg/l, 66mg/l. Therefore, the proposed *Bacillus subtilis k1* strain causes degradation of polycaproamide fibrous materials with the formation of ε-aminocaproic acid.

Thus, basing of the data obtained inference should be drawn that PCA fibers of 0.3 tex are more accessible to microorganisms, which is confirmed by the data of microscopic studies. The results obtained also indicate the possibility of using *Bacillus subtilis k1* strain for the disposal of polycaproamide fibrous materials in order to obtain ε-aminocaproic acid as a secondary raw material and in order to protect the environment against pollution by over-age polyamide materials. The mechanism of PCA fibrous materials degradation releasing ε-aminocaproic acid was established. Apparently, when the amide bond is broken, terminal amino and carboxyl groups are formed. Based on this assumption, an attempt was made to prove the increase in the number of active terminal carboxyl and amino groups by the sorption capacity method.

Analysis of the results obtained indicates (Table 4) that as PCA fiber is exposed to *Bacillus subtilis k1* bacterium, the sorption capacity increases. Bacteria impacting a weak amide bond in the macromolecular chain of nylon break it and release ε-aminocaproic acid. This translates to an increase of active terminal carboxyl and amino groups. In this case, cationic and anionic sorption capacities increase. It should be emphasized that after 12 months of exposure, the anionic sorption capacity increased 2.0 times for 0.7 tex PCA fibers, while the cationic capacity of 0.7 tex fibers increased 1.2 times and for 0.3 tex fibers it increased 1.4 times. Therefore, the sorption capacity of 0.3 tex fibers increases more intensively, which is confirmed by data on the degradation level of nonwoven materials.

Table 4. Variation in static exchange capacity of PCA fibers impacted by *Bacillus subtilis k1* culture (in mol/g)*

Time of infection, days	End group content		Exposure time, days	End group content	
	–COOH	–NH₂		–COOH	–NH₂
30	2.76	1.06	270	3.30	1.49
90	2.95	1.37	360	3.50	1.53
180	3.14	1.41	Original	2.47	0.61

Note: the relative precision ranged from 3 to 5%. *Developed by the authors.

This method can be used to study dynamics of the biological damage and to identify the ability of microorganisms to affect the polymer.

CONCLUSION

As determined by the studies, the culture of the bacterium *Bacillus subtilis k1* affects polycaproamide fibers, both the structure of fibers at the supramolecular level and the chemical structure of the fibers at the molecular level.

REFERENCES

1. I. A. Yermilova, Theoretical and practical bases of microbial degradation of chemical fibres*, Nauka, Moscow, Russia, 1991.
2. J. Szostak-Kotowa, *International Biodeterioration & Biodegradation*, **53**, 165 (2004).
3. E. Pekhtasheva, A. Neverov, G. E. Zaikov, Biodamage and biodegradation of polymeric materials, new frontiers, Shawbury, UK, Smithers Rapra, 2012.
4. S. A. Semenov, K. Z. Gumargalieva, G. E. Zaikov, Biodegradation and durability of materials under the effect of microorganisms, VSP International Publishers, Utrecht, The Netherlands, 2003.
5. D. Adamcova, M. Radziemska, J. Fronczyk, J. Zloch, M. D. Vaverkova, *Przegląd Naukowy. Inżynieria i Kształtowanie Środowiska,* **26,** 3 (2017), DOI:10.22630/PNIKS.
6. N. Mohanan, Z. Montazer, P. K. Sharma, D. B. Levin, *Frontiers in Microbiology*, **11,** 580709 (2020).
7. K. Janczak, G. B. Dąbrowska, A. Raszkowska-Kaczor, D. Kaczor, K. Hrynkiewicz, A. Richert, *International Biodeterioration & Biodegradation*, **155**, 105087 (2020).
8. T. Bubpachat, N. Sombatsompop, B. Prapagdee, *Polymer Degradation and Stability*, **152**, 75 (2018).
9. P. A. Faccia, Fr. M. Pardini, A. C. Agnello, J. I. Amalvy, M. T. Del Panno, *International Biodeterioration & Biodegradation*, **160**, 105205, 2021.
10. Ph. Stiefel, J. Schneider, C. Amberg, K. Maniura-Weber, Q. Ren, *Scientific Report*, 6 (2016).
11. J. Hoult, N. Krieg, P. Snit, *Bergey's Manual of Systematic Bacteriology*, Mir Publ., **1-2**, 800 (1997).

Section

Physics

Optical quartz fibers as non-linear media and four-wave mixing method for determination of fibers geometrical parameters

L. M. Ivanov [1,2*], T. D. Cholakov[1]

[1]*South West University, 66 Ivan Mihailov str., 2700 Blagoevgrad, Bulgaria*
[2]*Institute of Electronics, Bulgarian Academy of Sciences, 72 Tzarigradsko chaussee, 1784, Sofia, Bulgaria*

Because of their ability to maintain high energy density over long distances due to the small cross sections and low optical losses the fused quartz fibers are very appropriate media for observation of nonlinear optical effects. In this article the possibility is examined of using non-linear optical processes occurring in the fused quartz fibers to determine their geometrical parameters.

Keywords: non-linear optics, optical fibers, stimulated Raman scattering, four-wave mixing

INTRODUCTION

One of the most rapidly advancing areas in optics during the last few decades was non-linear optics. As a result, not only the fundamental dependencies of the non-linear processes were explained but also a lot of applied devices were developed. The non-linear optics gives wide possibilities for frequency conversion of coherent radiation thus strongly enlarging the laser technology abilities to create new coherent sources of light. We can hardly imagine the modern scientific researches without using the parametric light generators, without generating second and third harmonic, Raman lasers [1] and a lot of other devices [2]. Due to several reasons which we will discuss later the fused quartz fibers turn out to be very appropriate media for observation of the nonlinear optical processes. The following article is devoted to clarifying the possibilities for determining the geometrical parameters of the fibers by means of occurring non-linear optical processes. The proposed method is based on the fact that the frequency of the spectral components arising as a result of the four-photon mixing process directly depends on the fiber parameters. The method was experimentally verified.

Geometrical parameters of the fused quartz fibers

In its simplest form an optical fiber consists of a cylindrical core of silica glass surrounded by a cladding whose refractive index is lower than that of the core. This requirement is needed to ensure total internal reflection of the light on the core-cladding interface. The entire structure is covered by a protected jacket. Because of an abrupt index change at the core-cladding interface, such fibers are called step index fibers.

The fibers are characterized with their geometrical parameters such as core diameter $2a$, cladding diameter $2b$, core refractive index n_1, cladding refractive index n_2, and respectively, core cladding refractive index difference $\Delta n = n_1 - n_2$. These parameters are very important because they determine the fiber communication parameters, in particular the information speed. There is a most important integral parameter that describes the fiber properties. It is called normalized frequency or simply V parameter and is defined as:

$$V = \frac{2\pi a}{\lambda}\sqrt{n_1^2 - n_2^2} \approx \frac{2\pi a}{\lambda}\sqrt{2n_1\Delta n} \qquad (1)$$

We have to mention that two fibers with different geometrical parameters are identical if their V parameters are equal. It means that their information properties are the same.

During its propagation through the fiber, light forms waveguide modes that have a different effective propagation constant β. The number of excited waveguide modes depends on the parameter V. When a parameter V is less than 2.405 only one mode is formed in the fiber. Such fibers are called single-mode fibers. With parameter $V > 2.405$ more than one mode gets excited and these fibers are classified as multi-mode fibers. As can be seen from formula (1) each fiber can be single-mode for one wave length and multi-mode for other shorter wave length. Therefore, with appropriate choice of the light launched into the fiber multiple modes can get excited.

* To whom all correspondence should be sent:
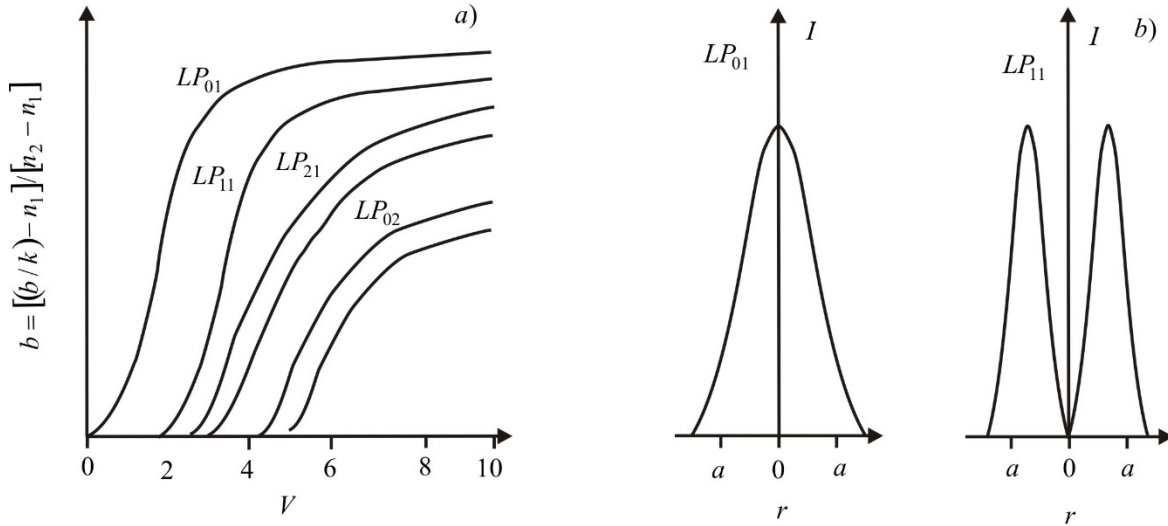E-mail: *mihovli@abv.bg*

Fig. 1. Normalized propagation constant (a) and field distribution (b) for first two fibers modes.

The propagation constants for the different modes can be calculated in dependence to the V parameter of the fiber. The result is shown in Fig. 1a. Furthermore, the wave analysis gives information about the distribution of the light intensity in the cross section of the fiber. Fig. 1b shows the results for the first two modes marked as LP_{01} and LP_{11}. As can be seen at the figure the axially symmetrical LP_{01} mode has maximum intensity at the center of the core. This conclusion turns out to be true for all the axially symmetrical modes (all modes with first index 0). On the contrary, axially nonsymmetrical mode LP_{11} has minimum intensity at the center of the fiber. This also turns out to be correct for all the other modes with first index different from zero.

Fused quartz fibers as nonlinear media

It is well known that fused quartz has a very low coefficient of nonlinearity in comparison to the other conventional nonlinear media. This fact is the main disadvantage of quartz as a nonlinear medium. However, the fibers have a lot of other advantages. The small cross sections of the cores of the fibers give them the ability to maintain high density of the energy. Also, the small losses and the great lengths of the fibers guarantee a great interaction length between the waves. As a result, in the fibers the product of the coefficient of nonlinearity and the length of interaction which determines the effectiveness of the nonlinear process exceeds many times those of the volumetric media. This makes the fibers very effective media for non-linear processes [3]. The non-linear processes occurring in the fibers are quite numerous. We will focus our attention on two of them – stimulated Raman scattering (SRS) and four-wave mixing (FWM) with an accent on the

second one which, we believe, allows determining the geometrical parameters of the fibers. The Raman scattering is a non-linear process where a new wave length in the Stokes area is generated which frequency shift from the pumping radiation corresponds to the maximum in the spontaneous vibrational spectrum of the nonlinear medium. The amplification line of spontaneous Raman scattering in the fused quartz is quite wide but has a maximum at $\Delta v = 440$ cm^{-1}. That is why the occurring stimulated Raman scattering has this frequency shift. The process is very effective because phase synchronism is not required.

As it is well known, the stimulated FWM is a non-linear process, when two pump photons of frequency v_p are transformed in Stokes and anti-Stokes pair of frequency, respectively v_s and v_a, which obey the energy balance:

$$v_p - v_s = v_a - v_p$$

The process is efficient if the phase matching condition is fulfilled:

$$\Delta k = k(v_s) + k(v_a) - 2k(v_p) = 0$$

Perfect phase-matching cannot be achieved in volumetric optical glasses because in the normal (anomalous) dispersion region Δk is always greater (less) than zero. Exact phase-matching is possible in optical fibers, when the material dispersion is compensated by the modal dispersion for a suitable combination of the modes [4, 5] (Fig. 1a), i.e.

$$\Delta\beta = \beta_{p1} + \beta_{p2} - \beta_a - \beta_s . \tag{2}$$

The dynamics of both processes *versus* the pump power is shown on Fig. 2. The fiber is pumped with second harmonic radiation of Q switched Nd:YAG laser.
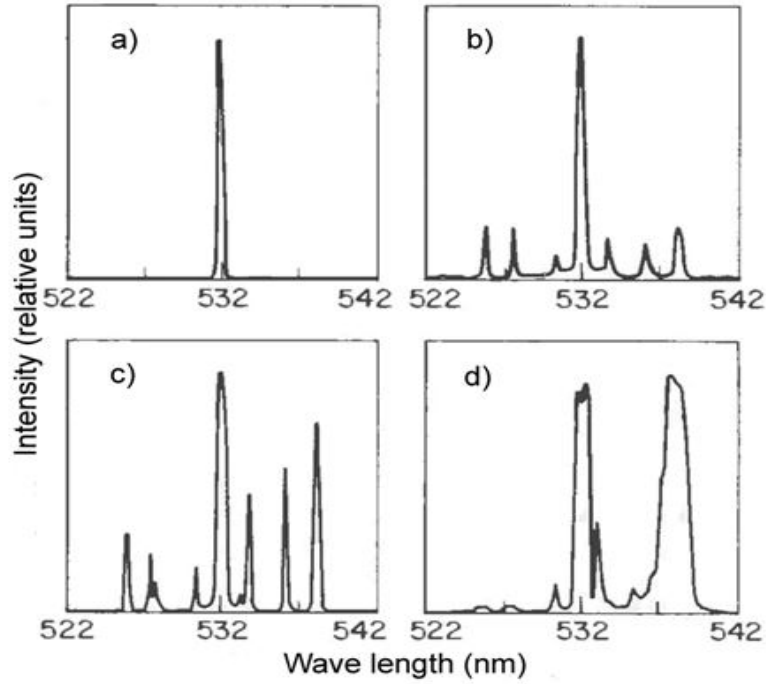
Fig. 2. Dynamics of SRS and FWM processes *versus* the power of the pumping pulses.

In Fig. 2a the power of the pump radiation is low and at the out of the fiber only the pumping radiation is registered. With increasing of the pumping power radiation (Fig. 2b) several new components symmetrical to the pump frequency appear. These spectrum lines occur as a result of the FWM process. The energy of the Stokes and anti-Stokes components is approximately equal. Further increasing of the pumping power (Fig. 2c) leads to increased power of the Stokes components because they get additional amplification as a result of the SRS process because these lines are within the spontaneous Raman amplification. The last Fig. 2d presents the spectrum of a very high pumping power. In this case the SRS process occurs. The energy of the pumping frequency almost completely transforms into Raman line and there is not enough energy left for the FWM process.

Non-linear method for determining of fiber parameters

The frequencies generated by the FWM process can be exactly predicted, if the parameters of the fiber are known. Our aim is the solving of the inverse problem – to find the fiber parameters from the given FMW frequencies.

For the case of weakly guided fibers [6] in a divided pump process (that is the Stokes and one of the pump waves propagate in one fiber mode, while the anti-Stokes and other pump wave propagate in another fiber mode) the frequency shift Δv is

determined by fiber parameters and can be written as follows:

$$\Delta v \lambda_p D(\lambda_p) = \Delta n \left[\frac{d(bV_s)}{dV} - \frac{d(bV_{as})}{dV} \right] \quad (3)$$

where V is the normalized frequency, λ_p is the pump wavelength, $D(\lambda) = \lambda^2 \left(\frac{d^2 n}{d\lambda^2} \right)$ is the core material dispersion and the expression $\frac{d(bV)}{dV}$ is differential mode delays of the propagating Stokes and anti-Stokes waves. For two distinct combinations of modes the following characteristic equation for the parameter V can be written [7]:

$$\frac{\Delta v^{(1)}}{\Delta v^{(2)}} = \frac{\frac{d(bV_s^{(1)})}{dV} - \frac{d(bV_{as}^{(1)})}{dV}}{\frac{d(bV_s^{(2)})}{dV} - \frac{d(bV_{as}^{(2)})}{dV}} = R(V) \quad (4)$$

Indices 1 and 2 denote the first and the second modal combination, respectively. The right side of eq. 4 depends only on the V parameter. This fact established the possibility to obtain V parameter, and then the other fiber parameters.

Fig. 3 shows the dependencies $R(V)$ for the rectangular refractive index profile for three different combinations of the pump wave modes, including 0, 1 and 2 axially symmetrical modes, respectively. Curve 1 corresponds to $\Delta v^{(1)}$ obtained with the pair LP_{31} - LP_{21} and to $\Delta v^{(2)}$ obtained with $LP_{21} - LP_{11}$, curve 2 to $\Delta v^{(1)}$ obtained with LP_{31} - LP_{21} and $\Delta v^{(2)}$ obtained with $LP_{11} - LP_{01}$, curve 3 to $\Delta v^{(1)}$ obtained with $LP_{02} - LP_{11}$ and $\Delta v^{(2)}$ obtained

75

with $LP_{11} - LP_{01}$. It is interesting to mention that these are combinations of the lowest order modes.
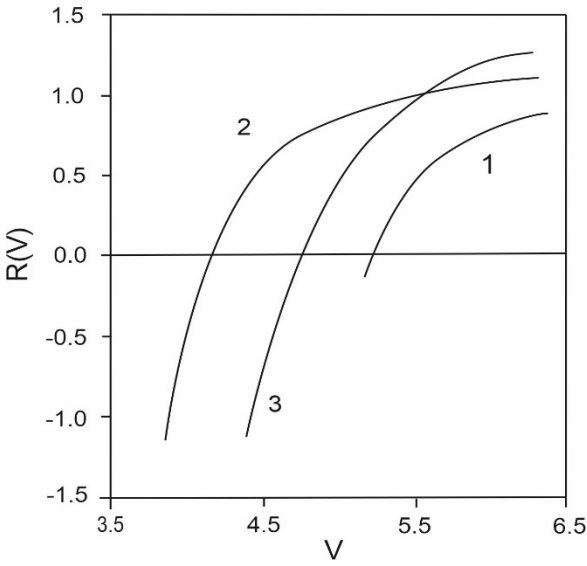

Fig. 3. Dependencies $R(V)$ for rectangular refractive index profile of the fiber. curve 1 – $\Delta v^{(1)}$ obtained with $LP_{31} - LP_{21}$, and to $\Delta v^{(2)}$ obtained with $LP_{21} - LP_{11}$; curve 2 - $\Delta v^{(1)}$ obtained with $LP_{21} - LP_{11}$, and $\Delta v^{(2)}$ obtained with $LP_{11} - LP_{01}$; curve 3 - $\Delta v^{(1)}$ obtained with $LP_{02} - LP_{11}$ and $\Delta v^{(2)}$ obtained with $LP_{11} - LP_{01}$.

From Fig. 3 it is seen that $R(V)$ has zeros for certain values of V. Consequently, for those values of V the normalized group delays participating in the numerator of eq. 4 are equal. The negative value of $R(V)$ corresponds to the case when the anti-Stokes wave of the modal combination in the numerator of eq. 4 propagates in a higher mode than the Stokes wave. The positive values correspond respectively to the case when the Stokes wave is in the higher mode.

If the V parameter is already known, the determination of the other parameters (core radius a and core cladding refractive index difference Δn) requires information about the doping composition of the fiber. As its concentration is very small we can use the data for the pure fused quartz and obtain good accuracy.

In order to examine experimentally the possibility of determining the fiber parameter using FWM process, we studied a fiber with known V parameter, which was approximately 3.9 at pump wavelength $\lambda_p = 532$ nm. An experimental set up, which is widely used for studying non-linear phenomena in optical fibers, was employed for obtaining the stimulated FWM spectra. The fiber was pumped by the second harmonic of a Q-switched and mode-locked CW Nd:YAG laser. The fiber had pure silica cladding and Ge-doped core.

In the experiments the excitation of the different groups of modes was accomplished by varying the

launching conditions for the pump beam. The modal structure of the generated radiation was identified visually, after splitting a fraction of the fiber output with a grating. FWM frequencies were recorded by OMA.

In Fig. 4 the anti-Stokes sides of the FMW spectra are shown. The Stokes sector of the spectra expects the symmetrical Stokes frequency, contains also the stimulated Raman scattering (SRS) line. It seriously complicates the spectra. This figure shows also the modal combination of the Stokes and anti-Stokes components for the respective frequency.
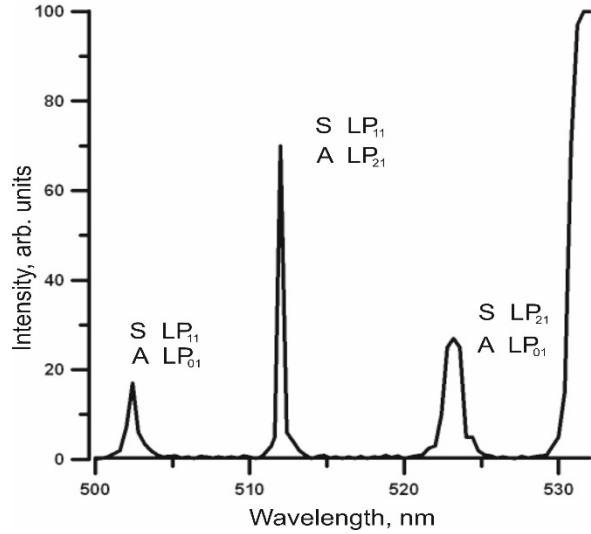

Fig. 4. Anti-Stokes components of the experimental FWM spectrum.

For this sample we used as first line the one with $\Delta v^{(1)} = 722$ cm^{-1} obtained for modal combination $LP_{21} - LP_{11}$ and as second line that with $\Delta v^{(2)} = 1089$ cm^{-1} for modal combination $LP_{11} - LP_{01}$. The frequency shift $\Delta v^{(1)} = 722$ cm^1 was obtained when the anti-Stokes component was in the higher mode. That's why we take this value as a negative. Using eq. 4 we found that the V value of the pump wavelength is 3.96.

Using this value, the parameters of the fiber were easily calculated. The standard optical fibers are made from pure silica with *Ge*-doped core. But the doping concentration weakly affects the core refractive index n_1, core material dispersion

$$D(\lambda) = \lambda^2 \left(\frac{d^2 n}{d\lambda^2} \right)$$ and differential mode delays $\frac{d(bV)}{dV}$

[8]. Then if we use the data for pure silica the error will be negligible. Solving eq. 3 we obtain for the core-cladding refractive index difference $\Delta n = 3.04 \times 10^{-2}$. From eq. 1 we find out for the core diameter $2a = 2.25$ μm. We have to mention that the passport data are correspondingly $\Delta n = 3.2 \times 10^{-2}$ and $2a = 2.2$ μm.

CONCLUSION

In conclusion, a method based on a nonlinear optical process is proposed for the first time to determine the geometrical parameters of optical quartz fibers. The method is based on the dependence of the frequency shift of the spectral components arising as a result of the four-photon mixing process on the fiber parameters. Unlike the others classical methods, the proposed method allows simultaneous determination of all practically important parameters of light guides - core radius, core refractive index, difference in refractive index between the core and the sheath, and the corresponding normalized frequency. These parameters directly determine the information capacity of optical communication lines. The method was experimentally demonstrated. The accuracy of the obtained results is completely satisfactory.

REFERENCES

1. G. A. Hariharan, J. W. Nicholson, *Proc. SPIE 11665*, 116650P (2021), doi:10.1117/12.2583068
2. M.-J. Yin, B. Gu, Q.-F. An, Ch. Yang, Y. L. Guan, K.-T. Yong, *Coordination Chemistry Reviews,* **376,** 348 (2018), *doi:10.1016/j.ccr.2018.08.001.*]
3. G. Agrawal, Nonlinear fibre optics, Fourth edn., San Diego, 2007.
4. R. H. Stolen, *IEEE J. Quantum Electron.*, **11**, 100, (1975).
5. R. H. Stolen, J. Bjorkholm, *IEEE J. Quantum Electron.,* **18**, 1062 (1982).
6. D. Gloge, *Appl. Opt.*, **10**, 2252 (1971).
7. S. J. Garth, C. Pask, G. E. Rosman, *Opt. and Quantum Electron.*, **20,**79 (1988).
8. J. W. Fleming, *Appl. Opt.*, **23,** 4486 (1984).

Welding of copper and 304L stainless steel with continuous electron beam

D. Kaisheva[1,2*], A. Anchev[3], V. Dunchev[3], B. Stoyanov[3], S. Valkov[1,3], M. Ormanova[1], G. Kotlarski[1], V. Todorov[3], M. Atanasova[3], P. Petrov[1]

[1]*Institute of Electronics „Acad. E. Djakov", Bulgarian Academy of Sciences, 72 Tzarigradsko Chaussee Blvd, 1784 Sofia, Bulgaria*
[2]*South-West University „Neofit Rilski", 66 Ivan Michailov Str., 2700 Blagoevgrad, Bulgaria*
[3]*Technical University of Gabrovo, 4 H. Dimitar Str., 5300 Gabrovo, Bulgaria*

The electron beam welding (EBW) is one of the few technologies that allow welding of materials with different thermophysical characteristics. This paper presents the results of the study of the structure and the mechanical properties of electron beam welded samples of copper and stainless steel. The samples were welded with different source power, changing the beam current. The specimens were examined by X-ray diffraction and scanning electron microscopy. They were also subjected to mechanical tests, such as hardness and tensile strength measurement. The welded zone is a solid solution of copper and γ-iron with inclusions of pure copper and a small amount of α-iron. Higher values of the beam power lead to finer microstructure of the weld. It was found that an increase in the beam power leads to improvement in the mechanical properties.

Keywords: electron beam welding, dissimilar materials, copper, stainless steel

Many methods and techniques were developed for joining of similar materials [1-3]. However, more and more often in practice there is a need for welding of dissimilar materials. Heavy all-steel structures are being replaced by lighter ones containing welded steel parts with copper, aluminium, titanium, etc., leading to energy savings and improved mechanical properties. Complex joints of different materials are used in a number of industries such as automotive, shipping and aerospace [4]. Obtaining a strong compound of two materials with very different thermophysical properties and behavior is a difficult task and a real challenge for scientists and engineers.

Studies of welds of copper and stainless steel produced *via* explosion welding [5, 6], laser welding [7-9], and electron beam welding [10, 11] are reported. The authors of [5] summarized the possibilities of joining the similar and dissimilar materials by explosive welding. They discussed the joining of copper to steel with respect to the technological conditions. The intermetallic phases were not found in the investigations [6]. The analysis shows that diffusion did not take place between bonding plates, and diffusion was observed after annealing of the bonded samples [5, 6]. The laser welding is widely studied and used in practice. It allows joining of materials with tiny geometry and different optical and thermal properties. The authors of [8] investigated the influence of the laser process conditions on the

properties of the copper-stainless steel welds. The joining mode was transformed to welding-brazing from fusion welding. The welding-brazing mode joins liquid stainless steel to solid copper, whereas the fusion zone mode joins stainless steel and copper by melting and mixing both metals. The melting of the copper can be effectively suppressed by offsetting and inclining the laser beam to the stainless steel. The microstructure and the tensile characteristics of EBW and TIG welded samples of copper and stainless steel were compared in [9]. It is marked that the main advantages of EBW in the case of dissimilar metal joints are lack of fusion, lack of penetration and no heat loss which in turn improves the weld quality. EBW of copper and three kinds of austenitic stainless steel was presented in [10]. The authors reported a complex heterogeneous fusion zone with porosity and microfissures due to the process with rapid cooling and poor mixing of the materials and due to the geometry parameters. They draw the conclusion that dissimilar metal welding can be very critical and sound welds can be obtained only if an accurate optimisation of the process parameters is performed. EBW with beam oscillation improves the mechanical properties of the copper-stainless steel welds in comparison with non-oscillating beam [11]. This improvement is due to the adequate mixing of copper in the welded zone and the backfilling of the microcracks on stainless steel by copper.

* To whom all correspondence should be sent:
E-mail: *darinakaisheva@ie.bas.bg*

However, investigations of the structure and mechanical properties of EBW of copper and 304L stainless steel, as well as of the influence of the beam power on the discussed functional properties are currently less well investigated. Therefore, this paper presents the results of the study of the structure and the mechanical properties of electron beam welded samples of copper and 304L stainless steel. The results are discussed concerning the applied technological conditions of electron-beam welding procedure.

EXPERIMENTAL

Three kinds of welded specimens of copper and AISI 304L stainless steel (SS) with the following chemical composition (wt %): 0.03% C; 2.0% Mn; 0.75% Si; 0.045% P; 0.030% S; 17.5 – 19.5% Cr; 8.0 – 12.0% Ni; 0.10% N, were examined. The samples were flat plates with sizes of 100 × 50 × 8 mm.

Electron beam welding (EBW) was carried out on the EvoBeam Cube 400 welding machine. Fig. 1 shows the scheme of the process. The technological conditions of the EBW process were the following: accelerating voltage U = 60 kV; welding speed v = 0.5 cm/s; beam current I_1 = 30 mA (sample 1), I_2 = 40 mA (sample 2), and I_3 = 50 mA (sample 3), corresponding to a beam power of P_1 = 1800 W, P_2 = 2400 W, and P_3 = 3000 W, respectively. A stationary electron beam without deflection was used.
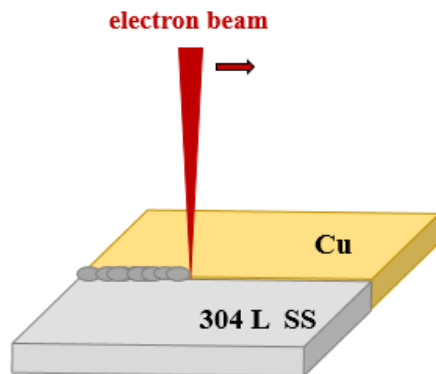

Figure 1. Scheme of the experiment of EBW of copper and stainless steel AISI 304L.

The phase analysis was conducted on a X-ray diffractometer "Bruker D8 Advance". The used method was "Coupled Two Theta", using Co Kα radiation with wavelength 1.78897 Å and line focus orientation. The range of the research was from 40° to 120°, the X-ray generator current was 40 mA and the used voltage was 35 kV. Other characteristics of the test were 0.05° step size and 0.25 s time for the step. The standard database used to identify

diffraction peaks was Crystallography Open Database (COD).

Scanning electron microscopy (SEM) was used for the investigation of the structure of the welded specimens. Secondary electrons were employed. The distribution of chemical elements in the fusion zone and near the fusion zone was analysed by energy-dispersive X-ray spectroscopy (EDX).

The mechanical properties were investigated by a machine for static and dynamic tests ZWICK Vibrophore 100. Tensile specimens were tested, which were welded at a different power of the beam. The test was performed in accordance with the requirements of ISO 6892-1 Method B. Also, samples made of pure copper and 304 L SS were investigated for comparison.

The microhardness experiment was performed on a semi-automatic microhardness tester ZWICK/Indentec - ZHVμ-S. Metallographic cross-sections of specimens were made of welded materials in the transverse direction of the weld. The line along which the microhardness was measured was located in the middle of the weld seam. A load force of 0.49 N was used for all experimental points.

RESULTS AND DISCUSSION

The application of the technological conditions of sample 1 lead to partial joint penetration weld, while the use of the conditions related to the specimens 2 and 3 lead to complete joint penetration depth.

In Fig. 2 the X-ray diffraction patterns of the investigated samples are shown. The XRD phase exhibits a solid solution of copper and γ-iron in the form of face-centred cubic (fcc), as well as α-iron with body-centred cubic structure (bcc). Additionally, considering the welds formed by a beam current of 30 and 40 mA, peaks corresponding to pure Cu were detected. This means that at these specimens, the copper has not been completely dissolved into the steel matrix. Prerequisites for the formation of a solid solution are the close atomic radii and the same crystal lattice of copper and γ-iron (fcc crystal structure), which is in agreement with the results obtained in the present study. The α-iron phase is formed due to the high temperature in the EBW process. The bcc phase is metastable at room temperature, and can be formed at 1200 ºC. Obviously, this temperature has been obtained during the welding process, meaning that the bcc structure has been successfully formed. Also, at the electron-beam welding process, the thermal cycling gradient is very high, and the solidification behaviour is non-equilibrium. This

means that metastable phases, such as the bcc structure of α-iron, can be obtained [12, 13]. It is clear that the peak corresponding to bcc phase has a different height at different technological conditions. It is highest for the sample welded by a beam c/urrent of 50 mA, and consequently this sample has the highest amount of α-iron. This could be attributed to the highest cooling rate at the EBW process. The highest value of electron beam power leads to the greatest temperature gradient. Therefore, these statements are consistent with the results obtained in our study.
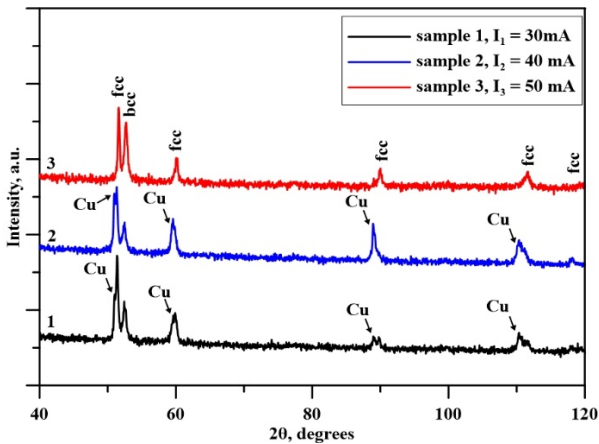

Figure 2. X-ray diffraction patterns of the welded joints.

In Fig. 3 cross-sectional SEM images of the welded specimen are shown. Fig. 3(a) shows the microstructure of the fusion zone of sample 1. Fig. 3 (b) presents the microstructure of the fusion zone of sample 2 and Fig. 3 (c) – the microstructure of the fusion zone of sample 3. According to the authors of [14], the increase in the beam current leads to the formation of finer microstructure of the weld. As already mentioned higher values of the discussed technological parameter cause a larger cooling rate. In the same time, the cooling rate is of significant importance for the formed weld structure, where larger values of the thermal cycling gradient lead to the formation of finer microstructure. Therefore, the highest value of the beam current leads to the largest cooling rate and the finest microstructure. These statements are completely in agreement with our results.

The results of the tensile test of welded samples of copper and steel are presented in Table 1. Tensile experiments were also carried out of pure copper and 304 L SS for comparison. As already mentioned, for sample 1 the beam power is not enough to form a complete joint penetration depth of the welded plates. This affects the mechanical properties, as the yield strength is by approximately 20% lower than that of the pure copper, the tensile

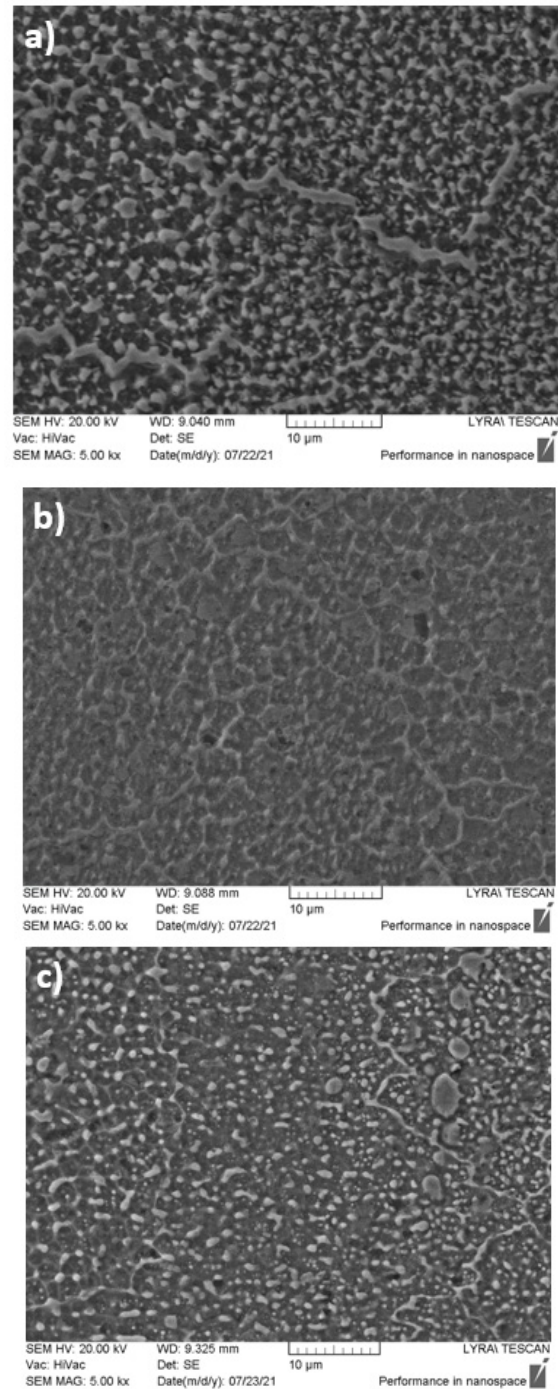strength is by 43% lower and the elongation is by 39% lower than these of copper.

Figure 3. Cross-sectional SEM images of the fusion zone of sample 1 (a), sample 2 (b) and sample 3 (c).

As the electron beam current increases, a weld is available along the entire depth of the welded plates. The mechanical parameters also increase and for sample 3 they reach a tensile limit, a tensile strength and a relative elongation of 35%, 79%, and 87% of the values obtained for pure copper, respectively. As already mentioned, the presence of a larger amount of the bcc phase in sample 3 may explain its better mechanical properties.

Table 1. Results of the tensile test of welded dissimilar samples of copper and stainless steel and pure Cu and 304 L SS.

Sample	Yield strength $R_{p0,2}$, MPa	Tensile strength R_m, MPa	Elongation A_t, %
Cu	267	275	16.8
AISI 304L	298	608	35.8
Sample 1	52	119	6.5
Sample 2	78	137	7.7
Sample 3	93	218	14.6

In Fig. 4 the results of the measured microhardness in a cross-section of the weld are shown. The microhardness of non heat-affected areas of the copper and the stainless steel is 60-100 µHV and 250-350 µHV, respectively. In the fusion zone there is no difference in the microhardness values for the three samples. In sample 1 a significant increase in microhardness is observed on approaching the welded zone, in contrast to the other two samples. In the heat-affected area on the side of the copper, a decrease in microhardness is observed compared to heat-unaffected pure copper. This decrease for samples 1 and 3 is approximately 35%, for sample 2 it is 3.2%. This reduction in the microhardness of the heat-affected zone at the Cu side could be a reason for the deteriorated mechanical parameters in the tensile test.
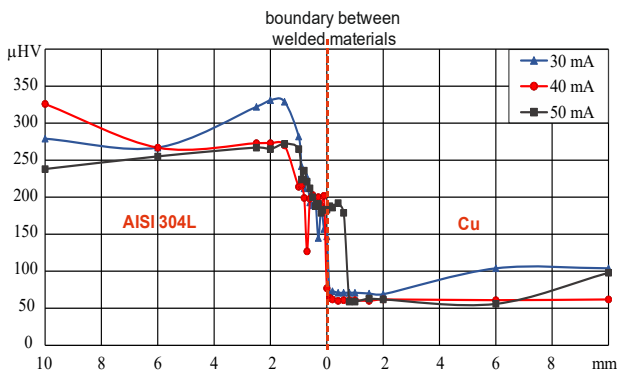

Figure 4. Distribution of the microhardness along the line perpendicular to the welding seam in the middle of the depth of the welded samples.

CONCLUSIONS

1. Copper and 304L stainless steel specimens have been successfully welded using electron beam welding technology. A beam power of 1800 W is sufficient to weld 8 mm thick specimens in partial joint penetration weld. At a beam power of 2400 and 3000 W complete penetration weld has been formed at the same sample thickness.

2. The welded zone is a solid solution of copper and γ-iron with inclusions of pure copper and a small amount of α-iron. The technological conditions have a significant effect on the microstructure of the welded samples. Higher values of the beam power lead to finer microstructure of the weld.

3. Higher values of the beam power lead to better mechanical properties. In the sample welded with the highest power of 3000 W, the highest values of yield strength and tensile strength were measured - 93 MPa and 218 MPa, respectively.

4. There is no difference in the microhardness values for the three samples in the fusion zone. In the heat-affected area on the copper side, a decrease in microhardness is observed compared to heat-unaffected pure copper. It is the reduced microhardness in the heat affected zone on the copper side that is one of the reasons for the deteriorated mechanical parameters in the tensile test.

REFERENCES

1. K. Weman, Welding processes handbook, Woodhead Publishing, 2012.
2. V. Mihailov, V. Karhin, P. Petrov, Fundamentals of welding, Polytechnic University Publishing, St. Petersburg, 2016.
3. L. Jeffus, Welding - principles and applications, 5th edn., New York: Delmar Publication, 2004.
4. U. Dilthey L. Stein, *Sci. Techno.l Weld. Join.*, **11,** 135 (2006).
5. F. Findik, *Materials and Design,* **32**(3),1081 (2011).
6. A. Durgutlu, B. Gulenc, F. Findik, *Materials and Design*, **26**, 497 (2005).
7. T.A. Mai, A.C. Spowage, *Materials Science and Engineering, A*, **374**(1–2), 224 (2004).
8. S. H. Chen, J. H. Huang, J. Xia, X. K. Zhao, S. B. Lin, *Journal of Materials Processing Technology*, **222**, 43 (2015).
9. R. Ajith, M. Dev Anand, *International Journal of Mechanical Engineering and Technology*, **9**(3), 519 (2018).
10. I. Magnabosco, P. Ferro, F. Bonollo, L. Arnberg, *Materials Science and Engineering, A,* **424,** 163 (2006).
11. J. Kar, S.K. Roy, G.G. Roy, *Journal of Materials Processing Technology*, **233**, 174 (2016).
12. J. W. Fu, Y. S. Yang, J. J. Guo, J. C. Ma, W.H. Tong, *J. Mater. Res.,* **24(7),** 2385 (2009).
13. S. Tosto, F. Nenci, Hu Jiandong, G. Corniani, F. Pierdominici, *Mater. Sci. Technol.*, **19,** 519, (2003).
14. S. Valkov, M. Ormanova, P. Petrov, *Metals*, **10**, 1219 (2020).

Influence of humidity on surface potential decay of gamma irradiated polypropylene and poly(ethylene terephthalate) electrets

A. P. Viraneva[1], I. Y. Vlaeva[2]*, T. A. Yovcheva[1]

[1] University of Plovdiv "Paisii Hilendarski", Faculty of Physics and Technology, 24 Tzar Assen str. 4000 Plovdiv, Bulgaria

[2] University of Food Technologies, Department of Mathematics, Physics and Information Technologies, 26 Maritsa Blvd., 4002 Plovdiv, Bulgaria

In the present paper gamma irradiated polypropylene (PP) and poly(ethylene terephthalate) (PET) electrets stored at different humidity levels were studied. Polymer films were irradiated in air by a ^{60}Co source with total doses of 5 kGy accumulated in a single step at a dose rate of 0.25 kGy/h. After irradiation, the samples were charged in a corona discharge system, which consists of a corona electrode, a grounded plate electrode, and a metal grid placed between them at two polarities - positive or negative. All investigated samples were stored in desiccators at different humidity levels (0%, 55% and 100%). After that, the surface potential was measured periodically out of the desiccators by the method of the vibrating electrode with compensation. Time storage dependences of electrets surface potential at different relative humidity levels for all samples were investigated. The results obtained were analyzed with the percolation model. The percolation model was used to consider the surface potential decay of electrets. The model allowed to analyze the surface potential decay of the gamma irradiated electrets, caused by the influence of the humidity at which they were stored. It was established that the higher values of the relative humidity led to a faster decay of the surface potential.

Keywords: polypropylene, poly(ethylene terephthalate), electrets, humidity, gamma irradiated

INTRODUCTION

Electrets are dielectric materials capable to retain electric charges over a long period of time and to create an external quasistatic electric field. They have been a field of investigations for many years [1, 2]. Over the years, considerable interest has been shown in the surface potential decay of corona charged polymeric materials. Besides the electrets materials and conditions of producing electrets the surface potential decay depends on a number of factors under which the electrets have been stored or used, for example temperature, humidity, pressure, gamma irradiation, etc. [3-6]. For the formation of electrets different polymeric materials as polypropylene and poly(ethylene terephthalate) are widely used, because of their important commercial significance, structure and appropriate mechanical and electrical properties [7-9].

The influence of gamma irradiation of 5 kGy and 25 kGy on the stability of electret characteristics of corona charged PP and PET films was investigated by following the surface potential decay with time and with sample's storage temperature [10]. Significant changes in the electrets behavior of the polymer films after gamma irradiation were established. The surface potential decay depended on factors such as the corona polarity, the type of material and the irradiation dose. At 25 kGy the gamma irradiation induced enhancement of the electrets efficiency of the PP films which achieved the highest value. The possible mechanisms of surface potential decay responsible for the observed irradiation dependent behavior are discussed.

The aim of this paper is to investigate the influence of relative humidity on the surface potential decay of non-irradiated and gamma irradiated PP and PET corona electrets.

EXPERIMENTAL

Sample preparation

Isotactic polypropylene films with thickness of 20 μm (Assenova Krepost LTD, Bulgaria) and poly(ethylene terephthalate) films with thickness of 40 μm (Hostaphan RNK, Mitsubishi Polyester Films GmbH, Germany) were used. The polymer films were cleaned in an ultrasonic bath with ethanol for four minutes then washed in distilled water and dried on filter paper under room conditions. Samples of 30 mm diameter were cut from the clean films and subjected to gamma irradiation treatment.

* To whom all correspondence should be sent:
E-mail: *ivlaeva@yahoo.com*;
         i_vlaeva@uft-plovdiv.bg

Gamma irradiation of the samples

Right after the samples were prepared, they were gamma irradiated. The samples were placed in special holders inside a metal tube under the ^{60}Co gamma source. The irradiation was performed in air at room temperature by a ^{60}Co source with total dose of 5 kGy at dose rates of 0.25 kGy/h. It was checked by thermometric control that the sample temperatures during the irradiation did not appreciably increase above room temperature. This was expected because of the low dose rate of the irradiation.

Corona charging and surface potential measurements

The samples obtained were charged in a corona discharge. The experimental set up described in [11] consists of a corona electrode (needle), a grounded plate electrode and a grid placed between them. The samples of the non-irradiated (0 kGy) and gamma irradiated (5 kGy) PP and PET films were charged at a room temperature for 1 minute. Positive or negative 5 kV voltage was applied to the corona electrode. 1 kV voltage of the same polarity as that of the corona electrode was applied to the grid. The electrets surface potential of the charged samples was measured by the vibrating electrode method with compensation by which the estimated error was better than 5%.

Storage of the samples at different relative humidity

After charging, all investigated samples were stored in desiccators at different relative humidity (RH = 0%, RH = 55% and RH = 100%) for 200 days at room temperature. The relative humidity in the desiccators was measured with hygrometers. The surface potential was measured periodically out of the desiccators.

The values of the relative humidity were obtained by chemical solutions shown in Table 1.

Table 1. Relative humidity.

Number of the desiccator	RH, %	
1	dry air	0
2	water solution of $Mg(NO_3)_2$	55
3	water	100

Computer analysis

The percolation model was used to analyze the experimental results obtained. A model that allows to analyze electrets surface discharge and to reveal the significant influence of the humidity level at which they have been stored is the model proposed by Kuzmin and Tairov [12, 13] based on the simultaneous utilization of the percolation theory, and the Kolmogorov's concept for the 2D kinetics of nuclei formation.

A computer program based on the percolation model was developed. The program selects the most appropriate parameters for which possible ranges of values have been created. Five parameters determining the relaxation of the electrets charge were obtained:

$X_1 = \alpha(t)$ – the rate of nuclei formation per unit time and unit area;

$X_2 = q(\tau)$ – the part of the electrets surface remaining free from such nuclei at the time of completion of electrification;

$X_3 = V_{01}$ and $X_4 = V_{02}$ – the rate of growth of the adsorbed nuclei as $V(t) = V_{01} \exp(-t/\tau) + V_{02}$;

$X_5 = f/g$, where $f = V$ – the steady state values of the surface potential and $g = V_0$ – initial surface potential.

RESULTS AND DISCUSSION

Time storage influence on the electrets surface potential decay

The dependences of the normalized surface potential on time storage for positively and negatively charged non-irradiated and gamma irradiated PP and PET films were studied for 200 days. The surface potential was measured periodically once in a week for the first 80 days when the charge was rapidly decaying. After this period, steady state values of the surface potential were established for all investigated samples. Time dependences of the normalized surface potential for positively and negatively charged non-irradiated and gamma irradiated PP samples are presented in Figs. 1 and 2, respectively.

In Figs. 3 and 4 the time dependences of the normalized surface potential for positively and negatively charged non-irradiated and gamma irradiated PET samples are presented.

Each point in the figures is a mean value of 5 samples. The calculated standard deviation was better than 5% of the mean value with confidence level 95%.

The experimental results presented in Figures 1–4 show that:

✓ The values of the normalized surface potential are initially decaying exponentially for the first 80 days after which they are slowly decreasing and are practically stabilized at 200 days. In the initial period of time the surface potential decreases rapidly due to the release of poorly captured charges from the shallow energy states. After that the steady

state value is reached caused by the tightly captured charges in the deep energy traps. This was observed for all investigated samples. Similarly, exponential decay of the electrets charge was observed in [14].

✓ The steady state values of the normalized surface potential for the samples charged in a negative corona are lower than those for the samples charged in a positive corona independently of material type, gamma irradiation and relative humidity.

Probably this is due to the fact that in case of a positive corona the dominant ions are $H^+(H_2O)_n$ and the ones for a negative corona - CO_3^{3-}. Those ions are bound in traps of various depths and they are

released from them depending on the surrounding conditions.

✓ The steady state values of the normalized surface potential depend on the relative humidity. It was established that the steady state values of the normalized surface potential are lowest for the RH = 100%, independently of material type, gamma irradiation and corona polarity.

We assume that on the electrets surface an adsorption of water molecules happens, additionally stimulated by the electrets own electric field. The higher humidity of the medium in which the electrets are stored leads to the higher rate of adsorption.
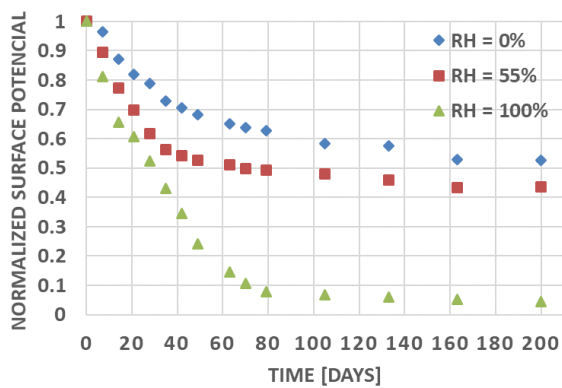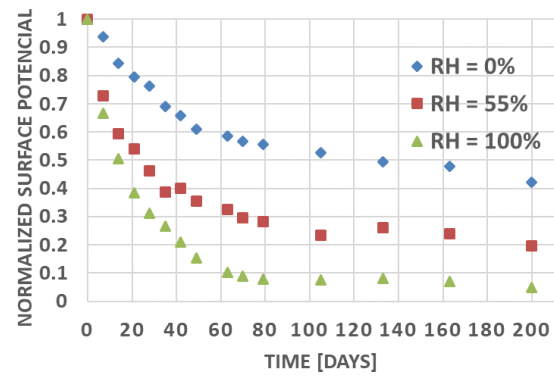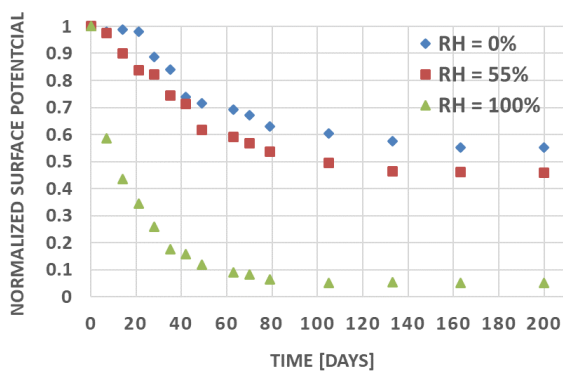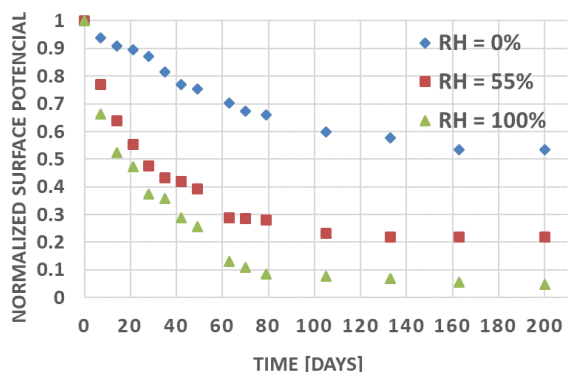

a   b

Fig. 1. Time dependences of the normalized surface potential for PP non-irradiated samples at both types corona charging: a) positive and b) negative.

a   b

Fig. 2. Time dependences of the normalized surface potential for PP gamma irradiated samples at both types corona charging: a) positive and b) negative.
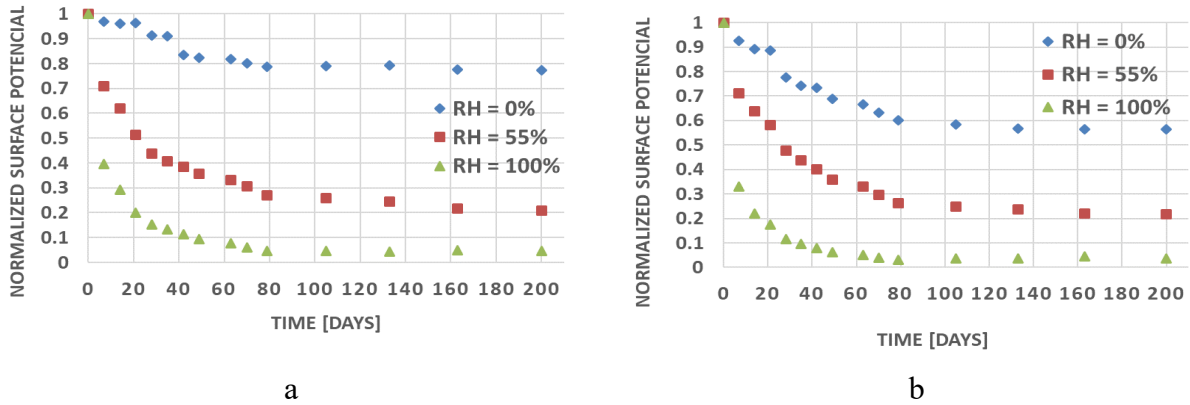
a

b

Fig. 3. Time dependences of the normalized surface potential for PET non-irradiated samples at both types corona charging: a) positive and b) negative.
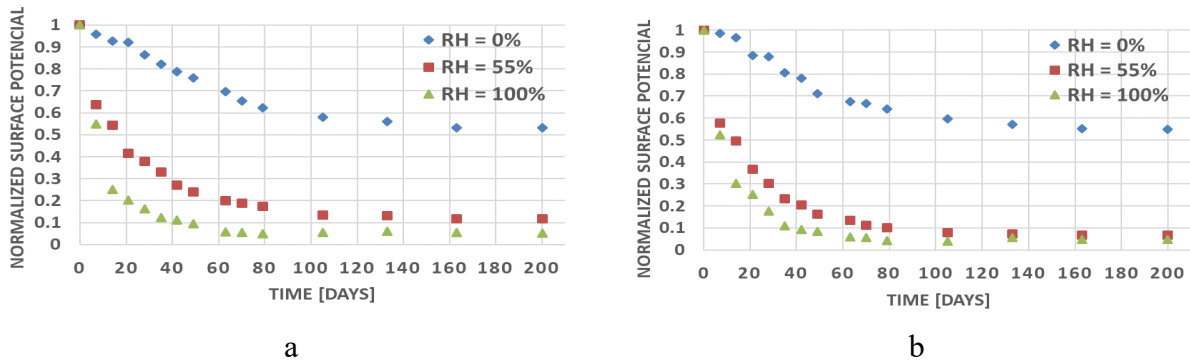

a

b

Fig. 4. Time dependences of the normalized surface potential for PET gamma irradiated samples at both types corona charging: a) positive and b) negative.
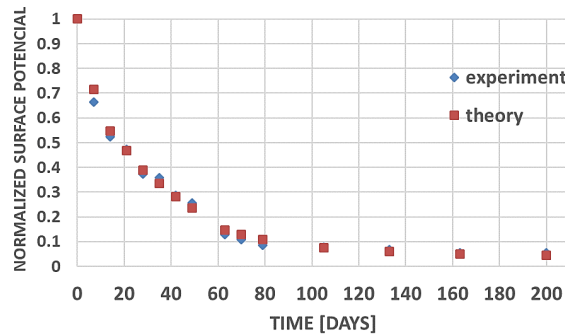

Fig. 5. Time dependences of the normalized surface potential for PP gamma irradiated samples, charged in a positive corona and stored at RH = 100%.

Comparison of the theoretical and experimental time dependences of the normalized surface potential

The experimental results obtained were analyzed by a computer program based on the percolation model. Experimental and theoretical curves for gamma irradiated PP and PET samples charged in a positive corona and stored at relative humidity 100% are presented in Figs. 5 and 6. Analogous curves

were obtained for all investigated samples. The results presented in Figs. 5 and 6 show very good coincidence of the experimental and theoretical data. Therefore, the percolation model describes very well the influence of relative humidity for all investigated electrets.

The values of the five parameters determining the relaxation of the electrets charge obtained after the computer processing of the experimental results for PET samples are presented in Table 2.
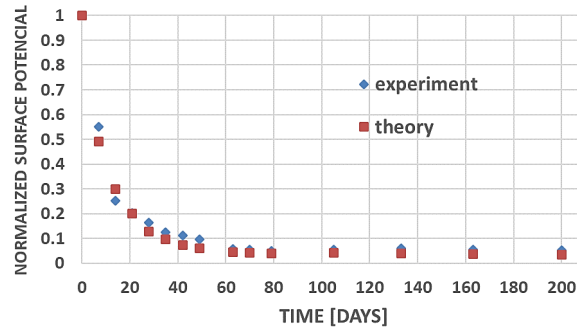
Fig. 6. Time dependences of the normalized surface potential for PET gamma irradiated samples, charged in a positive corona and stored at RH = 100%.

Table 2. Parameters determining the relaxation of electrets charge for non-irradiated and gamma irradiated PET samples, stored at RH = 0% and RH = 100%.

Samples	$\alpha.10^9$, m^{-2}s^{-1}	q	$V_{01}.10^{-13}$, ms^{-1}	$V_{02}.10^{-15}$, ms^{-1}	f/g
Positive corona, non-irradiated, RH = 0%	0.033	0.570	0.079	0.065	0.650
Negative corona, non-irradiated, RH = 0%	0.194	0.570	0.005	0.003	0.550
Positive corona, gamma irradiated, RH = 0%	0.071	0.570	0.003	0.068	0.500
Negative corona, gamma irradiated, RH = 0%	0,089	0.570	0.003	0.042	0.460
Positive corona, non-irradiated, RH = 100%	0.173	0.570	0.055	0.032	0.029
Negative corona, non-irradiated, RH = 100%	0.332	0.570	0.052	0.022	0.027
Positive corona, gamma irradiated, RH = 100%	0.373	0.570	0.072	0.001	0.035
Negative corona, gamma irradiated, RH = 100%	0/.384	0.570	0.063	0.003	0,031

Analogous data were obtained for all investigated samples. The results presented in Table 2 show that:

✓ The values of parameter X_2 are equal for all investigated samples, i.e. the part of the electrets surface remaining free of the adsorbed phase until charging is complete is the same. We suppose that the adsorption on the electrets surface and the formation of clusters is significantly stimulated during electrification. However, it is obvious that the charging conditions of the electrets (positive and negative corona) do not affect the amount of adsorbed phase.

✓ The rate of growth of the adsorbed nuclei depends on the parameters X_3 and X_4. X_3 has a determining role at the initial moment after charging, and X_4 determines the electrets behavior after a sufficiently long time.

✓ The parameter X_5 depends on the relative humidity. It was established that X_5 is lowest for the RH = 100%, independently of material type, gamma irradiation and corona polarity. Therefore, the higher humidity in which the electrets were stored leads to the greater rate of adsorption.

CONCLUSION

The influence of different relative humidity levels on surface potential decay of PP and PET non-irradiated and gamma irradiated films were studied. It was established that the higher values of the relative humidity led to a faster decay of the surface potential. The percolation model allowed to analyze electrets surface discharge, and to reveal the significant influence of the humidity level at which they have been stored. This is extremely important, and should be taken into account in the study of the stability of electret sensors and devices that are used at room temperature and function under real conditions involving various humidity levels.

REFERENCES

1. G. Sessler, R. Gerhard-Multhaupt, Electrets 3rd edn., Laplacian: Press Morgan Hill, California, 1999.
2. H. S. Nalwa, Ferroelectric polymers, Marcel Dekker Inc., New York, 1995.
3. X. Zhongfu, W. Yuda, Y. Guamao, S. Ximin. *IEEE Proc. 7th Int. Symp. Electrets (ISE7),* 651 (1991).
4. C. Gang-Jin, X. Hui-ming, Z. Chun-feng, *J. Zhejiang Univ. Sci.,* **5**, 923 (2004).
5. P. Ribeiro, J. Giacometti, M. Raposo, J. Marat Mendes*, 7th Int. Symp. Electrets*, 322 (1991).
6. K. Chikaoui, *Rad. Phys. Chem.,* **162,** 18 (2019).
7. J. Li, F. Zhou, D. Min, S. Li, R. Xia, *IEEE Trans. Diel. Electr. Insul.*, **22**, 1723 (2015).
8. L. Herous, M. Nemamcha, M. Remadnia, L. Dascalescu, *J. Electrostat.*, **67**, 198 (2009).
9. L. Herous, M. Remadnia, M. Kachi, M. Nemamcha, *J. Eng. Sci. Technol. Rev.*, **2(1)**, 87 (2009).
10. A. Viraneva, T. Yovcheva, K. Krezhov, S. Sotirov, *Bulg. Chem. Commun.*, **47B**, 121 (2015).
11. T. Yovcheva, Corona charging of synthetic polymer films, Nova Science Publishers Inc., New York, 2010.
12. Y. Kuzmin, V. Tairov, *J. Tech. Phys.*, **54**, 964 (1984).
13. Y. Kuzmin, *Proc. 10th Int. Symp. on Electrets* A, Konsta, A. Vassilikou-Dova, K. Vartzeli-Nikaki (eds.), **55** (1999).
14. G. Sessler, *J. Electrostat.,* **51-52**, 137 (2001)

Impedimetric response of phospholipid Langmuir-Blodgett films to methanol vapors

T. E. Vlakhov, G. B. Hadjichristov*, Y. G. Marinov

Institute of Solid State Physics, Bulgarian Academy of Sciences, 72 Tzarigradsko Chaussee Blvd., BG-1874, Sofia, Bulgaria

Aimed chemical biosensor applications, we have experimentally studied the electrical impedimetric response of Langmuir-Blodgett (LB) nano-thin monomolecular films of phospholipid dipalmitoyl-phosphatidyl-ethanolamine (DPPE) to methanol vapors. DPPE LB films were deposited on planar interdigital electrodes. The ability of such sensing element based on LB films with a thickness of about 3 nm to detect methanol vapors at ambient temperature was estimated by measurements with electrochemical impedance spectroscopy in the frequency range 0.1 Hz – 100 KHz of the applied electric field. DPPE LB films were exposed to methanol vapors at concentrations in the range from 80 to 320 mg/dm^3. Being in contact with methanol vapors, a significant decrease in the surface resistance of the studied LB films was observed. This effect was reversible. The results also showed a clear change in dielectric properties of the DPPE LB films affected by methanol vapors.

Keywords: electrochemical impedance spectroscopy (EIS); gas detection; Langmuir-Blodgett films; methanol vapors; phospholipids.

INTRODUCTION

Methanol is widely used in various industries (organic synthesis, pharmaceutical and plastics industry) for the production of e.g. dyes, drugs, detergents, pesticides, explosives. Methanol is a toxic compound, in particular by inhalation of its vapors and can injure the eyes. Furthermore, the methanol vapors are flammable and explosive. That is why the detection of the presence of methanol vapors is very important for protection of both human health and the environment. For detection of methanol and for safety purpose, various methods can be used. Most of the high-performance analytical methods currently used, e.g. gas chromatography or mass spectroscopy, are laboratory methods for measurement and thorough analyses. More desirable option is the use of an appropriate sensor because of the possibility of quick measurement in the place of potential threat. Among the large variety of sensor elements, micro-devices and systems for chemical sensing, are those based on films prepared by Langmuir-Blodgett (LB) technique [1–7]. In particular, LB films have been employed as active layers for gas sensing [8], including surface-acoustic-wave resonator (SAWR) sensors for methanol vapors [9]. The application of lipid LB films to design biosensors for harmful gases is of research and practical interest. In this direction, besides the optical methods, appropriate and advantageous is the use of electrochemical impedance spectroscopy technique (EIS) as an electrical method of detection.

The employment of interdigitated array electrodes is promising for bio- and chemical sensor applications because in this case the detection sensitivity becomes much higher than the sensing by use of conventional configuration of two metallic electrodes [10–14]. Such microelectrode arrays are very suitable for gas sensor and biosensor applications, and for construction of micro-sensor devices owing to their simple structural design and ease of fabrication [10, 15]. Interdigitated microelectrodes and EIS have been used as chemical sensors and to identify odors [11, 16]. Very recently, a measuring technique using surface acoustic-wave resonators and gravimetric method for detection were successfully applied to assess the impact of vapors of several volatile organic compounds on LB films of phospholipid dipalmitoyl-phosphatidyl-ethanolamine (DPPE) deposited on interdigitated microelectrode arrays [17]. In particular, the influence of the adsorbed methanol on the properties of such mass-sensitive sensor element was studied [17]. In the present work, we tested DPPE LB nano-thin LB molecular monolayers deposited on interdigitated microelectrodes to detect and quantify methanol vapors by means of EIS. DPPE molecule is appropriate and promising for biosensor applications owing to the two long hydrocarbon tails with 15 CH_2 groups each (Fig. 1a) that may provide excellent adsorption of some gases (such as methanol) with possible high sensitivity by sensor applications.

* To whom all correspondence should be sent:
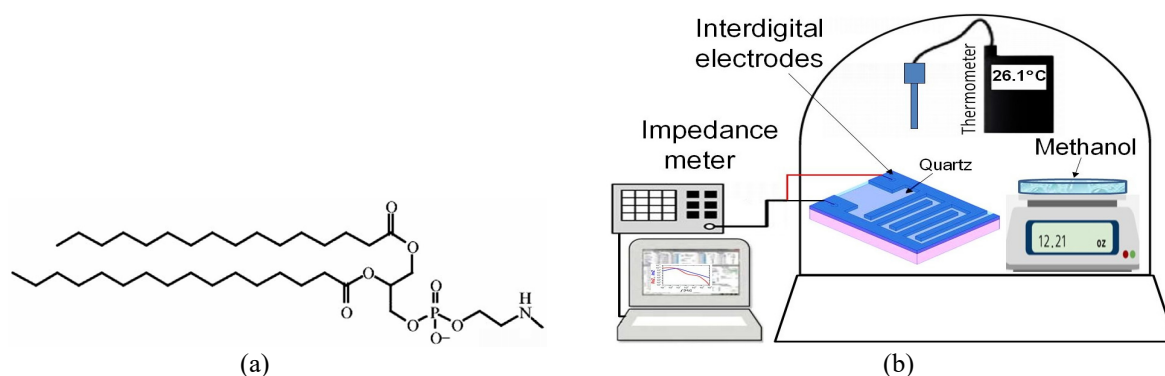E-mail: *georgibh@issp.bas.bg*

Fig. 1. (a) Chemical structure of DPPE; (b) a sketch of the experimental set-up.

EXPERIMENTAL

LB molecular monolayer of phospholipid DPPE with a nanometer thickness [17] was deposited on the surface area of patterned planar interdigitated gold microelectrodes. For the purpose, microelectrode array structure of SAWR [17, 18] was used. The substrate material of SAWR was quartz. The mean thickness of the studied DPPE LB films was estimated to be about 3 nm according to the measurements by small-angle X-ray diffraction (similar to those described in [19]), as well as measured with atomic force microscopy [17, 18]. The use of interdigitatal electrodes (two metallic electrodes in a comb shape, Fig. 1b) aims at considerably enhanced sensitivity of the electrical detection. In our case, they had a height (thickness) of 100 nm and a width of 1.7 μm, the electrode spacing (separation gap) was 1.7 μm (Fig. 1a). The other technical parameters and the topology of the planar interdigitated microelectrode array are given in details in [20]. EIS combined with similar microelectrode structures is advantageous for electrical sensing [10, 15].

The experimental set-up used in the present work is illustrated in Fig. 1(b). The examined gas detector element, composed of DPPE LB film deposited on interdigitated microelectrodes was placed inside a glass exicator and connected to an electrical impedance-meter (outside the exicator). Liquid methanol in a Petri dish was evaporated at constant temperature in the exicator. The concentration of methanol vapor in the exicator volume was varied from 80 to 320 mg/dm³. The vapor concentration was determined by measurement of the weight loss of the liquid methanol in the dish by means of sensitive electronic balance. The experiments were conducted after temperature stabilization of the exicator. During the measurements, the temperature was kept fixed at 26 ± 0.1 °C, outside as well as inside the exicator. A sensitive thermo-couple inside the exicator was used as a reference sensor interfaced to an electronic device for additional control of the interior temperature in the measurement chamber.

The electrical impedimetric behavior of the DPPE LB molecular monolayer upon exposure to methanol vapors was studied by EIS technique in the frequency range 0.1 Hz – 100 kHz. This range was selected because no clearly observable effect of methanol vapors on the impedances was observed at frequency above 100 kHz in our tests under the present experimental conditions. EIS measurements were performed at room temperature, with an electrical impedance meter SP–200 (BioLogic Science Instruments, France) controlled by a computer. The frequency spectra of complex electrical impedance in the plane of the LB film were recorded at AC sinusoidal probe voltage of amplitude 1 V (RMS). The measurements were performed in a grounded Faraday cage to avoid the interference of the external field strength with the measured electrical signal.

RESULTS AND DISCUSSION

By EIS technique [21–23], the raw experimental data - both real and imaginary parts of the complex electrical impedance, *ReZ* and *ImZ*, respectively, were simultaneously measured as a function of the frequency *f* of the AC electric field applied on the sample. Fig. 2 presents the frequency spectra of *ReZ* and *ImZ* measured for the studied DPPE LB film exposed to methanol vapors at various concentrations. It can be seen that in the presence of methanol vapors, the impedance values of the DPPE LB monolayer may greatly decrease. By gradually increasing concentration of methanol vapors, gradually reduced impedances are registered in the low-frequency region of the spectra. The effect is more clearly pronounced for *ImZ* spectra. It is well known that the decrease in *ReZ*(*f*) and *ImZ*(*f*) values toward the zero frequency is related to the decrease of the Ohmic resistance

and the electrical capacitance, respectively [21–23]. By dielectric in capacitor-like geometry, the decrease in $ReZ(f)$ and $ImZ(f)$ values toward the zero frequency is caused by the electrode polarization (EP) effect. At low frequencies, this process dominates over the other dielectric polarization processes. EP is an accumulation of long-distance traveled charges at the interfaces between the electrode and the dielectric film. The strong contribution of EP could be expected by the interdigital microelectrode arrays like the configuration used in this work.
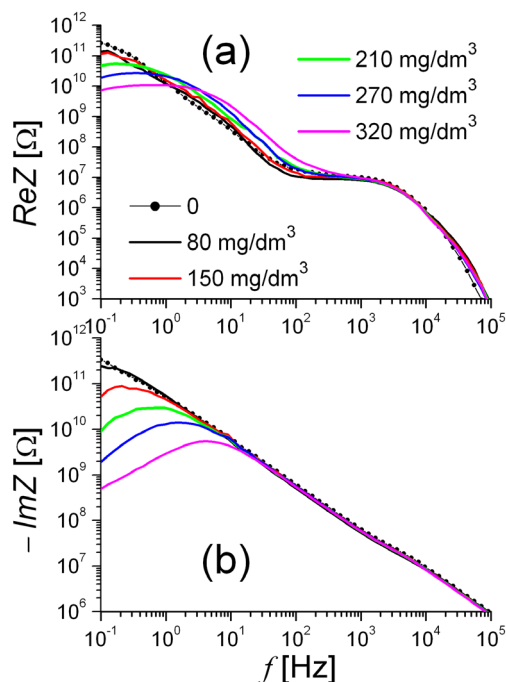

Fig. 2. Frequency spectra of real *ReZ* (a) and imaginary *ImZ* (b) parts of complex electrical impedances measured for DPPE LB film deposited on interdigital electrodes, being exposed to methanol vapors. The concentrations (mg/dm^3) of the vapors are given; 0 corresponds to methanol gas-free case. The temperature was 26 °C.

The observed changes of the impedance behavior were reproducible and reversible – by removal of methanol both *ReZ* and *ImZ* impedances return to the spectra corresponding to the initial vapors-free case. Because of considerable methanol gas-induced change, the impedimetric response of the examined DPPE LB films can be used for detection of methanol in gas phase.

Fig. 3 shows the Nyquist plots (*-ImZ versus ReZ*) for the DPPE LB film. The depressed semicircles in the high to medium frequency regions of the analyzed frequency range in these complex impedance diagrams point out an electrical conduction process [21–23]. The conduction can be attributed to the adsorption of

the methanol gas molecules on the surface of the DPPE LB film. The adsorption of methanol gas molecules on the surface of the DPPE LB film deposited on interdigital microelectrodes was evidenced by a gravimetric method of detection where the mass of the adsorbed gas is directly measured [17, 18]. The mechanism of interaction between methanol gas molecules and phospholipid DPPE LB molecular monolayer is rather complicated because of the competition between the rates of adsorption and desorption of the gas molecules. Generally, the stable detection of methanol vapors by the considered DPPE LB films should be achieved at the equilibrium of the rates of adsorption and desorption (the equilibrium is hard to be described by mathematical equations).

In our case, the adsorption of the methanol gas molecules on the surface of the phospholipid DPPE LB film is assisted by the electrostatic interactions at the surface or near the surface [24, 25] of the phospholipidic LB film, namely electric dipole-dipole intermolecular interactions between the polar head of phospholipid DPPE molecular structure and the dipolar methanol molecules. As known, the permanent electric dipole moment of methanol molecule in the gas phase at room temperature is 1.7 D. As a result, an increase of the concentration of adsorbed methanol gas molecules leads to a strong effect on the electrical impedances of the DPPE LB molecular monolayer, expressed in an increase of its electrical surface conductivity.
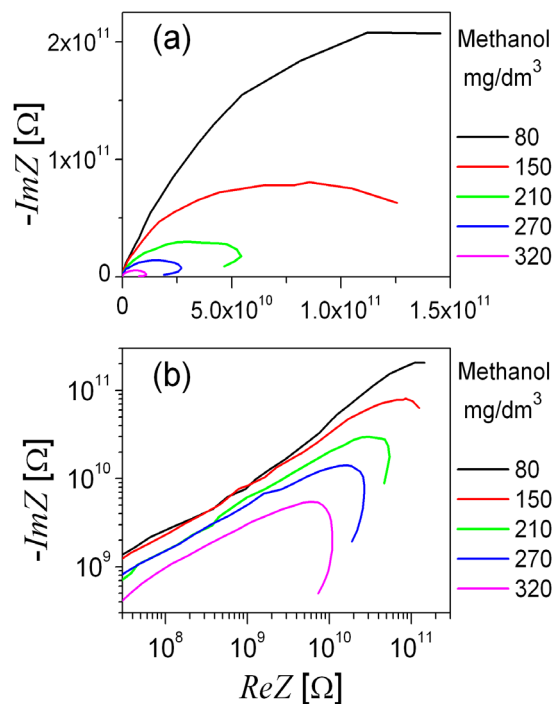

Fig. 3. Nyquist plots for complex electrical impedance measured for DPPE LB film exposed to

methanol vapors at various concentrations: (a) and (b) are the plots in linear and logarithmic scale, respectively.

From the Nyquist plots one can see that the diameter of the semicircles decreases with methanol concentration. The points of interception of the semicircles, or their extrapolations, with the *ReZ*-axis move to the lower impedance values as the concentration of methanol vapors increases (Fig. 3). This large change can be clearly registered by EIS. In particular, the reduction of *ReZ* values is related to a decrease of electrical resistivity of the DPPE LB film, in our case the surface resistivity. Hence, the influence of methanol gas on the impedance of DPPE LB film deposited on interdigital microelectrodes studied here can be used for reliable detection and quantification of methanol vapors by means of EIS. Note that the decrease of surface resistivity is relevant to an increase of the in-plane electrical conductivity of the DPPE LB film. The LB film can be considered to have a domain structure like many slabs that are closely located at the LB film surface and have close but somewhat different dielectric properties. The electrical current rises due to the flow of free electric charges across each slab, and the capacitive current rises due to the accumulation of charges at the boundaries between the slabs [26, 27].

In Fig. 3 it is also seen that at low frequencies the large depressed semicircle is followed by a loop. The latter is due to capacitive charging of gold interdigital microelectrodes and corresponding decrease in LB film resistance at low frequencies. Actually, the loops that takes place in the two-electrode setup applied in the present study result from the change in the resistance of the LB film due to diffusion of mobile electric charges into the LB film.

Clearly, the variations in the frequency-dependent electrical impedance values due to the impact of the methanol vapors is relevant to the modification of dielectric properties of the LB film, i.e., the change in its complex dielectric permittivity. The semicircles in Nyquist plots (Fig. 3) contain information on the change of dielectric properties of the studied DPPE LB film. The spectral changes seen in Fig. 2(a,b) suggest changes of dielectric relaxations [28–31] in the LB monolayer exposed to methanol vapors. This response of the LB film is related to the modification of its dielectric properties due to adsorbed methanol gas molecules. Such modification can be correlated with the frequency f_{max} corresponding to the characteristic local maximum in each of the *ImZ(f)* spectra recorded for DPPE LB films in the presence of the methanol

vapors (Fig. 2b). As seen from Fig. 2(b), the observed peak in *ImZ(f)* spectra is shifted towards the higher frequencies as the concentration of the methanol vapors increases. This frequency shift (Fig. 4) can be also used for detection and quantification of methanol vapors by EIS technique.

Additionally, the tangent loss (*tanδ*) can also be used to characterize the change of the dielectric properties of the studied DPPE LB monolayer affected by methanol vapors. The value of *tanδ* can be determined from the measured impedances: $tanδ = Imε/Reε = ReZ/(-ImZ)$, where $ε$ is the complex dielectric permittivity of the studied LB layer. Note, the values of $ε$ for the tested conditions could be very difficult to be exactly determined owing to the complicated geometry of the electrodes and the geometry of the deposited LB layer.

As a demonstration of the change in the dielectric properties of the studied DPPE LB monolayer affected by methanol vapors, Fig. 4(b) presents the calculated *tanδ vs* the frequency of the applied electric field. In contrast to the measured impedances (recall Fig. 2), the sensing effect is well pronounced in a larger frequency range, in our case 0.1 Hz < f < 1 kHz), where a straightforward increase of *tanδ* value with the increase of methanol gas concentration takes place (Fig. 4b). Clearly, in this way one can perform a secondary quantification of the methanol gas concentration by use of DPPE LB molecular monolayer and EIS.
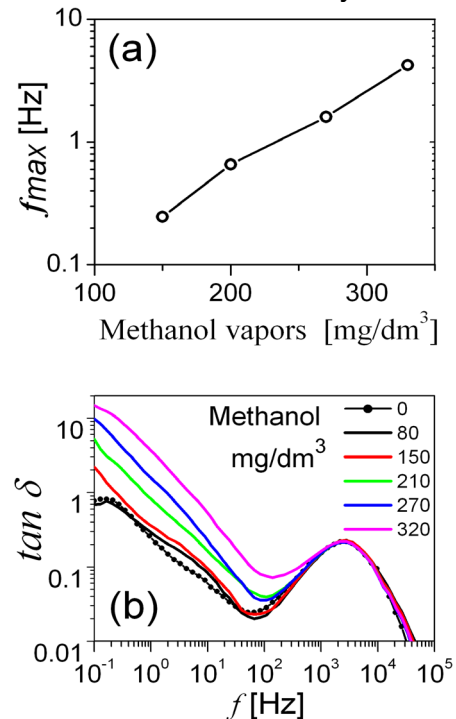

Fig. 4. (a) Frequency f_{max} determined for the studied DPPE LB film *vs* the concentration of methanol vapors;

(b) Tangent loss for DPPE LB film *vs* the frequency of the applied electric field.

The full description and physical interpretation of the modification of the electrical and dielectric properties of the DPPE LB film exposed to methanol vapors requires data obtained by modeling of the complex electrical impedance and complex dielectric spectra, as well data from complementary electrical measurements, e.g., by use of linear voltage sweeping voltammetry and cyclic voltammetry. Since the LB film morphology could affect the process of adsorption of methanol gas molecules on the film surface, the structural properties of the LB film at macro- to nano-level have to be also taken into account, hence the physical interpretation would be rather complicated. In particular, the LB film morphology will strongly affect the analysis of impedance spectra for extraction of numerical information by fitting an equivalent electrical circuit [27, 32] assembled by resistors and capacitors representing the dominant components of the studied LB film [26, 27].

CONCLUSIONS

In summary, the electrical impedimetric response of a phospholipid DPPE LB film to methanol vapors was studied at room temperature by applying electrochemical impedance spectroscopy (EIS). DPPE LB film deposited on interdigitated microelectrodes was examined at various concentrations of methanol vapors. The results show that the changes in the complex electrical impedance of DPPE LB film due to adsorption of methanol gas molecules are well detectable. In particular, the reduction of the surface resistivity of the DPPE LB film deposited on interdigitated microelectrodes can be used for detection of methanol vapors. Besides the electrical impedance characteristics of the DPPE LB film, the adsorbed methanol gas molecules lead to frequency-dependent variations in its dielectric properties. Such changes of the impedimetric response can be also used to detect methanol vapors.

The results obtained from this study are certainly promising and the methodology will be further investigated, e.g., by measurements with a four-electrode setup of EIS. Combining EIS and phospholipid LB films one can develop electrochemical biosensor micro-devices. Further, EIS measurements can provide information on the electrical and dielectric properties of phospholipid LB films in the in-plane direction, as well as on their change upon vapors of volatile organic compounds, such as methanol.

REFERENCES

1. M. C. Petty, C. Pearson, A. P. Monkman, R. Casalini, S. Capaccioli, J. Nagel, *Colloids Surf. A: Physicochem. Eng. Asp.*, **171**, 159 (2000).
2. M. Penza, P. Aversa, G. Cassano, D. Suriano, W. Wlodarski, *IEEE Trans. Electron. Devices*, **55**, 1237 (2008).
3. C. Martensson, V. A. Hernandez, *Bioelectrochem.*, **88**, 171 (2012).
4. J. J. Giner-Casares, G. Brezesinsk, H. Möhwald, *Curr. Opin. Colloid Interface Sci.*, **19**, 176 (2014).
5. H. Wang, H. Ohnuki, H. Endo, M. Izumi, *Bioelectrochem.*, **101**, 1 (2015).
6. M. Y. K. Meynaq, K. Shimizu, M. S. Aghbolagh, S. Tesfalidet, B. Lindholm-Sethson, *J. Colloid Interface Sci.*, **482**, 212 (2016).
7. J. Alvarez-Malmagro, E. Jablonowska, E. Nazaruk, P. Szwedziak, R. Bilewicz, *Bioelectrochem.*, **134**, 107516 (2020).
8. Y. Lu, Y. Chang, N. Tang, H. Qu, J. Liu, W. Pang, H. Zhang, D. Zhang, X. Duan, *ACS Appl. Mater. Interfaces*, **7**, 17893 (2015).
9. A. Balcerzak, M. Aleksiejuk, G. Zhavnerko, V. Agabekov, *Thin Solid Films*, **518**, 3402 (2010).
10. A. V. Mamishev, K. Sundara-Rajan, F. Yang, Y. Du, M. Zahn, *Proc. IEEE*, **92**, 808 (2004).
11. V. Dharuman, T. Grunwald, E. Nebling, J. Albers, L. Blohm, R. Hintschea, *Biosens. Bioelectron.*, **21**, 645 (2005).
12. T. T. Ngo, A. Bourjilat, J. Claudel, D. Kourtiche, M. Nadi, in: Next Generation Sensors and Systems, S. C. Mukhopadhyay (eds.), vol. 16, Springer International Publishing, Sham, 2016, p. 23.
13. N. S. Mazlan, *AIP Conf. Proc.*, **1885**, 020276 (2017).
14. K. Mitsubayashi, O. Niwa, Y. Ueno, Chemical, Gas, and Biosensors for Internet of Things and Related Applications, Elsevier, Amsterdam, 2019.
15. S. C. Mukhopadhyay, B. George, J. K. Roy, T. Islam, Interdigital Sensors: Progress Over the Last Two Decades, Springer Nature, Sham, 2021.
16. L. Yanli, Y. Yao, Q. Zhang, D. Zhang, S. Zhuang, H. Li, Q. Liu, *Biosens. Bioelectron.*, **67**, 662 (2015).
17. G. R. Ivanov, I. D. Avramov, V. J. Strijkova, Y. G. Marinov, T. E. Vlakhov, E. Bogdanova, G. B.

Hadjichristov, *J. Phys. Conf. Ser.*, **1762**, 012002 (2021).

18. G. R. Ivanov, I. Avramov, *J. Phys. Conf. Ser.*, **1186**, 012007 (2019).
19. P. J. Lukes, G. R. Ivanov, M. C. Petty, J. Yarwood, M. H. Greenhall, Y. Lvov, *Langmuir*, **10**, 1877 (1994).
20. I. D. Avramov, A. Voigt, M. Rapp, *Electron. Lett.*, **41**, 450 (2005).
21. J. R. MacDonald, in: Impedance Spectroscopy-Emphasizing Solid Materials and Systems, J. R. Macdonald (ed.), John Wiley and Sons Inc., New York, 1987, p. 13.
22. E. Barsoukov, J. R. Macdonald, Impedance Spectroscopy: Theory, Experiment, and Applications, Wiley, Hoboken, 2005.
23. V. F. Lvovich, Impedance Spectroscopy: Applications to Electrochemical and Dielectric Phenomena, John Wiley & Sons, Inc., Hoboken, 2012.
24. A. M. Gabovich, A. I. Voitenko, *Low Temp. Phys./Fizika Nizkikh Temperatur*, **42**, 841 (2016).
25. R. B. Gennis, Biomembranes: Molecular Structure and Function, Springer-Verlag, New York, 1989.
26. R. Guidelli, L. Becucci, in: Applications of Electrochemistry and Nanotechnology in Biology and Medicine II, N. Eliaz (ed.), Springer, Boston, 2012, p. 147.
27. K. Mallaiya, S. Rameshkumar, S. S. Subramanian, S. Ramalingam, T. Ramachandran, *Electrochim. Acta*, **138**, 360 (2014).
28. A. K. Jonscher, Dielectric Relaxation in Solids, Chelsea Dielectric Press, London, 1983.
29. V. I. Gaiduk, Dielectric Relaxation and Dynamics of Polar Molecules, World Scientific, Singapore, 1999.
30. F. Kremer, A. Schönhals, Broadband Dielectric Spectroscopy, Springer Verlag, Berlin, 2003.
31. Y. D. Feldman, A. Puzenko, Y. Ryabov, in: Fractals, Diffusion, and Relaxation in Disordered Complex Systems, W. T. Coffey, Y. P. Kalmykov (eds.), vol.133, John Wiley & Sons, Inc., Hoboken, 2006, p. 1.
32. H. T. Tien, A. L. Ottova, *J. Membr. Sci.*, **189**, 83 (2001).

Section

Methodology in Education

The potential of YouTube as a learning tool in physics education: a survey among secondary students

I. Kotseva[1], N. Nikolov[2]*

[1]Sofia University „St. Kliment Ohridski", Faculty of Physics, 5 James Bourchier Blvd., Sofia 1164, Bulgaria
[2]119. High School „Acad. Mihail Arnaudov", Sofia, Bulgaria

Online education is based on modern ICTs, the potential of which is being revealed more and more recently. During the long-distance learning in the pandemic conditions of COVID-19 in Bulgaria, we decided to explore the potential for creating video lessons on YouTube and to explore some attitudes among students. A YouTube physics training channel was set up, and students had to answer a few questions. The report presents an algorithm for creating an educational YouTube channel and video lessons in physics, as well as summarized results of the survey among students. The questions in the survey are designed to assess the effectiveness, visibility, and accessibility of video lessons, as well as the motivation of students to learn from YouTube.

Keywords: Online education, physics, YouTube, video lessons

INTRODUCTION

There is an active introduction of modern information and communication technologies (ICTs) in modern distance learning. ICTs benefit the presentation of teaching materials, the interaction of teachers with their students, and the intermediate and final control of students' advancement [1].

One of the most suitable learning tools is video tutorials. They allow to make the lesson more interesting, dynamic, and convincing, and a huge flow of information is easily accessible. Such a methodological technique as video learning allows to better visualize the learning material and can be an important tool for students' self-learning. This approach can also be used as a form of distance learning.

The relevance of the introduction of video lessons in education is determined for several reasons:

• When studying the teaching material in video format, the student can regulate the learning process, namely to review the video from the required place, to pause for viewing, thus studying in detail incomprehensible (complex) or especially important moments for him.

• The effectiveness of video lessons is increased by the fact that the student perceives the material given to him by two senses - sight and hearing, therefore such material contains more information than a single text presentation or audio reproduction and comments.

• The training can be held at any convenient time and place while creating in the student a sense of personal presence in class.

As a result, it can be concluded that maintaining an educational information channel for video lessons is extremely important.

The creation of educational video films today is impossible without the use of modern methods and technologies for video data processing and initial video recording skills. Unfortunately, not all teachers know where to start the process of creating a video lesson, how to write a script (or to make a scenario of the lesson), and how to make the video lesson more attractive according to the requirements of the students. Based on this, one of the ways to improve the educational process is to create guidelines for teachers to develop video lessons.

RESEARCH METHODS

The research questions we asked ourselves at the beginning of this study were related to the opportunities that YouTube provides for the development of educational channels and what are the attitudes of students to learning from YouTube. We also initially looked at articles on these issues. Some of them address issues related to the potential benefits, advantages, and disadvantages of YouTube in the classroom [2-5], while others are more specific concerning certain disciplines [6-9]. As a result of our theoretical research, we concluded that there is a need for more research, especially in connection with the attitude of students to the educational opportunities of YouTube.

Thus, our research work went through the following stages:

(1) Creating a YouTube channel for the needs of physics education in seventh grade;

(2) Developing a questionnaire to study attitudes and motivation among students;

(3) Processing and analysis of the survey results.

Creating a YouTube channel

When creating your own YouTube video channel, you have several tutorials available, such as [10], or you can simply use YouTube itself to do so (creatoracademy.youtube.com/page/home). The YouTube video-sharing platform has its pedagogical benefits in several ways:

• creating specific playlists with materials on a given subject. This supports the learning of the students and is a convenience for the teacher;

• creating video lessons that are recorded outside the classroom;

• students are taught to follow the rules for sharing content on relevant platforms, not to violate copyright laws, to be ethical and fair to others;

• "learning by doing" method can be implemented to encourage students' creativity by creating their videos with an educational goal.

The structure of a lesson and a video lesson may vary in some stages. According to the structure of the modern lesson and the requirements for each stage in the creation of educational videos, the following points must be taken into account:

1) Stage of motivation for learning activities - a necessary component of learning that must be maintained throughout the lesson. Of great importance is the clearly defined goal that is set for students.

2) Setting a training goal - the student from the very beginning of working with a multimedia didactic tool must know what is required of him. Learning objectives should be clearly stated during the lesson.

3) Stage of updating - creating prerequisites that support the perception of the learning material.

4) Stage of choosing a strategy to achieve the goal.

5) Stage of initial consolidation - students solve typical problems using the new method of action shown in the video lesson.

6) Summary of the lesson - there must be a connection between the set goal and the obtained results. Additional goals of the activity may be outlined.

It is necessary to create video lessons which should be expressed in simple language, without using complex definitions and formulas. This is because when a person watches video fragments, he first perceives the visual information and only then the auditory information. It is also not advisable to create long video tutorials. It is recommended that the duration be up to 10-15 minutes.

It should be noted that the effectiveness of video courses on a YouTube channel is directly dependent on the quality of the video lessons and the technical means used. The video method places great demands on the organization of the learning process, which must be characterized by clarity, thoughtfulness, and expediency. A teacher using the video method is required to develop the ability to introduce students to the range of studied problems, direct their activities, and draw general conclusions.

After getting acquainted in detail with the possibilities of YouTube for creating and maintaining the channel, we created a short guide to help teachers who would benefit from this. In conclusion of our work on creating the channel (we have chosen the video logo to be PHYSICS TV), we can say that it is within everyone's ability to maintain their channel.

When recording the lessons, we used BANDICAM - a multimedia program that records actions on a computer screen, audio, and more (www.bandicam.com) and is easy to use. A specific feature of the program is that it can record for up to 12 minutes for free.

Survey and target groups

For our study, we chose to make a lesson on "Sound and Hearing" from the physics program for 7th grade. The duration of the video lesson is about 10 minutes and it includes explanations from the physics textbook that students study and also contains embedded videos. The link to this video lesson is given in [11]. You can subscribe to the channel and see the other lessons as well. The target audience is seventh-graders from 119. Secondary school "Acad. Mihail Arnaudov", Sofia and the video tutorial is available on the Internet for everyone. Creating a similar video lesson is within a day.

After the students watched the video lesson, they were asked to fill out an online questionnaire consisting of a total of 7 questions, of which 4 with optional answers and 3 open. The survey is anonymous and involved 40 students.

RESULTS AND DISCUSSION

Here are the questions and the summarized results. We provide only descriptive statistics due to the small sample size.

Question 1: How often do you visit YouTube?

✓ Very rarely -1 student;
✓ Rather a several times a week - 10 students;

✓ Every day - 29 students.

The answer "Every day" was most often chosen (≈73%), followed by the answer "Rather a several times a week" (≈25%), and finally, the answer "Very rarely" was chosen by only one person (≈2 %) (Figure 1).

How often do you visit Youtube?

2%
25%
73%

■ Very rarely
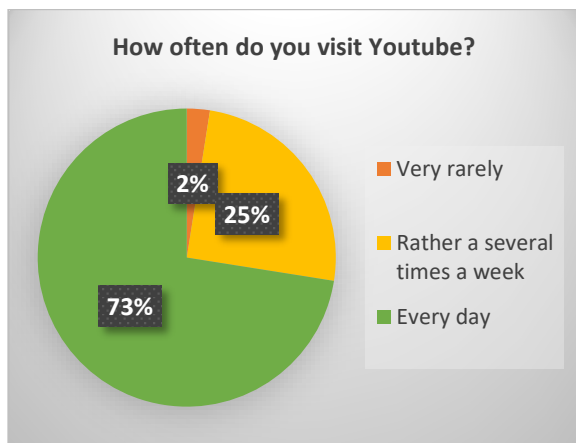■ Rather a several times a week
■ Every day

Figure 1. Answers to Question 1

These results confirm the global statistics, according to which YouTube is the second most visited site on the Internet after Google. It is therefore interesting to find out for what purpose students visit YouTube most often.

Question 2: For what purpose do you visit YouTube?

This question is open, but the answers allowed them to be grouped into three main groups:

✓ Music and movies - 28 students;
✓ I'm looking for information about something - 9 students;
✓ Education - 3 students.

This means that for the largest percentage of students (approximately 70%), YouTube is a source of entertainment. For approximately 22% YouTube is a source of information and for only 8% it is a learning tool (Figure 2).
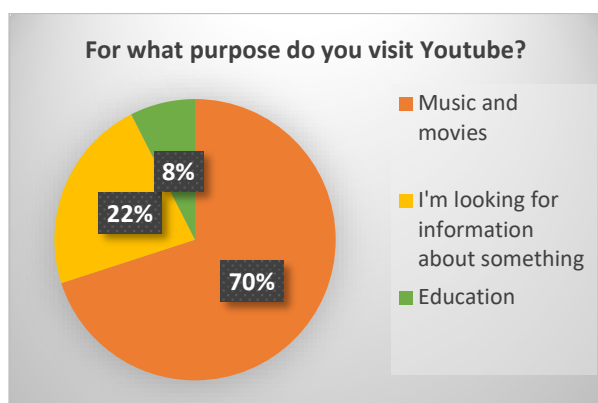
For what purpose do you visit Youtube?

8%
22%
70%

■ Music and movies
■ I'm looking for information about something
■ Education

Figure 2. Answers to Question 2

The purpose of Question 3 of the survey is to assess the educational opportunities of YouTube according to the opinion of the students, after watching the video lesson "Sound and Hearing". The question has 5 optional answers, which are designed to evaluate 4 main characteristics of video lessons: a) effectiveness; b) clarity; c) repeatability (information is not lost); d) accessibility. It is possible also to choose a neutral position (only 1 student found it difficult to choose from the other options). The summarized results are the following:

Question 3: Which of the following statements most accurately reflects your view of YouTube's educational opportunities after watching the Sound and Hearing video tutorial?

✓ Video lessons save time for self-preparation - 4 students;
✓ The information is clearer and more understandable - 18 students;
✓ If something is not clear, I can watch the lesson again - 5 students;
✓ The lesson is available anytime and anywhere - 11 students;
✓ I do not have a clearly defined opinion - 1 student.

From these results, we see that the most students rate the clarity and comprehensibility of video lessons (almost 46%). Almost the same percentage (if we combine answers 2 and 3, as they are close in meaning) receive the other characteristics - repeatability and accessibility (41%). Only 10% believe that video tutorials would save time for self-preparation. Finally, the conclusion is that video lessons are more a means of better visibility and comprehensibility of information, but can also be part of students' self-preparation (Figure 3).

Question № 4 assesses students' attitudes towards video lessons, and the answers (see below) can guide students' attitudes if teachers use such lessons.

Which of the following statements most accurately reflects your view of YouTube's educational opportunities after watching the Sound and Hearing video tutorial?

3%
10%
28%
13%
46%

■ Video lessons save time for self-preparation
■ The information is clearer and more understandable
■ If something is not clear, I can watch the lesson again
■ The lesson is available anytime and anywhere
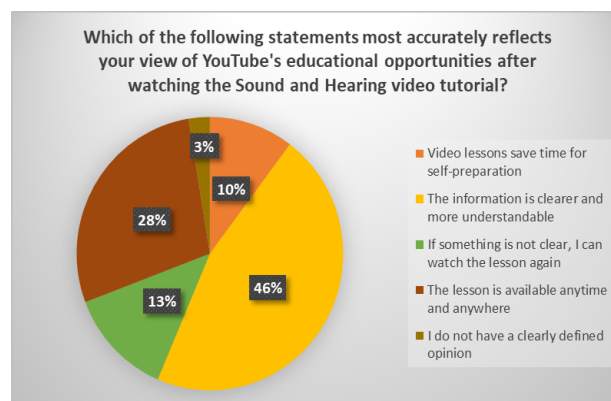■ I do not have a clearly defined opinion

Figure 3. Answers to Question 3

Question 4: Which of the following statements most accurately reflects your attitude towards video tutorials?

✓ They are more interesting - 20 students;
✓ They motivate me to study - 6 students;
✓ I like them the most - 4 students;
✓ There should be more such lessons - 10 students;
✓ I have no definite attitude - 0 students.

There is not a single student who has found it difficult to choose a position. Half of the students find this type of lesson more interesting. Twice fewer students (25%) are adamant that there should be more such lessons. 15% will be motivated to learn if there are such lessons, and 10% are adamant that they like this type of lesson the most (Figure 4).
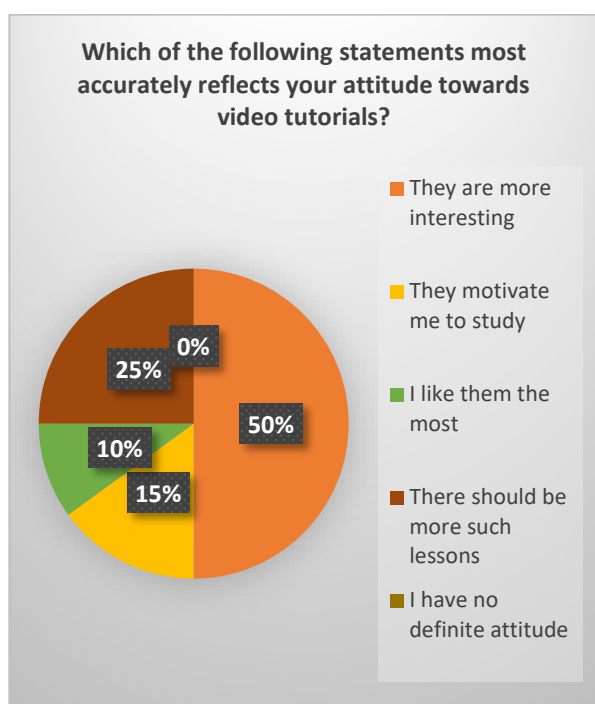

Figure 4. Answers to Question 4

Question 5 was open-ended, but the answers allowed them to be grouped into 4 main categories:

Question 5: Indicate what you liked the most in the lesson you watched.

✓ Everything - 7 students;
✓ There is 3D - 5 students;
✓ The presentation of the lesson as a whole - 20 students;
✓ Its duration – 8 students.

Half of the students liked the idea that the lesson could be presented in the form of a video and the video itself. 20% believe that the duration (about 10 minutes) is optimal for this type of lesson; 17% liked everything and 13% liked the 3D (Figure 5).
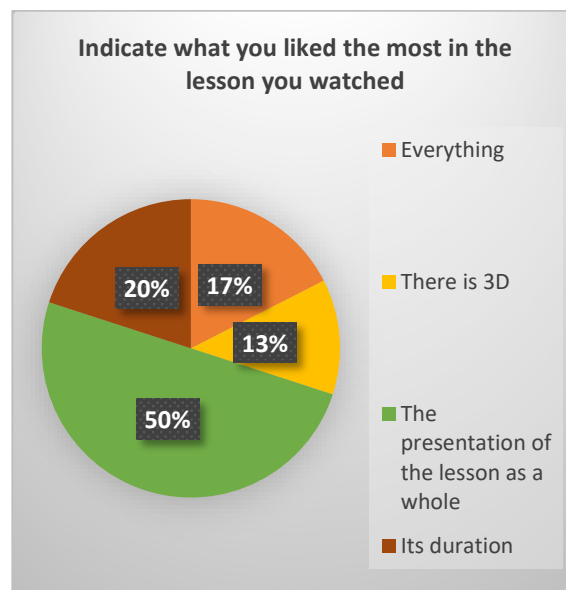
Figure 5. Answers to Question 5

And on **Question 6:** What did you not like in the lesson?" 36 students (90%) have no remarks, two - speaking more slowly and two more - write down the unit of decibel.

To the last **Question 7**, would they give any recommendations to the teachers who want to create similar video lessons (or what they expect the most from such video lessons), almost half of the students (17 in number) do not have recommendations, 12 in number express a wish to have more such lessons and 11 in number, the video lessons to be of similar duration.

CONCLUSION

At present, the problems and issues related to distance learning are extremely relevant, and the final product of this thesis - the created information and education channel, is an appropriate solution. Adding to the technological and informational capabilities of YouTube, more work should be done in the future to develop video tutorials, especially since this opinion was also expressed by the majority of surveyed students.

We hope that the modest research we have done will motivate many teachers who are willing to improve the quality of education and increase students' interest in the subjects they teach to benefit from the potential of YouTube as a learning tool.

REFERENCES

1. G. Kalpachka, *Bulgarian Chemical Communications*, **52**, Special Issue A, 109 (2020).

2. T. Jones, K. Cuthrell, *Computers in the Schools,* **28(1)**, 75 (2011).
3. B. K. Fleck, L. M. Beckman, J. L. Sterns, H. D. Hussey, *Journal of Effective Teaching*, **14(3)**, 21 (2014).
4. M. Gilroy, *The Education Digest*, **75(7)**, 18 (2010).
5. J. J. Jenkins, P. J. Dillon, Learning through YouTube, in: *The plugged-in professor*, Chandos Publishing, 2013, p. 81.
6. J. Allgaier, Science and medicine on YouTube, Second international handbook of Internet research, 2020, p. 7.
7. C. Snelson, YouTube across the net: A review of the literature, *MERLOT Journal of Online learning and teaching*, **7(1)** (2011).
8. D. DeWitt, N. Alias, S. Siraj, M. Y. Yaakub, J. Ayob, R. Ishak, *Procedia-Social and Behavioral Sciences*, **103**, 1118 (2013).
9. S. C. Burke, S. L. Snyder, *International Electronic Journal of Health Education,* **11**, 39 (2008).
10. R. Ciampa, T. Moore, YouTube channels for dummies, John Wiley & Sons, 2015.
11. https://www.youtube.com/watch?v=jTluT14EqdE&t=24s.

Analysis of problem-based learning in physics from the perspective of integrated STEM education

I. Kotseva*, M. Gaydarova, F. Kunis, K. Ilchev

Sofia University „St. Kliment Ohridski", Faculty of Physics, 5 James Bourchier Blvd., Sofia 1164, Bulgaria

Problem-based learning is a specific instructional strategy that applies to the teaching of a variety of scientific content in school. In this article, we analyze the main characteristics of problem-based learning and argue that it is one of the most appropriate practices for integrated STEM education. Our arguments are based on several key concepts and principles that are common to problem-based learning and the integrated approach to STEM. In addition, we find common difficulties in the implementation of problem-based learning and the integrated approach, which are also discussed. This offers new perspectives for problem-based learning in connection with the future development of integrated STEM education.

Keywords: problem-based learning, integrated STEM education, physics

INTRODUCTION

Recently, in science education, the focus has been on the world-famous STEM (science-technology-engineering-mathematics) education. As a result of several years of research on this phenomenon called STEM, we have gained a very thorough knowledge of its origin, its impact on education, and the approaches and models through which it is applied in education. The modern analysis of the approaches and models in STEM education reveals a tendency towards the improvement of the integral approach. In recent years, the integral approach in STEM has been developing under the pressure of influential international organizations of engineers and technologists. The question of where "T" and "E" are in STEM education is quite fair and standards for technological literacy are consequently developed [1, 2]. Let us remember that the ideas of active learning and learning by doing are inherent in technology education and let's admit that problem-based learning began to develop in the early 20th century through the work of John Dewey precisely in connection with technology education [3]. So it's no surprise that we're looking for intersections between problem-based learning (hereinafter referred to as PBL) and integrated STEM (hereinafter referred to as I-STEM).

PBL is the focus of many universities, which aim to modernize their curricula and programs and shift the burden from teacher-centered instruction to student-centered learning. Other reasons to focus on PBL are, that learning is more enjoyable with PBL. PBL helps you learn 'how to learn' and critical skills for the workplace are developed with PBL [4].

It is also interesting, "what employers want to see from new graduates entering the workplace" [4]. The author George Watson refers to a Sigma Pi Sigma Survey of "*Skills Used Frequently by Physics Bachelors in Selected Employment Sectors, 1994*" and although it was done in the distant 1994, the listed characteristics are even more relevant: high level of communication skills, ability to define problems, gather and evaluate information, good teamwork skills and the ability to work with others, and the ability to use all of the above to address problems and find solutions in a complex real-world setting. It is interesting that in the list of self-reported skills used frequently by physics bachelors in selected employment sectors - industry, government laboratories, and high school teaching, knowledge of physics is placed just before advanced mathematics in one of the last places, and not surprisingly, problem-solving is put in the first place [4].

METHODS OF RESEARCH

This is primarily an exploratory report, the purpose of which is to analyze PBL in physics education but from the perspective of I-STEM education because PBL and context-based real-life problems in themselves or the interdisciplinary approach are not a novelty to physics education [5-10]. This implies a good knowledge of the characteristics and trends of both the PBL and the integrated STEM. Based on the available sources in PBL and STEM education (not all of them are cited here), we have formed our point of view on some current issues of physics (and STEM) education in general.

* To whom all correspondence should be sent:
E-mail: iva_georgieva@phys.uni-sofia.bg

In the analysis, we also take into account two additional facts - that PBL and I-STEM intersect with the new 21st-century paradigm in education, namely the emphasis on developing certain skills on the one hand, and the highest taxonomic level in Andersen's taxonomy – creativity, on the other hand.

Characteristics of PBL

The basis of PBL is the research of a problem most often through teamwork. Problems can be clearly defined by the teacher, or unstructured by defining different levels of problem definition [11]. Problems are also divided into routine (with a clear decision procedure) and non-routine (without a clear decision procedure). They can be in only one subject area or they can be integral - combining knowledge from different areas. PBL is a student-centered approach in which, instead of memorizing knowledge and solving such problems, oriented to the use of this knowledge, a real problem is posed and information necessary to solve this problem is collected by the students. This approach also forms skills for teamwork and research and develops critical thinking and lifelong learning skills [12]. The motivation to learn increases due to the challenge of finding the necessary information, not just applying what is learned in class. Seeking information also contributes to strengthening the motivational element in learning, strengthening the student's self-confidence and building a sense of competence. The reflection related to the self-assessment of the student's activity and the evaluation of the work of the other students is also brought up. Communication skills, skills for presenting and defending positions, defined as soft skills, are formed at the stage of presenting decisions and sharing with others their own decisions.

Some authors determine that the use of PBL has the following main advantages: the student's responsibility for his own achievements increases, the learning also has an emotional character, the skills for group activity in the distribution of roles in the team improve, the comprehension of content is facilitated [13].

The most difficult thing for the teacher when applying PBL is to determine within the studied curriculum a real significant problem suitable for research. It must be consistent with the age of the students and the competencies declared in the curriculum. A preliminary analysis of the problem is needed regarding the difficulties and challenges that students may encounter. The different roles in the teams, as well as the resources available to the students should be defined. It is also necessary to plan feedback with students at each stage when solving the problem.

Characteristics of I-STEM

In the integrated approach in STEM, the disciplines are studied as one discipline, without barriers between them. This approach requires the integration of at least two disciplines, and in recent years there have been models of integration in all four areas of STEM [14, 15]. This is made possible by the entry of engineering design into curricula and the understanding, supported by the Next Generation Science Standards (NGSS), that the study of practical applications of science can provide a framework for integrated STEM education. This new generation of standards has three dimensions involved in teaching at all levels: (1) basic ideas derived from the specific content of individual disciplines; (2) scientific and engineering practices (students are expected not only to study content but also to understand the methods that scientists and engineers use in their practice); (3) crosscutting concepts applicable in all areas, such as *pattern, cause and effect, scale, proportion, quantity, systems and system models, energy and matter, structure and function, stability and change* [16].

We see that an important element of these standards is the integration between content and scientific and engineering practices. It should be noted that NGSS focuses equally on engineering design and scientific inquiry. The entry of engineering and technological design greatly changes the landscape of STEM education. While in science education students learn ideas about the world previously accepted by science, this is not the case with technology and engineering. Technology and engineering acquire knowledge through design starting from a technological problem and there are elements of trial and error in this process. Technological knowledge is predetermined by the nature of the problem. The information needed to solve a technological problem constitutes this new knowledge, which must be acquired and which is therefore not known before an analysis of the problem is made. Hence the conclusion is that content cannot be studied without a design problem [17].

The different epistemologies of science, technology, engineering, and mathematics are the biggest challenge to I-STEM [17]. This predetermines the different connections that science, technology, engineering, and mathematics can have in pairs. This must be taken into account in any model of the integral approach [14]. Yet integration can be achieved based on the goal that has been set

and the goal is not only to acquire knowledge but also to develop certain skills.

Intersections with 21ˢᵗ century skills

Both PBL and I-STEM have intersections with 21ˢᵗ-century skills. The skills of the 21ˢᵗ century, which are fundamental to shaping the prosperity of future generations, are defined by the National Research Council of the United States and more specifically, by the Board on Science Education at a workshop in May 2007 as follows:

➢ *adaptability* - sustainable behavior in a changing and uncertain environment;

➢ *social and communicative skills* – a manifestation of tolerance, empathy, and acceptance of the different;

➢ *non-routine problem solving* - recognizing and defining the problem, developing a strategy for solving it, searching for new solutions;

➢ *self-control* - exercise of reflection, need to learn, self-assessment;

➢ *systems thinking* - the ability to understand how things work, how the parts are connected to the whole, how they interact and how they change, and how to improve and refine the system [18, 19].

Two of these skills - systems thinking and non-routine problem solving - are related to science education, in particular physics. The PBL strategy can be integrated to achieve effectiveness in terms of these two qualitative characteristics of personal behavior. Systems and non-routine thinking are the basis for the formation of the cognitive level of creativity in physics education.

Systems thinking is formed in science education as a system of knowledge that is classified in the process of its creation and is based on the use of conceptual apparatus, models and laws – the core of science. Systems thinking requires knowledge of the structure of scientific theory, the limits of the models we use, and the methods of scientific research. This is knowledge of epistemological and procedural nature, defined in the PISA programs [20].

Scientific knowledge, part of which is studied in school, is structured - there is a system of concepts, laws, models, and theories. It has a collective character and develops by changing models. Its purpose is to reach a conceptual description, explanation, and prediction of facts and phenomena. Through systems thinking we can distinguish the different categories of knowledge - facts, concepts, laws, and models, which are in different relationships and different degrees of generalization. For example, physical laws have great predictive power, and the theory explains the facts. The formation of systems thinking in the study of physics is also presupposed by its object of study - natural phenomena and processes that take place in different systems [21].

The conditions in which the systems exist determine the causes and consequences of natural phenomena. Understanding how changing conditions affect consequences is an important element of systems thinking and is the basis for understanding how systems work. Nature itself teaches us to think systematically when we study it. It sustains life by creating and operating systems. Understanding that the behavior of systems in nature depends on all its parts, and that the lack or imbalance in one part of the system affects the normal functioning of others, is a basic idea in the formation of systems thinking in students. Important concepts here are the modeling and visualization of systems, as well as defining the boundaries within which they exist.

PBL is an approach through which systems thinking can be formed by organizing learning so that in the process of solving physics problems clearly distinguish the individual elements of scientific knowledge - fact, concept, law, model, theory, etc. This also forms competencies related to the application of procedural and epistemological knowledge, defined as important in the study of natural sciences.

Non-routine problem solving requires researching a wide range of information, recognizing existing models and developing a strategy, integrating seemingly unrelated information, as well as generating new solutions, and switching to another strategy if the developed one works no longer [22]. It also requires creative thinking, which is the highest cognitive level in Anderson's taxonomy [23].

In connection with I-STEM and creativity, some authors believe that Anderson's taxonomy is more relevant and helpful for engineering and technological education because "creating lies at the heart of engineering and technology" [24]. We further agree that developing metacognitive knowledge which is the fourth category in Anderson & Krathwohl's knowledge dimension is a basis for active learning not only in engineering but in I-STEM and PBL as well. Both Bloom's and the revised Bloom's taxonomies are appropriate to develop the levels in the PST – the problem-solving taxonomy [24, 25]. We can also refer to a PPST – a physics problem-solving taxonomy presented as a useful instructional tool to teachers [26].

CONCLUSION

Both PBL and I-STEM are rooted in constructivism which means developing new knowledge rather than learning by heart. But other characteristics connect PBL in physics education and I-STEM. These are teamwork and developing other 21st-century skills. PBL is sometimes described as an instructional strategy in which students confront conceptually ill-structured problems and this type of task is very typical for engineering and consequently for I-STEM. Ill-structured problems are very often rooted in real-life situations and require meaningful solutions (not always unambiguous). Strategies for solving this kind of problem are developed in both PBL and I-STEM.

Both PBL and I-STEM have great potential to improve education in general but there are some challenges to their implementation. As oriented towards higher cognitive levels, they require new strategies at the policy and management level and flexible curricula that provide the time needed to accomplish goals and objectives. Certain changes in the educational space are necessary to facilitate teamwork regarding PBL and cooperation with communities of practice regarding I-STEM. Content that covers different areas of knowledge and competencies is based on both PBL and I-STEM and has to be found and included in cognitive problems. This also leads to changes in teachers' professional development and implementation of new instructional methods, like design-based methods, for example. Despite these difficulties, the challenges of the 21st century make us think that PBL and I-STEM should and will develop and the trends we notice prove it.

REFERENCES

1. J. Moye, P. A. Reed, *Technology & Engineering Teacher*, **80(3)**, 9 (2020).
2. T. R. Kelley, *Technology and Engineering Teacher*, **73(4)**, 18 (2013).
3. M. Sanders, 2008 Annual Conference & Exposition, 13 (2008).
4. D. Raine, S. Symons, PossiBiLities: A Practice Guide to Problem-based Learning, 2005.
5. T. J. McConnell, J. Parker, J. Eberhardt, Problem-Based Learning in the Physical Science Classroom, K-12. NSTA Press, 1840 Wilson Boulevard, Arlington, VA 22201, 2018.
6. R. I. Vassileva, *Bulgarian Chemical Communications*, **50**, Special Issue B, 72 (2018).
7. P. van Kampen, C. Banahan, M. Kelly, E. McLoughlin, E. O'Leary, *American Journal of Physics*, **72(6)**, 829 (2004).
8. B. J. Duch, AIP Conference proceedings, **399(1)**, American Institute of Physics, 1997.
9. A. K. Mody, H. C. Pradhan, *Problem-Based Learning in Basic Physics–III*, 36 (2017).
10. R. I. Vassileva, G. Malchev, *Bulgarian Chemical Communications,* **52**, Issue A, 121, (2020).
11. M. A. Ruiz-Primo, in: Workshop on Exploring the Intersection of Science Education and the Development of 21st Century Skills, Washington, DC, (2009).
12. S. Kurt, Problem-based learning (PBL), Educational Technology, in: Education Technology, retrieved from https://educationaltechnology.net/problem-based-learning-pbl, (2020).
13. E. Bate, J. Hommes, R. Duvivier, D. C. Taylor, Problem-based learning (PBL): Getting the most out of your students–Their roles and responsibilities: AMEE Guide No. 84, *Medical Teacher*, **36(1)**, 1 (2013).
14. T. R. Kelley, J. G. Knowles, *International Journal of STEM Education*, **3(1)**, 11, (2016).
15. J. G. Wells, *Technology and Engineering Teacher*, **75(6)**, 12 (2016).
16. National Research Council, A framework for K-12 science education: Practices, crosscutting concepts and core ideas, National Academies Press, 2012.
17. J. Williams, *Design and Technology Education: An International Journal*, **16(1)**, 26 (2011).
18. National Research Council, Exploring the intersection of science education and 21st-century skills: A workshop summary, 2010.
19. N. G. Peterson, M. D. Mumford, W. C. Borman, P. Jeanneret, E. A. Fleishman, An occupational information system for the 21st century: The development of O* NET, American Psychological Association, 1999.
20. OECD, PISA 2015 Assessment and Analytical Framework: Science, Reading, Mathematics and Financial Literacy, OECD Publishing, Paris, 2016.
21. W. A. Sandoval, *The Journal of the Learning Sciences*, **12(1)**, 5 (2003).
22. J. Houston, K. Ferstl, Future skill demands, from a corporate consultant perspective, National Research Council, 2007.
23. L. W. Anderson, D. R. Krathwohl, A taxonomy for learning, teaching, and assessing: A revision of Bloom's taxonomy of educational objectives, Longman, 2001.
24. M. Barak, *Journal of Engineering, Design, and Technology*, **11(3)**, 316 (2013).
25. H. L. Plants, R. K. Dean, J. T. Sears, W. S. Venable, A taxonomy of problem-solving activities and its implications for teaching, The teaching of elementary problem-solving in engineering and related fields, 1980, p. 21.
26. L. Shakhman, M. Barak, *EURASIA Journal of Mathematics, Science and Technology Education*, **15(11)**, 1 (2019).

Applying collaborative activities in high school physics course during a hybrid model of learning

F. Kunis[*], I. Kotseva, M. Gaydarova

[1]Sofia University „St. Kliment Ohridski", Faculty of Physics,5 James Bourchier, Sofia 1164, Bulgaria

Many large educational institutions and international studies point out that collaborative problem solving is a key competence for the successful integration of students into society and the workforce. Therefore, teachers need to apply methods and activities that develop students' teamwork skills. But for two school years now, we have been facing the challenges of distance learning because of the coronavirus crisis. Lacking the possibility of full attendance of students in the classroom, there is a need for an innovative and flexible approach to be applied by teachers to be able to cope with this emergency. This report examines the possibilities for implementing collaborative activities in the high school physics course during the hybrid model of learning. Surveys were conducted among students from ninth to eleventh grade to investigate whether there is an increase in interest in physics and STEM disciplines if collaborative activities are implemented in high school physics courses during the hybrid model of learning.

Keywords: collaborative activities, hybrid learning, collaborative problem solving, physics education

INTRODUCTION

There is no doubt that education systems around the world face enormous challenges. The coronavirus has caused huge changes around the world. Education is one of the most affected systems.

But even before the coronavirus, educational systems had to meet new challenges and change so that students could successfully integrate into the future world of innovation and technological change. Leading world organizations such as UNESCO at the UN, the European Parliament, the Council of Europe, the PISA program at the OECD, and others recommend focusing teaching efforts on developing the skills and competencies needed by today's students to live in the challenges of the 21st century [1, 2]. To achieve this goal, education systems are expected to provide high-quality education, training, and lifelong learning for all, as well as to assist teachers in implementing competency-based learning approaches [3].

The main competencies that students need for their successful integration into society and for their successful professional realization are critical thinking, creativity, collaboration, and communication [4].

Collaborative problem solving was chosen by the Organization for Economic Co-operation and Development (OECD) as a new competence, which was explored in the PISA international study in 2015. There are many reasons for collaborative problem solving to be in focus. International studies indicate that collaborative problem solving is a key competence for the successful integration of adolescents into society and the workforce. It is also believed that much of the planning, and problem-solving decision-making will be done by teams and teamwork [5].

The implementation and application of the new competencies are important for the Bulgarian educational system. In the PISA assessment from 2012 of the module problem solving of 43 participants, Bulgarian students were in 42nd place, and in 2015 in the PISA assessment of the module collaborative problem solving of 51 participants, Bulgarian students were in 40th place [6]. These examples show that serious changes are needed in the Bulgarian learning environment to lead to a qualitative improvement of skills and competencies of the 21st century.

BENEFITS

Teamwork is a key competence that students must possess to be successful in the 21st century. Therefore, it is important to have sufficient quantity and quality practices in the learning process for students to work in a team. In this way, we can guarantee with a high probability that students will develop their teamwork skills through appropriately selected team activities. Collaborative learning does not only develop students' teamwork skills. Many studies show different benefits of collaborative learning [7-12].

According to research, students show a higher level of knowledge if they have participated in team activities.

---

* To whom all correspondence should be sent:
E-mail: fabien.kunis@gmail.com

Research usually compares a group of students who have participated in collaborative learning and an active form of learning with a group of students who have only listened to a lecture. The differences in the achieved results vary, but there is a significant difference in the results. The explanation is that students should be an active part in discussing the problem when working together. This stimulates them more and makes them think more about the problem. Whereas if they only listen to a lecture, they are in a passive role. This passive role does not allow them to delve into the problem and therefore it is difficult to acquire quality and long-lasting knowledge.

CHALLENGES

Collaborative learning has many challenges and is not easy to implement in the curriculum. To successfully implement collaborative learning, it is necessary to have a proficient teacher. Many teachers do not feel confident enough to leave their comfort zone and try new teaching methods and techniques.

Unfortunately, many students have "group hate" [13]. Some students do not want to work in groups. This can be due to various factors. Some students are introverted. These students don't feel comfortable talking to other people. They usually remain silent and do not take part in discussing the problem. The other team members begin to ignore them and thus the opposite effect occurs. These students are increasingly starting to dislike teamwork [14]. In order not to get into such situations, the teacher must know the students and be able to make the groups feel comfortable. That's not easy. A teacher is required to know the students and to have some experience in managing teamwork.

Another challenge is loafing. There are usually students who don't take responsibility for their role, even if it is the smallest role in the group [15]. This leads to conflicts within the group. Students expect everyone to do their job conscientiously. In order not to get into such situations, the teacher should carefully monitor the progress of the groups and, if necessary, intervene.

An important issue in collaborative learning and common projects is evaluation. To avoid conflicts, the teacher from the very beginning must be sure that the work is fairly divided between the individual participants. Individual team members must have agreed from the outset on how the work will be divided. In the process of performing the tasks, the teacher must ensure that each member of the team performs his/her duties. The assessment should be formed based on the individual performance of the tasks by the student and the demonstrated skills for teamwork. Students need to know the criteria and agree to the procedure from the outset.

Our research in the presented report is oriented to study the attitudes of students to work in a team in a hybrid form learning environment using two methods - Peer instruction and JIGSAW. The main method of research is a survey, which is conducted twice - during the first term without the use of both methods and during the second term, after training students in employing the suggested methods.

We defined the research tasks as follows:

1. Compiling and evaluating questions to survey attitude to teamwork.

2. Analyzing survey data after the first term.

3. Developing methodological cases that apply methods of teamwork for three groups of classes.

4. Evaluating the results of the survey after applying the methods of Peer instruction and JIGSAW in the same sample of students in the second term.

5. Performing comparative statistical analysis for estimating the differences in attitudes based on the results of the two surveys.

EXPERIMENT

During the 2020-2021 school year, the learning process took place in a hybrid form that is alternated periods of face-to-face education and those in an online environment. In the online environment, the lessons were conducted *via* online video meetings, using the Google G Suite platform for education. During the study, the possibilities of information and communication technologies were used to see if collaborative learning could be used effectively by teachers in an online environment. For this purpose, we focused on two methods of collaborative learning. These methods are Peer instruction and JIGSAW. Many resources describe the implementation of Peer instruction and JIGSAW in a learning environment. But these resources describe face-to-face education. Therefore, we wanted to implement these methodologies in an online environment and see where the difficulties are.

To achieve the objectives of our study, we implemented both methodologies for cooperative learning during the second term of the 2020-2021 school year. During the first term, students did not have a learning process that used the methodologies of Peer instruction or Jigsaw. The students were in a hybrid form of learning. During online learning, students had cooperative projects. These

cooperative projects consisted in making joint presentations or posters on a particular topic. During the first term, students used the following software to conduct online classes: Google G Suite for Education, Google Meet, Google Slides, Google Sheets, Google Docs, and Jam Board. At the beginning of the second term, before implementing the two methodologies, we asked the students questions through the Likert scale. A five-point Likert scale was used for evaluation. The following scale was used: not at all (1), no (2), neutral (3), yes (4), and very much (5). After completing the educational process using both methodologies at the end of the second term, we asked the same questions again. The questions are:

Q1. Did you like the physics course?

Q2. Did you like the team projects during in-person learning?

Q3. Did you like the team projects during online learning?

Q4. Did you like the software tools?

Q5. Would you like to have more team activities?

Two ninth-grade classes, two tenth-grade classes, and one eleventh-grade class were included in the survey. The number of participants was 109, of which 49 were in ninth grade, 41 were in tenth grade and 19 were in eleventh grade. In ninth and tenth grade, one class majors in mathematics and physics, while the other has a humanities profile. In the eleventh grade, only the class with majors in mathematics and physics participated, because the humanities class does not study physics in a curriculum. Peer instruction is a very popular method for collaborative learning developed by Mazur [16]. The teacher prepares materials on the given topic in advance. These materials can be short text or video. The teacher then gives these materials to the students to get to know them before class. Students get acquainted with the materials and mark or comment on things that are unclear to them. Based on the comments, the teacher chooses what to specify in the short lecture. He/she then asks questions to test students' knowledge and understanding. Students have a short time to answer questions, usually one minute per question. It should be noted here that they respond individually. They then gather in groups of up to five people. In the group, students discuss the questions and discuss which answers are correct. They usually have three to five minutes to discuss. The teacher then asks the same questions again. Students again answer individually. The results are compared and depending on the number of correct answers the teacher decides whether additional explanations are

needed or can move on to the next topic. This method has proven its effectiveness in the educational process. Here we will note that the method has been tested in Bulgaria and found to give good results [17].

At first, we thought it would be very difficult to implement Peer instruction in online learning. But later we were even amazed at how easy and convenient it is to implement this method in online learning. The technologies we mainly used were Google G Suite for Education, Google Docs, Kahoot, VideoAnt, and Edpuzzle. Schools in Bulgaria mainly use Google G Suite for Education or Microsoft Teams for online learning. Google G Suite for Education is being used at Boyan Penev High School. Therefore, we had to implement a Peer instruction methodology so that it could be used through Google G Suite for Education. Before the beginning of each class, we posted materials on the topic and asked questions on the topic using Google docs for text information and VideoAnt and Edpuzzle for videos. Students answered questions or remarked on what they did not understand. We noticed that even with the comments on the questions, interesting discussions arose between the students. Based on these answers and notes, we created the conceptual questions to ask during the class. The technology we used to ask questions and poll is Kahoot. This proved to be very effective during online training. Teachers are used to judging by the reactions of their students whether they understand the material and whether additional explanations or additional examples are needed. But during online learning, it is very difficult to see the reactions of students. Therefore, we find this method very useful and at the same time, it engages students in the learning process. To make the most of our time, we asked a series of questions. We then divided the students into groups through breakout rooms. Then we asked the same questions and what we noticed was that the number of correct answers increased significantly. This indicates that students were able to better understand the material by communicating with each other. For each class, we did five lessons based on Peer instruction. Jigsaw is also a very popular method for collaborative learning. There are different variations of Jigsaw but we chose to focus on Aronson's concept [18].

The teacher introduces the strategy and the topic to be studied. She or he divides the students into groups. Typically, the groups consist of 3 to 5 students. These groups are commonly referred to as home groups or basic groups. The separation can be done at random or at the discretion of the teacher. The goal is to get equal groups. The teacher divides

the topic into several topics. Each student receives a specific topic to study. Usually, the students distribute the topics in the group themselves. The teacher then creates the so-called expert groups. Each expert group is responsible for a specific topic and consists of students from the home groups who are responsible for this topic. Students work collaboratively in expert groups. They discuss the problem together. Together they come to the formulation of the problem. They are looking for the necessary information to solve the problem. Each student is encouraged to make a hypothesis on the given problem and the corresponding argumentation. Then each student accepts or rejects the given hypothesis by presenting his arguments. Typically, the students in the expert groups unite around one working solution. The students then turn to their home groups. There, each student presents his/her topic and helps his/her classmates to understand it if there are any ambiguities. The overall solution to the problem is to combine the solutions of the individual subtopics. Again, students enter a discussion in shaping the overall solution. Finally, they must reach a general solution to the problem or a final product. Each group then presents its overall solution or product.

The implementation of this method in the Bulgarian educational system is a challenge. The main problem is that the lessons are 40 minutes. The other challenge is that teachers should be able to combine several lessons into one larger topic. Then divide this topic into sub-topics of the individual students. For the implementation in the online environment, we used the same technologies as in Peer instruction. We usually use Jigsaw when we give larger research projects, for example, the colonization of Mars. We divide the class into groups of three to five students. We divide the topic into separate parts. An expert group is responsible for each part. Each expert group receives materials and is also free to find materials on its own. In the online environment, each expert group works in separate breakout rooms and makes notes in Google docs. Students then return to their home groups. If we are in an online environment again in different breakout rooms students take notes and discuss issues in Google docs. Finally, the whole class comes together. Each home group presents its solution. We ask them questions and they answer using Kahoot. For each class, we did two lessons based on Jigsaw.

RESULTS AND DISCUSSION

The descriptive statistics (mean, standard deviation, and standard error) for both surveys (pre-test and post-test) are given in Table 1. The unidimensional reliability test shows an excellent value of Cronbach's alpha (0.974) in Table 2.

The exploratory factor analysis also confirms the high reliability of the scale and its one-dimensionality (Tables 3a, 3b).

Table 1. Descriptives

	N	Mean	SD	SE
Question1 (Pre-Test)	109	2.945	1.145	0.110
Question1 (Post-Test)	109	3.422	1.030	0.099
Question2 (Pre-Test)	109	3.174	1.177	0.113
Question2 (Post-Test)	109	3.661	0.983	0.094
Question3 (Pre-Test)	109	3.101	1.178	0.113
Question3 (Post-Test)	109	3.569	1.003	0.096
Question4 (Pre-Test)	109	3.101	1.146	0.110
Question4 (Post-Test)	109	3.550	0.995	0.095
Question5 (Pre-Test)	109	3.147	1.193	0.114
Question5 (Post-Test)	109	3.651	0.975	0.093

Table 2. Frequentist Scale Reliability Statistics

Estimate	Cronbach's α
Point estimate	0.974
95% CI lower bound	0.966
95% CI upper bound	0.981

Table 3a. Factor Loadings for Pre-Test Scores

	Factor 1	Uniqueness
Question3 (Pre-Test)	0.956	0.086
Question4 (Pre-Test)	0.946	0.105
Question2 (Pre-Test)	0.941	0.114
Question5 (Pre-Test)	0.937	0.122
Question1 (Pre-Test)	0.920	0.153

Table 3b. Factor Loadings for Post-Test Scores

	Factor 1	Uniqueness
Question3 (Post-Test)	0.943	0.112
Question2 (Post-Test)	0.912	0.167
Question5 (Post-Test)	0.911	0.170
Question1 (Post-Test)	0.904	0.183
Question4 (Post-Test)	0.904	0.183

Only one variable (one factor) is observed in both pre-test and post-test factor analysis. An interesting result is that Question 3 (Did you like the team projects during online learning?) has the greatest weight in the factor in both the pre-test and the post-test factor analysis. Question 2 (Did you like the team projects during in-person learning?) almost

retains its position. The same can be said for Question 1 (Did you like the physics course?), which ranks last and penultimate, respectively. Here it is necessary to make more detailed research as to why there is a big difference in the weights that the group activities and the physics course have in determining the factor. We will return to this question when we discuss the mean differences and the effect size in Table 5. For now, it is sufficient to say that the attitude towards the physics course has a little bit improved (the weight of Question 1 increased from 5th to 4th position comparing Tables 3a and 3b). The desire for more team activities has also increased, i.e., Question 5 (Would you like to have more team activities?) raised its weight from position 4 to position 3 in Tables 3a and 3b. The largest shift in weights is observed for Question 4 (Did you like the software tools?). Its weight dropped from the second position in Table 3a to the last position in Table 3b.

The mean differences in the results of the pre-test and the post-test scores will be analyzed for significance by the Paired Samples T-Test later

according to Table 5. We do not check for homogeneity variances with Levene's test like within the Independent T-test because we test the same group of students.

The descriptive statistics (mean, standard deviation, and standard error) for both of the surveys (pre-test and post-test) are given in Table 1.

Table 4. Test of Normality (Shapiro-Wilk)

		W	p
Question1 (Pre-Test)	Question1 (Post-Test)	0.844	< .001
Question2 (Pre-Test)	Question2 (Post-Test)	0.790	< .001
Question3 (Pre-Test)	Question3 (Post-Test)	0.824	< .001
Question4 (Pre-Test)	Question4 (Post-Test)	0.834	< .001
Question5 (Pre-Test)	Question5 (Post-Test)	0.845	< .001
Note. Significant results suggest a deviation from normality.

Table 5. Paired samples T-Test

Measure 1	Measure 2	Test	Statistic	z	df	p	Location Parameter	SE Diff.	Effect Size
Question1 (Pre-Test)	Question1 (Post-Test)	Student	67.500	-5.582	108	< .001	-1.000	0.071	
		Wilcoxon	-6.837			< .001	-0.468		-0.746
Question2 (Pre-Test)	Question2 (Post-Test)	Student	192.500	-5.227	108	< .001	-1.000	0.066	-0.706
		Wilcoxon	-6.578			< .001	-0.450		-0.898
Question3 (Pre-Test)	Question3 (Post-Test)	Student	216.000	-5.050	108	< .001	-1.000	0.068	-0.655
		Wilcoxon	-6.884			< .001	-0.505		-0.782
Question4 (Pre-Test)	Question4 (Post-Test)	Student	168.000	-5.323	108	< .001	-1.000	0.068	-0.630
		Wilcoxon				< .001	-1.000		-0.756
Question5 (Pre-Test)	Question5 (Post-Test)	Student			108	< .001	-0.468	0.073	-0.659
		Wilcoxon					-1.000		-0.804
Note. For the Student t-test, the effect size is given by Cohen's *d*. For the Wilcoxon test, the effect size is given by the matched rank biserial correlation.
Note. For the Student t-test, the location parameter is given by mean difference *d*. For the Wilcoxon test, the effect size is given by the Hodges-Lehmann estimate.

The unidimensional reliability test shows an excellent value of Cronbach's alpha (0.974) in Table 2. Therefore, the non-parametric Wilcoxon Signed Rank Test is preferred to the Student's t-test (Table 5). Again, the p-value is less than 0.05 for all five questions and we conclude that the differences in the mean values are statistically significant. The absolute value of the effect size given by the Hodges-Lehmann estimate for the Wilcoxon test shows how big the mean differences are. In descending order of the magnitude of the effect, we arrange the questions as follows: Q2, Q5, Q3, Q4, and Q1This means that the largest effects of the intervention between pre-and post-tests are the positive changes in the attitudes towards the team projects during in-person learning (Q2) and the willingness for more team activities (Q5). On the other hand, the intervention made the lowest effect on the attitude to the physics course and the software tools.

CONCLUSIONS

The article evaluates the change in students' attitudes towards teamwork in a hybrid learning environment for two terms using the Peer instruction and Jigsaw methods for teamwork during the second term.

After the statistical analysis of the results obtained through a survey of attitudes, the following conclusions can be drawn.

The questions from the survey show a great deal of consistency (Cronbach's alpha is above 0.9). All questions show a change with a different statistical difference. The use of both methods has a positive effect on attitudes towards teamwork. Students prefer face-to-face learning with a will to use more diverse methods, one of which is teamwork. The use of different software products does not affect the attitudes toward teamwork as this generation of students generally wants to work with computer technology regardless of the methods their teachers use. There is no significant change in the attitude towards physics as a subject. The attitude towards teamwork during the online training is the most significant change and a positive one that we can notice.

The use of surveys as a tool for establishing attitudes towards certain teaching methods and activities such as teamwork is a reliable method for research in education. These give better valid results with the statistical method of dependent samples. It can serve as a diagnosis of the effectiveness of the learning process and a basis for decision-making related to learning objectives.

These results give us a reason to conclude that the proposed methods can be used by teachers to increase students' interest and motivation for the acquisition of long-lasting skills and competencies in the 21st century in a different educational environment.

REFERENCES

1. P. Griffin, B. McGaw, E. Care, Assessment and teaching 21st-century skills, Springer, 2012.
2. T. Berger, C. Frey, Future Shocks and Shifts: Challenges for the Global Workforce and Skills Development, OECD, Paris, 2015.
3. J. Pellegrino, Teaching, learning and assessing 21st-century skills, OECD Publishing, Paris, 2017.
4. B. Trilling, C. Fadel, C., 21st-century skills: Learning for life in our times, Jossey-Bass/Wiley, 2009.
5. National Research Council, Successful K-12 STEM Education: Identifying Effective Approaches in Science, Technology, Engineering, and Mathematics, The National Academies Press, 2011.
6. PISA 2015 Results, Collaborative Problem Solving, PISA, OECD Publishing, Paris, 2017.
7. M. Tsay, M. Brady, A case study of cooperative learning and communication pedagogy: Does working in teams make a difference? *Journal of the Scholarship of Teaching and Learning*, **10**, 78 (2010).
8. D. Augustine, K. Gruber, L. Hanson, Cooperation works, Educational Leadership, 1990.
9. T. Good, B. Reys, D. Grouws, C. Mulryan, Using work groups in mathematics instruction, Educational leadership, 1989-1990.
10. R. Slavin, Cooperative learning, Prentice-Hall, 1990.
11. K. Wood, *Journal of Reading*, **31**(1), 10 (1987).
12. D. Johnson, R. Johnson, Cooperation and competition: Theory and research, Interaction Book Company, 1989.
13. S. Sorensen, Grouphate: a negative reaction to group work, International Communication Association, 1981.
14. L. Lewis, P. Hayward, *Communication Education*, **52** (2), 148 (2003).
15. M. Isaac, I hate group work social loafers, indignant peers, and the drama of the classroom, National Council of Teachers of English, 2012.
16. E. Mazur, Peer Instruction: A User's Manual Series in Educational Innovation, Prentice-Hall, 1997.
17. I. Kotseva, M. Gaydarova, N. Nencheva, *Chemistry*, **24 (**2), 187 (2015).
18. E. Aronson, The Jigsaw Classroom, Sage Publications, 1978.

An integrated approach to teaching the topic of *light and colors* from the seventh grade physics syllabus

R. I. Vassileva[*]

Department of Physics, Faculty of Mathematics and Natural Sciences, South-West University, 66 Ivan Mihailov Str., 2700 Blagoevgrad, Bulgaria

The paper presents a variant for integrating knowledge about the physical nature of colors and knowledge about the color as one of the basic artistic means in painting. The performing of real and virtual experiment provides the opportunity to introduce and compare on the qualitative level two different models of gaining color perception: (i) Obtaining light in random color by mixing in different proportions the light beams of three primary colors: red, green and blue; (ii) Obtaining new colors by the mechanical mixing of paints, as in this model the three primary colors are red, yellow and blue. Specific attention is paid to the practical application of the discussed models. The importance of the integrated lessons for the formation of an overall world picture in the students' minds is emphasized.

Keywords: physics education, painting, light, color, integrated approach

INTRODUCTION

According to the current syllabus, the topic of "Light and Colors" (section "Light and Sound") is an important part of the 7th grade *Physics and Astronomy* learning content in junior high school. It is planned to be studied in the framework of two lessons. The main goal is to clarify the physical nature of colors, which is closely related to grasping the new physical concept – *light spectrum*. The curricular of study are: the colors in the spectrum of white light; *the primary colors* and the result of their mixing; the possibilities for changing the white light through color filters and the answer to the question: when and why bodies change their color [1].

The current study was provoked by a common situation in the teaching practice of this particular learning content. When the physics teacher clarifies that *the primary colors are three: red, green and blue*, the students react that this fact contradicts their knowledge acquired in the curricular of art – *the three main colors are red, yellow and blue*. It is obvious that this contradiction must be resolved, and this requires the teacher to be prepared in advance in order to implement an adequate integrative approach in the learning process. This paper presents a methodological suggestion for studying part of the learning content on the topic, which helps students to acquire the necessary knowledge about the physical nature and origin of colors and *to understand and solve the problem themselves*. It is important to note that from a didactic point of view the situation is very favorable, as the modern concept of integration in education involves not only unification, complementing educational elements from different curricular areas, but also creating a product of new quality (idea, meaning, element, etc.) on the basis of *resolving contradictions* [2]. This fact reflects the specifics of integration in learning compared to interdisciplinary links.

As a matter of fact, the literature review shows that neither pedagogical knowledge nor the knowledge of teaching methodologies offers a unanimously accepted definition of the concept of *integration,* as well as the related concepts *integrative approach* and *integrative education.* For the purposes of this study, *interdisciplinary integration in educational practice is considered a process of connecting separate elements (knowledge, relations, evens modes of thought) into a whole by way of meaningful and stable associations, which satisfies a specific educational goal. A new system is formed as a result which has the following main characteristics – continuity and expedience* [3]. The integrative approach combines the paths and means of establishing integration and its realization results in a type of education that can be viewed both as a system and as a process of forming integrative associations.

Up until the middle of the 20th c. the conceptions of integration concern the level of interdisciplinary connections and most authors regard these as [4]:
- a didactic means of increasing the effectiveness of knowledge, skill, and habit acquisition;
- a condition for the development of cognitive activity and autonomy, for the formation of cognitive interests;

* To whom all correspondence should be sent:
E-mail: *radostiv@abv.bg*

- a means of realizing the principles of systematicity and science or as an independent principle of education;
- a means of achieving unity of mainstream and professional education and forming professional skills;
- as a condition for enhancing the scientific level of knowledge, etc.

Other researchers define interdisciplinary connections as a *didactic phenomenon* reflecting connections between sciences in education; as *a didactic condition* for the provision of coherence among syllabi and course books in various subjects; as a *didactic process* or *principle* pertinent to holistic knowledge of nature and society; as *an independent sphere of didactics* characterized by specific psychological and pedagogical rationale, principles, methods, means used to form qualitatively new knowledge – interdisciplinary one [5].

Scientific literature offers definitions of wider scope which reflect specific characteristics of integration considering it as a process and a result at the same time [6, 7, 8].

Importantly, a large number of researchers side with the idea that the core of integration in education cannot be limited to mechanic amalgamation of inter-subject and intra-subject connections. Unlike interdisciplinary connections, integration implies a transition from coherence in the teaching of different subjects towards their deep interaction. In connection with this idea, it is worth noting the works of M. N. Berulava. He defines three main levels of realization and integration of instructional content [9]:

- the level of interdisciplinary connections – associated with the actualization, generalization and systematicity of knowledge (content integration);
- the level of didactic synthesis – it is characterized not only by the content integration of the subjects, but also by the integration of the forms of educational activity (procedural integration);
- the level of completeness – it ends with the formation of a new subject of an integrative character.

The level of didactic synthesis is productive with respect to the improvement of the educational process. It reflects *the interaction* among the subjects taught, gives a comprehensive idea of the objects, phenomena and processes in the surrounding world and aids the realization of person-centered education.

The integrative lesson is among the most commonly used contemporary forms of educational activities which is conducive to the realization of didactic synthesis. The goal of integrative lessons is to achieve high systematicity of the instructional content, to create conditions for multi-faceted consideration of the objects of study solving didactic tasks coming from two or more subjects in the meantime. To plan such a lesson, it is crucial for the teacher to choose the integrative factor correctly – the rationale for the amalgamation of the elements into a unity. The role of such an integrative factor can be fulfilled by a phenomenon, an idea, a concept, an object, a technology, a method, etc. Pertinent to the nature of the present study is the situation when a specific *problem* serves as an integrative factor (integrator) which is related to controversial aspects of the instructional content. In other words, it is the problem that unites, groups heterogeneous content. And it is a widely known truth that involving students in the processes of uncovering and solving educational problems puts them into the shoes of explorers – an important factor improving the characteristics of their overall cognitive and practical activity.

PRACTICAL IMPLEMENTATION OF AN INTEGRATIVE APPROACH IN TEACHING THE TOPIC OF *LIGHT AND COLORS*

When introducing the topic, the teacher needs to emphasize the fact that until the 17th century there had not existed a scientific theory of the origin and nature of colors. The physical foundation of color science was laid by Isaac Newton with the discovery of the spectral composition of light. Therefore, the basis for structuring the learning content on the topic is Newton's experiment from 1671, which ought to be introduced to the students beforehand through a real or virtual experiment. As it is well known, Newton directed a beam of white sunlight at a triangular glass prism. On a screen placed behind the prism, he observed stripes of different colors, flowing from red to purple and arranged in a strictly defined order. Thus he proved that white light is actually a mixture of many colors. He introduced the term "spectrum" – the rays of all colors that are part of white light form the so called *light spectrum*. Here comes the logical question: what is the cause for the observed phenomenon, i.e. why does the glass prism decompose the white light into its constituent colors? From a methodological point of view, it is appropriate to hold a short discussion, using the students' knowledge about the phenomenon of *refraction of light*. The analysis of the experiment shows that in its passing through the glass prism the light is refracted twice: on entering the prism (on the air – glass border) and on leaving it (on the glass –

air border). In addition, it is obvious that the rays of the different colors are refracted differently (at different angles). The screen behind the prism shows clearly that the violet light is refracted the most and the red light the least. In this way the prism separates the rays, i.e. decomposes white light into its constituent colors, and behind it *the light spectrum* is observed. For the better acquisition of this knowledge, it is appropriate to make an analogy between Newton's experiment and the beautiful natural phenomenon of the *rainbow*, explaining the reasons and conditions for its formation.

The next important step is to make students understand that just as white light can be decomposed into its constituent colors, the mixing of all the spectrum colors can produce white light. However, is it possible to achieve this result by mixing a smaller number of colors? How many colors are needed at the least? To answer these questions, the following experiment can be performed [10]. In a darkened room, beams of red, green and blue light emitted by three spotlights simultaneously are directed to the same place on a white screen. A white circle is formed where the rays fall. In the same way, the light beams from any two spotlights can be used and the effect of mixing each pair of colors can be traced. The image of Fig. 1 illustrates this.
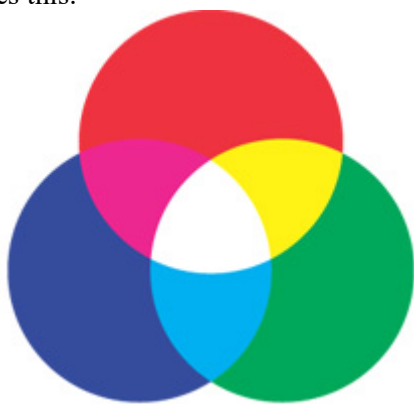
Fig. 1. Additive color mixing – *RGB*-model

Thus, students discover that *white light can be obtained by mixing three spectral colors – red, green and blue.* It is important for the teacher to emphasize that depending on the proportions in which they are mixed, different colors and their shades can be obtained, but *red, green and blue cannot be obtained by mixing other colors.* That is why these three colors are called *primary*. This fact is closely related to the peculiarities of human color vision. Here the teacher needs to explain that the millions of light-sensitive cells that cover the retina of the human eye are responsible for color vision and that they are of three types: some are sensitive to red light, others to

green, and still others to blue. Light detectors in these cells are special molecules that receive incoming light signals, convert them into electrical ones and direct them along the optic nerve to the brain. Thus, in the visual center of the brain, our visual perceptions are formed. Therefore, *when red, green, and blue lights enter the eye at the same time, and the contributions of these three primary colors are the same, after processing the signals, the brain forms a perception of white light*. If only two of the primary colors enter the eye at a time, we see respectively: red and green – yellow; red and blue – magenta; blue and green – cyan (Fig. 1). *Yellow, magenta* and *cyan* are called *secondary* colors. It is necessary to mention the fact that there is no such combination of primary colors that evokes the perception of black. In this case, *black is the absence of any light falling into the eye.*

Now the students' attention is focused on the following experiment: in three glasses there is the same amount of water, colored in red, green and blue, respectively. Watercolor paints can be used for this purpose. The question is whether mixing the three liquids colored in the primary colors will produce a white liquid. The experiment clearly demonstrates that a black liquid is obtained. *Why is the visual perception obtained as a result of mixing red, green and blue different in the two cases?* Thus, students' attention is focused on clarifying *the basic question*: *how bodies that are not sources of light get their color.* When answering this question, the teacher should remember that, as a rule, we judge the color of bodies when they are illuminated with white light. The following two cases are analyzed:

1) Let us choose a transparent object. In this case, it absorbs some of the colors of the light that falls on it and transmits the rest. *The color of transparent bodies is determined by the color of the light they transmit.* The feature of transparent bodies to transmit light selectively is used in so-called *color filters*. Through them we can *separate* (receive) the light of a certain color from the white light. After perceiving this information, students may realize by themselves that in this experiment we see the liquid in a glass as red, because it absorbs all the colors of light passing through it, and transmits only the red color. The liquid in the second glass is green because it absorbs all the colors of light passing through it, except green. It is the same with the blue color of the liquid in the third glass. When the three liquids mix, they absorb all the light (all colors) and we see a liquid that is black.

2) Let us choose an object that is not transparent. In this case, it *absorbs* some of the colors of the white light that falls on it, and *the components*

reflected in the eye determine its color. *The color of non-transparent bodies is determined by the color of the light they reflect.* Therefore, the red hat reflects only red and absorbs the other colors, the white sheet of paper reflects all colors equally, and the black jacket absorbs all colors. In explaining this learning content, the teacher can use videos of interesting physical experiments that cannot be carried out in the classroom. For example, the experiments with colorful balloons and red laser beam presented in [11] are very attractive. Through a discussion with students, they provoke the answer to a number of questions related to the concept of color from a physical point of view.

As a result of the experiments made so far, the following important conclusions can be drawn:

1. It is not the objects that generate the colors, but the color is the result of the interaction of the objects with the light.

2. No matter whether the bodies are transparent or non-transparent, what is important is the fact that the color of an object depends mainly on which components of white light are *"subtracted"* from it due to absorption.

3. Visual perception when *mixing colors* may be different because it can be formed in different ways:

    - by *adding (summing)* colors from white light (additive color mixing)

    - by *"subtracting"* colors from white light (subtractive color mixing).

The first option is the case when the light emitted from light sources, such as TV screens, computer monitors, color displays of mobile phones, etc. falls directly into the eye. In such devices, the variety of colors is obtained as a result of superimposition of the three primary colors – red, green and blue in different proportions. This is an additive model of color perception, known in practice as the *RGB*-model (Fig. 1).

The second option is the case when we perceive light not directly from its sources, but the light that is reflected from different objects, as in our perception of works of artists, color photographs, color images in works of printing, etc. This requires the use of subtractive models of color perception, i.e. models that consider the formation of color images based on the "*subtraction*" of colors from white light, in which *the three primary colors are different from those of the RGB-model.* For example, in printing, a model is often used in which *cyan, magenta and yellow* (secondary in the *RGB*-model) *are considered primary colors*. In practice, it is called the *CMY*-model.

After these discussions, the students have the necessary preparation to answer the question why the primary colors in physics are different from the primary colors known from their art classes. They have already realized that the light of any color can be obtained by mixing light beams with three primary colors: red, green and blue. In this case we are talking about the so-called *optical mixing of colors*. However, it is completely different from the *mechanical mixing of colors*, which is realized when we mix paints in different proportions on a palette, canvas or sheet of paper to get new colors. This type of practical activity has been repeatedly performed by the students, creating a variety of drawings. When white light falls on a drawing, some colors are absorbed, while others are reflected, and after a contact with the eyes, the corresponding color perception is formed. Obviously, in this case it is a matter of subtractive mixing of colors, i.e. the color image is obtained by "subtracting" those colors from the white light that are absorbed by the colors in the drawing. As practice shows, in this model of color perception (originated centuries ago) the main colors are *red, yellow and blue* [12].

The image of Fig. 2 illustrates the result of mixing these primary colors.

Fig. 2. Subtractive color mixing – *RYB*-model

It is visible that from blue and red, for example, *purple* is obtained, from yellow and red – *orange*, and from blue and yellow – *green*. These three colors are called *secondary*. From the mixing of *primary* and *secondary* colors, *tertiary* colors are obtained, etc. Another feature is that the mixing of the three primary colors gives a black color. Thus, by using a rich variety of appropriately combined colors, artists create (achieve) the aesthetic and emotional impact of their paintings.

CONCLUSIONS

The proposed teaching strategy regarding part of the topic "Light and Colors" requires the use of information about the practical application of some models of color perception. However, it is important to note that this additional information is not

compulsory. Its aim is merely to help students understand and acquire better the knowledge about the physical nature and origin of colors. The proposed teaching suggestion has a significant advantage – it allows students by integrating knowledge from different curricular areas - physics and art, *to resolve a contradiction* they initially face *by themselves*. Such situations are beneficial to the educational process. In this way, students form a complete picture of the world, develop their thinking and increase their motivation to participate in learning.

The elaboration of the conception of education discussed here in view of its practical realization implies the design of a suitable inventory for the evaluation of educational results. Since integrative knowledge and skills are being tackled, it will be highly productive if ways are sought to use the so called *authentic evaluation*, along with traditional methods.

REFERENCES

1. M. Maksimov, G. Ruseva, Physics and astronomy – 7. grade, Bulvest 2000, Sofia, 2018 (in Bulgarian).
2. L. I. Gritsenko, Theory and practice of teaching. An integrative approach, Akademiya, Moscow, 2008 (in Russian).
3. N. Raycheva, Interdisciplinary integration in high school, Sofia University Publishing House, Sofia, 2019 (in Bulgarian).
4. N. A. Krel', Interdisciplinary connections as a didactic foundation for the design of inter-disciplinary laboratory work, https://superinf.ru/view_helpstud.php?id=4033, 2012 (in Russian).
5. A. I. Gurev, Proceedings from National Russian scientific and applicative conference, Gorno-Altaysk, Univer-Print Publishers, 1999, p. 27 (in Russian).
6. N. G. Lederman, M. L. Niess, *School Science and Mathematics*, **97** (2), 57 (1997).
7. G. J. Venville, V. M. Dawson, The art of teaching primary science. Crows Nest, Australia, Allen & Unwin Publishers, 2004.
8. L. Tsvetanova-Churukova, Integrative education in primary school, South-West University Publishing House, Blagoevgrad, 2010 (in Bulgarian).
9. M. N. Berulava, Integrative processes in education, in: Integration of education content in pedagogical higher schools, Biysk, 1994, p. 5 (in Russian).
10. D. T. Ivanov, Fun experiments in physics. Optics, Prosveta – Sofia AD, Sofia, 2006 (in Bulgarian).
11. https://www.youtube.com/watch?v=PwM2xwIVCHM.
12. https://www.youtube.com/watch?v=yg8UyOdDhCU

Section

Technical Sciences

Investigation of the operation of a thermoelectric converter

P. Kissabekova, D. Karabekova[*], A. Khassenov, L. Chirkova, A. Satybaldin

E.A. Buketov Karaganda University Kazakhstan

In this article, a heat flux meter is considered for diagnosing the state of thermal insulation of underground pipelines by measuring the surface distributions of the heat radiation density over the laying. The heat flux meter is an indicator of the state of the underground heat pipeline by the nature of changes in heat losses or the temperature of the ground surface above the researched object. The developed heat flow meter is based on the principle of using an "auxiliary wall". On the transducer of heat flux, which is applied to the surface of the enclosing structure, a temperature difference is created in the steady-state heat exchange mode, proportional to the density of the heat flux passing through the barrier. This heat flux meter consists of a thermometric unit, which is based on a battery-operated thermoelectric transducer. The battery sensor is a sealed laminated round disk, which is mounted in a stainless steel ring with an internal groove and filled with epoxy resin. The lamp soot is added to the epoxy resin to increase the level of disc absorption. The disk provides the same conditions for heating the sensor element by the radiation flow and the electric current passed through the heater. This allows the equivalent heating of the sensor element by the radiation current flow. The developed device is designed to analyze the state of thermal insulation of underground pipelines of heat networks.

Keywords: heat flux meter, heat flow, thermometric unit, battery-operated thermoelectric transducer

INTRODUCTION

Research and modernization of thermal power plants and energy-intensive technologies are now particularly relevant in connection with energy and resource conservation issues. In these conditions, measurements, operational control and regulation of thermal parameters are essential, among which a significant place is occupied by heat flow, which has become today the same informative parameter as temperature, pressure, consumption, etc.

Measurements of heat flow density are of great importance in engineering, they are necessary in thermophysical experiments devoted to the study of the properties of substances and heat exchange processes, as well as for the diagnosis of industrial thermal power equipment and technological processes and control of its operation modes. The methods of heat measurement can be successfully used for the operational quality control of thermal insulation of power plants and pipelines and determination of heat-protective properties of building structures. Such control contributes, on the one hand, to the rational use of insulating materials and, on the other, to the saving of thermal energy. Therefore, the new course in the field of energy development is aimed at increasing, promoting and introducing new methods and devices aimed at reducing heat losses [1].

In order to increase the efficiency of the Republic of Kazakhstan's heat supply and reduce the shortage of thermal energy, the use of devices for operational quality control of heating installations and heating networks, as well as modernization of production at existing capacities and expansion of the possibilities of modern methods of heat saving is needed.

Numerous studies have shown that the methods of non-destructive testing, which are based on the observation and automated registration of the temperature state of processes, currently meet all the requirements of technical diagnostics of heating networks and technological facilities. The experience of foreign countries shows the effective use of heat flow meters of non-destructive testing for the purposes of the normative state of objects and construction structures [2].

Heat flow devices are used not only for research but also for control and regulation of processes in various fields of science and technology. In devices of heat flow measuring, the basis of all achievements is a thermoelectric battery converter, where the auxiliary wall method is used.

This article discusses the developed modifications of devices for measuring the heat flow. A distinctive design of the heat flow device is that it contains a thermoelectric battery converter and a receiving plate, additionally equipped with a temperature-dependent heating element. In this case, the thermoelectric battery converter is combined with the heating element, and its "hot" junctions are combined with the receiving plate, and the "cold" junctions are brought into thermal

* To whom all correspondence should be sent:
E-mail: *karabekova71@mail.ru*

contact with the heating element. The article is devoted to the principle and creation of the main element of the device, a battery thermoelectric converter [3].

The heat flow converter is embodied in the form of an auxiliary wall and consists of a battery of identical galvanic thermoelectric conductors which are connected in parallel according to the measured heat flow and in series according to the electrical signal being generated. The monolithic converter in a rigid or flexible design is provided by a pouring electrical insulation compound. When operating a converter installed on the surface of the object under study, in a stationary heat exchange mode, a temperature drop proportional to the measured density of the passing heat flow occurs on opposite flat surfaces of the converter, due to which a thermo-EMF is generated in the battery of thermoelements [4].

The principle of operation of a thermocouple is the thermoelectric effect, or the Seebeck effect, which is based on the occurrence of a potential difference in conductors, so the metals of thermoelectrodes should differ in chemical and physical characteristics.

EXPERIMENTAL

In the laboratory "Measurement of thermophysical quantities" of the Department of Engineering Thermophysics named after Professor Zh. S. Akylbayev of the Faculty of Physics and Technology of E. A. Buketov Karaganda University a device for measuring heat flow for recording and measuring heat flows was developed.

Heat flow instruments are used not only for research but also for the control and regulation of processes in a wide variety of fields of science and technology. In heat flow measuring devices, the basis of all achievements is a thermoelectric battery converter, where the auxiliary wall method is used.

The heat flow converter is a disk with a thickness of 1.80 mm and a diameter of 26 mm. There is a battery of galvanic thermoelements, which are rigidly held in a given position by an epoxy compound placed between the end surfaces. The technology for producing galvanic laminated sensors is carried out on the winding machine of two wires with filament insulation on a celluloid strip. The wire is served by rubber rollers. The wire is winded on a spool which rotates around a celluloid strip in the form of a spiral of a bifilar winding in the form of a circle. The pitch is approximately 2-2.5 times the diameter of the wire. The length of the covered 20-30 m is limited to the capacity of the spool. For a size of 20×20 mm, the

length of the necessary blank must be 800 mm, which is approximately more than 50 pairs of elementary junctions. Further control takes place by electric resistance of the fixed wire, strips of strips are twice covered with zapon. The battery transducer shall be dried after each coating for one hour and installed in a special mist box. During the copper plating process, the frame is lowered into a galvanic bath to precipitate copper. About 1% if ethyl alcohol is added to the electrolyte, which improves the density and strength of the coating. For copper-constant wires with a diameter of 0.7 mm, the thickness of the coating should be between 6 and 6.5 µm. The copper-plated celluloid base and the zapon are dissolved in acetone, the helix is varnished and kept at room temperature for 60 minutes. A helix coated with varnish is placed in the drying oven and conditioned at a temperature of 70-90°C for 150 minutes. The resultant blank is lubricated with an ED-6 resin hardener and a FAED-13 furano-epoxy resin, the operating temperature of the converter can be increased to 130°C and placed in the mold and compressed on all sides, respectively, is heated in a thermostat up to 100°C and held for 5 hours for glue polymerization (Figure 1).
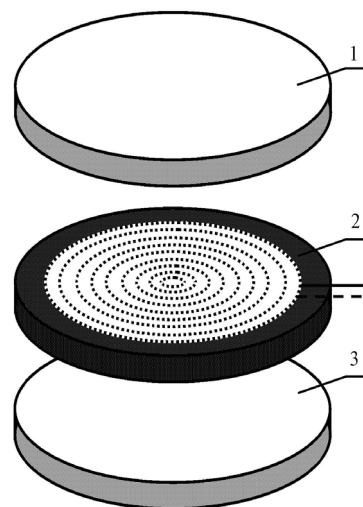

Figure 1. Appearance of the thermoelectric battery converter: 1,3 - upper and lower disc; 2 - thermoelectric battery converter.

As a result, a compact laminated round disc is obtained, the quality being evaluated on a grading board, where the values of its operating coefficients are determined [5].

The resulting disc is mounted in a ring made of stainless steel with an internal duct and is filled with epoxy resin, into which lamp soot is added in order to increase the degree of absorption.

RESULTS AND DISCUSSION

Previously, we carried out experimental work on the calibration of thermocouples used to determine the temperature change in the ground and calculating the calibration coefficient, which relates the value of the thermo-EMF of thermocouples with the temperature value in Celsius [6]. The laboratory stand for the calibration of thermocouples is shown in Figure 2.
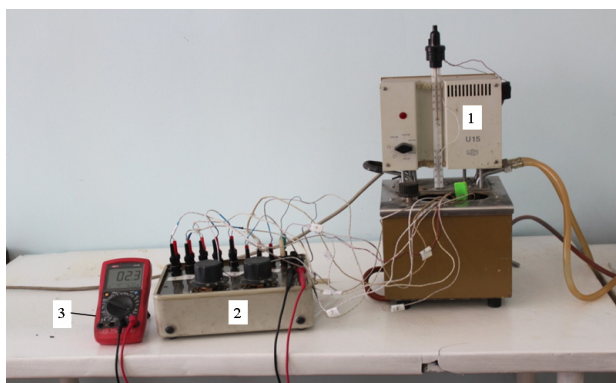

Figure 2. Calibration of thermocouples: 1 - thermostat, 2 - thermocouple switch, 3 - measuring device

Temperature changes were investigated using an earlier developed heat flow meter [7] with a device for measuring heat flow [8]. Based on the results of experimental data, a calibration graph of the thermocouple was constructed (Figure 3).
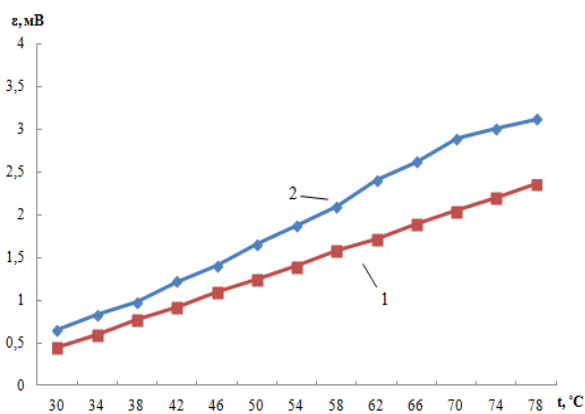
Figure 3. Graph of the calibration thermocouple: 1 – heat flow meter [8]; 2 - device for measuring heat flow [9].

In the device for measuring the heat flow [8], the sensitivity of the device has been increased, that is increase the number of hot junctions in the thermal battery per unit area of the sensing element. The obtained studies of the thermal batteries of these converters showed (Fig. 3) that by increasing the number of hot junctions, we increased the sensitivity of the newly developed sensor.

CONCLUSIONS

Numerous studies of the converter have shown that the manufactured heat flow device has a high sensitivity, which allows it to be used for measuring heat flows of not only high, but also low intensity. Heat flow devices are of great interest, since they do not need an additional power source, therefore, the appearance of current noise characteristic of others is excluded. These methods made it possible to increase the sensitivity and reduce the temperature measurement error. The analysis of errors in measuring the energy parameters of radiation is carried out. It is shown that the relative non-excluded error of measuring energy parameters using the developed devices and methods does not exceed 2.0% [9, 10].

Thus, the control and measurement of heat flows are of interest for many branches of science, technology and industry, but, above all, for solving issues of rational use of energy resources.

REFERENCES

1. A. K. Azhkenova, Improving the efficiency of heat supply systems based on monitoring of heat losses and optimization of thermal insulation parameters, Almaty, Institute of Energy Research, 2009, p. 370 [in Russian].
2. V. V. Klyuev, F. R. Sosnin, A. V. Kovalev *et al.,* Non-destructive testing and diagnostics: handbook, Moscow, Mashinostroenie, 2005, p. 656 [in Russian].
3. D. Z. Karabekova, P. A. Kissabekova, B. R. Nussupbekov, A. K. Khassenov, *Thermal Engineering*, **68**(10), 802 (2021).
4. B. R. Nussupbekov, D. Zh. Karabekova, A. K. Khassenov, Proceedings of SPIE Photonics Applications in Astronomy, Communications, Industry, and High-Energy Physics Experiments, Wilga, 2016, p. 348.
5. O. A. Gerashchenko, T. G. Grishchenko, Devices for thermophysical measurements, Kiev, Chas, 1991, p. 73 [in Russian].
6. O. A. Gerashchenko, Fundamentals of thermometry, Kiev, Naukova dumka, 1984, p. 192 [in Russian].
7. B. R. Nusupbekov, D. Zh. Karabekova, A. K. Khassenov, U. B. Nusupbekov, O. B. Aukeev, *Patent* № 1588 RK, 2016, [in Russian].
8. D. Zh. Karabekova, P. A. Kissabekova, A. K. Khassenov, Sh. Azatbek, *Patent* № 6393 RK, 2021, [in Russian].
9. D. Zh. Karabekova, A. K. Khassenov, P. A. Kissabekova, A. Zh. Satybaldin, M. K. Tungushbekova, *Eurasian Physical Technical Journal,* **17**(1), 113 (2020).
10. B. R. Nussupbekov, D. Zh. Karabekova, A. K. Khassenov, *Measurement Techniques*, **59**, (6), 644 (2016).

Special session

"Low-carbon energy for transport and household"

Membraneless fuel cells for remediation of sulfide- and nitrate-contaminated fluxes

S. Stefanov*, Ts. Parvanova-Mancheva, L. Ljutzkanov, E. Razkazova-Velkova

Institute of Chemical Engineering, Bulgarian Academy of Sciences, Acad. G. Bonchev str., bldg. 103, 1113 Sofia, Bulgaria

Sulfides and nitrates are dangerous environmental pollutants with sources both natural and anthropogenic. The search for cheaper wastewater treatment techniques and alternative energy sources has led to a new branch of scientific interest – fuel cells for wastewater treatment. The present research is dedicated to remediation of sulfide- and nitrate-polluted fluxes in the anodic and cathodic compartments, respectively, of a membraneless fuel cell of our own design. The core of the fuel cell is a cylindrical tube of activated carbon, playing the role of both an electrode and a non-selective membrane. Both abiotic and microbial fuel cells (FCs and MFCs, respectively) are being investigated for their efficiency at neutralization of contaminated fluxes with different initial concentrations of sulfide and nitrate ions, as well as their electrical power output. *Pseudomonas putida* 1046 is used in the MFC for sulfide oxidation.

Keywords: Membraneless fuel cell, remediation of contaminated fluxes, sulfides, nitrates, *Pseudomonas putida*.

INTRODUCTION

The constant reduction of fossil fuel sources and quantities makes the search for new renewable energy sources a priority. Another major problem facing humanity is the generation of increasing amounts of wastes – in liquid, solid, or gaseous form. Fuel cells, although still not widely implemented in this context, represent a good prospect for redox waste disposal, combined with electricity generation.

Generally, a fuel cell (FC) consists of anode and cathode with catalysts incorporated into them and separated by a membrane [1]. A lot of the scientific efforts in the field are focused on increasing the FC power output, directly proportional to the rate of the oxidation / reduction of the fuel, and in the case of FCs for waste decontamination of the polluted fluxes. To this end, research is dedicated to increasing the efficiency of the catalysts for different redox reactions [2], their incorporation on the electrode surface [3], the configuration of the electrodes within the FC and the characteristics of the membranes used. The latter are an essential component for both high electricity yields and waste disposal. The main difficulties lie in their reliable installation and especially the preservation of their properties during operation. Of scientific interest is the degradation of the membrane's electrochemical characteristics during operation and under varying conditions [4, 5, 6, 7, 8]. Another limitation of the polymer membranes are their operating temperatures – polymer electrolyte membrane (PEM) fuel cells typically operate at temperatures no higher than 60-80 °C due to structural limitations of the membranes, though attempts are made for elevation of the operation temperature of the PEM fuel cells [9]. Factors such as durability and cost still remain as major barriers to fuel cell commercialization [7].

An interesting and innovative approach in the development of FCs is the construction, design and investigation of membraneless fuel cells [10, 11, 12].

The aim of the present study is the preliminary investigation of a membraneless FC constructed from a tube of activated carbon that serves both as a semi-permeable non-selective membrane and an electrode.

Sulfide- and nitrate-contaminated fluxes are chosen as pollutants to be remediated into the anodic and the cathodic compartments of the FC, respectively. As there are a lot of sources of these severe pollutants (both anthropogenic and natural) and the classical methods used for their neutralization and disposal are expensive and energy intensive, they are appropriate candidates to be processed in FCs.

The most effective and widely applied method for efficiency increase for classical FCs is the incorporation of catalysts. Another way to increase the efficiency is the use of microorganisms instead of conventional catalysts in the so called microbial fuel cells (MFCs). *Pseudomonas* sp. are known to oxidize sulfides [13, 14] so *Pseudomonas putida* is chosen for comparison between abiotic membraneless FC without catalyst and membraneless MFC.

* To whom all correspondence should be sent:
E-mail: *s.stefanov@iche.bas.bg*

MATERIALS AND METHODS

Experimental set-up

A scheme of the laboratory-scale fuel cell is presented on Fig. 1A. The core of the fuel cell is a pyrolyzed cylindrical carbon tube (Fig. 1B), used as both electrode and semi-permeable non-selective membrane. The initial material for pyrolysis of the tubes are cellulose rolls. The once pyrolyzed tube is plugged at one end, thus forming two separate spaces (internal (30 mL) and external (130 mL)) that can be used as the cathodic and anodic compartments of the fuel cell. Additionally, the inner compartment is fitted with a standard graphite rod (SGR, Fig. 2A) attached firmly to the wall of the tube to be used as a current collector for the compartment. The tube is pyrolyzed by a patented technology with simultaneous activation [15]. The process allows easy incorporation of different catalysts, making the design very flexible.
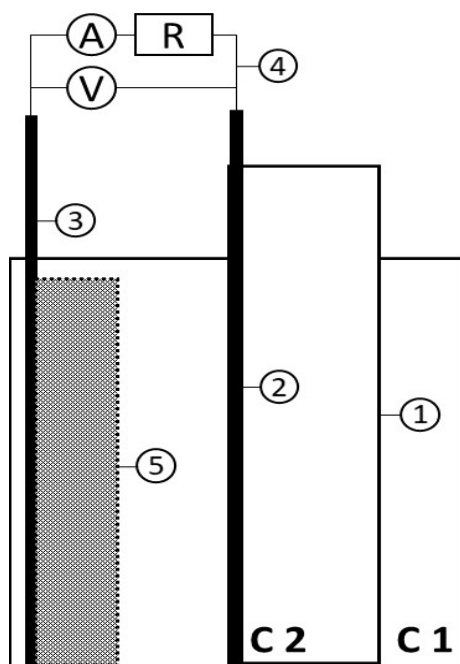
Fig. 1A. Scheme of the membraneless fuel cell: C 1 – Compartment 1 (external); C 2 – Compartment 2 (internal); 1 – pyrolyzed carbon tube; 2 – graphite electrode (of Comp. 2), 3 – graphite electrode (of Comp. 1); 4 – external electrical wiring; 5 – (optional) pyrolyzed carbon felt.

Different electrode configurations for the anodic compartment are investigated: i) three standard graphite rods; and ii) two pyrolyzed and activated carbon felts (ACFs, Fig. 2B) and three SGRs (used as a current collectors). The source material of the felts is commercially available as PAN carbon felt SCF510001000 and is pyrolyzed and activated by the same technology as the tubes [15]. The ACFs are situated in the external compartment next to the

pyrolyzed carbon tube and the SGRs pierce the felt, ensuring good electrical connection. To evaluate the influence of an increased surface area of the cathodic electrode some of the experiments (Experiments № [12-18], Table 1) were performed with 15 g (30 mL) of activated carbon (AC, Fujikasau®, Japan, 680 $m^2 \cdot g^{-1}$) added in the cathodic compartment.

Fig. 1B. Pyrolyzed cylindrical carbon tube.

Fig. 2A. Standard graphite rods (SGR).
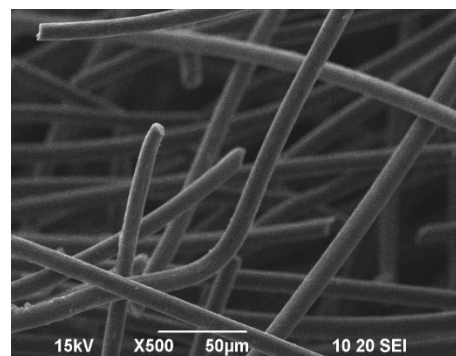
Fig. 2B. Activated carbon felt (ACF, SEM image).

The main reactions taking place in the anodic and in the cathodic compartment are as follows:
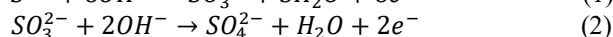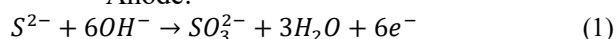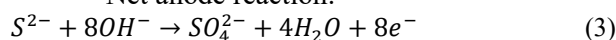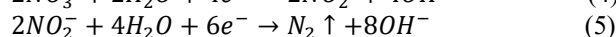
Anode:
$$S^{2-} + 6OH^- \rightarrow SO_3^{2-} + 3H_2O + 6e^- \qquad (1)$$
$$SO_3^{2-} + 2OH^- \rightarrow SO_4^{2-} + H_2O + 2e^- \qquad (2)$$
Net anode reaction:
$$S^{2-} + 8OH^- \rightarrow SO_4^{2-} + 4H_2O + 8e^- \qquad (3)$$
Cathode:
$$2NO_3^- + 2H_2O + 4e^- \rightarrow 2NO_2^- + 4OH^- \qquad (4)$$
$$2NO_2^- + 4H_2O + 6e^- \rightarrow N_2 \uparrow + 8OH^- \qquad (5)$$
Net cathode reaction:
$$2NO_3^- + 6H_2O + 10e^- \rightarrow N_2 \uparrow + 12OH^- \qquad (6)$$
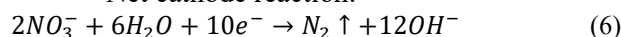
Table 1. Experimental parameters.

№	Cell Resistance, Ω		Anodic					Cathodic				
	0 hour	1 hour	Electrode	Concentration				Electrode	Concentration			
				Initial, mg·L^{-1}	FFD level	Final, mg·L^{-1}	Depletion, %		Initial, mg·L^{-1}	FFD level	Final, mg·L^{-1}	Depletion, %
1	250	163	3 SGR	60	(-1)	2	96.67	1 SGR	500	(+1)	497	0.60
2	327	254	3 SGR	60	(-1)	28	53.33	1 SGR	100	(-1)	99	1.00
3	334	244	3 SGR	150	(0)	95	36.67	1 SGR	100	(-1)	99	1.00
4	333	190	3 SGR	240	(+1)	136	43.33	1 SGR	100	(-1)	99	1.00
5	357	215	3 SGR	60	(-1)	29	51.67	1 SGR	300	(0)	284	5.33
6	347	194	3 SGR	150	(0)	70	53.33	1 SGR	300	(0)	299	0.33
7	204	169	3 SGR	240	(+1)	137	42.92	1 SGR	300	(0)	299	0.33
8	238	171	3 SGR	60	(-1)	28	53.33	1 SGR	500	(+1)	499	0.20
9	296	168	3 SGR	150	(0)	86	42.67	1 SGR	500	(+1)	498	0.40
10	238	168	3 SGR	240	(+1)	155	35.42	1 SGR	500	(+1)	493	1.40
11	322	191	3 SGR	150	(0)	85	43.33	1 SGR	1000 [4]		960	4.00
12[1]	96	94	Wet ACF	74 [2]		4	94.59	AC+1 SGR	504		-	-
13	74	65	Dry ACF	56 [2]		Traces	100.00	AC+1 SGR	504		67 [3]	86.71
14	103	98	Wet ACF	65 [2]		3	95.38	AC+1 SGR	504		-	-
15	107	95	Dry ACF	68		-	-	AC+1 SGR	500		132 [3]	73.60
16	128	119	Wet ACF	63		-	-	AC+1 SGR	500		71 [3]	85.80
17	59	55	Dry ACF	61 [2]		3	95.08	AC+1 SGR	502		341	32.07
18[1]	70	60	Wet ACF	62 [2]		3	95.16	AC+1 SGR	505		390	22.77

[1] Microbial fuel cell (MFC); [2] Sulfide solution with phosphate buffer; [3] Concentration at 24th hour mark; [4] Nitrate concentration twice higher than the highest examined in the full factorial design.

Analytical procedures

The anodic and cathodic solutions were prepared by dissolving the appropriate amounts of analytical grade Na$_2$S·9H$_2$O and KNO$_3$ (Sigma Aldrich), respectively. For improving the conductivity of both solutions, NaCl (analytical grade) with concentration of 16.5 g·L^{-1} was used for all experiments. For the experiments with constant pH of the anodic (sulfide) solution phosphate buffer was used (Experiments № [12-14] and [17-18], Table 1).

The concentration of the sulfide ions was determined photometrically by converting them to methylene blue by addition of N,N-p-phenylenediamine [16], and the concentration of nitrates was determined by UV photometry following the method of Goldman & Jacobs [17]. All analyses of the concentration of the sulfide and nitrate ions were performed for the initial solutions and at the 2nd hour mark, except in the cases explicitly stated otherwise.

Electrical measurements

Current and voltage output of the FC at a fixed load (100 Ω) were measured simultaneously during operation. Prior to the initiation of the experiment and after one hour of work, by varying the external resistance in the range [∞ - 1 Ω] the resistance of the fuel cell was calculated as the slope of the curve U = f (I) and is presented in Table 1.

Pseudomonas putida 1046 cultivation and immobilization

Pseudomonas putida 1046 was chosen as an electrogenic strain capable of oxidizing sulfide ions [13, 14]. The medium used for its cultivation was: 10 g·L^{-1} meat extract, 10 g·L^{-1} peptone and 5 g·L^{-1} NaCl and the cultivation was performed for 24 hours at 30 °C on a shaker (50 rpm).

The pyrolyzed carbon felt was immersed into the pre-cultured bacterial suspension. It was then transferred to shaking flasks and incubated at 30 °C for 48 hours. Following this methodology the immobilized cells of the *Pseudomonas putida* strain are able to produce exo-polysaccharides, which serve as binding agents between the microbial cells and the carbon felt [18].

RESULTS AND DISCUSSION

Electrical power output and depletion of sulfides and nitrates with graphite rods used as electrodes in membraneless FC

In order to evaluate the influence of the initial concentration of both contaminants a full factorial design (3^2) (FFD) was performed (Experiments № [2-10]), varying the concentration of sulfide (60, 150 and 240 mg·L^{-1} as levels -1, 0 and +1, respectively) and nitrate (100, 300 and 500 mg·L^{-1} as levels -1, 0 and +1, respectively) ions. The concentration ranges were chosen based on previous experience of the research group [19, 20]. A preliminary run (Experiment № 1) was performed to assess the

influence of the volume of each solution (with the anodic compartment being the internal one (30 mL) and the cathodic being the external one (130 mL)). When comparing Experiments № 1 and № 8 (same concentrations, but the anodic compartment being 130 mL and the cathodic – 30 mL) the latter vastly exceeds the former in terms of electrical characteristics. Following this evaluation a decision was made that all the experiments from the factorial design, as well as the additional ones presented in

Table 1 will be performed with the anodic compartment being the larger (external) one.

The electrical power output per unit volume of the catholyte of selected experiments is presented in Fig. 3. The experimental conditions are described in Table 1. Although the concentration ranges being investigated are relatively wide, the electrical performance of the FC does not differ significantly except for the initial output at higher concentrations.
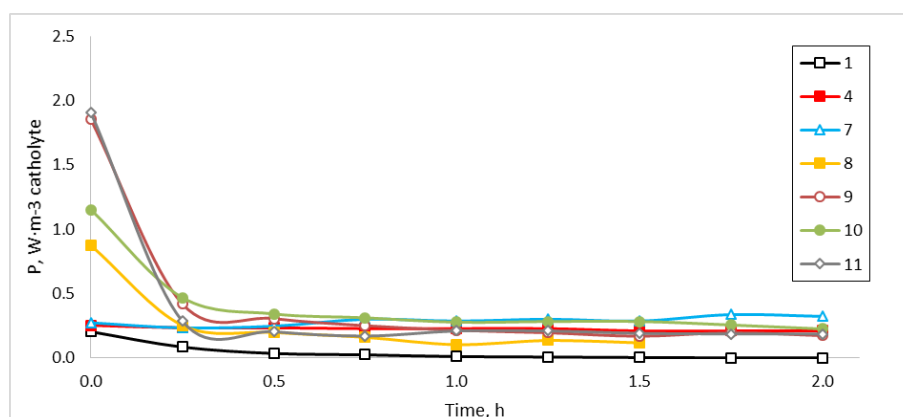
Fig. 3. Power output of the FC per unit volume of catholyte – selected experiments.
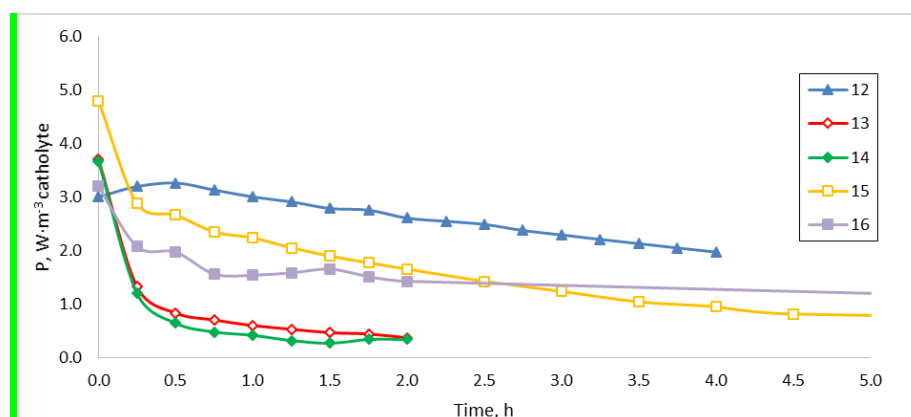
Fig. 4. Power output per unit volume of catholyte for membraneless FC with activated carbon felt electrode: dry ACF (empty symbols), wet ACF (filled symbols).

The depletion of the ions of the investigated configurations in Fig. 3. is presented in Table 1. The oxidation of sulfide ions corresponds closely to the electrical output obtained and is in the range of [35-55] % at the 2nd hour mark. The outlying fast oxidation of the sulfides of Experiment № 1 is due to the fact that the volume of the sulfide solution used in this experiment is only 30 mL (as opposed to all others experiments – 130 mL), making the amount of sulfide ions about 4 times less. The reduction of nitrates does not exceed 6 % in all cases for 2 hours of work as a FC, in accordance with the chemical characteristics of nitrate ions – a very

stable and hard to reduce pollutant, in contrast to the very active and easily oxidized sulfide ions.

Electrical power output and depletion of sulfides and nitrates with pyrolyzed carbon felts used as electrodes in the anodic compartment of membraneless FC.

In order to increase the electrical power output of the FC a different type of electrodes were used – pyrolyzed activated carbon felt. Two square-shaped felts (100 cm² each) were used as anode. Additionally, to increase the surface area of the cathode 15 g (30 mL) of activated carbon was added in the cathodic compartment. The power output of

the cell per unit volume of catholyte *vs* time is given on Fig. 4. The experimental conditions are summarized in Table 1, Experiments № [12-16]. Previous work of the research team [19] has shown that *Pseudomonas putida* is a viable microorganism for use in sulfide-driven microbial fuel cells. The research also showed that substantial substrate inhibition occurs at sulfide concentrations over 70 mg·L^{-1}, so for this part of the study sulfide concentrations were limited to about 70 mg·L^{-1}. In order to further compare the results for the FC and MFC two sets of experiments were conducted – with dry (Experiment № 15) and wet (Experiment № 16) ACFs. The felts with immobilized *P. putida* for the MFC were stored in saline solution (0.9 % NaCl), meaning they are always wet, while those for the FC can be either dry or wetted (with sterile saline solution) prior to being put into the fuel cell. The higher initial power output of the experiments with dry AFCs is due to fact that the dry AFCs adsorb immediately a large quantity of the sulfide ions, substantially increasing the local concentration of the sulfides in the pores of the felt.

On the other hand, the experiments with wet felts show lower resistance drops between the initial cell resistance and the 1 hour one. We attribute this to the fact that the felts are already soaked with conducting saline solution and the resistance drop is a consequence of the substitution of the saline solution with the more conducting anolyte (9 g·L^{-1} *vs* 16.5 g·L^{-1} NaCl, respectively, plus the additional conductivity provided by the sulfide ions present). This effect is even more prominent for the experiments with dry carbon tube and graphite rods, where the tube is the only adsorbing material – it takes a lot longer to soak than the felts, hence the difference in the internal resistance reaches up to 40 % (Experiments № [1-11]). Additional experiments with buffered sulfide solutions were performed (Experiments № [13-14]) in order to assess the viability of the configuration at lower (and stable) pH values and to compare it to the MFC, which operates at pH = 7.00. As can be seen on Fig. 4. the electrical output of the FC with buffered anodic solutions is lower which is partly due to the fact that at this pH value (7.00) part of the sulfide ions are in the form of hydrogen sulfide and they desorb from the anodic solution, lowering the concentration of the "fuel" [21]. Regardless of this effect the highest power output was obtained with the MFC (Experiment № 12), showing the viability of the MFC in generating energy in addition to the decontamination of polluted fluxes. The depletion of the ions follows the same tendency as the

experiments without buffered solutions (Experiments № [12-14] *vs* № [15, 16]), although in contrast to the experiments with only SGR used as electrodes (Experiments № [1-11]) the neutralization of sulfide ions is twice as effective, reaching up to [94 – 100] % (compared to [35-50] % for the SGR ones). The reduction of nitrates, on the other hand, reaches up to [73-87] % for 24 hours, while that of the SGR experiments is in the range of [0.2-5.3] % for 2 hours of work. Part of the depletion of nitrate ions concentration may be due to adsorption by the activated carbon used to increase the surface area of the cathode – this has the added benefit of boosting the electrical and electrochemical parameters of the FC (by increasing the local concentration of ions contacting the cathode), but at the same time impairs the direct and accurate determination of nitrate ions concentration.

Comparison between classical PEM FC and membraneless FC

In order to evaluate the viability of the membraneless FC design investigated in this work we compared its electrical and chemical parameters with those of a classical PEM FC (using Fumapem® membrane) from our previous work (Experiments № [17-19]). The initial concentrations for both experiments were identical – 65 mg·L^{-1} sulfide ions and 500 mg·L^{-1} nitrate ions. The reference membrane FC was designed with equal anodic and cathodic compartments of 300 mL, in contrast to the disproportional compartments of the membraneless FC evaluated in this study (130 mL for the anodic and 30 mL for the cathodic), but when the power output was normalized to a unit volume the two designs showed comparable values (Fig. 5). Additionally, in terms of oxidation of sulfide ions the depletion percent for the FC (with carbon felt used as anode) shows identical results and the FC with standard graphite rods is half as effective as the PEM FC for 2 hours of operation. In terms of nitrate ions reduction, though, the PEM FC outperforms both set-ups of membraneless FC presented, achieving [23-32] % depletion in 2 hours, while for the SGR set-up the depletion was in the range of [0.2-5.3] % for the same amount of time and for the ACF it was in the range of [74-87] % for 24 hours of operation.

These results prove that the proposed membraneless fuel cell design is competitive in terms of energy harvest and sulfide oxidation to established FC designs and at the same time eliminates one of the classical PEM FCs main disadvantages – the very expensive and delicate membranes.
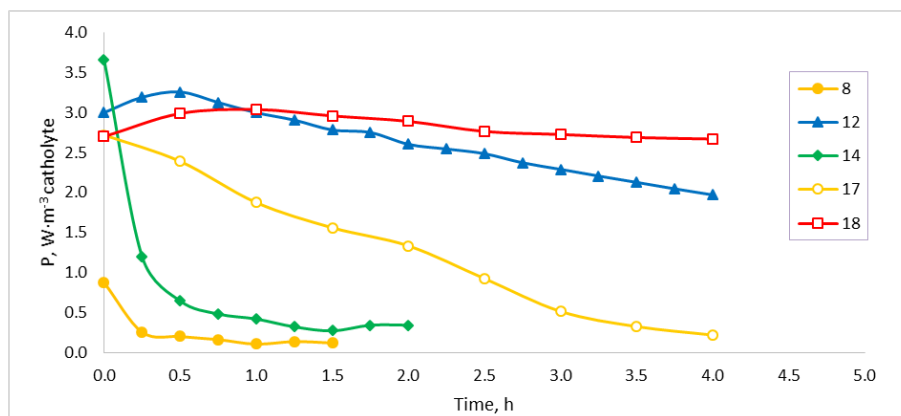
Fig. 5. Power output per unit volume of the catholyte: membraneless FC with graphite rods (Exp. 8); membraneless MFC (Exp. 12) and FC (Exp. 14) with carbon felt; PEM FC (Exp. 17) and PEM MFC (Exp. 18).

Additionally, the carbon felt electrodes improve both electricity generation and oxidation/ reduction of the investigated pollutants when compared to pure graphite electrodes.

Coulombic efficiency of the fuel cell

Based on the main reactions presented in Eq. [1-6] and the experimental results obtained the Coulombic efficiency for the anodic and cathodic reactions was calculated and is presented in Table 2.

Table 2. Coulombic efficiency of the fuel cell for anodic and cathodic reactions.

Exp. №	Anodic Reaction [1]	Cathodic Reaction [2]
1	1.25	7.04
2	1.58	235.58
3	0.90	230.72
4	0.57	273.67
5	1.51	13.61
6	0.78	290.56
7	0.65	310.68
8	1.61	238.97
9	0.92	137.41
10	0.74	41.76
11	0.91	6.86
12	4.26	2.75
13	2.72	1.62
14	2.15	1.23
15	3.90	3.41
16	3.65	2.52
17	11.39	19.08
18	15.78	37.66

[1] 6 electron transfer by Eq. (1); [2] 10 electron transfer by Eq. (6).

Qualitative analysis performed on the anodic solution proved that no elemental sulfur was present in the solution or deposited onto the anode during operation of the FC, while the presence of sulfite and sulfate ions in the anolyte was confirmed (with sulfite ones being more prominent than sulfate ones).

Thus, the Coulombic efficiency presented corresponds to the sulfide-to-sulfite reaction ($S^{2-} \rightarrow SO_3^{2-}$, Eq. (1)) and the transfer of 6 electrons. In terms of electrical efficiency, the results for Experiments № [1-11] were low [0.6-1.6] % but a 2 to 3 times increase was observed for the experiments with carbon felt (Experiments № [12-16]) and up to [11-16] % efficiency was achieved by the membrane FC (Experiments № [17-18]). Highest efficiencies (in their respective sets) were achieved by the MFCs compared to the same condition FCs (Experiments № 12 *vs* № 14 and Experiments № 18 *vs* № 17, with 4.26 % *vs* 2.15 % and 15.78 % *vs* 11.39 % efficiency, respectively). Still, in terms of ecological parameters for the anodic solution neutralization the novel design of the FC (with activated carbon felts used as anode) showed comparable results with traditional PEM FC.

The Coulombic efficiency for the reduction reaction is based on Eq. (6) with 10 electrons transferred. When examining the results presented in Table 2 an interesting phenomenon is observed – the first batch of experiments (Experiments № [1-11] with just graphite electrodes) show efficiencies over the maximum theoretical values, especially the lower initial nitrate concentrations (100 and 300 mg·L^{-1}). We attribute this to two factors: i) at lower nitrate concentrations reduction of dissolved oxygen in the catholyte is also contributing to the cathodic reactions, while for the higher concentration examined (500 mg·L^{-1}) the majority of the electron transfer is related to nitrate reduction; and ii) as nitrate ions are very stable ions it takes a lot longer to reduce them than to oxidize the sulfide ones in the anodic compartment. This is evident from the depletion percent presented in Table 1 – for 2 hours of operation of the FC only [0.2-5.3] % of the nitrates present are reduced, compared to [73-87] % for 24 hours of operation of the FC, albeit with different electrodes used (Experiments № [1-11] *vs*

130

Experiments № [12-16]). The addition of activated carbon in the cathodic compartment, while increasing the power output, drastically reduces the cathodic efficiency. Both of these effects are consequence of the adsorption of the nitrate ions onto the surface of the carbon – on one hand the adsorption increases the local concentration on the surface of the electrode, thus the power output; while on the other hand as the nitrate ions are very stable the reduction rate is low, thus part of the ions are still not converted to nitrogen, yet they are not in the solution and because the chemical analysis cannot account for this adsorbed quantity the actual amount of converted ions is most likely lower than the analyses show.

CONCLUSIONS

A membraneless fuel cell for remediation of contaminated fluxes is presented and investigated. Compared to a classical membrane fuel cell it shows comparable characteristics. Its advantage is the elimination of the expensive and difficult for exploitation polymer membrane. Additional advantages are the possibility to work at elevated temperatures and the relatively cheap manufacture and exploitation costs.

From an ecological standpoint the innovative FC design has a couple of advantages – it converts a waste (the carbon tube) into a product that further helps remediate sulfide- and nitrate-contaminated fluxes, effectively applying the principles of the circular economy. Depending on the initial concentrations [35-53] % of the sulfide ions present are remediated in the first two hours of operation when standard graphite rods are used as electrodes and [94-100] % are converted when activated carbon felt is used as an electrode in addition to the graphite one over the same time period. In terms of nitrate reduction the conversion rate is low when only SGR are used for two hours of work [0.2-5.3] %, while when activated carbon is employed in addition to the SGR as cathode and activated carbon felt is used as an anode reduction of up to 87 % can be achieved at the 24th hour mark.

All experiments show a drop in the internal cell resistance of the FC after 1 hour of operation due to the fact that conducting solution enters the pores of the electrodes. This effect is more prominent when the only adsorbent material is the pyrolyzed tube itself (up to 40 % resistance drop), though the use of pyrolyzed felt as anode lowers the internal resistance of the FC two to three times, making it comparable to a membrane FC.

Coulombic efficiency for the anodic reaction is low when SGR are used as anode [0.6-1.6] % but the use of carbon felts as anode increases the efficiency to [2.1-4.3] %. These results are still far from the ones obtained by a traditional PEM FC [11.4-15.8] %. MFCs show better efficiencies than FCs of the same design and at the same conditions (4.3 % *vs* 2.1 % and 15.8 % *vs* 11.4 % efficiency for the membraneless and PEM MFC *vs* FC, respectively).

The Coulombic efficiency for the cathodic reaction with SGR shows that additional reaction takes place, most likely reduction of dissolved oxygen. This can be avoided by using higher initial concentrations of nitrate ions. The electrical efficiency drops to [1.2-3.4] % for 24 hours of operation, yet the depletion percent increases from [0.2-5.3] % to [74-87] %. Similar to the anodic efficiency, MFCs show better cathodic efficiency than the corresponding FCs.

Microbial fuel cells (both membraneless and classical membrane ones) show better electrochemical characteristics than regular FCs of the same design. The use of immobilized electrogenic cells in the anodic compartment allows their repeated use, on one hand, and on the other hand, it lessens the effect of substrate inhibition at higher concentrations of sulfide ions, thus expanding the range of application of the MFC.

Based on all the results obtained a process can be designed to tap into the advantages of the rapid and not so electrochemically effective oxidation of sulfide ions and the steady, efficient reduction of nitrate ones – fresh anolyte can be fed to the anodic compartment while a static, nitrate-rich catholyte can be used to realize an effective fuel cell for remediation of sulfide- and nitrate-contaminated fluxes.

REFERENCES

1. K. Scott, H. Y. Eileen, Amsterdam, Elsevier WP Woodhead Publishing 2016, 2015.
2. T. Napporn, Y. Holade, Electrolyzers, and Metal-Air Batteries, 1st edn., G. Korotcenkov (ed.), Elsevier, 2021.
3. S. Bapat, C. Giehl, S. Kohsakowski, V. Peinecke, M. Schäffler, D. Segets, *Adv. Powder. Technol.,* **32**, 3845 (2021).
4. H. M. A. Sharif, M. Farooq, I. Hussain, M. Ali, M. A. Mujtaba, M. Sultan, B. Yang, *J. Taiwan Inst. Chem. Eng.,* **129**, 207 (2021).

5. J. Zhao, X. Li, C. Shum, J. McPhee, *Energy and AI,* **6**, 100114 (2021).

6. Y. Liu, B. Xiao, J. Zhao, L. Fan, X. Luo, Z. Tu, S. H. Chan, *Energy Convers. Manag.: X,* **12**, 100114 (2021).

7. Y. Wang, K. S. Chen, J. Mishler, S. C. Cho, X. C. Adroher, *Appl. Energy,* **88**, 981 (2011).

8. P. C. Okonkwo, I. B. Belgacem, W. Emori, P. C. Uzoma, *Int. J. Hydrog. Energy,* **46**, 27956 (2011).

9. C. Zhang, W. Zhou, M. M. Ehteshami, Y. Wang, S. H. Chan, *Energy Convers. Manag.,* **105**, 433 (2015).

10. Q. Wang, F. Chen, Y. Liu, T. T. Gebremariam, J. Wang, L. An, R. L. Johnson, *J. Power Sources,* **404**, 106 (2018).

11. H. An, H. Jeon, J. Ji, Y. Kwon, Y. Chung, *J. Energy Chem.,* **58**, 463 (2021).

12. Y. Yang, P. Xu, S. Dong, Y. Yu, H. Chen, J. Xiao, *J. Clean. Prod.,* **307**, 127306 (2021).

13. H. Guo, C. Chen, D.-J. Lee, A. Wang, N. Ren, *Enzyme Microb. Technol.,* **53**, 6 (2013).

14. Y.-C. Chung, C. Huang, C.-P. Tseng, *Biotechnol. Prog.,* **12**, 773 (1996).

15. L. Ljutzkanov, A. Anastasov, Method of processing carbon containing materials, Bulg. Pat. 63594, 2002.

16. T. D. Rees, A. B. Gyllenspetz, A. C. Docherty, *Analyst,* **96**, 201 (1971).

17. E. Goldman, R. Jacobs, *J. Am. Water Work,* **53**, 187 (1961).

18. F. H. Romano, V. Beschkov, in: Biocatalysis Research Progress, Nova Science Publishers Inc., 2008, p. 281.

19. E. Razkazova-Velkova, S. Stefanov, T. Parvanova-Mancheva, M. Martinov, *Bulg. Chem. Commun.*, **52** (A), 87 (2020).

20. E. Razkazova-Velkova, M. Martinov S. Stefanov, *Sci. Works Univ. Food Technol.,* (2017).

21. H. Marianne H. Hasler-Sheetal, *Front. Mar. Sci.,* **1**, 11 (2014).

BULGARIAN CHEMICAL COMMUNICATIONS

Instructions about Preparation of Manuscripts

General remarks: Manuscripts are submitted in English by e-mail or by mail (in duplicate). The text must be typed double-spaced, on A4 format paper using Times New Roman font size 12, normal character spacing. The manuscript should not exceed 15 pages (about 3500 words), including photographs, tables, drawings, formulae, etc. Authors are requested to use margins of 3 cm on all sides. For mail submission hard copies, made by a clearly legible duplication process, are requested. Manuscripts should be subdivided into labelled sections, e.g. **Introduction, Experimental, Results and Discussion**, *etc*.

The title page comprises headline, author's names and affiliations, abstract and key words.

Attention is drawn to the following:

a) **The title** of the manuscript should reflect concisely the purpose and findings of the work. Abbreviations, symbols, chemical formulas, references and footnotes should be avoided. If indispensable, abbreviations and formulas should be given in parentheses immediately after the respective full form.

b) **The author**'s first and middle name initials, and family name in full should be given, followed by the address (or addresses) of the contributing laboratory (laboratories). **The affiliation** of the author(s) should be listed in detail (no abbreviations!). The author to whom correspondence and/or inquiries should be sent should be indicated by asterisk (*).

The abstract should be self-explanatory and intelligible without any references to the text and containing not more than 250 words. It should be followed by key words (not more than six).

References should be numbered sequentially in the order, in which they are cited in the text. The numbers in the text should be enclosed in brackets [2], [5, 6], [9–12], etc., set on the text line. References, typed with double spacing, are to be listed in numerical order on a separate sheet. All references are to be given in Latin letters. The names of the authors are given without inversion. Titles of journals must be abbreviated according to Chemical Abstracts and given in italics, the volume is typed in bold, the initial page is given and the year in parentheses. Attention is drawn to the following conventions:

a) The names of all authors of a certain publications should be given. The use of "*et al*." in the list of references is not acceptable.

b) Only the initials of the first and middle names should be given.

In the manuscripts, the reference to author(s) of cited works should be made without giving initials, e.g. "Bush and Smith [7] pioneered...". If the reference carries the names of three or more authors it should be quoted as "Bush *et al*. [7]", if Bush is the first author, or as "Bush and co-workers [7]", if Bush is the senior author.

Footnotes should be reduced to a minimum. Each footnote should be typed double-spaced at the bottom of the page, on which its subject is first mentioned.

Tables are numbered with Arabic numerals on the left-hand top. Each table should be referred to in the text. Column headings should be as short as possible but they must define units unambiguously. The units are to be separated from the preceding symbols by a comma or brackets.

Note: The following format should be used when figures, equations, *etc*. are referred to the text (followed by the respective numbers): Fig., Eqns., Table, Scheme.

Schemes and figures. Each manuscript (hard copy) should contain or be accompanied by the respective illustrative material as well as by the respective figure captions in a separate file (sheet). As far as presentation of units is concerned, SI units are to be used. However, some non-SI units are also acceptable, such as °C, ml, l, etc.

The author(s) name(s), the title of the manuscript, the number of drawings, photographs, diagrams, etc., should be written in black pencil on the back of the illustrative material (hard copies) in accordance with the list enclosed. Avoid using more than 6 (12 for reviews, respectively) figures in the manuscript. Since most of the illustrative materials are to be presented as 8-cm wide pictures, attention should be paid that all axis titles, numerals, legend(s) and texts are legible.

The authors are asked to submit **the final text** (after the manuscript has been accepted for publication) in electronic form either by e-mail or mail on a 3.5'' diskette (CD) using a PC Word-processor. The main text, list of references, tables and figure captions should be saved in separate files (as *.rtf or *.doc) with clearly identifiable file names. It is essential that the name and version of

the word-processing program and the format of the text files is clearly indicated. It is recommended that the pictures are presented in *.tif, *.jpg, *.cdr or *.bmp format, the equations are written using "Equation Editor" and chemical reaction schemes are written using ISIS Draw or ChemDraw programme.

The authors are required to submit the final text with a list of three individuals and their e-mail addresses that can be considered by the Editors as potential reviewers. Please, note that the reviewers should be outside the authors' own institution or organization. The Editorial Board of the journal is not obliged to accept these proposals.

EXAMPLES FOR PRESENTATION OF REFERENCES

REFERENCES

1. D. S. Newsome, *Catal. Rev.–Sci. Eng.*, **21**, 275 (1980).
2. C.-H. Lin, C.-Y. Hsu, *J. Chem. Soc. Chem. Commun.*, 1479 (1992).
3. R. G. Parr, W. Yang, Density Functional Theory of Atoms and Molecules, Oxford Univ. Press, New York, 1989.
4. V. Ponec, G. C. Bond, Catalysis by Metals and Alloys (Stud. Surf. Sci. Catal., vol. 95), Elsevier, Amsterdam, 1995.
5. G. Kadinov, S. Todorova, A. Palazov, in: New Frontiers in Catalysis (Proc. 10th Int. Congr. Catal., Budapest, 1992), L. Guczi, F. Solymosi, P. Tetenyi (eds.), Akademiai Kiado, Budapest, 1993, Part C, p. 2817.
6. G. L. C. Maire, F. Garin, in: Catalysis. Science and Technology, J. R. Anderson, M. Boudart (eds), vol. 6, Springer-Verlag, Berlin, 1984, p. 161.
7. D. Pocknell, *GB Patent* 2 207 355 (1949).
8. G. Angelov, PhD Thesis, UCTM, Sofia, 2001.
9. JCPDS International Center for Diffraction Data, Power Diffraction File, Swarthmore, PA, 1991.
10. CA **127**, 184 762q (1998).
11. P. Hou, H. Wise, *J. Catal.*, in press.
12. M. Sinev, private communication.
13. http://www.chemweb.com/alchem/articles/1051611477211.html.

CONTENTS

Ninth International Conference of FMNS (FMNS-2021) "Modern Trends in Science",
Blagoevgrad, Bulgaria, September 15-19, 2021